Topologically Optimised Cast Glass Grid Shell Nodes

Exploring Topology Optimisation as a design tool for Structural Cast Glass elements with reduced annealing time

Wilfried Damen TU Delft

Topologically Optimised Cast Glass Grid Shell Nodes

Exploring Topology Optimisation as a design tool for Structural Cast Glass elements with reduced annealing time

P5 graduation thesis

Faculty of Architecture
and the Built Environment

Msc. Architecture, Urbanism
& Building Sciences

Building Technology Track

Student
Wilfried Damen Bsc.
4277031

First mentor
Faidra Oikonomopoulou Msc.
Structural Mechnaics and Design

Second mentor
Dr. Michela Turrin
Design Informatics

External Examiner
Dr. Erik Louw
Urban and Regional Developement

Juli 2019

TU Delft Delft University of Technology

Acknowledgement

This project is the conclusion of my education at the TU Delft. It was a busy and wonderful time, and it taught me a lot. I could not have done this alone, as I was supported by many who went out of their way to help me.

First and foremost, I would like to thank my mentor Faidra Oikonomopoulou. Her knowledge of the subject was invaluable for this project, while her endless enthusiasm and great stories worked wonders in keeping our group of glass students excited and motivated during the last seven months.

It was a pleasure to work with Michela Turrin. Her solid advice and critical questions helped me a lot to improve the quality of my work, and remain focussed throughout the project.

I would also like to thank Telesilla Bristogianni for her help in the glass lab. Her expertise and experience with the casting process proved valuable, and helped me realise the wonderful final glass models.

Many thanks to Jackson Jewett from MIT and Dimitris Vitalis from ARUP for their solid and in-depth advice on the topology optimisation and glass; you really helped me in understanding the complex workings of structural optimisation and glass design

I am very grateful to Andreas Müller from ExOne for kindly providing some amazing printed sand moulds, and to Andres Sevtsuk from the Harvard Graduate School of design, for sharing extensive documentation and a digital model of the SUTD pavilion he helped design. Furthermore, many thanks to Paul de Ruiter for his thoughts on wax printing, Ate Snijder for sharing his experience on designing and detailing hybrid glass beams, and Fred Veer for his advice on structural analysis and ANSYS.

I had a great time working with my fellow student Ivneet Bhatia, who did most of the work on exploring the sand mould casting for his thesis, and whom I worked with closely during the entire project. You make a great cup of tea!

Finally, I would like to thank my parents and my girlfriend for supporting me, and keeping me sane over the last months. I could not have done this without you.

1. Table of contents

2. Introduction

2.1 Background

In recent years, cast glass has been receiving increasing attention as a structural material. Projects such as the Crystal Houses (Oikonomopoulou, 2017) or the Atocha Memorial (Göppert, Paech, 2008) have proven that structural cast glass is capable to function as a fully self-supporting material (Fig. 1). In the currently realised projects however, little exploration has been made on the forms that can be achieved by cast glass (Oikonomopoulou, 2018). The currently used structural cast glass components copy the design language of the common ceramic brick, as this is a geometry that is easy to produce and uses the high compressive strength of glass.

These glass bricks are not without flaws. Large cast glass elements require long cooling times during production, in a process referred to as annealing. Due to this, the size of cast glass bricks has remained limited. In structural behaviour, glass has great potential. Though brittle, under compression glass has a strength that close to that of steel (Veer, 2005). Used as a simple brick wall, much of this potential strength is wasted.

Topology Optimisation (TO) is a method for creating material efficient, optimised structural designs. It is a tool for finding the most optimal material distribution within a given design space, taking into account specified loads, supports and constraints. (Bensoe, Sigmund, 2003)) Often this results in shapes that are complex and not always intuitive (Fig. 2). Unlike most conventional production processes, computer guided additive manufacturing (AM) offers near complete freedom of shape, which makes it possible to directly translate these geometries to a physical object. (Saadlaoui et al. 2017) AM can be used to directly produce the object, or alternatively be used to simplify the production process by automatically generating moulds for casting. (Niehe, 2017)

Topology optimisation has so far mainly seen use in common structural materials such as metals and plastics; applications in glass structures have as of yet remained unexplored. Yet there appear to be potential advantages of using this optimisation method for designing cast glass elements. By following the flow of forces in the material, elements optimised with TO have organic looking, rounded geometries, in addition of having a relatively low mass. As will be further explained in the following chapters, these properties have the potential of greatly reducing fabrication time of cast glass allowing for a much faster cooling process compared to solid glass objects.

Fig. 1 *Top: Atocha Memorial, Madrid Bottom: Crystal Houses, Amsterdam*

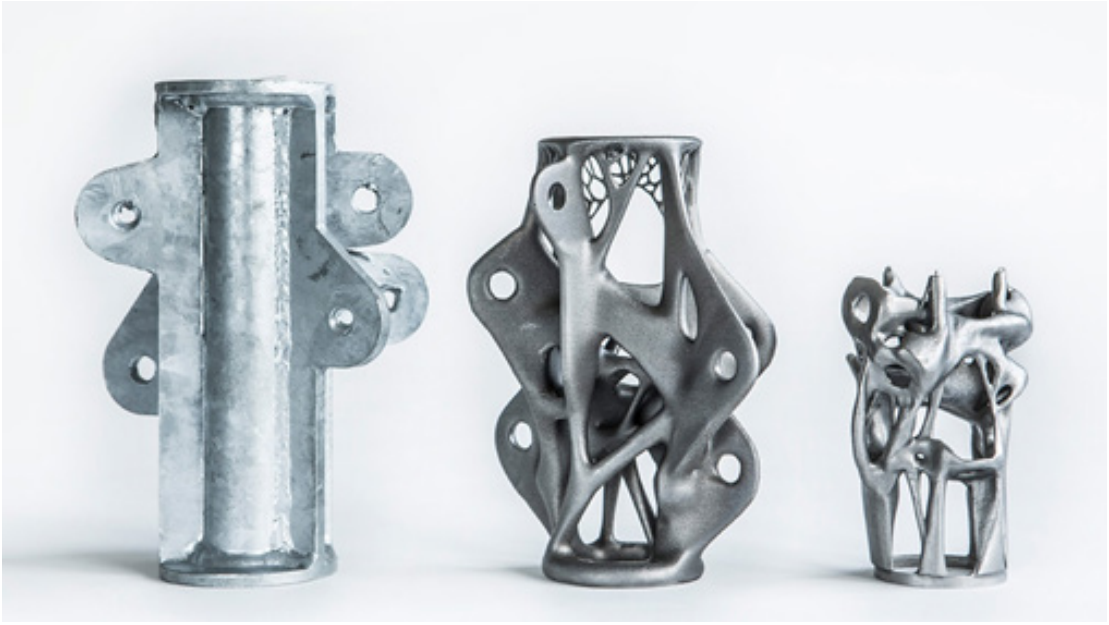

Fig. 2 *Topological Optimisation and Additive Manufacturing. Left: original conventional component. Middle: Topologically optimised node, fabricated with Metal Laser Sintering. Right: Improved TO node, cast in 3D-printed sand mould*

The applicability of topology optimisation on structural cast glass design will be explored in this thesis. This will be done through a design project; creating a node for a grid shell structure using cast-glass.

A grid shell node was chosen for a couple of reasons. Grid shell roofs are attractive for architects due to the very transparent structure that can be realised, as little structural material is required to achieve great spans (Fig. 3). By replacing the structural elements with glass, unparalleled transparency can be achieved. From a mechanics point of view, shells are compression based structures. A node will therefore mostly be loaded in compression, which glass can withstand well. Finally, grid shell nodes have a complex shape. In freeform shells, it is not uncommon for each node to be unique, making manufacturing both complex and time-consuming. As additive manufacturing is required to realise the complex geometries designed by TO, a large degree of complexity can be achieved in these elements with little added effort.

A case-study project of a small grid-shell based pavilion will be used as a tool for designing the node. The shell-structure will be redesigned with a glass support structure, with a focus on the cast connecting nodes.

Fig. 3 *Lightweight and open: gridshell covering the Queen Elisabeth II Great Court, British Museum, London. Foster and partners*

2.2 Objective

The objective of this research is to explore the potential of using Topology Optimisation as a design tool for complex structural cast-glass elements with a reduced annealing time.

2.3 Research question

What is the potential of using Topology Optimisation as a design tool for a structural cast glass grid shell node that is optimised for fabrication, structural behaviour and assembly?

2.4 Subquestions

- What design criteria should be used when using topology optimisation for cast glass design?
- How should the connection between the glass node and the remainder of the structure be designed?
- What are the most suitable methods to fabricate the nodes with the aid of additive manufacturing?
- What is the influence of TO design on the annealing time of the glass elements?

2.5 Methodology

Literature research

Looking at existing literature will give insight to what the possibilities and limitations of Topology Optimization and cast glass are. Looking at precedents can tell what is possible using these methods, while also revealing issues that might arise. Researching grid shells is necessary to know what the requirements are that the final design need to fulfil. Meanwhile, a suitable case study is selected where the theory can be applied.

The following literature research questions have been formulated to investigate cast glass, topology optimisation and grid shells.

- What are the physical and structural properties of different compositions of glass?
- How is glass cast, and what are the possibilities and limitations of this production process?
- What uses has cast glass seen in the built environment?
- What various methodologies have been developed for topology optimisation?
- What applications has topology optimisation seen in the build environment and beyond?
- What are the challenges for using topology optimisation for glass?
- How do grid shells function and what are the requirements for the grid shell joints?

Tool development and design

Based on the lessons learned during the literature research, design proposals for the glass grid shell node will be made. Different methods and settings for TO will be tested, based on these designs. A series of parametric tools will be developed to allow to faster generate and test different design variations. During this process, structural behaviour will be tested using FEM analysis. Fabrication and assembly should also be taken into account, for example by using physical models.

Prototyping

To test whether the developed geometries are suitable for casting, some of the designed nodes will be cast in glass. This also gives the opportunity to test various methods of mould making with the aid of additive manufacturing.

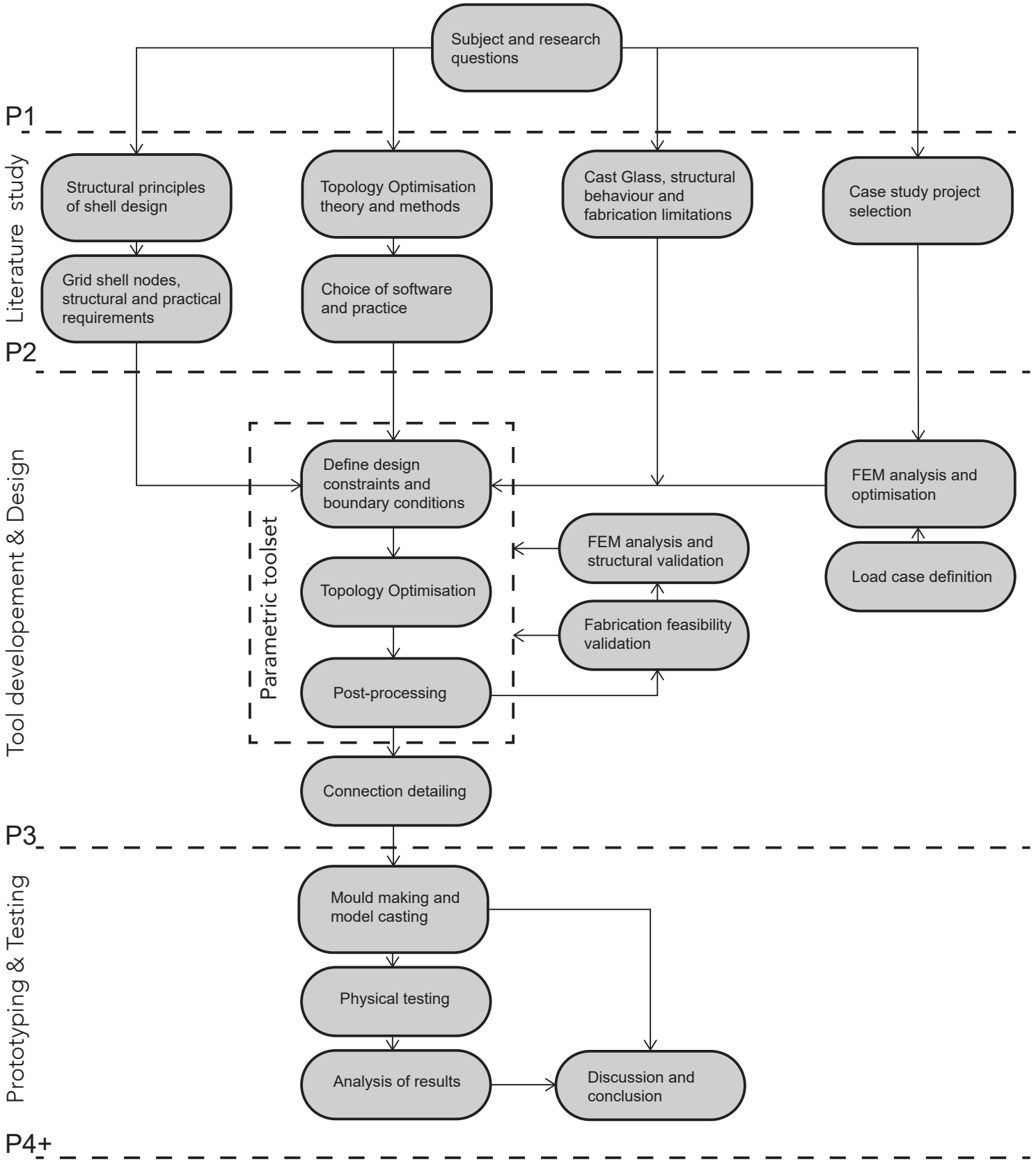
Subject and research questions
P1
Literature study
Structural principles of shell design
Topology Optimisation theory and methods
Cast Glass, structural behaviour and fabrication limitations
Case study project selection
Grid shell nodes, structural and practical requirements
Choice of software and practice
P2
Tool developement & Design
Parametric toolset
Define design constraints and boundary conditions
FEM analysis and optimisation
FEM analysis and structural validation
Load case definition
Topology Optimisation
Fabrication feasibility validation
Post-processing
Connection detailing
P3
Prototyping & Testing
Mould making and model casting
Physical testing
Analysis of results
Discussion and conclusion
P4+

2.6 Outline of this thesis

This thesis has been split up into two parts. First, a literature review is used to provide a scientific context for the research. This literature review has been divided in four chapters, each covering a different aspect of the design assignment.

After this, the design process of the case study structure is described, as are the physical tests performed, based on this design. Finally, the concluding chapters try to provide an answer for the research question, and give some further reflection.

Chapter 2 focusses on Topology Optimisation (TO). There, it will be explained what its role is within the field of structural optimisation. Multiple different methods developed to perform TO will be briefly explained, and the expected challenges associated with using TO for a brittle material such as glass are considered. Next, a couple examples of TO used in practice are described. Finally, a couple of software packages capable of TO are briefly reviewed.

Chapter 3 gives an explanation of grid shells, and shell structures in general. First, the structural principles behind shell structures, and ways of finding an optimal shell shape are described. Following this, the subfamily of grid shells is introduced, and the requirements of the grid shells nodes are listed. Lastly, three existing projects researching TO gridshell node designs are summarised.

Chapter 4 focusses on the material of glass, focussing on cast glass. First of all, the potential of cast glass as a structural material in the built environment is discussed. Next, the physical and structural properties of glass are described, followed by an overview of different glass compositions and their applications. The glass casting process and different moulds available for this are described. To close the chapter, two existing structures using cast glass as a structural material are mentioned.

Chapter 5 concerns the case study that will be used. First, the criteria used to choose this project are briefly explained. After a description of the chosen project, a series of analyses is performed to check the structural feasibility of the structure. These conclusions are used to make some changes to the pavilion geometry

Chapter 6 follows the design process of the new shell pavilion, in which the structure is re-imagined as a glass building. Based on a couple design criteria, a glass beam design is chosen, and the connection between the node and the beams is detailed.

In chapter 7, the precise goals and methodology of the topology optimisation are explained. Following this, chapter 8 describes the various optimisations attempted, and their results. Three iterations of designs are made, each one taking into account the lessons of the previous step.

In chapter 9, the fabrication of the found geometries is tested. Two different mould designs, using additive manufacturing with sand and lost-wax investment casting have been used.

Chapter 10 contains technical drawings and visualisations of the finalised pavilion and node. Furthermore, the potential of mass production of the glass elements is discussed.

Chapter 11 concludes the research. An answer is given to the main research question and the sub-questions, based on the research results. Next, a more general perspective on topology optimisation is given. What lessons about topology optimisation in the built environment have been learned during this research, which might be of use for future research? Finally, the entire research project is reflected upon. Is it realistic that this project will be applied in practice, and why? What are the limitations of the research, and what potential follow-up research can be done to further expand on this topic?

3. Cast glass

3.1 Potential of structural cast glass

"Architecture is the masterly, correct and magnificent play of volumes brought together in light, (…) the history of architecture was the history of the struggle for the window."

–Le Corbusier
(in: Whitney & Kipnis, 1993)

Transparency plays an important role in architecture. Natural daylight, and a connection to our environment are essential for functional residential and commercial buildings (Arbab & Finley, 2010). Glass is a unique material in this context, as it is one of the few widely available materials that can function as a barrier while still offering transparency. Due to this, glass has been sought out as building material time and time again.

For most of the history of construction, advancements in glass manufacturing aimed at improving the material for use in window glazing. New production techniques enabled larger and thinner panes to be produced in ever increasing quantities, while many more recent innovations aim at improving building physics performance of glass by introducing cavities, coatings and insulated framing. (Structural use of glass, 2014).

Striving for a more transparent architecture, structural glass has been introduced, beginning with greenhouses where glass was used as a bracing element providing stability to the structure. This was a clear shift away from glass used purely as an infill material, and towards a fully glass architecture. Advancements in glass technologies and engineering have transformed glass from a brittle, fragile material to a structural component of high compressive, load bearing capacity. (Oikonomopoulou, 2018)

Despite this, glass is still primarily regarded as a two-dimensional material, used in flat panes. Though this ensures high transparency, it means the material is prone to buckling. Additional steps need to be taken to increase the stiffness of the glass. This is usually achieved by the following measures (Fig. 4).

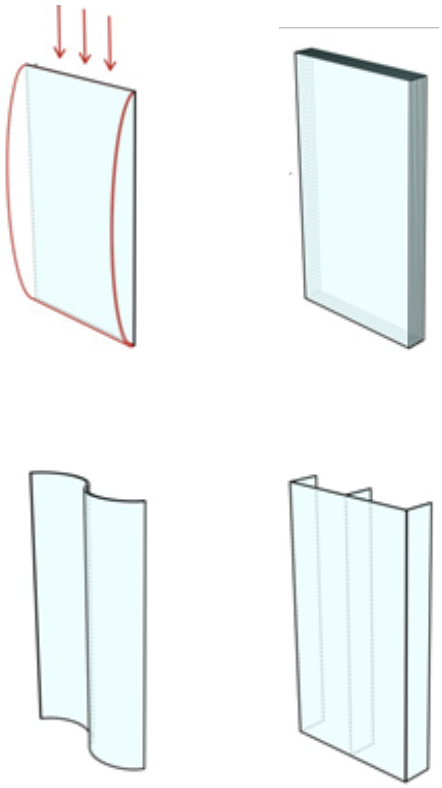

Fig. 4 *Improving buckling resistance. From left to right: laminating, curving and support structure.*

- Laminating, to increase the thickness of the material
- Curving the glass, to change the geometry of the material
- Adding glass fins for support

These solutions bring with them many complications, such as for example the requirement of opaque steel elements to form connections, and high production costs associated with curving or laminating glass Furthermore, the brittleness of pane glass means extensive security measures need to be taken. This includes over dimensioning of elements and the designing of alternate load paths to account for failure of elements. (O'Reghan, 2014; Pariafsain, 2016)

A promising alternative to this is cast glass. Cast glass involves the pouring of molten glass into a mould, in a manner reminiscent to metal casting. This change in production

process allows for a completely different design language than pane glass. It makes it possible to make solid, monolithic elements in a great variety of shapes. Structurally, greatly increased cross-sections can be achieved, decreasing the risk of buckling and allowing to make structures without additional stiffening.

So far, cast glass has seen limited use in architecture. Application has been discouraged by high manufacturing costs caused by for example the long and complicated annealing process.

However as will be explained in the chapter on annealing, experiences from for example large-scale cast glass telescopes have shown that smart design can at least partly overcome these challenges.

3.2 Properties of glass

'If you think of Brick, you say to Brick, 'What do you want, Brick?' And Brick says to you, 'I like an Arch.'

-Louis Kahn

In essence, any structural design task is a material science challenge. The material that will be used dictates the structural limitations for the structure, and determines how, and where it can be used. Knowing the physical and mechanical properties of materials is therefore essential. This is especially true for a unique material such as glass.

On a molecular level, glass is an amorphous material. Although there are some discernible structural elements, there is no systematic repetition of this structure and thus no crystallinity by the standard definition. This lack of a crystal structure means that there is no possibility of dislocations. Due to this, glass is cannot deform plastically. (Veer, 2005) This makes glass a brittle material, as it will yield suddenly, without showing plastic behaviour. The lack of plastic behaviour also means that the material is unable to reduce local peak stresses by flowing. The material can only deform elastically, or fracture. (Haldiman, 2008; Veer, 2005)

Glass does not undergo phase changes. Instead, its viscosity gradually changes based the temperature of the material. At high temperatures, the glass behaves as a viscous liquid; when cooled the material can be considered solid (Fig. 6). The low viscosity during cooling prevents crystallisation, as the glass molecules move too slow to reorganise themselves into a crystal structure. This gives glass its transparent properties. If the glass is cooled sufficiently slowly to enable crystallisation, the glass loses its transparency and is considered a glass ceramic.

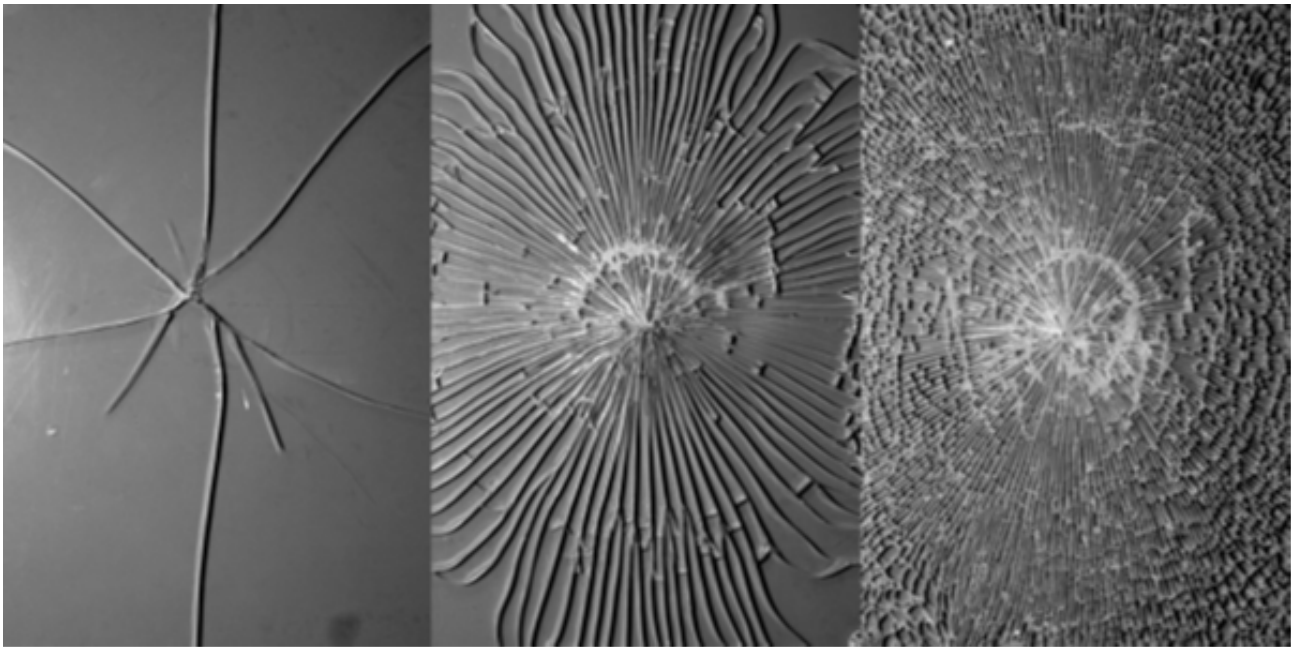

Fig. 5 *Failure behaviour of float glass. Left to right: Annealed, heat strengthened, fully tempered*

Based on the molecular forces in the material, glass has an exceptionally high theoretical yield strength, estimated between 6 000 and 10 000 MPa. (Haldiman, 2008) This is many times higher than even the strongest steel currently available. These theoretical results are however of little use in practice. Due its brittle behaviour, its strength is greatly reduced by mechanical flaws in the material. If, under loading, the local stress around a defect exceeds the chemical bond strength, a crack will form. As this further increases the local stresses, the crack will propagate further, causing the material to shatter below the theoretical limit. (Veer, 2005) (Fig. 7)

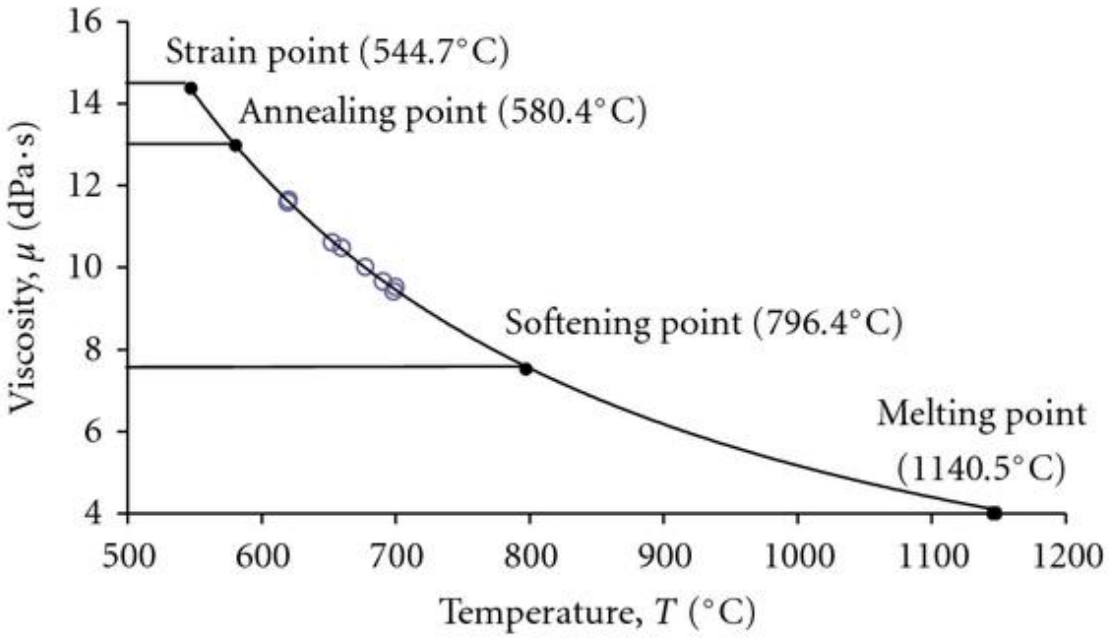

Fig. 6 *Relation between glass temperature and viscosity*

Therefore, the yield strength of glass is not so much a material property, as it is a property of each element, based on the quality of its surface and the presence of defects. Even when testing seemingly identical samples, the stresses at which the material fails have a wide range that do not follow any statistical distribution. (O'Regan, 2014)

Under compression, the flaws and defects of glass do not grow or fail, as they are closed by elastic deformation of the material. Due to this, glass has a much higher compressive strengths in comparison to its tensile strength. The compressive limit is however rarely reached. Even under compression, tensile stresses will appear in the material, due to either buckling or deformation caused by the Poisson ratio effect. Therefore the tensile yield strength can be considered the limiting factor. (Haldiman, 2008)

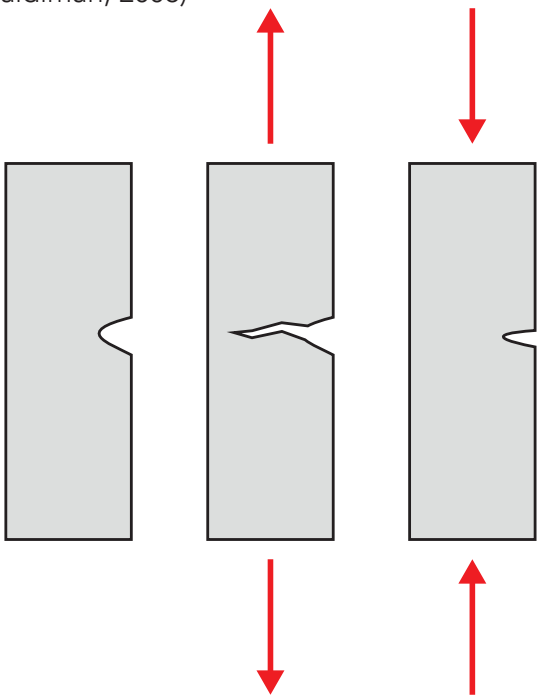

Fig. 7 *Structural behaviour of a brittle material with a surface flaw. Under tension, the flaw results in a local stress concentration, causing a crack. Under compression, the flaw is closed*

To cope with this uncertainty about glass strength, high material safety factors are employed in glass engineering. This results in structures that are generally over dimensioned to avoid failure in the weakest components. Taking into account these safety factors, a tensile failure strength of 20 N/mm^2 is used for most types of annealed glass (Veer, 2005). For compression, a failure strength of 200 N/mm^2 is used.

Soda-lime	Approximate Composition
	73% SiO2
	17% Na2O
	5% CaO
	4% MgO
	1% Al2O3

Melting point: 1350-1400°C
Used for: window panes, bottles, façade glazing.

Borosilicate	Approximate Composition
	80% SiO2
	13% B2O3
	4% Na2O
	2.3% Al2O3
	0.1% K2O

Melting point: 1450-1550°C
Used for: Light bulbs, laboratory ware, household ovenware, large telescope mirrors

Lead silicate	Approximate Composition
	63% SiO2
	21% PbO
	7.6% Na2O
	6% K2O
	0.3% CaO
	0.2% MgO
	0.2% B2O3
	0.6% Al2O3

Melting point: 1200-1300°C
Used for: Crystal glassware, Glass art, Neon-signs, Television screens

3.3 Glass compositions

Many properties of glass are determined by the exact composition of the material. In its purest form, glass has a molecular structure consisting of silica oxide. This structure can be broken up with other elements, changing how the material behaves. Especially many temperature-related properties of the glass, such as the working temperature at which the material is fully liquid, thermal expansion and viscosity are greatly influenced by the material composition. For example, pure silica oxide has a working point of around 1710 degrees; whereas the addition of alkali will reduce this to around 1300-1600 degrees. (Haldiman, 2008) Commercial glass generally can be subdivided in six categories, based on their material composition. (Corning, 2011; Oikonomopoulou, 2018)

Soda-lime glass

By far the most commonly produced and cheapest type of glass. Due to its composition, it has a low working temperature, which reduces manufacturing costs, while still being durable. Downsides of this material is limited resistance to high temperatures, and vulnerability to sudden temperature changes due to thermal shock.

Borosilicate glass

The addition of at least 5% boron oxide gives this glass a low thermal expansion rate, which makes it more resilient to thermal shock. In addition, it means the glass can be formed with a shorter annealing time, which makes it attractive for large-scale cast glass. Lastly, it has good resistance against chemical corrosion. This material is moderately expensive, costing more than Soda-lime or Lead Silicate glass.

Lead Silicate glass

This glass has around 20% percentage of lead oxide added to it. This makes the material relatively soft, and gives it a low melting point. In addition, its high refractive index gives it an interesting visual brilliance. It is popular under glass artists as it is easier to grind and polish than other types of glass. It is the second cheapest glass available.

However, this glass is very vulnerable to thermal shock and high temperatures, and is

easily scrached.

Alluminosilicate

Glass containing aluminium oxide. Its properties are similar to Borosilicate glass; but with even higher resistance to high temperature, thermal shock and chemicals. In addition to this, it is also stronger than most other types of glass. Downsides of this glass is the high temperature needed for production, which complicates the production process and makes it expensive.

96% Silica and Fused-silica

These two types of glass contain little to no additives to reduce their melting temperature. This results in high performance glass with very high temperature shock resistance which can still be used in conditions of around 900 degrees. Due to this, very high temperatures are required to melt and fabricate the material. This limits the possible shapes it can be manufactured in, and makes these the most expensive glass compositions to produce. They are used in specialised circumstances, such as the windows of space vehicles.

Aluminosilicate	Approximate Composition
	57% SiO_2
	20.5% Al_2O_3
	12% MgO
	1% Na_2O
	5.5% CaO

Melting point: 1500-1600°C

Used for: Telephone screens, fibre glass, high-temperature thermometers

96% silica	Approximate Composition
	96% SiO_2
	3% B_2O_3

Fused-silica	Approximate Composition
	99.5% SiO_2

Melting point: >>2000°C

Used in: space vehicle windows, furnace windows

3.4 Casting glass

In principle, glass casting can be compared to the casting metal. It involves heating the material until it reaches a liquid state, before pouring it into a mould where the material takes the required shape. Afterwards, the material is allowed to cool down and solidify.

Despite the similarities, some additional complications arise in glass casting due to the unique properties of the material. In the following chapter the process of casting glass will be described.

Two types of glass casting can be distinguished, based on the initial state of the material. In primary casting, the raw ingredients for glass are heated to form new, liquid glass for casting. Secondary casting is a form of recycling, in which existing glass pieces are re-heated until liquid, and cast. (Oikonomopoulou, 2018) Secondary casting requires lower temperatures to work, however care needs to be taken that a single composition of glass is used, as mixing different types of glass will lead to internal stresses and likely failure after cooling (Cummings, 2001).

For both primary and secondary casting, different forming processes are suitable. (Fig. 8). Hot-pouring (or melt-quenching), is usually employed for primary casting. In this process, the glass is brought to its liquid working temperature, and then poured into a mould. The mould with the liquid glass is then placed in a secondary furnace, where the material can anneal.

For secondary casting, kiln-casting is used. Here, glass is placed in a hear resistant container (for example, a flower pot) and heated. As the glass becomes liquid, it flows out of the container, into the mould. The mould generally remains in the oven while annealing. (Oikonomopoulou, 2018)

Annealing is the gradual cooling of glass to avoid the forming of internal strain and stress. If left to cool down naturally, a solid glass element will quickly start solidifying on the outer layers, while remaining liquid inside. The difference of thermal expansion between these layers will create internal stresses, which will weaken the final object, or even cause outright failure due to the tension in the material. (Cummings, 2001).

After casting the glass is first rapidly cooled from the liquid working point to its softening point. This rapid cooling, or quenching, gives the molecules in the glass no time to arrange themselves into a crystalline structure, resulting in the amorphous structure described before.

Fig. 8 *Two methods of glass casting. Left, hot pouring, or melt-quenching. Pre-molten glass is taken out of a furnace (seen in the background) and poured into a mould. Right, kiln casting. Shown is the oven with the glass in ceramic pots and the moulds placed beneath. Heating the oven will cause the glass to melt and pour into the moulds.*

At this temperature, the glass is viscous enough to support its own weight, and can be removed from the mould if the geometry of the mould supports this. From here on, the material is further cooled down until right above the annealing point. This is the lowest temperature at which the material is still liquid enough for the internal stresses in the material to equalise and relax in a few minutes. The glass is kept at this temperature to give the residual internal stresses time to dissipate. Following this, the temperature of the annealing oven is slowly decreased, making sure the glass has time to cool evenly. This is done until it reaches the transition temperature. Below this temperature, internal stresses can no longer be relaxed, and the material can be considered solid. After this, the material can be left to cool down to ambient temperature quickly, taking into account that breakage due to thermal shock needs to be avoided. (Oikonomopoulou, 2017; Haldiman, 2008)

Annealing is a meticulous and often slow process, and is one of the largest limitations for large scale cast glass application. As the dimensions of the object increases, the required annealing time increases exponentially. In the Crystal Houses project, a solid 65 × 105 × 210 mm brick of soda-lime glass required an annealing cycle of about 8 hours. Doubling one of the dimensions, to 65 x 210 x 210 mm, increased the annealing time to approximately 36-38 hours. (Oikonomopoulou, 2017). On a more extreme scale, the largest solid cast glass telescope mirror, with a diameter of 2.5m and a mass of 20T took 12 months of gradual cooling, despite being made from the easier to anneal borosilicate glass (Zirker, 2005)

Determining the ideal required annealing time and oven heat flow for a model is complicated, as it is determined by a multitude of factors. Not only the model's shape and mass distribution, but also the amount of surface exposed to cooling, other thermal masses present in the oven and the properties of the oven itself, all influence the annealing cycle. (Oikonomopoulou, 2018). Though literature exists that attempts to precisely guide the annealing process, they often rely on unstated assumptions and specific circumstances that cannot be widely applied. (Watson, 1999,) Because of this, in practice the annealing schedule of cast glass is largely decided intuitively, based on previous experiences and observations. (Watson, 1999; Oikonomopoulou, 2017; Cummings, 2001)

3.5 Designing cast glass

The goal of annealing is a uniform cooling of the glass throughout the object, minimising temperature differences within the material. By taking the cooling behaviour into consideration during design, annealing times can be drastically reduced.

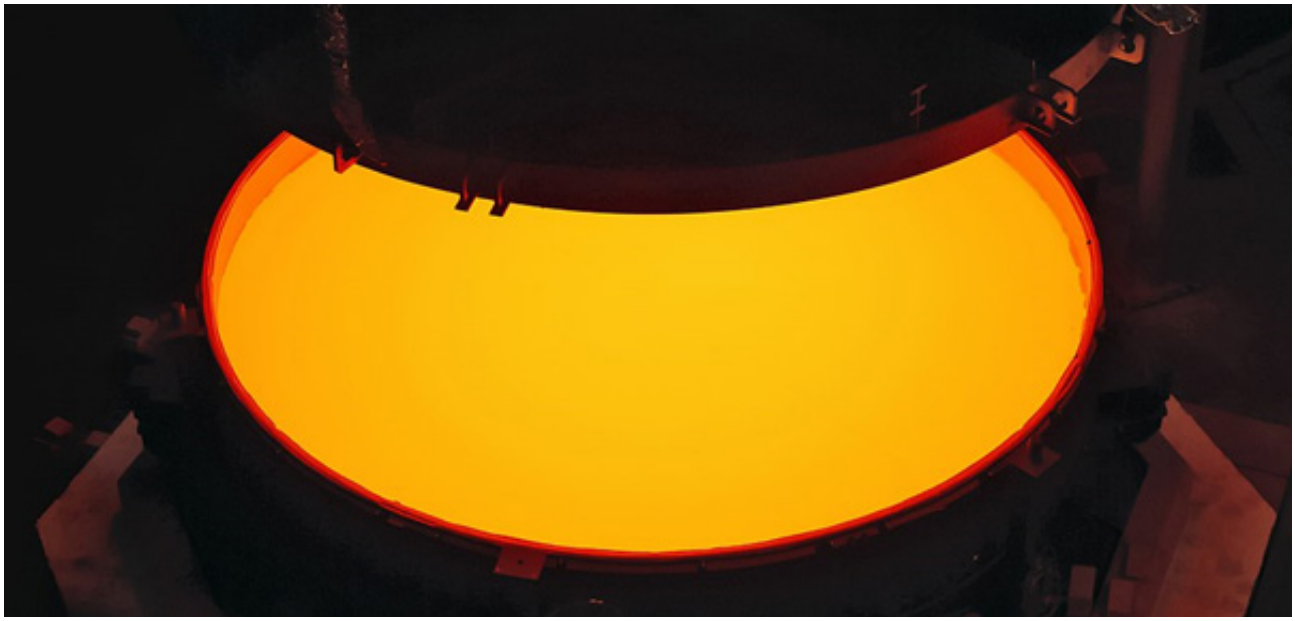

Fig. 9 *Annealing of a glass telescope lens*

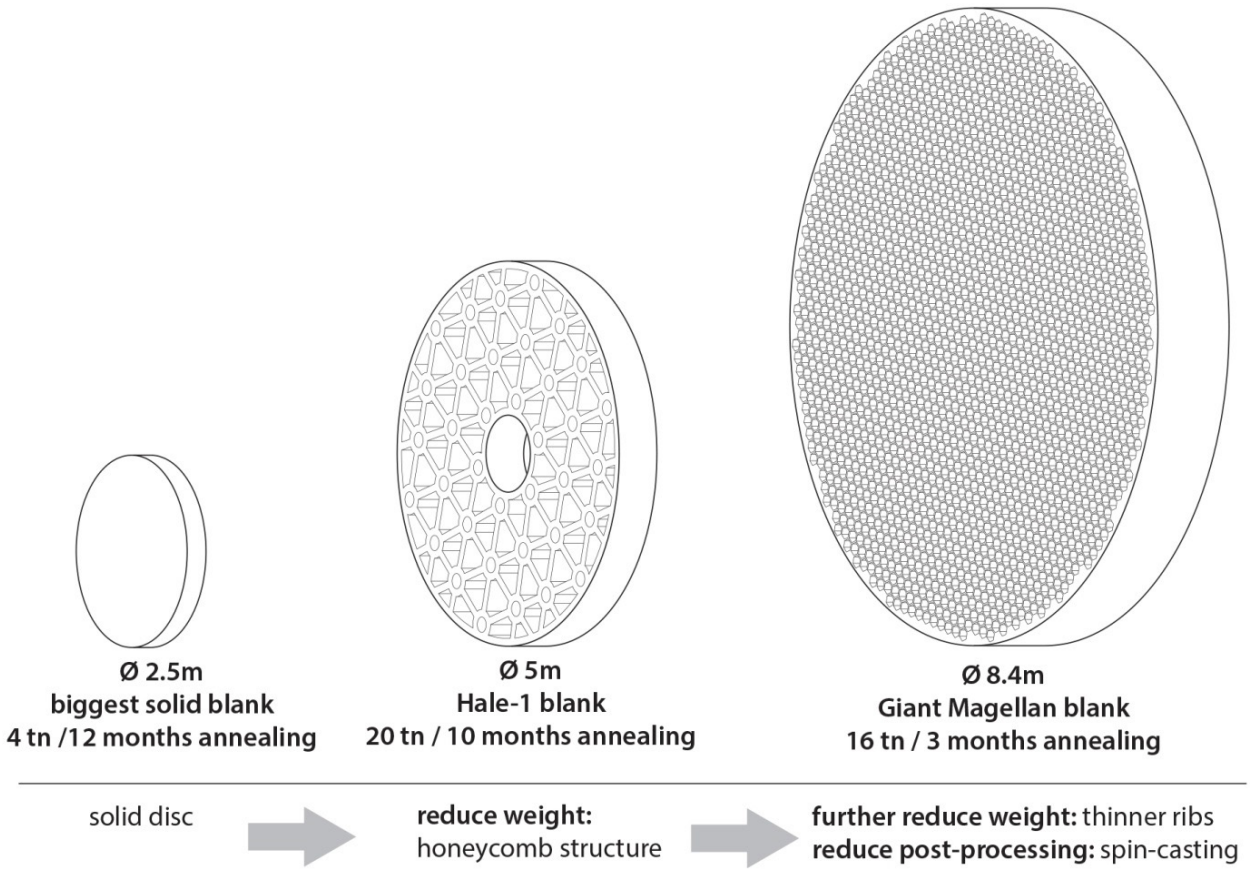

Fig. 10 *Evolution of cast glass telescope mirrors, with their annealing times. It can be seen that smart design allows for larger elements to be cast, in less time*

This has been most clearly demonstrated with large telescope mirrors described before. (Fig. 10) The largest solid cast telescope mirror, with a mass of 20T and a diameter of 2.5m, required 12 months of annealing. In contrast to this, the more recently produced Giant Maghellan telescope mirror has a larger diameter of 8 m, yet weighs only 12 tonnes. The mirror was partly hollow, using a honeycomb structure to reduce the lenses' mass (Fig. 12). Due to this, this larger mirror required only three months of annealing. (Zirker 2005)

Three basic principles of glass design exist that can help reduce annealing time (Fig. 11). Reducing the mass of the element will greatly shorten cooling times as there is simply less material to cool. In addition, large temperature differences within the material should be avoided. Sharp edges and corners sticking out of the object should be avoided, as these will cool much faster than the remaining object. More gradual, smoothed shapes are preferable. Large temperature differences can also be avoided by equalising the material distribution throughout the object. A cast

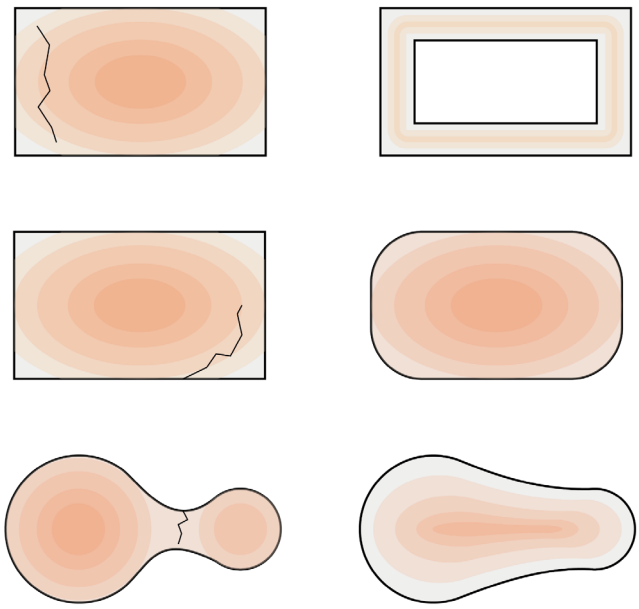

Fig. 11 *Three primary design principles to reduce annealing times of glass components. From top to bottom: Weight reduction, rounded shapes, equalised mass distribution*

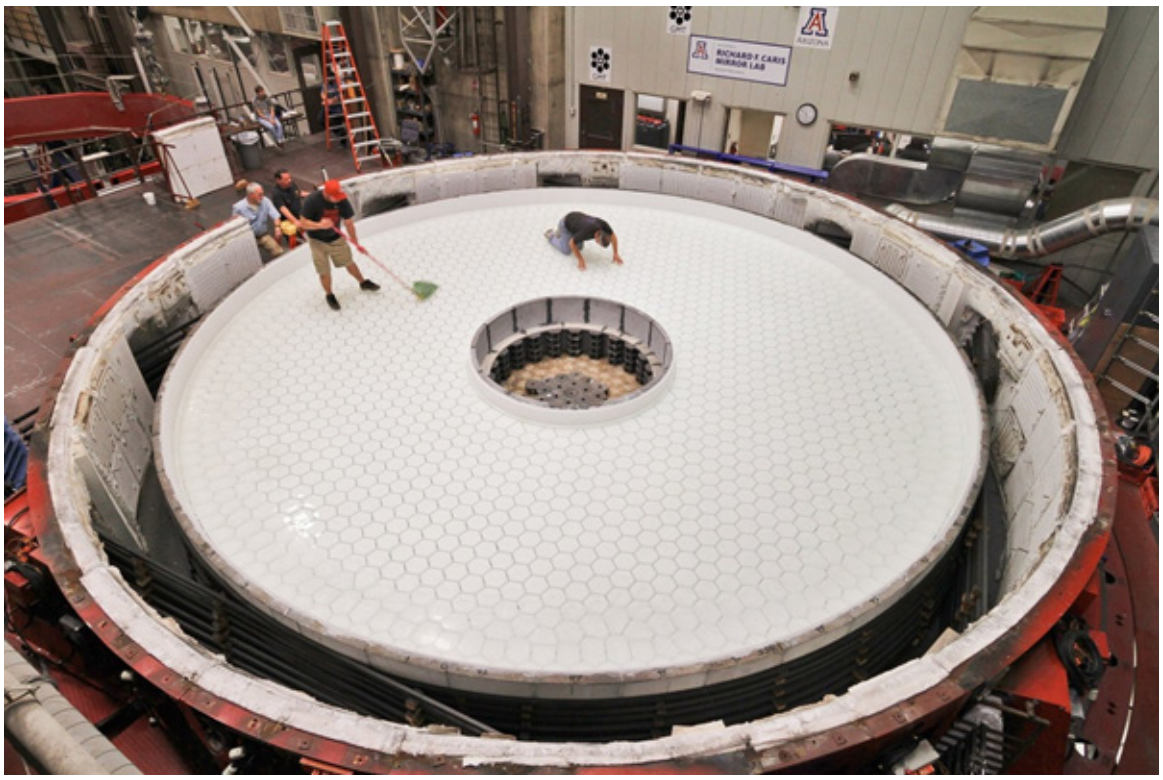

Fig. 12 *The Giant Maghellan telescope mirror being produced. The weight-reducing honeycomb mould structure can clearly be discerned.*

glass object should therefore be designed in a way that all parts are of comparable mass and thickness.

The limitations of the manufacturing process should also be taken into account when designing cast glass. The casting itself has relatively few limitations. Unlike for example concrete, there are no solid particles within the cast liquid that could lead to clogging, which means rather small element sizes can be achieved. Compared to molten metal, molten glass considerable more viscous, which means it will take longer to fill the entire mould. Examples from for example glass art have shown that even the slow-flowing, viscous glass can fill complexly shaped moulds if sufficient time at a high temperature is given for the glass to settle.

3.6 Moulds

It is important to choose the correct type of mould when casting glass. The available options mentioned here are described in (Oikonomopoulou, 2018).

Two categories of mould for glass are generally discerned: single-use disposable moulds, and reusable permanent moulds. The choice of mould is mainly dependent on the geometry of the cast object, the production volume needed, the required precision of the final object, and the type of glass used.

Different types of disposable moulds are available. Investment-cast silica plaster moulds are cheap to produce, and allow for easy demoulding as the material falls apart when submersed in water. However, they have a lower precision than other types of moulds, and can only be used for castings under 1200 degrees, limiting the types of glass that can be used. Higher precision is offered by CNC-milled moulds from alumina-silica fibre ceramic, while also withstanding higher temperatures of up to around 1650 degrees. This comes at a substantially higher cost.

Due to the contact of the glass to the mould, the glass produced by these disposable moulds will have a rough, translucent surface after demoulding. Additional grinding and polishing is needed to restore transparency and improve the accuracy if the object. Due to their brittle nature, temporary moulds are mostly used in kiln-casting, with the glass remaining within the mould during cooling and annealing.

As the disposable moulds are broken down after casting, it is possible to create complex geometries without being limited by mould disassembly. The investment-cast silica plaster moulds are most suitable for this, however production of these moulds is complex and labour intensive (Fig. 13) (Bristogianni et al., 2016). Disposable moulds are therefore most suitable when a small production volume of uniquely shaped objects is required.

Permanent moulds are used when high production volumes are needed, as the high production costs of these moulds make them uneconomical for small batches. Permanent moulds are often used in combination with the melt-quenching technique, which is more suitable for fast production.

Steel is often employed to create permanent moulds, either welded from multiple parts, or CNC-milled when high accuracy is required. These moulds can be either of a fixed shape, or can be adjusted to facilitate different shapes, at the cost of some precision. Steel moulds can be used up to around 1200-1260 degrees. For higher temperatures, CNC-milled graphite moulds are used, as no maximum temperature limit has been found for this material.

Both types of permanent moulds have high precision. Before use, a release coating needs to be applied and the moulds need to pre heated to avoid surface chilling of the glass. If this is done properly, little to no post processing is required after demoulding. The glass can usually be taken out of the mould after the glass has reached the softening point, but it can also be left in the mould during the entire annealing process to increase accuracy.

The complexity of objects cast in permanent moulds is limited, as the mould remains intact during demoulding. Multi-part moulds that can be disassembled to create more elaborate geometries are available, but are expensive and do not have the same flexibility that disposable moulds offer.

An alternative for conventional disposable moulds is the production of sand moulds using additive manufacturing. This method is already widely employed in the metal casting industry, and has proven to be suitable to produce complex geometries with high precision. (Niehe, 2017) The automated additive manufacturing allows for fast production at relative low cost, making it suitable for the production of individual, customised components.

This this moulding technique has not yet been applied for glass casting. Though the material can withstand high temperatures for a brief time, its behaviour when heated for an extended annealing cycle is not known. Removing the mould after casting is another potential challenge, as this needs to happen with care to not damage the glass. Finally, the surface properties of the glass in contact with the mould needs to be investigated. Despite this, it has the potential to revolutionise the way cast glass components are designed and produced.

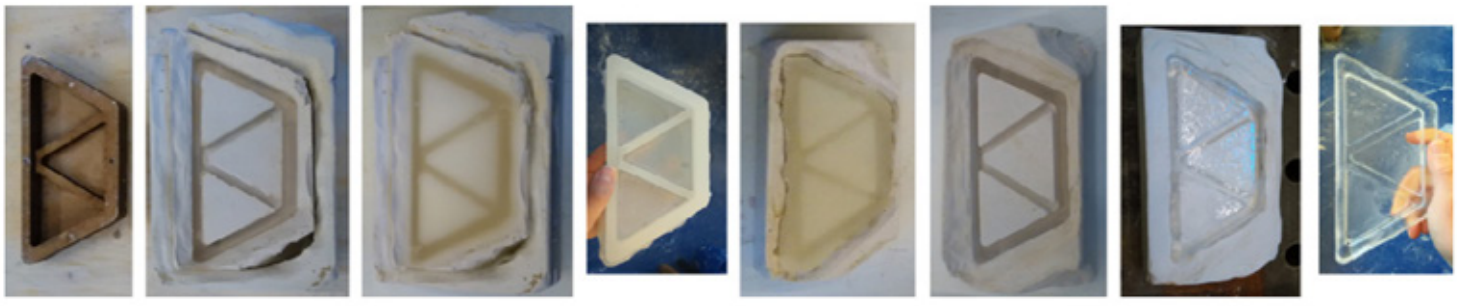

Fig. 13 *Disposable mould making process as documented by Bristogianni et al., 2016. The shape to be cast is first recreated in MDF (1). This is used to make a mould (2) that is used to make a wax representation of the cast object (3,4). The wax model is used for a new mould (5) from which the wax is removed using steam (6), leaving a mould suitable for glass casting (7,8). The first mould (2,3) is re-used, and is sometimes made from silicon to allow for more complicated shapes.*

3.7 Examples of cast glass architecture

Crystal Houses

Following a design of MVRDV, an Amsterdam storefront has been built partially using cast glass. In this project, cast glass bricks were used to create a transparent interpretation of a traditional Dutch façade of 10 x 12 m, which is fully self-supported. (MVRDV, 2016)

The 6500 bricks are adhesively connected. Finding a suitable glue proved challenging, as it needed to be not only strong and durable enough but also be colourless and have a refractive factor close to that of glass, to not interfere with the transparency of the façade. In the end, Delo Photobond 4468 was chosen, which is a UV-cured adhesive (Fig. 14). For this adhesive to form a proper bond, a thickness of between 0.2 and 0.3 mm was found to be optimal, with minimal deviation allowed.

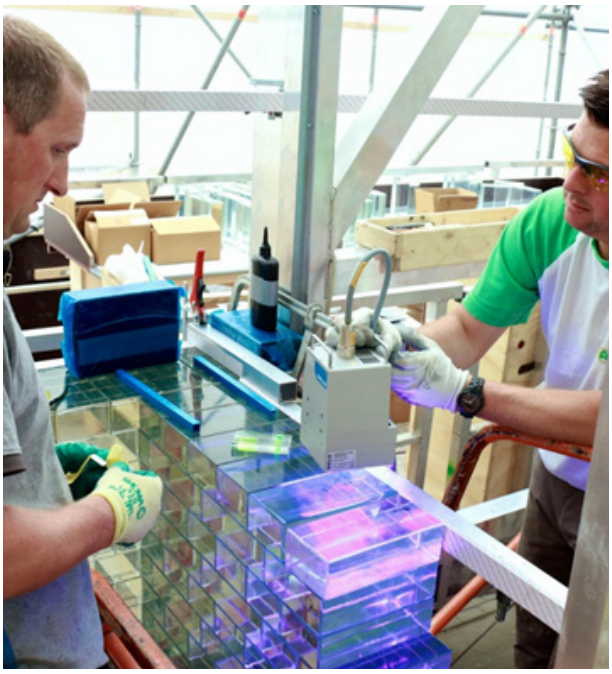

Fig. 14 *UV-curing the adhesive in the Crystal Houses project.*

Fig. 15 *The finished, part glass brick facade of the Crystal Houses*

The bricks were cast from Soda-lime glass, using the melt-quenching technique and high precision, milled steel moulds. Due to the very high precision dictated by the used adhesive, the bricks had to be additionally CNC milled in post-processing, which considerably increased production costs. (Oikonomopoulou et al., 2017)

Atocha Memorial

To commemorate the Madrid bombings of 2004, a monument was erected close to the site of the attack. At the centre of the monument stands a tower made from structural cast-glass bricks (Fig. 17). The tower is 11 m high and has a near-oval floor plan of 8 x 11 m. The tower is covered by a laminated-glass roof.

The solid cast bricks measure 200 x 300 x 70 mm, and weigh 8.4 kg each. The bricks have opposed concave and convex geometry, which allows the irregular shape to be built using one type of brick (Fig. 16). The bricks were pressure cast, using borosilicate glass to reduce the annealing time. For assembly a UV-curing acrylic adhesive, developed specially for this project, was used. To ensure that the adhesive layer would have a proper thickness, a 1 mm tolerance for the bricks was used. After assembly, the brick seams on the outside were sealed using an ultra-transparent acid silicone. This was done to protect the adhesive and ensure a water tight structure. (Göppert et al., 2008)

Fig. 16 *The brick design used for the Atocha Memorial*

Fig. 17 *The Atocha Memorial*

3.8 Additive manufacturing of glass

An alternative for the casting of glass is producing objects by additive manufacturing. Research on this has mainly been performed on small applications of glass for use in medical or optical equipment (Luo et al., 2014; Witzendorf et al., 2018). Glass additive manufacturing on a scale with potential in the build environment has been explored extensively by Klein, 2015 (Fig. 18). Here, a process was used comparable to the 3d-printing of polymers. It involves heating the glass beyond its softening point, after which the liquid glass is printed into an annealing oven, using a CNC-controlled nozzle. The oven is kept right above the annealing point during the printing, to ensure each new layer of glass properly fuses with the underlying layers. Once the print is completed, the temperature is carefully lowered in a regular annealing procedure. Subsequent testing showed that this results in negligible internal stress. A simpler setup was tested in which the glass was deposited outside the oven, at ambient temperature, but this was found to result in internal stresses between the deposited layers. Even after the sample was reheated and annealed, these stresses could not be fully removed.

Compared to regular casting, the current additive manufacturing process takes considerably longer to produce an object of similar shape. However, this is offset by the fact that no mould needs to be made. This simplifies the production process considerably, and could make the overall process faster, cheaper and more flexible.

A large drawback of glass additive manufacturing is the need to keep the material at the annealing temperature during the printing process. This limits the dimensions of the object that can be printed. As the material remains in a somewhat liquid state, the increasing weight of the model during printing can lead to the lowest layers to be deformed, leading to inaccuracies and deformation of the model. Furthermore, the inclusion of an annealing oven in the printer greatly complicates the equipment setup. Due to these limitations, so far the model size has been limited to 300 x 300 x 250 mm.

Furthermore, currently only single layer, hollow samples have been produced. It is so far unclear how solid elements produced with this technique would perform structurally.

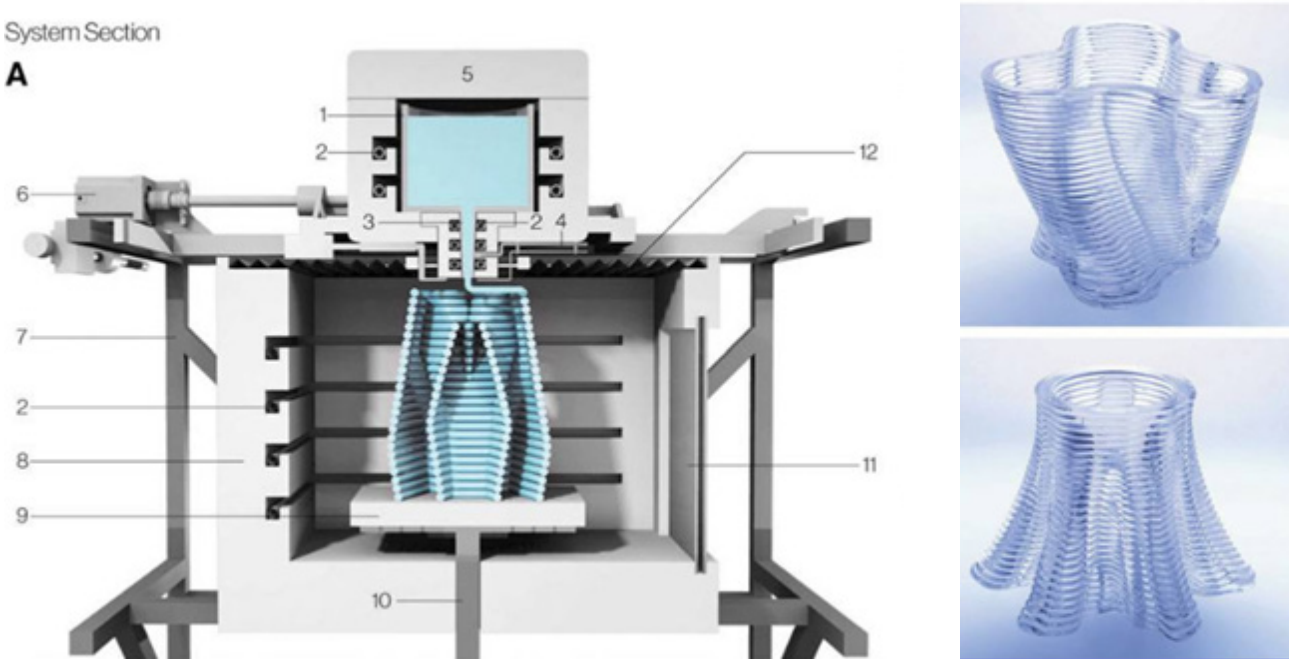

Fig. 18 *Additive manufacturing of glass, as shown by Klein, 2015. Left, a section of the machine setup is shown. A reservoir containing molten glass (1-5) is mounted on a CNC frame (6,7) and deposits material into an annealing oven (8-12). Right, some of the produced elements are shown.*

3.9 Summary

In structural applications, glass is still mainly considered as a two-dimensional material. In comparison, casting glass makes it possible to create solid, three-dimensional and self-supporting structures. Structurally, glass is a brittle material. Though its theoretical yield strength is exceptionally high, in practice these values are never reached as any surface imperfections lead to highly reduced tensile strength. This dependence on geometrical imperfections makes it hard to reliably predict the failure behaviour of the material. Though glass is highly resistant against compressive stress, under compression it often shatter due to tensile stresses appearing under deformation. Furthermore, glass cannot flow under heavy loading, which means the material is unable to dissipate local stress concentrations by deforming.

Out of the six compositions of glass available commercially, two are most suitable for structural cast glass manufacturing. Soda-lime glass is cheap, and has acceptable structural and thermal properties while it can be worked at a relatively low temperature. Borosilicate glass is more expensive and requires higher temperatures to be cast, but offers more stable thermal behaviour, allowing faster production due to its improved annealing rate. Aluminosilicate has good structural and thermal properties, but the high temperatures needed to work it make it generally too expensive to use.

When casting glass, proper attention need to be paid to the annealing procedure. Too slow cooling can lead to crystallisation, whereas too fast cooling will lead to internal stresses. Rounded shapes and an equal distribution of mass help homogeneous cooling and will reduce annealing time. For the casting, cheaper disposable moulds are more suitable for low production quantities and allowing more complex shapes, whereas more expensive re-usable moulds allow high volume production, usually of simple geometries. Additive manufacturing of glass is in its early stages, and is currently only possible at small dimensions.


ROCK
SHOX

4. Topology Optimisation

4.1 Structural optimisation

Structural optimisation is a process that seeks to create a structure that is the most optimal while satisfying a given set of constraints, such as a set amount of material. It is becoming increasingly relevant due to an ever greater demand for lightweight, low-cost and high-performance structures due limited material resources, environmental impact and technological competition. (Huang, Xie, 2010)

Usually, structural optimisation aims to minimise or maximise a certain physical property of the model. This could for example include minimising local displacement, minimising stresses or maximising stiffness, all dependant on the load case applied. Other, less load dependant goals might include minimising volume, general dimensions or weight. The optimisation calculation itself is done while adhering to one or more predetermined constraints, which can be some the properties mentioned before.

Mathematically, this can be expressed as follows:

$$min_x f(x)$$

$$subject\ to:$$
$$g(x) < c$$
$$x_i \in \varphi$$
$$equilibrium\ condition$$

With f(x) being the function that is being minimised, g(x) the response that is being limited by one or more constraints c and $x_i = (x_1, x_2, \dots, x_n)$ the variables that are changed, within a range of φ. This is an iterative process, in which each step has to satisfy the equilibrium conditions. (Lundgren, Palmqvist, 2012)

Generally, three methods of structural optimisation are distinguished, these being sizing, shape and topology optimisation (Fig. 19) (Bendsoe & Sigmund, 2003).

Size optimisation is the simplest method and involves the dimensioning of elements within a structure; for example picking the optimal cross section for a beam within a truss, based on the forces acting on this beam. Characteristic of this method is that the domain of the design model is set beforehand, and remain unchanged during the optimisation. In contrast to this, shape optimisation involves changing the boundary of the design to improve structural performance; the domain itself has become a parameter. It is limited to changing the outlines of the existing boundaries, the topology remains unchanged. Topology optimisation takes this one step further, as it does allow changes to the topological layout of the geometry. For a solid shape this means new holes will appear where material is not needed, whereas for frame-like structure the connectivity and number of elements can be changed.

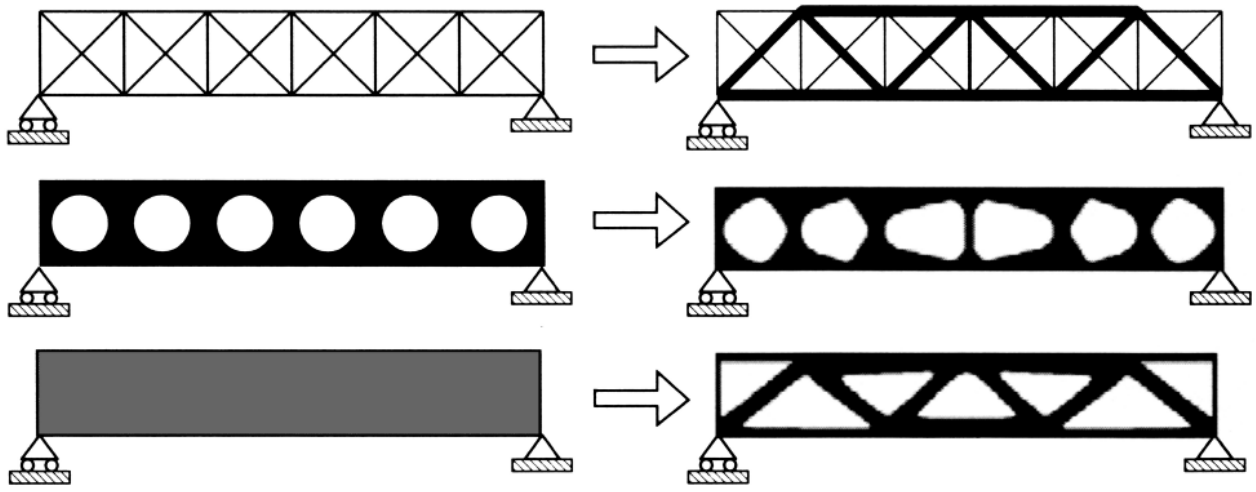

Fig. 19 *Three methods of structural optimisation. Top: Size optimisation, middle: Shape optimisation, Bottom: Topology optimisation. Bensoe and Sigmund, 2003.*

4.2 Topology optimisation methods

Topology optimisation is the process of determining where material needs to be placed within a design domain to most efficiently reach a set objective, within a series of constraints. Different ways of carrying out topology optimisation have been developed. The following four methods can be discerned: (Lundgren, Palmqvist, 2012).

- Homogenisation method
- Solid Isotropic Microstructure with Penalisation, SIMP
- (Bi-directional) Evolutionary Structural Optimisation, (B)ESO
- Level set method

Homogenisation method

The homogenisation method rebuilds the design geometry into a linear elastic structure by inserting a great number of micro-scale voids. By varying the size of these voids, an object with varying material densities can be simulated. By finding the most suitable density of the material within the design domain, the shape can be optimised. Elements that are found to be all solid are filled in with material, elements that consist of only voids are removed from the design area. Elements that are partly, but not fully void are expressed as an intermediate material. From a fabrication point of view, this intermediate material is difficult to translate to physical structure. To reduce the amount of this material in the final solution, it can be artificially weakened in comparison to solid material (Fig. 20) (Suzuki, K., Kikuchi, N., 1991; Lundgren, Palmqvist, 2012).

Solid Isotropic Microstructure with Penalisation, SIMP

In SIMP, a pseudo material density is used as the design variable for the optimisation. This density lies between 0, 1 ($x \in [0, 1]$) and represents the stiffness of each element. An element with a density of 0 is removed from the physical model, and is represented in white, whereas an element with maximised density 1 is shown in black. Values in between are indicated in shades of grey (Fig. 21).

From an engineering point of view, the final result should be a fully black and white solution. A penalisation factor is therefore employed, to

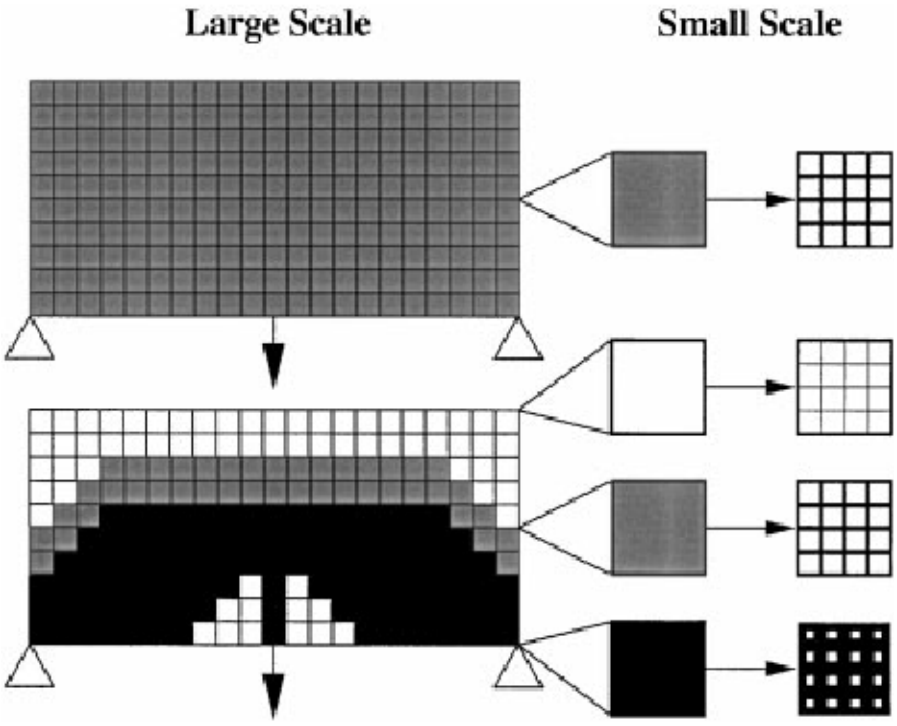

Fig. 20 *Homogenisation Topology Optimisation. Top: initial state with homogeneous micro voids. Bottom: optimised state with solid (black), void (white) and intermediate (grey) material distribution.*

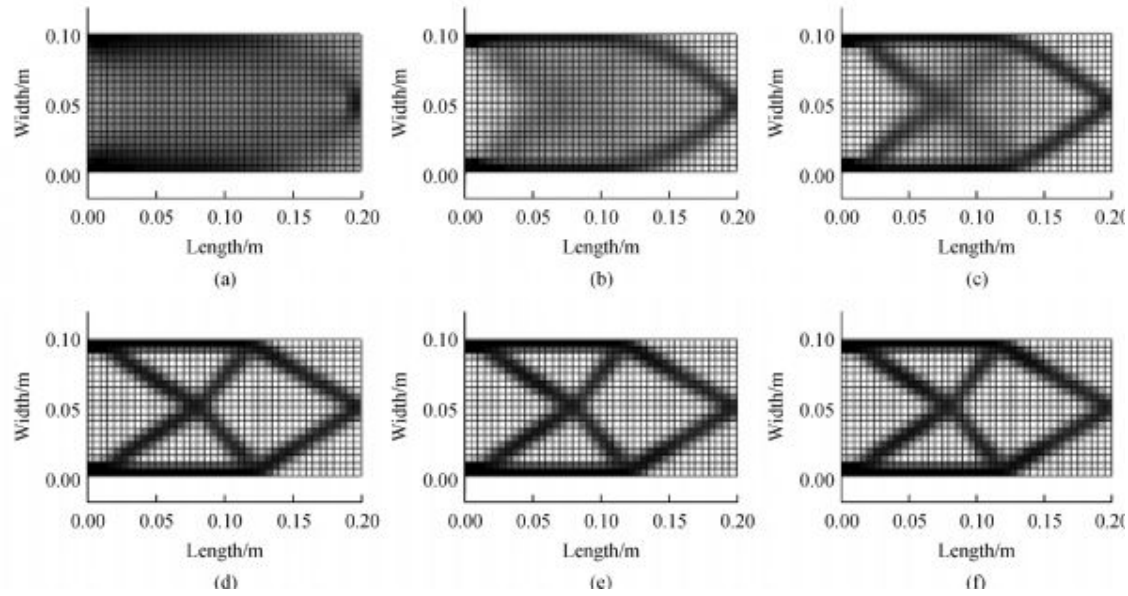

Fig. 21 *.SIMP Topology Optimisation process over multiple iterations. Top left to bottom right: material density is lowered from fully solid (black) to semi-solid (grey) or void (white). The bottom three pictures show how the penalisation factor pushes the structure to a fully black-and-white result.*

discourage the appearance of grey material in the resulting model. The element properties in the SIMP-model can be expressed with the following expression (Bendsø and Sigmund, 2003):

$$E_{ijkl}(x) = x^p E^0_{ijkl}, \qquad p > 1$$

With E^0_{ijkl} the material property of the material, usually the stiffness and x the design variable. p is the penalisation factor for intermediate grey values, with p > 1 indicating increasing amounts of penalisation. Usually, p ≥ 3 is required for a discrete black-and-white solution. However, occasionally the intermediate values are so efficient that, despite the penalisation, some grey elements will remain in the final model. (Lundgren, Palmqvist, 2012)

(Bi-directional) Evolutionary Structural Optimisation, (B)ESO

ESO uses the principle that a structure will evolve to a more optimised shape if the least contributing elements are removed in each iteration. This optimisation can be based on either stress level or stiffness and displacement.

For stress, the stress level of each element is compared to the maximum stress level in the model. The elements are removed when the ratio between these values is below a certain pre-set rejection ratio. This is repeated until a steady state is found in which no more elements can be removed. Though this leads to structurally feasible results, it can lead to structures with sub-optimal stiffness. To overcome this, an ESO method using stiffness has been developed. Here, the influence of each element on the overall stiffness is measured. Elements with the least element strain are discarded from the geometry.

ESO makes use of a so-called 'hard-kill' method, which means that based on the performance of each element, this element is either kept, or removed. This means no intermediate, or grey elements can appear, removing the need for penalisation. However, it is a one-way process: no new elements can be added, nor can removed elements be restored. (Lundgren, Palmqvist, 2012)

An addition to this is the Bi-directional ESO method, or BESO (Fig. 22). Here, material can be both removed and added based on the performance of each element. Using Finite Element Analysis, each element is assigned a sensitivity number, indicating the contribution of the elements in the current structure. The surrounding voids are also

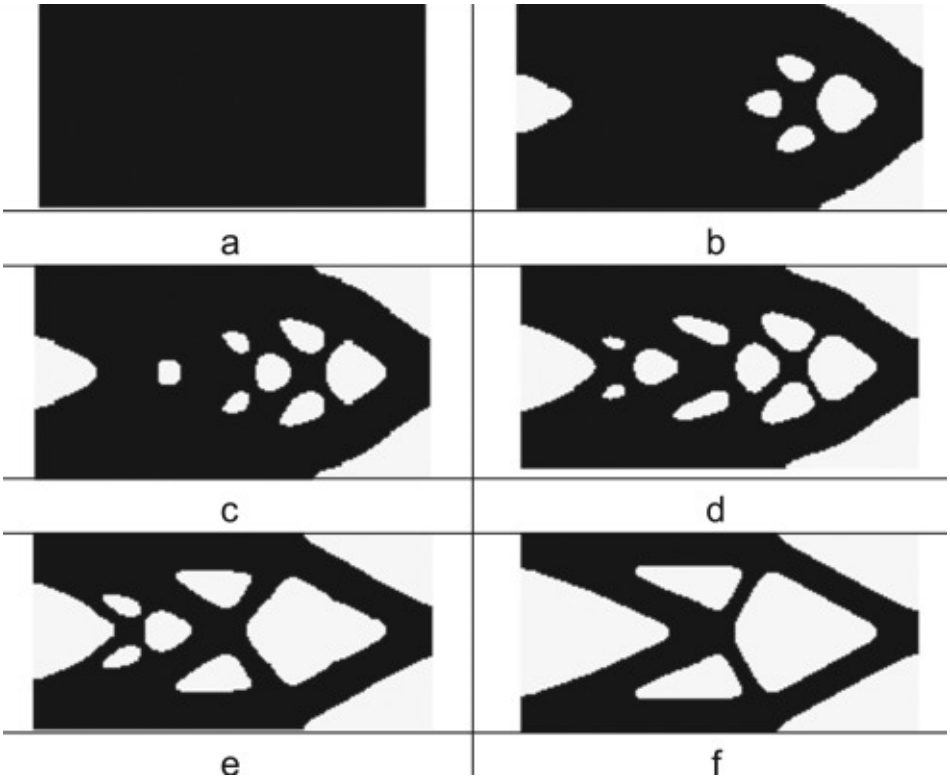

Fig. 22 *BESO topology optimisation. From top-left to bottom right, the removal of material in each iteration can be observed.*

assigned a sensitivity number, based on linear extrapolation of the FEA results. Based on a pre-determined rejection ratio and inclusion ratio, solid elements with the lowest sensitivities are removed, and voids with the highest sensitivity ratios are filled. These ratios need to be chosen with care, otherwise it is possible that the algorithm will not find an optimal solution. (Huang, Xie, 2010)

The advantage of ESO over the SIMP and the homogenisation method is the lack of

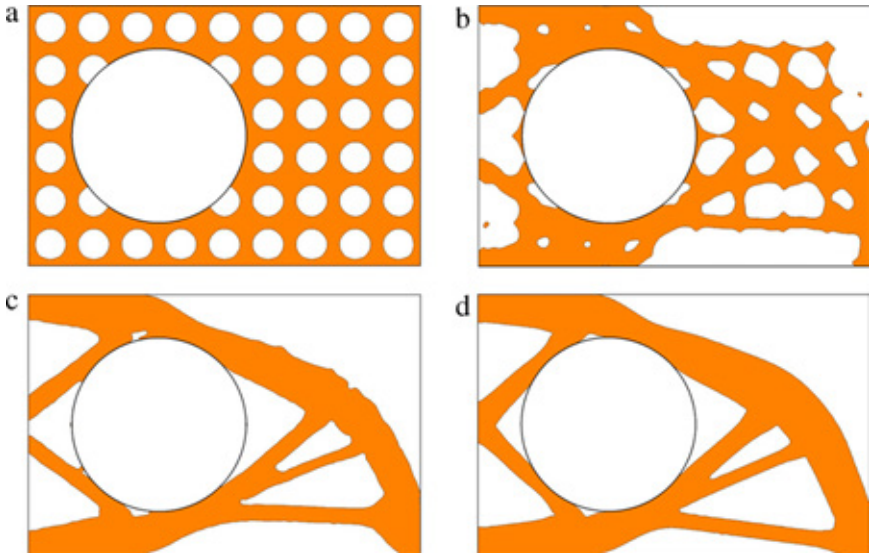

Fig. 23 *Level Set topology optimisation. Top-left, the initial state with the pre-placed voids is shown. In the following steps, it can be seen how the void boundaries are moved, and holes start merging and disappearing. In the final result, the original voids can no longer be discerned.*

intermediate grey zones, which is preferred from an engineering point of view. However, it has been criticized for being less efficient, requiring considerably more iterations to converge, compared to other methods. ESO also has the risk of not reaching a globally optimal structure, but stopping at a local optimum. (Rozvany, 2008). BESO greatly improves on these factors, but the risk of a globally sub-optimal result remains. (Lundgren, Palmqvist, 2012)

Level set method

The level set method can be characterised by the iterative moving of boundaries in the design domain. The initial structure is designed to have a series of arbitrarily placed voids in it. Dependant on the stresses at the boundaries of the material, material is either subtracted or added with each iteration. Material is added if the stress is above a certain percentage of the maximal initial stress; or subtracted if the stress is under this value (Fig. 23).

During this process, the holes that were initially placed at the wrong places will gradually shift to more optimal locations. Holes may fuse together or disappear altogether. Placing more voids in the initial geometry does not noticeably affect the final shape, but does decrease the amount of iteration needed to come to a stable end result. (Wang, Wang, Guo, 2003)

4.3 Glass topology optimisation

Though topology optimisation has been available for some years, its application so far has been mostly for ductile materials, such as steel or plastics. Research on the optimisation of brittle materials has been done, but has mostly been limited to concrete design. Glass topology optimisation is therefore a novelty. Some complications arise when trying to use topology optimisation on brittle glass.

TO is often based on minimising Von Mises stresses. Von Mises stresses are generally used for FEA analysis, as it simplifies the results to a single critical value per element. This makes it attractive for complex processes such as TO. However, Mises stresses is in essence a failure criterion for ductile materials such as steel, which display similar properties under both compression and tension. Brittle materials such as glass on the other hand have a tensile strength that is considerably lower than their compressive strength. For these materials, principle stresses should be used to check structural performance, as this allows to locate critical tensile stresses.

Ideally, a principle-stress based topology optimisation methodology that supports different goals for tension and compression stresses should be used. However, whereas Mises stress gives a single stress value per element; principle stresses are dependent on the reference plane of the element, which is difficult to reliably determine in a changing design object such as found in TO. This makes it considerably harder for the optimisation to converge to a final result. Principle-stress based TO has been achieved in academic research considering 2D assignments (Guan et al. 1999; Cai & Shi, 2010; Jewett & Carstensen, 2019); however is yet to be implemented in commercially available software packages (Fig. 24).

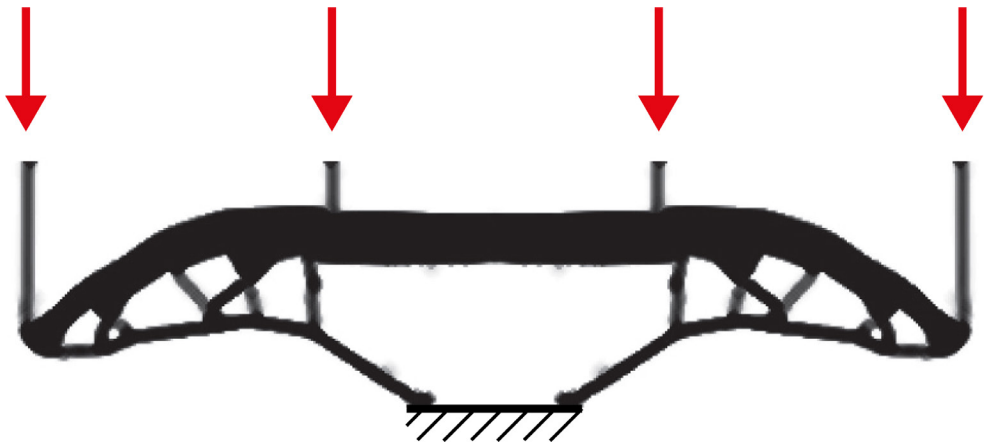

Fig. 24 *Stress based optimisation by Jackson & Carstensen, 2019. The difference between the thicker tension-loaded elements, and the thinner comression loaded elements can be clearly discerned*

A variation of this principle-stress based optimisation that is of potential interest for glass structures is multi-material optimisation. In this methodology, two different materials are placed to carry respectively tensile and compressive forces. This can be used for a hybrid structure combining a brittle material such as glass with for example steel in a way that ensures that little to no tensile stresses will occur in the glass. However, joining the two materials can still pose a challenge in practice. This methodology has so far only been developed for 2D designs. (Gaynor et al., 2013)

For topology optimisation of brittle materials, using a strain-optimisation goal is expected to lead to more reliable results. In post-processing, the basic geometry found has to be further analysed to check the principle stresses and locate possible peak stresses. Based on these findings, it can then be decided to change the parameters of the optimisation, or to manually modify the geometry to reduce stresses. (Dimitris Vitalis from ARUP, in personal correspondence).

4.4 Examples of TO design

Light Rider

An area of design in which topology optimisation in combination with additive manufacturing has already been widely utilised is the aircraft industry. When designing airplanes, safely reducing weight is of utmost importance as this decreases fuel consumption, which reduces emissions and lowers costs. For this purpose, in 2013 Airbus founded APworks, a subsidiary focused on exploring the possibilities of AM and TO. To showcase these innovations, an electric motorbike featuring a topology optimised frame was designed and build (Fig. 25). Optistruct software from Altair was used to generate the structural topology, which was then manually reworked for production. The frame was then laser-sintered from Scalmalloy, a high-performance aluminium alloy developed by airbus.

APworks reports the resulting bike weighing 35 kg, of which the frame is 6 kg. This is a weight reduction of 30% for the complete bike, compared to the bike with a conventional frame; without a reduction of strength of stiffness. (Weaver, T., September 2016)

Fig. 26 *Detail of the APWorks Light Rider*

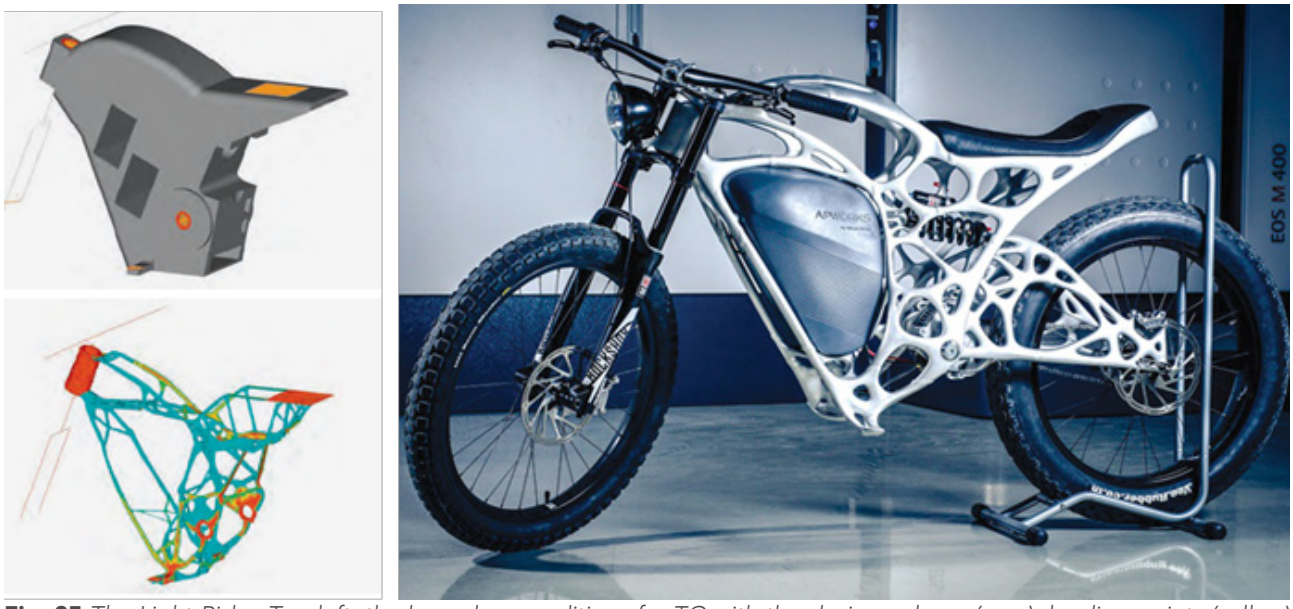

Fig. 25 *The Light Rider. Top-left: the boundary conditions for TO,with the design volume (grey), loading points (yellow) and voids. Bottom-left: the approximate material distribution given by Optistruct*

Fig. 27 *ETH Zurich TO designed concrete slabs. Left, the slab that was calculated using the free Millipede software to be supported on three points. On the right, the slab calculated using professional ABAQUS software, to be supported at the four corners.*

Concrete slab ETH Zurich

In their research on construction automatization, the department of Digital Building Technologies at the ETH Zurich have created a series of topologically optimised concrete slab structures (Fig. 27). The goal of the project was to show that large-scale elements for the building industry can be fabricated using additive manufacturing. A topologically optimised structure was chosen, as the complex geometries generated using this methodology often cannot be directly manufactured using production processes such as CNC milling or conventional casting. The slabs were produced using additively manufactured sand moulds and cast concrete.

Two slabs have been designed using two different TO applications. The first slab was optimised using Millipede, a free plug-in for McNeal Rhinoceros and the parametric Grasshopper software (Fig. 28). For the second slab the SIMP topology algorithm of Simulia ABAQUS was used, a more robust commercial application.

After the topology optimisation, the slabs were refined for production. This involved removing elements that were too fine for sand 3d-printing or too narrow for concrete flow, smoothing the surface and removing artefacts from the topology optimisation. For casting a special concrete mix, containing 2.75 vol. % steel fibres 10 mm long and 0.16 mm in diameter was used. The fibres act as reinforcement, and makes the concrete display isotropic behaviour; which is easier to model for TO. (Jipa et al., 2016)

The structural performance of the second slab was tested by applying a 2 500 kN/m2 distributed load, which proved the validity of the TO process. An average concrete thickness of 30 mm was realised, which indicates that weight reductions of up to 70% might be achievable.

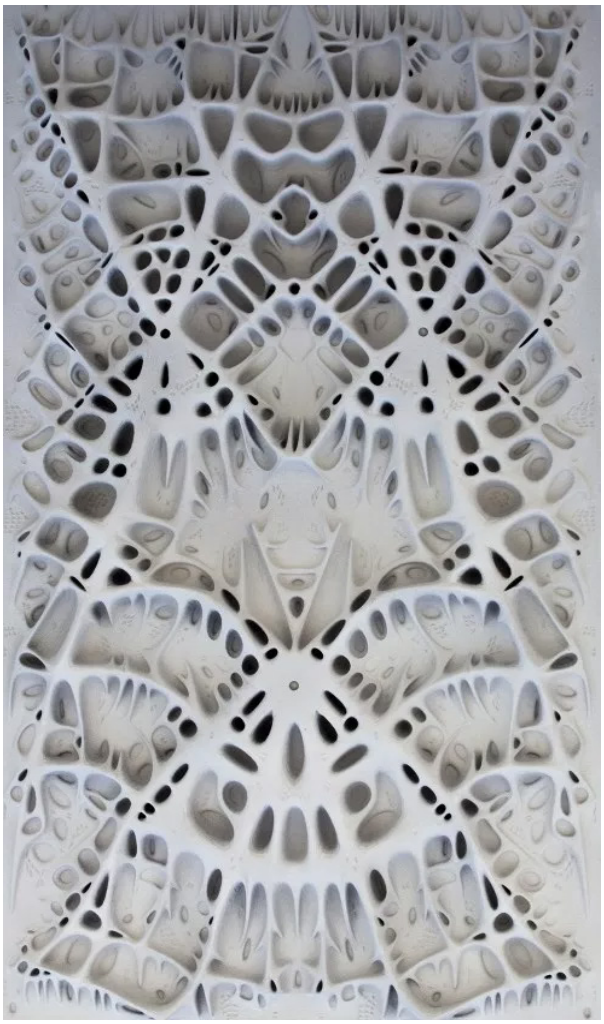

Fig. 28 *Concrete slab designed using Millipede*

Autodesk/JPL interplanetary lander

To show the potential of their Generative Design software (Autodesk, 2019), Autodesk collaborated with the NASA Jet Propulsion Lab to design and fabricate an interplanetary lander module. The task of this module is to safely carry scientific equipment down to the surface of extra-terrestrial landscapes. For space travel, reducing weight is of high importance as every reduction in weight causes a significant reduction of fuel required to launch the object into space.

At its core, the Generative Design software uses a Level Set topology optimisation algorithm for form finding. In addition to structural optimisation, the software takes into account fabrication limitations of the chosen material. To display this, the final prototype consists of elements fabricated using various tools. This includes a main body that has been cast in a 3d-printed sand mould, optimised legs that were CNC-milled and additional components that were directly 3d-printed in metal (Fig. 29). The final design was found to be around 35% lighter than a conventional design.

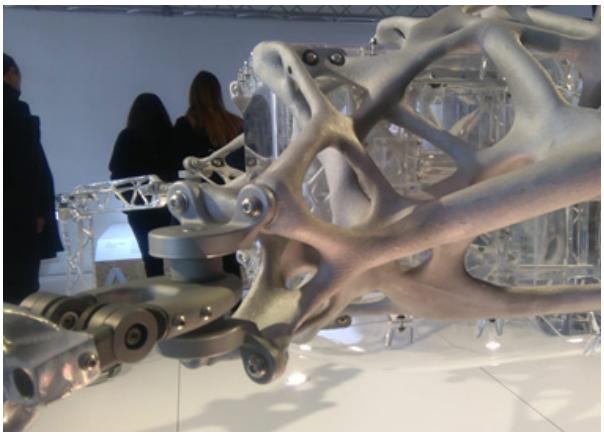

Fig. 30 *a close-up of the sand-mould cast frame and connections*

4.5 Available software

Some available TO software programs will be discussed here. Especially in recent years, a large variety of programs capable of performing TO have become available. Five programs that are freely usable with an academic licence are compared.

Millipede

This is a plug-in for Rhino Grasshopper used for structural analysis and topology optimisation. (Sawapan, 2018). It uses a structural analysis algorithm for linear elastic systems and performs TO using the

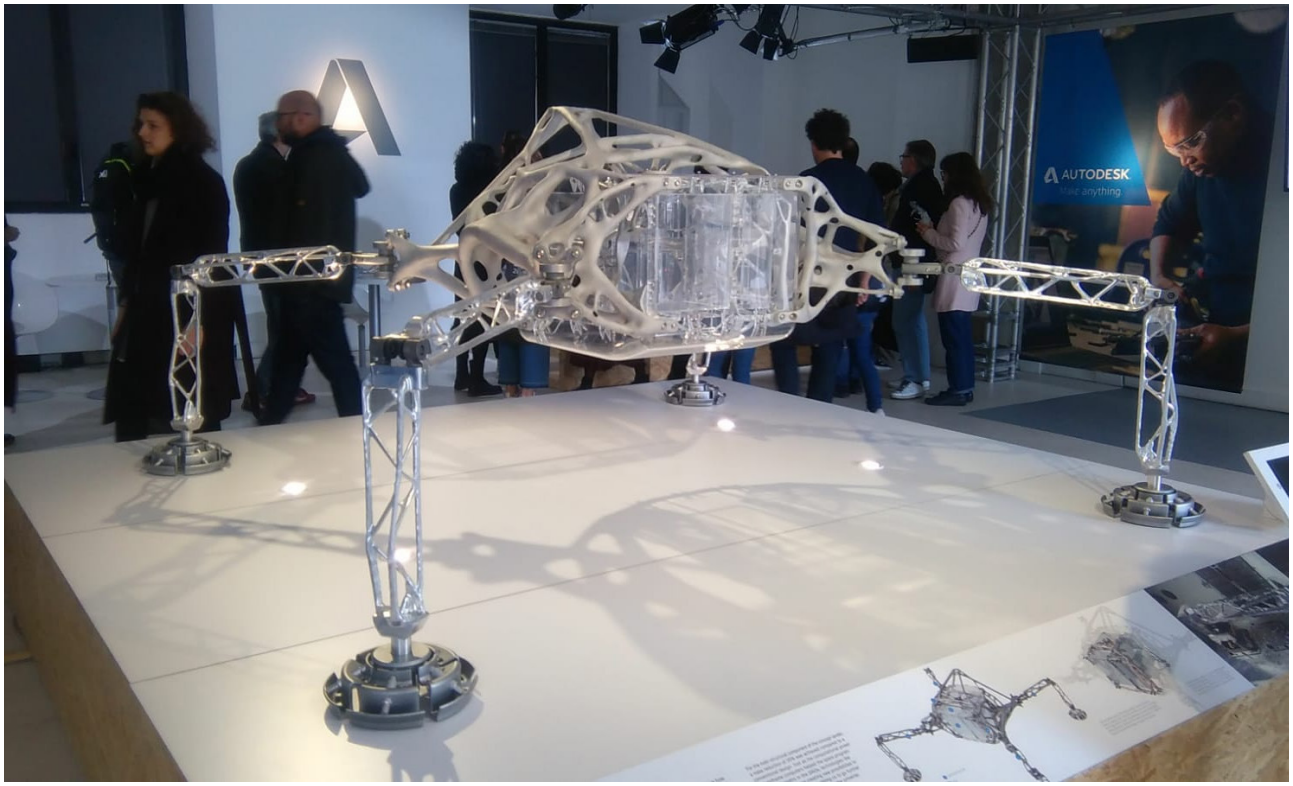

Fig. 29 *Autodesk/JPL planetary lander.*

homogenisation method. It provides fast results, which for example allows it to be used in combination with evolutionary optimisation algorithm plug-ins such as Galapagos for Grasshopper. A desired density for the final object is given as a goal, which the solver will try to achieve within the provided design volume. This plug in is relatively easy to set up and use, and gives fast results. As a drawback, the options provided are somewhat limited. As mentioned in the previous section, this plugin was used by ETH Zurich for the optimisation of a concrete slab.

Ameba

Formerly known as BESO3D, this program was developed by researchers of RMIT Australia. It is a plug-in for Grasshopper, which uses the BESO method for topology optimisation. Ameba can be set to minimise either displacement or Mises stress while moving to a set volume reduction. Additionally, the Young's modulus and Poisson ratio of the used material can be set.

An interesting property of Ameba is that its calculations are performed online using cloud computing. A mesh file can be generated offline, which can then be sent to one of the two servers used by Ameba. This gives the user access to extensive calculating power, allowing for faster calculation times. In addition, Ameba has integrated re-meshing and mesh smoothing components.

ANSYS

ANSYS is a software suite that offers software for many areas of engineering and building physics. It has an extensive structural design and analysis package which includes TO, using the SIMP methodology. As a standalone commercial program, ANSYS TO offers detailed control of material properties, optimisation goals and constraints. Furthermore, manufacturing constraints, such as limits to the member size, can be included in the optimisation.

Besides this, ANSYS offers extensive and proven structural FEA software, that can easily be transferred from the TO process. Finally, ANSYS Spaceclaim offers an extensive geometry modelling and post-processing tool that is integrated in the FEA workflow.

Autodesk Fusion 360

The Autodesk Fusion 360 software package combines multiple existing Autodesk programs into a single CAD program. Amongst the different functionalities is a SIMP-based topology optimisation and FEA tool, formerly known as NASTRAN In-CAD. This TO tool supports both stress and compliance-based optimisation. The FEA tool linked to it has an extensive material library, and allows for custom materials to be defined. Autodesk offers cloud computing to perform the TO calculation. (Autodesk, n.d.)

In addition, the Autodesk ReCap software allows for easy post-processing of topology optimised meshes and supports quad mesh modeling, which can be brought back into Fusion360 for editing using T-splines. This modelling method is very suited for digital sculpting of rounded organic shapes, making it a strong tool to supplement TO.

Autodesk Generative Design

The Generative Design software from Autodesk is a new tool aimed at simplifying design and engineering by using advanced computer programs and powerful cloud computing. Though at its core it includes level-set topology optimisation algorithms, this software uses a different approach compared to generic Topology Optimisation software. Instead of giving a single, optimal design within the given parameters, Generative Design creates a series of possible design solutions for the designer to choose from. It also can take into account a much wider range of design criteria, such as cost and production time. The solutions proposed by the system include for example suggested materials (taking into account manufacturing limitations), and can give estimations on weight, structural behaviour, cost and production time. It then lets the designer choose the preferred design, picking between for example a cheaper or lighter variation of the design.

By integrating design constraints such as fabrication into the design process from the start, Generative Design aims at avoiding the iterative back-and-forth workflow that is currently often seen between designer, manufacturer and client, accelerating the design process. (Harvard Business Review, 2018)

4.6 Summary

Topology optimisation is a structural optimisation process that uses finite element methodology to determine an optimal material distribution within a given design volume to most efficiently reach a predetermined objective, within a series of limitations. Different approaches to tackle this challenge have been developed. The Homogenisation and SIMP methodologies work by applying material over a gradient, between solid and void. A form of penalisation is required to push the results to a solution containing only fully solid or void materials, which is suitable for fabrication. In contrast, the BESO and Level Set method function by adding and removing material based on structural performance, leaving only material that is needed to reach the set goals.

Topology optimisation is generally set to minimise either stresses, or mean compliance (ie. strain). Stress based topology optimisation will avoid yield stresses, however does not always result in sufficiently stiff structures. Additionally, this method is noticeably influenced by mesh density, reducing reliability. Finally, the commercially available stress based TO software utilises Mises stresses, which are unsuitable when brittle materials such as glass are considered. Principle stress based TO brings with it many complications, and has not been reliably implemented outside academic work. Strain based TO is generally more reliable, but does lead to increased peak stresses.

TO is a tool in the concept designing phase to assess optimal material distribution. Post-processing is usually required to remove flaws and artefacts, smooth out geometry to avoid stress peaks and optimise the geometry for fabrication. In practice, it is found that additive manufacturing is often used in combination with TO, as it has the freedom to fabricate the often highly complex geometries with relatively little effort needed.

5. Grid Shells

5.1 Shell theory

Grid shells are part of the family of lightweight structures. These structures can be described by a philosophy of economical load-bearing: material use is optimised by efficient use of shape. (Fritzsche, 2013). In the case of grid-shells, this allows for large spans being achieved with an open, lightweight and slender structure. These properties make it popular amongst architects.

Grid shells are closely linked to the structural principles of plane shells. A plane shell can be generalised as an isotropic homogenous plate. The dimensions of this plate are in two directions much larger than in the third, the thickness. A plate or shell can be defined by its middle plane, thickness and material properties. (Blauwendraad, Hoefakker, 2014)

A flat plate loaded in plane will experience normal stress along its x-axis and y-axis and shear stress perpendicular to these axes (Fig. 31, top). The behaviour of these membrane stresses are described by membrane theory. Once an out of plane load is applied, these membrane stresses are no longer sufficient; a bending moment will appear within the plate to transfer the load (Fig. 31, bottom). The analysis of this behaviour is called bending theory. Membrane theory combined with bending theory is the basis of shell theory.

By curving the flat plate, a three-dimensional shell is formed. Due to the curvature, this shell is able to withstand out-of-plane loading with in-plane membrane stresses. This makes for a thin, efficient structure, as a plate is more suitable for withstanding membrane stress than bending stresses. It is simply easier to bend a plate than to stretch it. (Williams, 2014)

Usually bending moments need to be introduced in some areas of the structure, as the shell is unable to achieve local equilibrium purely with membrane action. Localised concentrated loads, sudden changes in geometry or incompatible supports are some of the things that will disturb membrane behaviour and cause bending moments to compensate. (Van der Linden, 2015)

Furthermore, shells need a certain

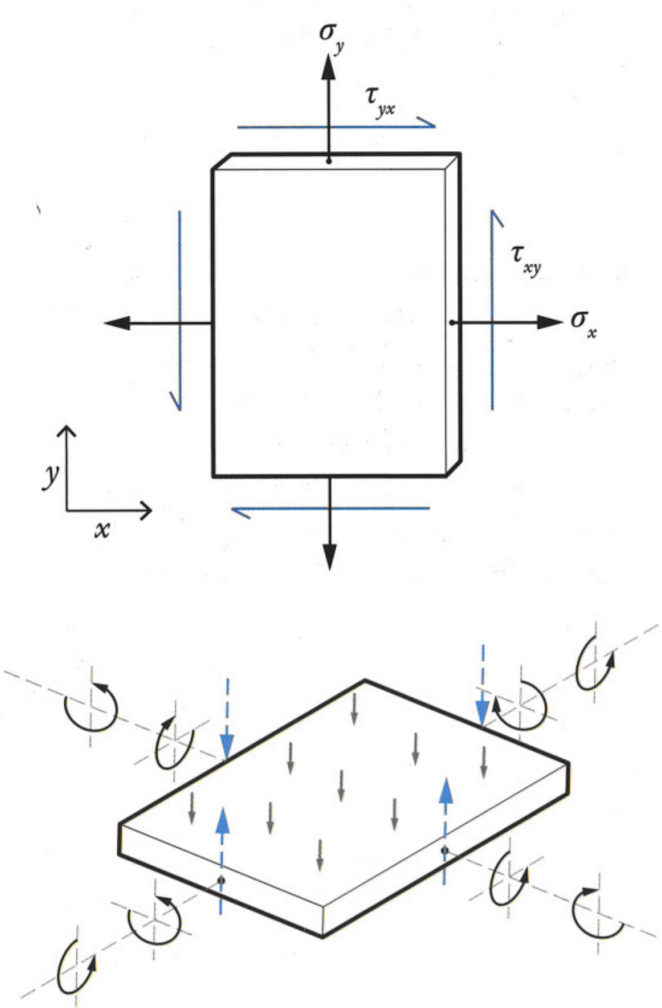

Fig. 31 *Plates. Top, a plate with an in-plane loading along the x and y axes. Bottom, a plate with an out of plane load. The right plate will need bending moments to resist such loads.*

bending stiffness to avoid buckling. Shell buckling is particularly dangerous, as most shells are in a state of unstable equilibrium. A large disturbance in the membrane forces, such as localised buckling, will lead to advancing and irreversible collapse of the structure. (Ney, Adriaenssen, 2014; Williams, 2014)

5.2 Shape optimisation

Double curved shells need a specific geometry to show compression-based shell behaviour and avoid bending moments. Form finding procedures are used to assure that a shell design is capable of carrying applied loads in axial compression.

For a long time, physical form finding was used. The main principle behind this was first published by Robert Hooke, who in 1676 stated (in the form of a riddle) 'as hangs the

flexible line, so but inverted stands the rigid arch' (Fig. 32). In other words, a flexible cable unable to withstand compressive forces or bending moments. Therefore, when hanging between two points, the cable will form a tension-based shape that contains neither compression nor moments. Inverting this shape will give to an arch that acts in pure compression. Under self-weight, a catenary arch is formed; additional loads will cause the cable to shift to adapt to these new loads. This natural shape is referred to as the funicular shape. The principle of the funicular cable can be extended to a cable net or fabric, which makes it possible to simulate a three – dimensional shell structure (Fig. 33) (Williams, 2014). This principle has used extensively by designers such as Candela or Isler (Garlock & Billington, 2014).

In more recent years, the rise of CAD and increasing computational power have led to shell form finding being performed mostly digitally. The introduction of FEA software has made it possible to more easily combine form generation with structural analysis. Additionally, it allows for larger freedom of shape, as the designs are no longer limited to the funicular shapes from physical optimisation. Different methods have been developed for the computational form-finding of shells.

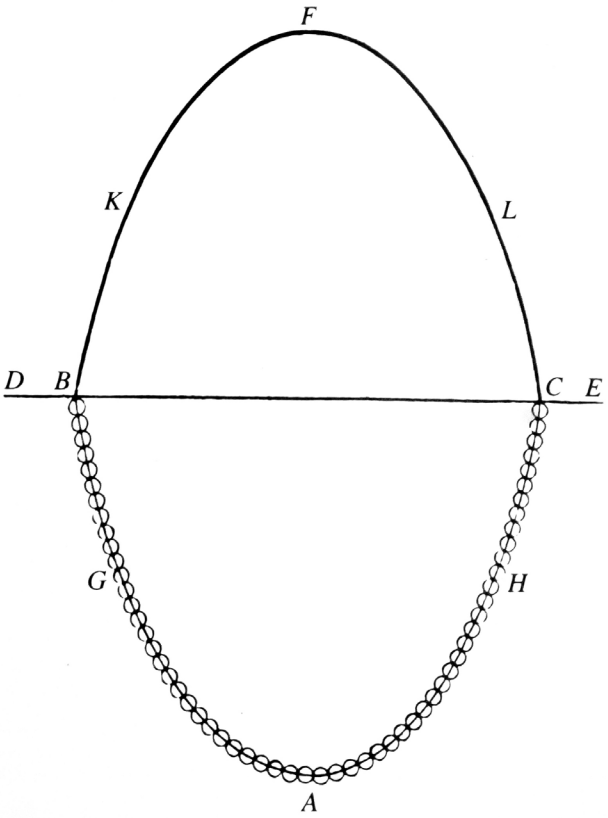

Fig. 32 *Hooke's hanging chain and arch.*

5.3 Grid shells

A grid shell is in essence a plane shell with the structural members concentrated into individual members in a relatively fine grid relative to the overall dimensions of the grid (Adriaens et al., 2014). Whereas in a plane shell loads can be transferred in infinitely many directions, in grid shells there is a limited amount of load paths, as forces can only be transferred along the structural members.

To properly function as a shell, a grid shell needs to be able to activate both membrane and bending action. Membrane behaviour requires that the shell elements must have in-plane rigidity to be able to transfer shear forces. A triangular grid consists of rigid elements and is rigid in itself; whereas for example a rectangular grid is non-rigid and will need additional stiffening. This can be done by using for example rigid connecting joints, or by applying cables in cross-direction.

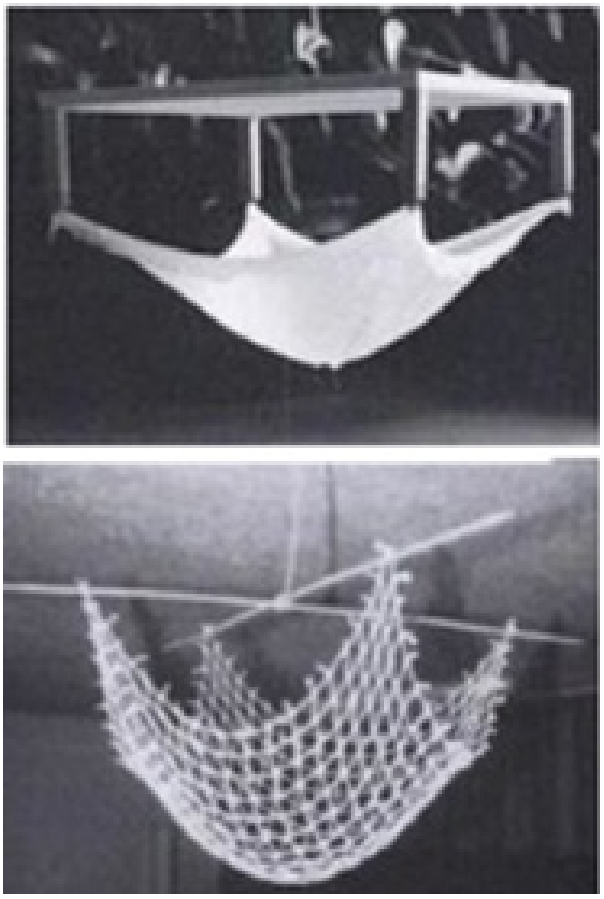

Fig. 33 *Form-finding models employed by Heinz Isler. Top: a fabric model of a continuous shell. Bottom: a net-like model that simulates a reversed gridshell.*

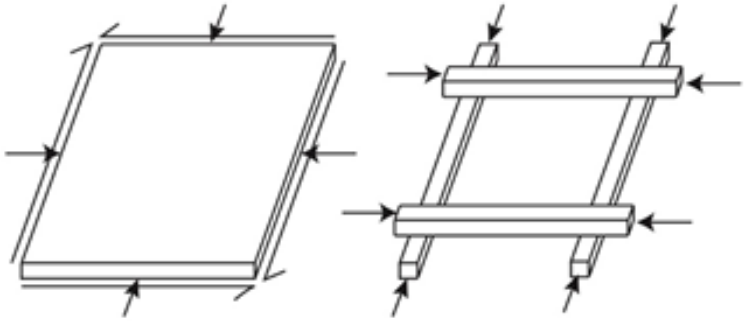

Fig. 34 *Continuous shell and grid shell. A continuous shell can transfer both in-plane normal forces and shear forces. A grid shell can transfer in-plane axial forces, but needs additional measures to resist shear*

In bending behaviour, a grid shell behaves like a plane shell. For areas where the membrane behaviour is disturbed, bending stiffness is required to create local equilibrium. Furthermore, bending stiffness is required to prevent buckling (Fig. 34).

In a grid shell, multiple types of failure mechanisms due to buckling can be discerned (Bulenda, Knippers, 2001):

- Member buckling, in which a single beam element buckles.
- Local instability, which means one or more nodes buckling. This is also referred to as 'snap-through' of the nodes. (Fig. 35)
- Global instability. Here the entire shell buckles, in a way comparable to continuous shells.

As shells are normally highly optimised for a certain load limit, exceeding this can lead to multiple of these mechanisms occurring simultaneously. The interacting of multiple failure modes that might be harmless individually, can interact to create one dangerous failure mode. Proper buckling resistance is important: buckling behaviour is almost impossible to predict analytically, and even computational results can be inaccurate. (Williams, 2014)

5.4 Gridshell nodes

Properly designed nodes are essential for constructing an efficiently functioning grid shell. Not only structural behaviour, but also practical and economical requirements need to be taken into account.

Structurally, the design of the joints connecting the grid shell beams greatly influences the stability of the structure. Locally, an insufficiently rigid connection can lead to member buckling and local snap through. (Bulenda, Knipper, 2001; Williams, from book). Globally, buckling can be caused by imperfections in the shell, such as for example non-rigid joints. (Bulenda, Knipper, 2001) This concerns out-of-plane stiffness, as in plane stiffness can also be provided using a rigid

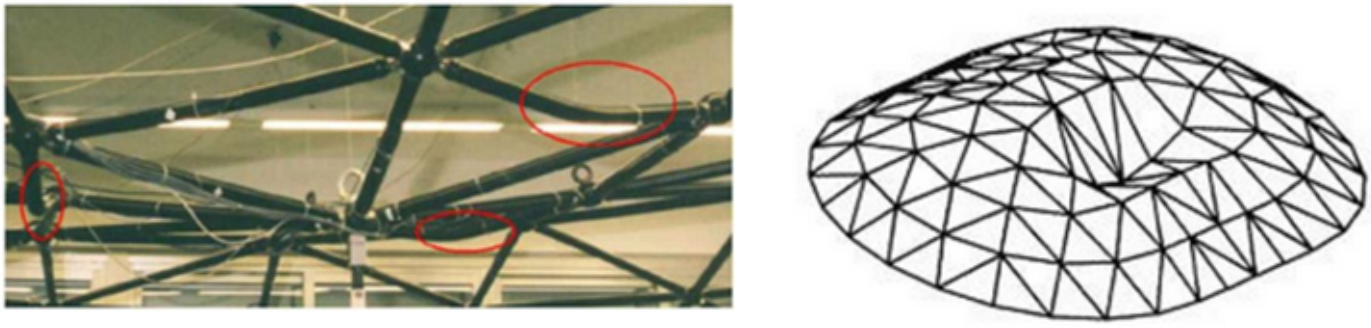

Fig. 35 *Gridshell buckling. Left, member buckling of seperate beam elements. Right, snap-through of multiple nodes.*

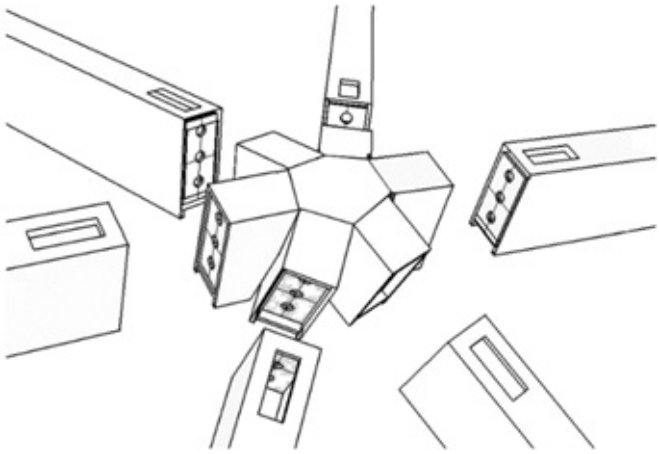

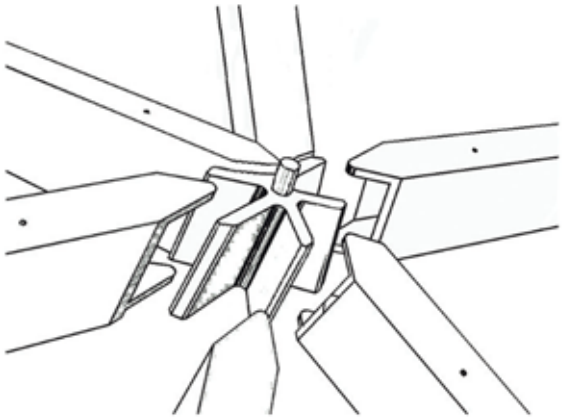

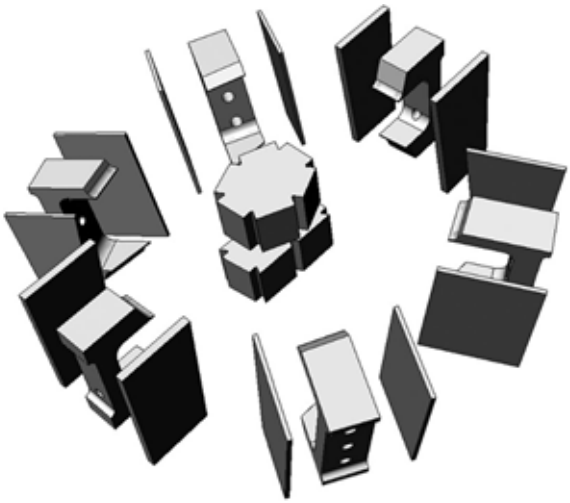

Fig. 36 *The Westfield Shopping centre node design. The finalised node on the left has bolted connections which allow for fast on-site assembly. On the right, the many components that make up the node are shown. CNC milling was extensively employed to speed up production and ensure an accurate structure.*

Fig. 37 *The Frankfurt Hoch Vier shopping centre node design. A simpler design that requires on-site welding. CNC milling allowed for quick manufacturing of the beams and node, but the need for welding lead to a slower assembly. Pre-made shell elements in the form of ladders was employed to speed up construction.*

triangular grid or cross-bracing cables.

From a fabrication point of view, grid shells are challenging as they require a large amount of unique, complexly shaped nodes. In conventional manufacturing structural nodes are one of the most costly parts in constructing three-dimensional structures (El-Sheikh, 1996). Designing a node system that can easily be produced using for example CNC milling or additive manufacturing is therefore preferred.

Fig. 38 *Simplified on-site assembly using pre-assembled ' ladders'*

(Fig. 36, Fig. 37)

Ease of assembly needs to be taken into consideration. Mechanically fastened connections are generally easier to assemble than welded connections, and are more suited to deal with tolerances. Pre-assembling sections of a grid shell into so-called 'ladders' can be used to shorten on-site construction time (Fig. 38).

Reducing the weight of the nodes is another design preference. Not only does this safe material in the nodes, a reduced dead weight will result in more slender beam being viable, further reducing material use. Finally, a lighter weight simplifies the assembly process of the shell.

5.5 Topologically optimised grid shell nodes

Some research has already been done on the designing of topologically optimised grid shell nodes in combination of additive manufacturing. Research particularly focuses on manufacturability using AM, the methodology of setting up the TO, potentially using parametric design, and structural

performance of TO nodes compared to conventional nodes.

No designs like these have been implemented in practice as of yet, as additive manufacturing is generally too slow and expensive to be used at a large scale. Furthermore, this production technique is generally not covered by building regulations, which makes it hard to certify and approve such structures. Continued research is needed for these designs to find use in practice. (Salome Galjaard, in personal correspondence)

Prayudhi, 2016

In collaboration with ARUP, this graduation project set out to find a design strategy to optimise structural performance and material efficiency in freeform envelope structure, using additive manufacturing. For this project, a small shell model of around 2 x 2 x 1 m was designed to test the proposed methodology (Fig. 40). Two work-flows were used. First, the required nodes under self-weight were designed. For this, a linear FEA was performed using Karamba3D, a structural analysis plug-in for Rhino Grasshopper. Grasshopper was also used to parametrically generate the boundary conditions for the TO. After this, TO was performed on each node separately with Altair Optistruct software, using the loads found with Karamba3D.

A secondary load, of a person standing on the shell, was taken into account separately. For this, both structural analysis and TO was performed on the entire model simultaneously in Altair Optistruct. This lead to a higher accuracy, as the effect of TO weight reduction could be immediately included in the entire model. In addition, the risk of data getting lost in the transition between software packages was reduced. The downside of simultaneous calculation and optimisation did lead to a significant increase of computation power and time required and might not be viable for large-scale structures. After optimisation, the found meshed were merged together, cleaned up and smoothened for additive manufacturing. For the scale model, a carbon-fibre reinforced polymer filament was used. The completed scale model was able to carry a person, despite large displacements.

Fig. 39 *Finalised node produced using direct laser metal sintering. Prayudhi, 2016*

For the case study, redesigning the shell from a triangular grid to a quad grid, and implementing the optimised nodes lead to an estimated total mass reduction of approximately 30%. One of the nodes was successfully produced at reduced scale using direct laser metal sintering (Fig. 39).

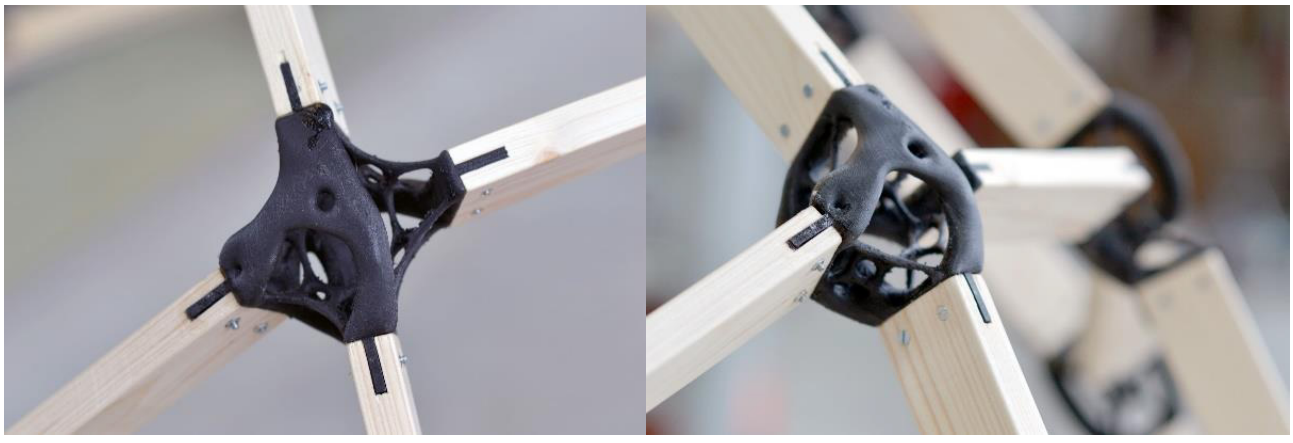

Fig. 40 *Small-scale prototype shell using conventionally 3D-printed nodes. Prayudhi, 2016*

Van der Linden, 2015

The goal of this research was to investigate what opportunities are created in the built environment by the introduction of Additive manufacturing. For this, structural joints in grid shells designed with the help of TO were investigated (Fig. 41).

The roof of the Zlote Tarasy shopping centre in Poland, a free-form grid shell made by Arup, was used as a case study. A structural linear static analysis of the roof under different loads was performed using Oasys GSA; the results from this analysis were used as the loads for TO in BESO3D. Analysis of the found joint geometry showed that the node had formed a double layered structure, capable of withstanding in-plane normal loads, and out-of-plane bending loads. The joints showed instability if considering out-of-plane shear forces. As the TO setup had not included shear loading, the TO algorithm had minimised shear resistance, despite the fact that shear might occur under some loading conditions. It showed the capability of TO to optimise for a specific load case, but also the risks of changing or unpredicted loads after assembly. Finally, though the average stresses in the final node were within limits, higher peak stresses were found compared to conventional nodes.

Using AM and TO, an estimated weight reduction of around 70% could be achieved for the nodes. A cost analysis showed that conventional node manufacturing would still be cheaper, due to the very high costs of metal AM. However, money can be saved due to easier and faster assembly of the structure due to its reduced weight.

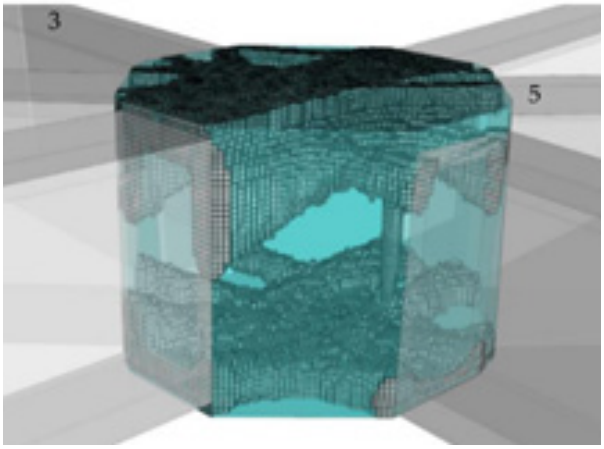

Fig. 42 *Design domain used by van der Linden*

The TO software required manual iterative tweaking to result in suitable geometry. Furthermore, considerable post-processing of the mesh was needed to come to a producible result. A more automated process is needed if this method is to be applied on a large-scale structure.

Seifi et al., 2018

This research compared two grid shell node designs for AM with three conventional nodes. One of the AM nodes was designed using BESO, the other using a transitional node of the authors design, using Laplacian smoothing algorithms. The BESO node was designed using only axial loads in all connecting beams,

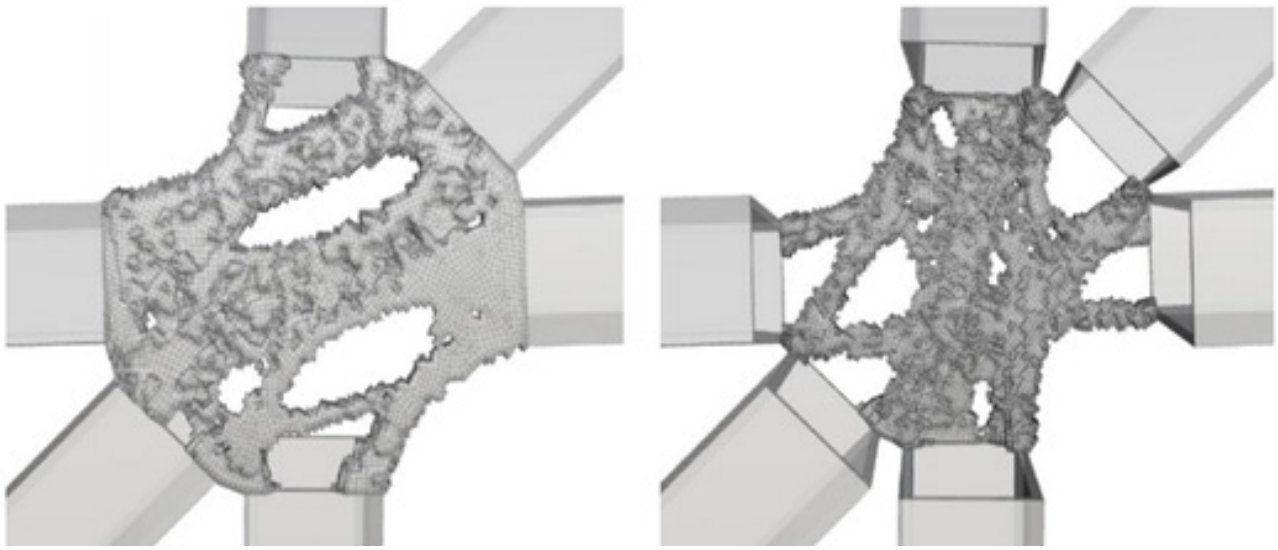

Fig. 41 *TO designed grid shell node by van der Linden, 2015. Due to the lack of out-of-plane shear loading, the found geometry consists of two, unconnected layers.*

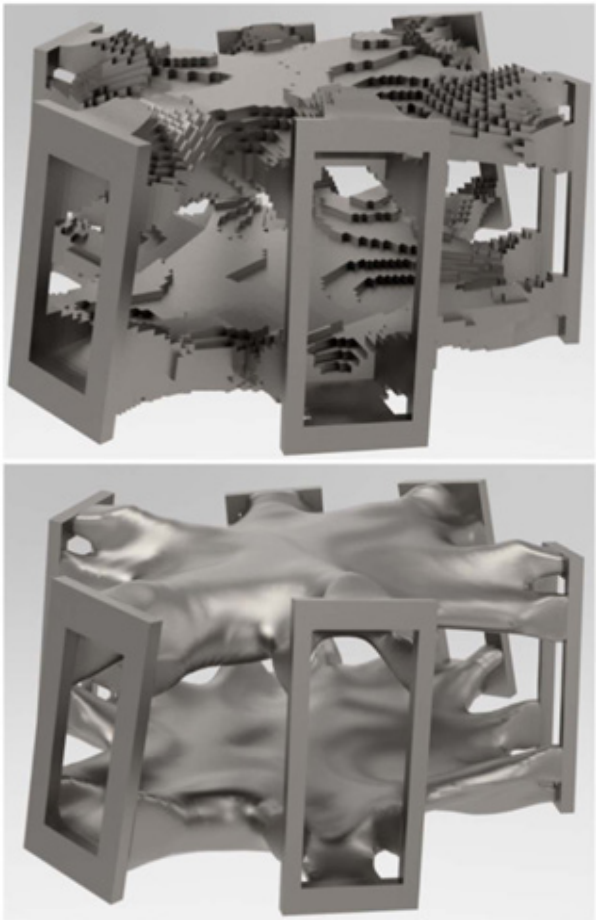

Fig. 43 *The BESO node as designed by Seifi et al., 2018. Top, the voxelised result from the TO; it can be seen a rather coarse element division was used. Bottom, the smoothened geometry after post-processing.*

with minimising mean compliance set as the goal (Fig. 43).

Linear structural analysis was performed using the same loads. The BESO-designed node showed less deformation, using less material compared to the other nodes. The increase in stiffness found was however small. Additionally, the BESO node showed increased local peak stresses compared to the other nodes.

5.6 Summary

Grid shells are part of the continuous plane shell family of structures, following the same structural principles. These shells can be described as a curved two-dimensional plate element. The curvature of the shell allows it to carry out of plane loads with in-plane forces, which makes it possible to achieve large spans with a thin, lightweight cross section. This can be explained using membrane theory. Where membrane behaviour is interrupted due to for example eccentric loads or shell imperfections, bending moments will be introduced to carry the loads. This is described with bending theory. Combining membrane and bending theory gives shell theory. Efficient shell design aims at minimising bending moments, allowing for thinner and lighter structures. However, bending stiffness is still required to ensure stability of the shell under eccentric loading and to avoid buckling of the shell.

Finding an optimal shape for the shell can be done physically, using a hanging-cable model, which can be expanded into a hanging net or fabric model to create a full shell model. Alternatively, computerised models have been introduced, allowing for integrated form-finding and structural analysis while enabling more elaborate geometries to be designed.

Grid shells can be described as a continuous shell, with the structure concentrated in individual members in a fine grid, connected by nodes. To show membrane behaviour, the grid needs to be capable to withstand in-plane normal and shear forces, which requires a rigid grid. This can be achieved by using a triangular grid that is rigid in itself, or by using for example clamped joints or cross-bracing cables. In the nodes, bending stiffness is required not only for shell stability, but also to avoid local member buckling and node snap-through.

In addition to the structural requirements, fabrication and assembly need to be taken into account. Designing a node that is easily to manufacture and assemble allows for faster construction and reduces costs. Decreasing weight saves material and allows for smaller profiles in the grid, as the self-weight load is decreased.

A few examples of steel grid shells designed using Topology Optimisation have been shown. Generally, it is found that this method finds structurally viable results and can significantly reduce element weight. However, higher peak stresses compared to conventional results seem to be found. As TO focuses on structural optimisation, post-processing is required to ensure the design is suitable for fabrication.

6. Case study

6.1 Selection criteria

An important part of this research will be performed using the principle of 'Research through Design'. It is believed that working on a tangible design challenge and solving the problems that arise is an helpful tool for performing research.

To test the idea of a cast glass grid shell node, an existing grid shell structure will be redesigned, using this new element. A case study was chosen on the basis of a few criteria. First of all, the structure should function as a compression-based shell, using membrane action for its structural stability. Often, grid shell-like structures are used for 'blob' architecture. Though this makes use of the free-form potential of the construction technique, it disregards the structural principles of shell theory, resulting in structures that require considerably more reinforcement than 'pure' shells. As structural glass is most suitable for compression loading, a compression-based shell is most suitable.

Secondly, the project should be free-form. Parametric design linked to additive manufacturing is most economical when a large quantity of uniquely shaped elements needs to be produced. For a symmetric structure such as a geodesic dome with more repetitive joints, more economical solutions should be used.

A small-scale project was preferred, with a shell span of around 10-12 meters. As mentioned in the chapter on glass, element size greatly affects how easy and fast a glass component can be made. It is decided to start with a small scale project to simplify the challenge and lay the groundwork for future, larger scale applications.

Finally, the availability of documentation was taken into account.

6.2 SUTD Gridshell Pavilion

Based on these requirements, the grid shell pavillion erected at the Singapore University of Technology and Design was chosen (Fig. 44). This pavilion has been designed to give function to a piece of "no man's land" at the edge of the Dover campus of the Singapore University of Technology and Design. The

Fig. 44 *Impressions of the SUTD Gridshell Pavilion*

pavilion turned this empty plot of land into a lively space between the university dormitory and lecture hall. During the day, the pavilion offers a shaded informal place to relax, work, and mingle for students and staff of the university. At night it is used for gatherings, evening lectures and community events.

The shape of the site was used to determine the plan of the pavilion. Out of multiple student designs, a grid shell was chosen, as this allowed covering the pavilion using a light-weight structure without columns, horizontal beams or walls. During the design of the grid shell, a numerical hanging chain model was used to create an efficient double-curved geometry, and create a beam structure that follows the line of thrust in compression.

The structure was assembled from flat plywood, CNC-milled to form a three-dimensional puzzle. By doing this, the shell could be assembled without the need to fabricate complex connectors. This allowed the pavilions complex form to be achieved with readily available materials, allowing it to be built at a low cost. A RhinoPython script was used to automatically translate the form-found mesh to a buildable structure.

6.3 Shell performance

To test the structural behaviour of the pavilion and find out whether its shape is suitable for shell behaviour, a basic linear structural analysis has been performed. Andres Sevtsuk of the SUTD was kind enough to provide extensive documentation of the project, including a digital model for McNeal Rhinoceros. Grasshopper, the parametric tool of Rhinoceros, was used for the analysis. The structural analysis plug-in Karamba3D was used within Grasshopper. For this analysis, the grid was modelled with arbitrary steel hollow tube profiles of 30 mm in diameter, 4 mm wall thickness, joint with rigid connections. Only self-weight loading was applied. This test is performed to locate peak stresses and high out of plane bending moments, indicating disturbances in the membrane action of the shell, and possibly locating flaws in the design that could be improved. The normal forces in the beams, in-plane and out of plane bending moments and shear forces found in Karamba are shown in Fig. 45-Fig. 49.

A few conclusions can be drawn from these

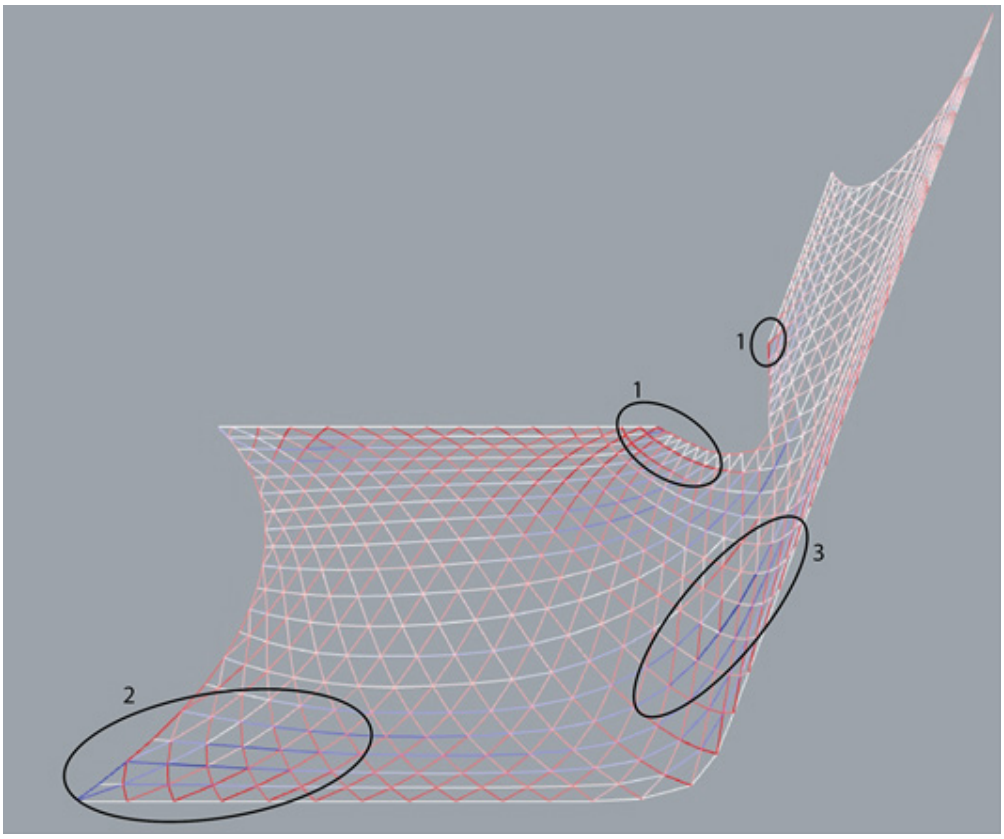

Fig. 45 *Axial forces in the shell, found using Karamba3D. Peak compressive forces are found around the middle opening (1), increased tensile forces appear around (2) and (3).*

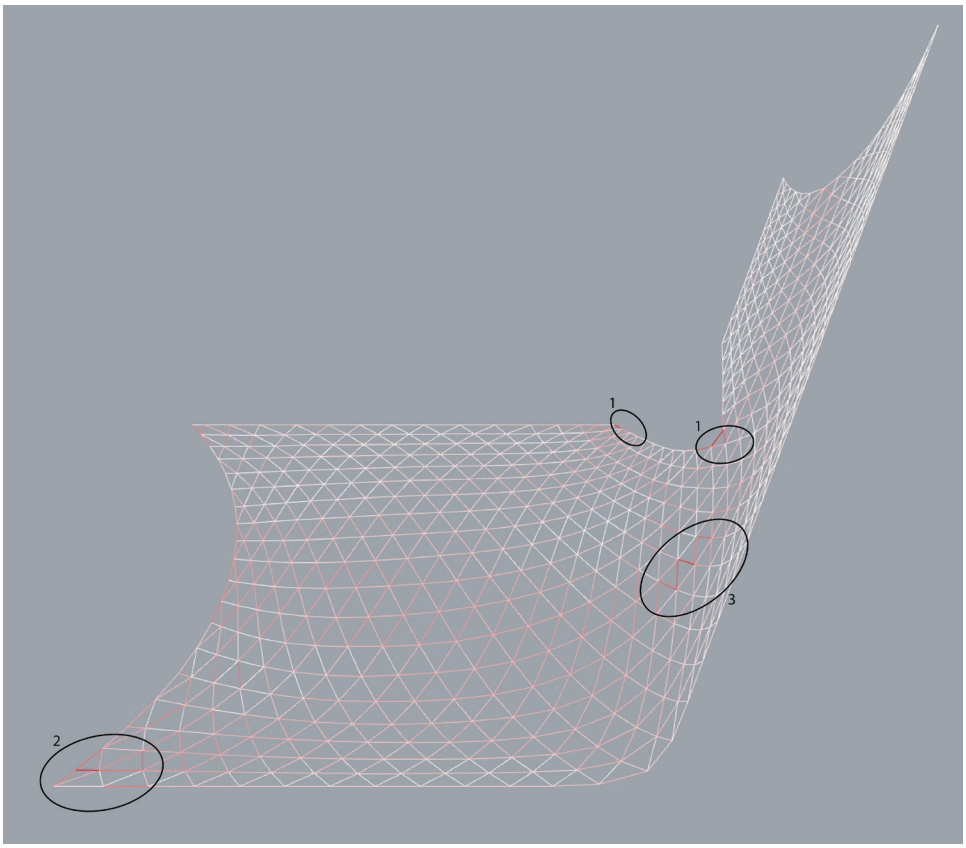

Fig. 46 *In-plane bending moments. Due to the rigid triangular grid, these moments are generally low, with a few peaks around the middle entrance (1) and in areas where increased axial tension was found (2,3).*

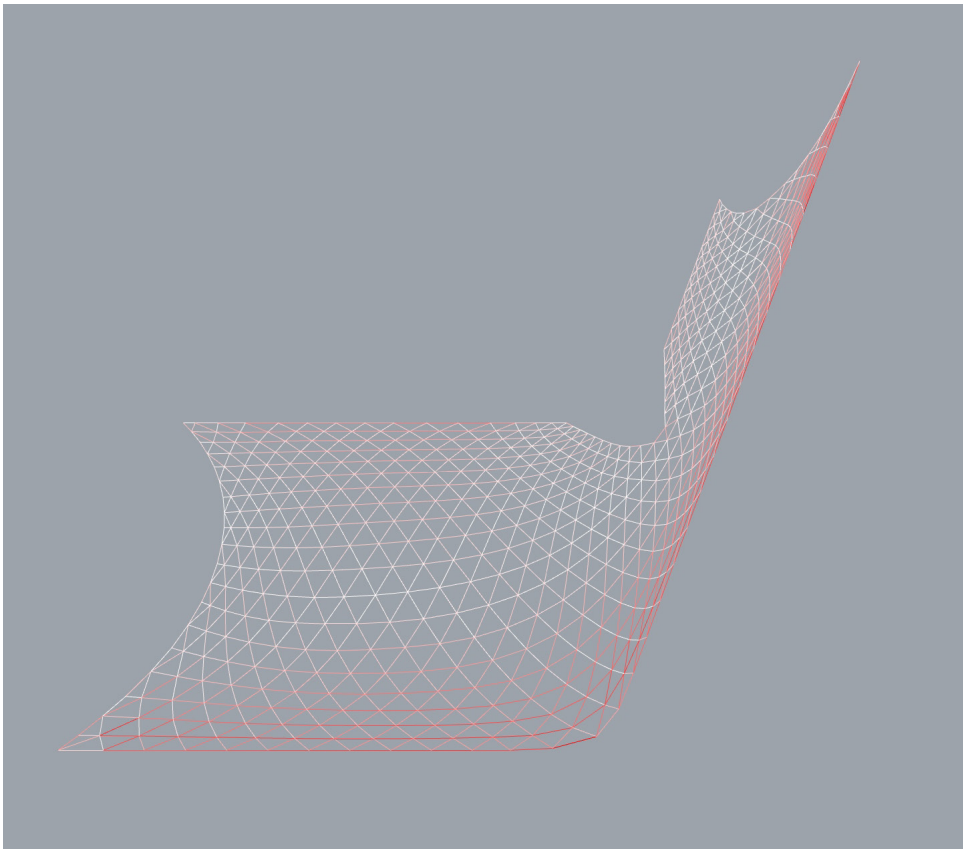

Fig. 47 *Out of plane bending moments. The higher values along the outer edge indicates that the shell is unable to transfer the loads with membrane-forces, leading to bending moments.*

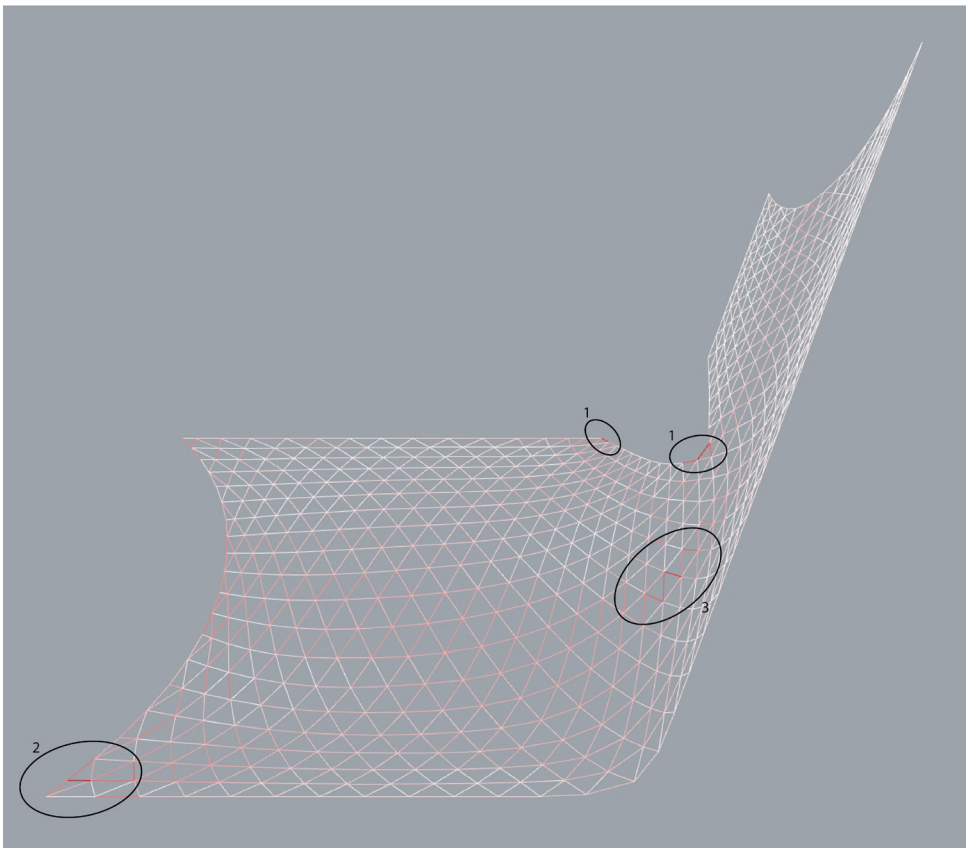

Fig. 48 *In plane shear stress is found to be low. Peaks are found around the middle opening (1) and in places with increased axial tensile forces (2,3)*

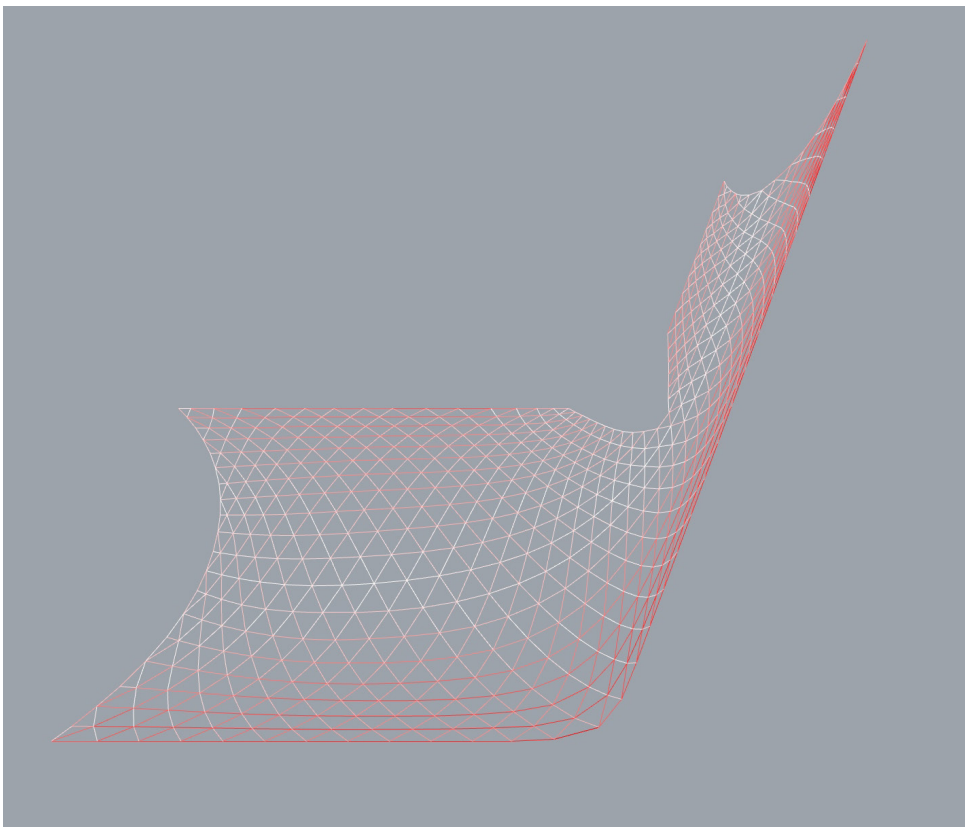

Fig. 49 *out of plane shear. It can be seen that along the edges, the in-plane membrane forces are disturbed, leading to out of plane disturbances.*

results. The opening in the middle of the structure interrups the shell action, leading to compressive stress peaks and in-plane moments and shear . Furthermore, the tensile stress peaks appear at one of the corners and at the ridge where the shell plan curves. Out of plane bending and shear stresses appear at the shell edges, indicating that the structure here does not fully perform as a shell.

6.4 Mesh relaxation

To see if the shell behaviour of the mesh can be improved, a hanging model mesh relaxation was performed on the structure. This method has further been described in chapter 4.2. Instead of using a physical net or cloth model, this optimisation was performed computationally. The Kangaroo2 plug-in for Grasshopper was used to perform this optimisation. In this model, each mesh line is converted into a spring element, free to rotate at each intersection. A small load is applied at each intersection, allowing the model to take the most optimal shape to carry the tensile loads without internal bending moments. For a more accurate result, each line element was split down the middle and connected with a hinge element. This helps in making a tensile-only structure, as any element under compression will automatically buckle. In the final, reversed model, this should lead to a fully compression-based shell structure.

The results of the mesh relaxation are shown in Fig. 50. In red the original mesh is shown, and yellow the optimised. Though some shifts can be seen, the geometry has remained mostly the same. It is likely that a similar hanging-model optimisation has already been performed on the design, with the differences explained as slight differences in the setup of the model. It is therefore decided to continue using the original mesh.

6.5 Beam length analysis

For fabrication, the length of the line elements was analysed. Ideally, beams of over 1.5 m should be avoided, as that is the maximally available element length available for many commercially available extruded glass elements, which are a likely candidate to be used in the glass redesign of the pavilion. In addition, elements of less than 30 cm should preferably be avoided, as these are not practical to produce or assemble. A grasshopper script has been written that colours the mesh elements based on their length, black for long elements and white for short. Elements that are more than 1.5 m, or less than 30 cm in length are labelled in red (Fig. 51).

A wide range of beam lengths can be found

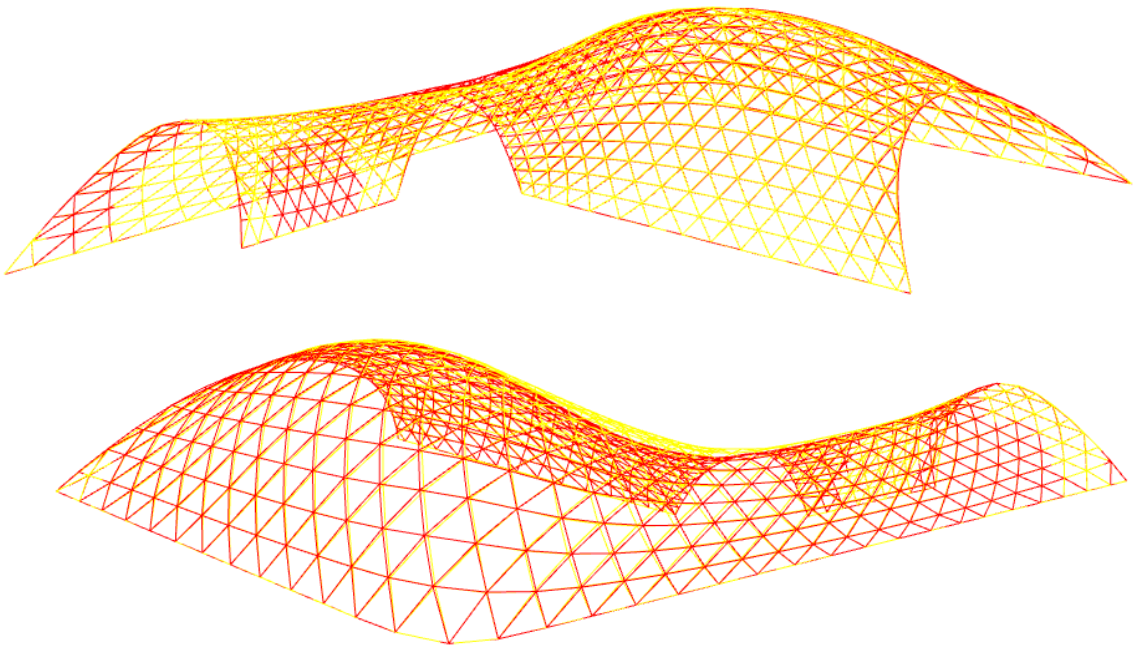

Fig. 50 *Hanging model mesh relaxation: before (red) and after (yellow)*

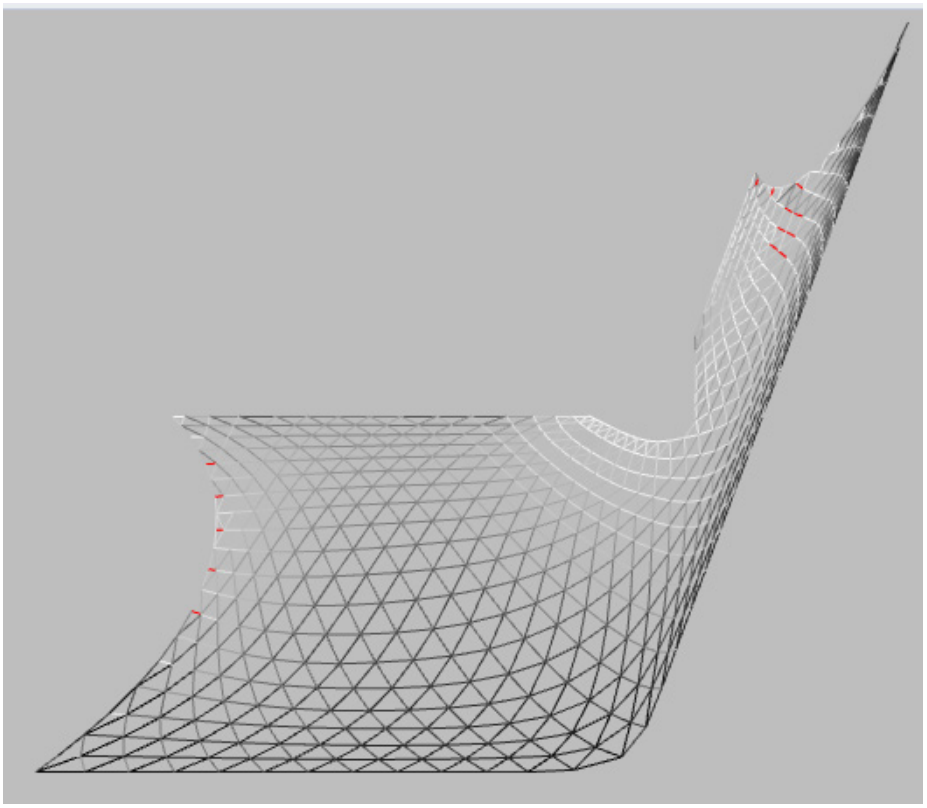

Fig. 51 *Beam length analysis. Long to short is labelled black to while, with elements <300 mm labelled in red*

in the pavilion. The longest element is 1.42 m, the shortest is 25 cm. These short elements can be found at two places throughout the mesh. At the edges of the shell, where the mesh is cut off, some very short elements are left over. These can be removed without noticeably affecting the structure. Secondly, at the top of the highly curved arm of the shell, some short elements can be found. These have been retained for now, though they should be taken into account for the final assembly of the shell.

6.6 Mesh redrawing

Based on the analysis results so far, it can be concluded that most of the shell is performing well, and will not be changed. Around the inner opening of the shell, however, some improvements should be made, as this is where most of the peak stresses, shear forces and bending moments appear. The mesh here has been modified to decrease the size of the opening, and better distribute the heavy load on this corner. The redrawn mesh can be seen in Fig. 52. A minimum element length of 30 cm was used.

Structural analysis shows that the corner remains an issue, with peak loads found at the corner. However, these loads are now better distributed and lower (Fig. 53). Considering the goals of the thesis, it is decided not to further pursue the optimisation of the shell. During the process, it should be kept in mind that the case study has been modified to fit a structure that it was not designed for originally. This leads to some heavy-loaded elements that should be avoided in a properly designed grid shell.

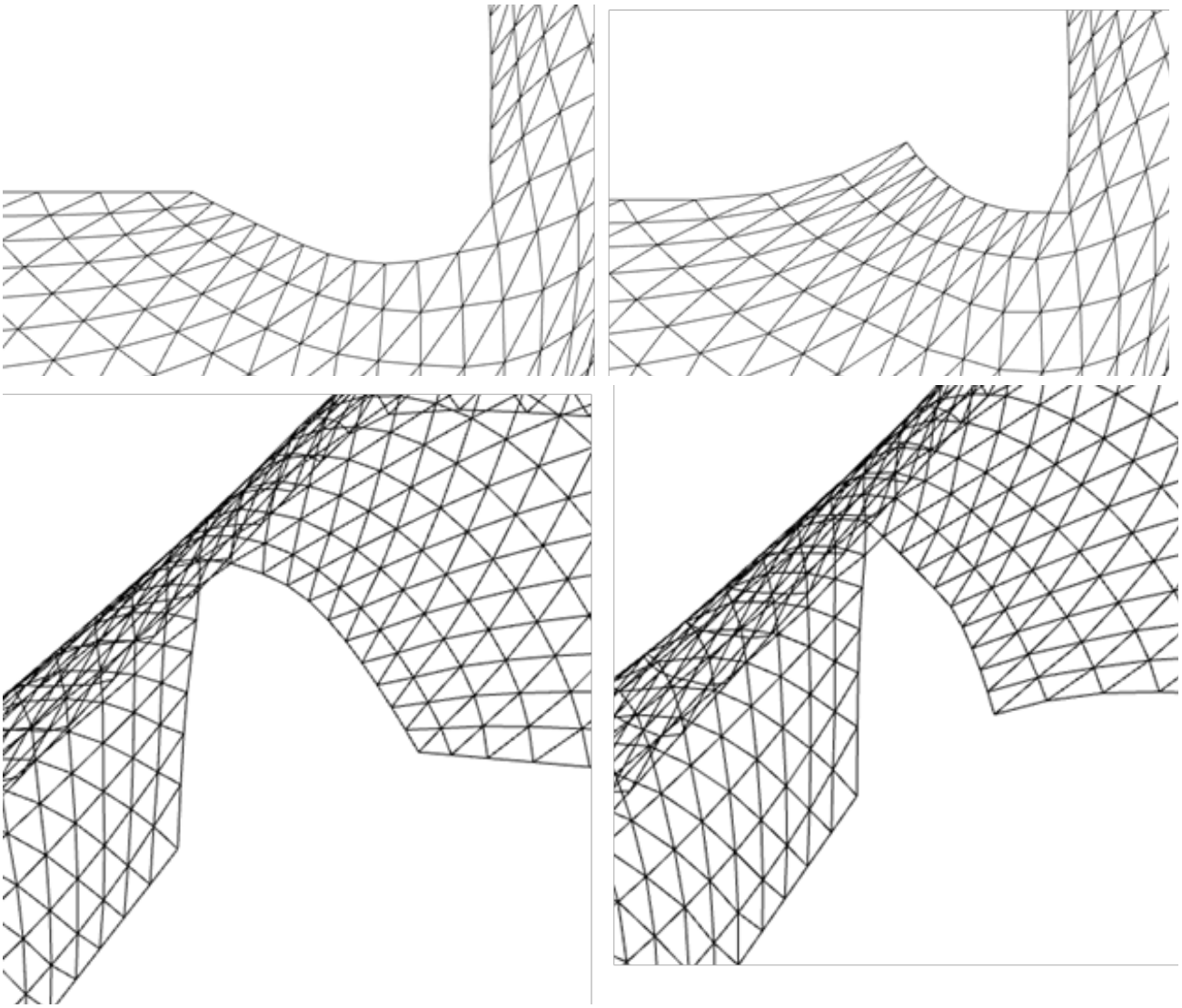

Fig. 52 *Mesh redesign. Left: the old mesh, Right: the redesigned corner*

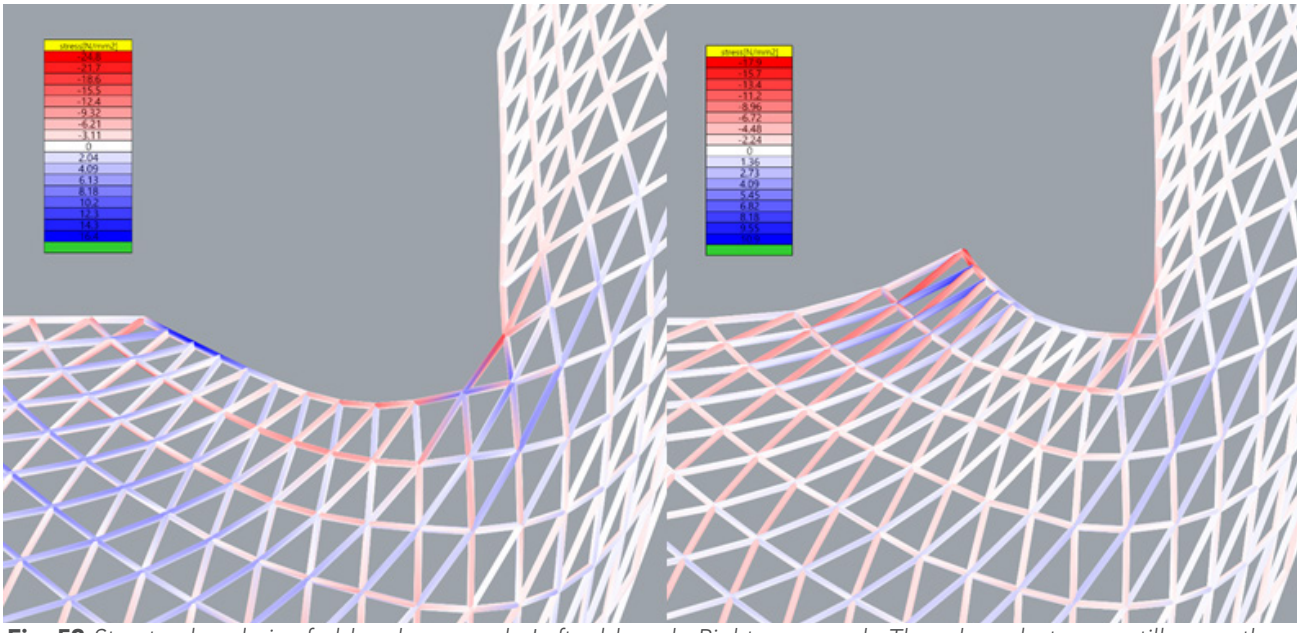

Fig. 53 *Structural analysis of old and new mesh. Left: old mesh. Right: new mesh. Though peak stresses still occur, the stresses are better distributed and lower.*

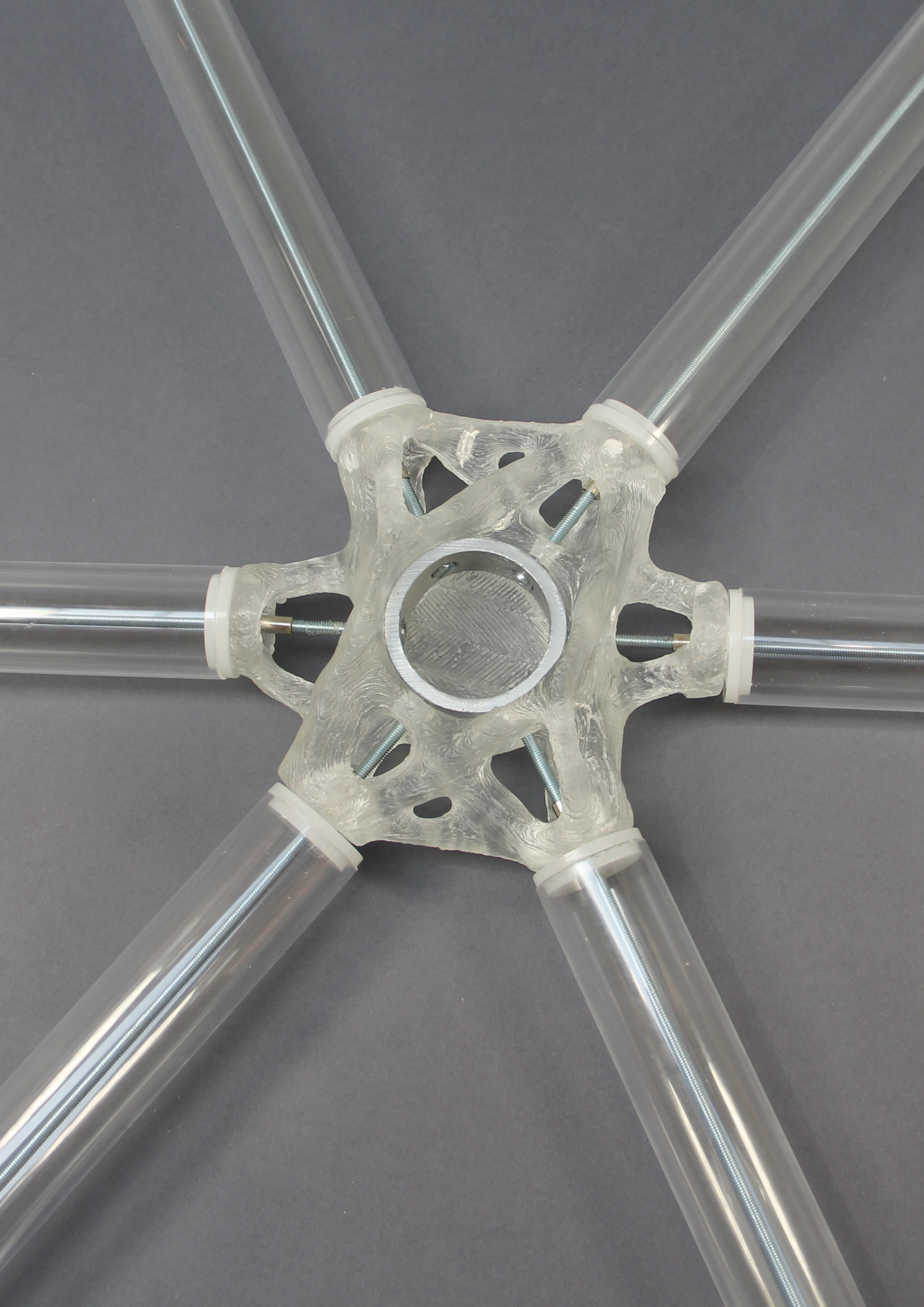

7. Pavilion design

7.1 Redesign principles

The modified mesh from the SUTD pavilion has been used to design a new pavilion, based around the use of cast glass nodes. This has been done on the basis of two design principles.

The aesthetic qualities of the structure should be kept in mind throughout the design process. For a glass structure, this is especially important. Not only should transparency be maximised, in addition each opaque element will be fully visible through the glass. Therefore, each element needs to be designed with care.

Secondly, as much functionality as possible should be included in the nodes. A high level of unique complexity that is possible with parametric design and additive manufacturing. This makes it relatively easy to include a lot of complexity in the cast elements, which can be used to shift the need for more complex custom elements away from the rest of the structure. Because of that, the remaining structure can be designed using more repetitive, generic elements; which is both cheaper and easier for assembly. This was shown well in a topology optimised, additively manufactured element designed by ARUP for a tensegrity structure. Here, many joining elements were eliminated by integrating their functionality into the printed metal node element simplifying the overall structure (Fig. 54-Fig. 55) (Galjaard et al., 2015). This is a great advantage of the free complexity offered by additive manufacturing.

Fig. 55 *Close-up of the ARUP node with integrated connections*

7.2 Beam design

It was decided to use glass for the beam elements of the grid shell to maximise its transparency. Different alternatives have been considered for these beams, these are described below. Not only should the beams be transparent and safe, they should also be easy to fabricate in various lengths, as each beam in the shell has a unique size.

Laminated glass

Laminated pane glass is an often used solution when glass beams are required (Fig. 56). These beams are formed by stacking multiple flat panes of glass and joining them with a transparent interlayer, allowing them to function as a single solid beam. The interlayer can keep the glass together even when one or multiple panes fail, adding

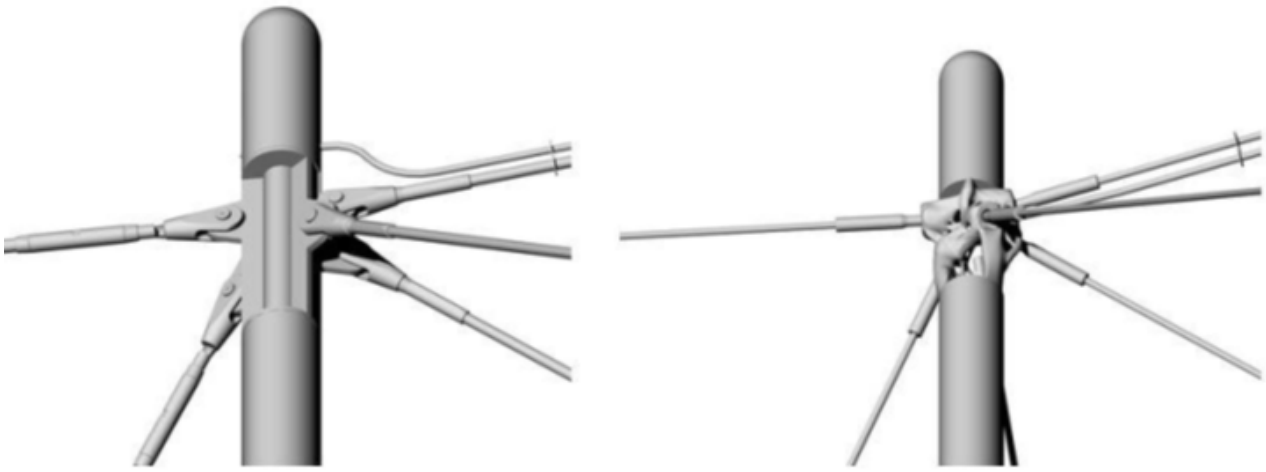

Fig. 54 *Integrating complexion. Left shows the conventional design, right the optimised element. Fewer connecting parts are required in the new design.*

Fig. 56 *Example of laminated glass beams*

structural redundancy. It is possible to use heat strengthened or fully tempered glass, increasing the structural performance of the beam. For connection the laminated beam, it is possible to insert metal elements in the glass before lamination.

However, the beams cannot be modified or cut after laminating. For a structure such as this, in which each beam has a different length, this means that each element need to be processed to the correct size before laminating and tempering the glass. This will increase production costs, and makes it difficult to replace beams that are broken. Structurally, these laminated beams can be weak when subjected to long-term loading, as the interlayer will start to creep when subjected to a load perpendicular to the interlayer direction (O'Regan, 2014).

Cast glass beams

It should be possible to cast the beams in glass. This would result in sturdy, solid elements, with good transparency. However, as said before, casting and annealing is a time-consuming and therefore costly process, and would be inefficient to use for a simple straight beam.

In the theme of this research it might be possible to design a more lightweight, truss-like optimised beam to be cast with disposable moulds (Fig. 57). This would be a much more material-efficient design, making use of the freeform potential of cast glass. However, the form-finding and mould-making required for this would increase the complexity of the project manifold, and lies beyond the scope of this research.

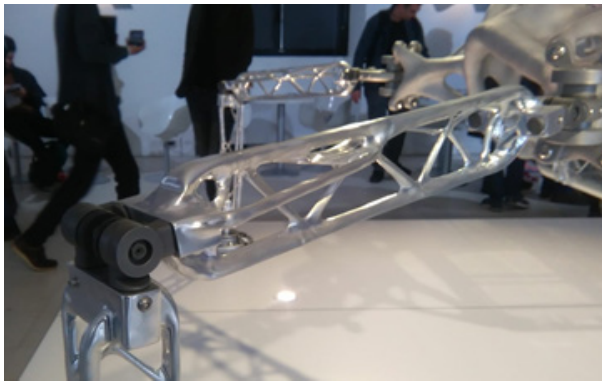

Fig. 57 *Leg of the Autodesk/JPL optimised lander. A similair optimised geometry fabricated in glass can be imagined for the beams of the shell pavilion*

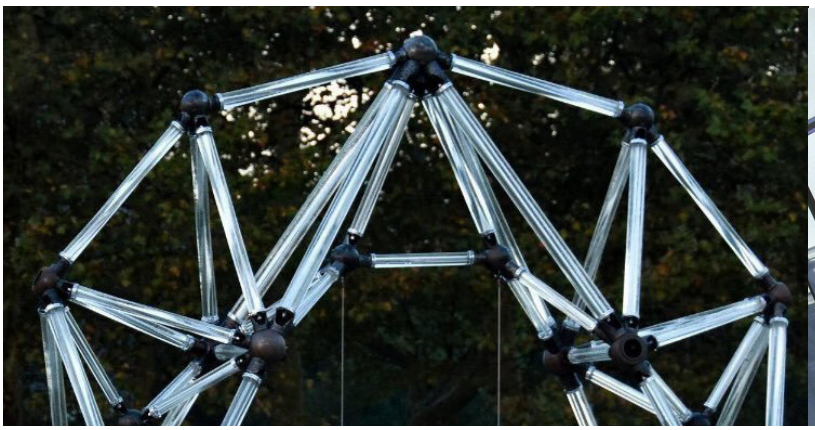

Fig. 58 *Glass bundle beam as seen in the TU Delft Glass Swing*

Fig. 59 *Glass tube field London*

Hybrid extruded glass beams

As an alternative, extruded glass can be used. Many different designs and dimensions of extruded glass elements are commercially available (www.schott.com). In structural applications, both solid glass rods (Fig. 58) and glass tubes (Fig. 59) have been used in beam elements. Both beam designs have a comparable assembly. It consists of metals caps placed at the ends of the extruded glass elements. These caps are pulled together by a metal cable or rod running through the centre of the beam. This mechanically clamps the glass in place and ensures that the glass is only ever loaded in compression, as the cable will carry any tension applied to the beam. The metal end pieces can then be bolted to the remaining structure (Fig. 60).

Solid glass rods are usually limited to smaller diameters due to annealing times. In pre-tensioned beams such as these, they are therefore applied in bundles. This has the additional advantage of providing redundancy in case one of the rods fails. Hollow glass tubes are available at larger dimensions, and can

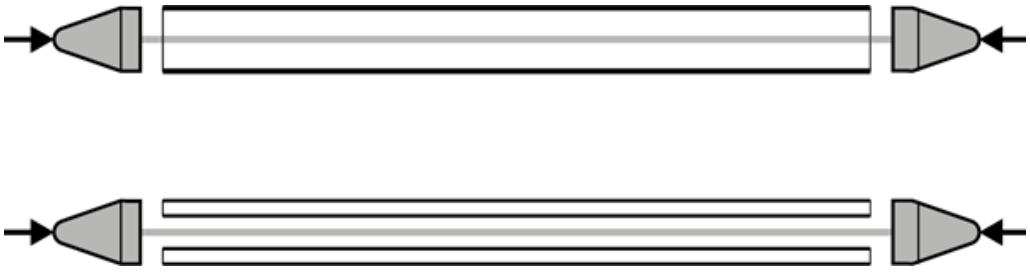

Fig. 60 *Basic principle of the hybrid extruded glass/steel beam. Top: glass tube. Bottom: glass rods*

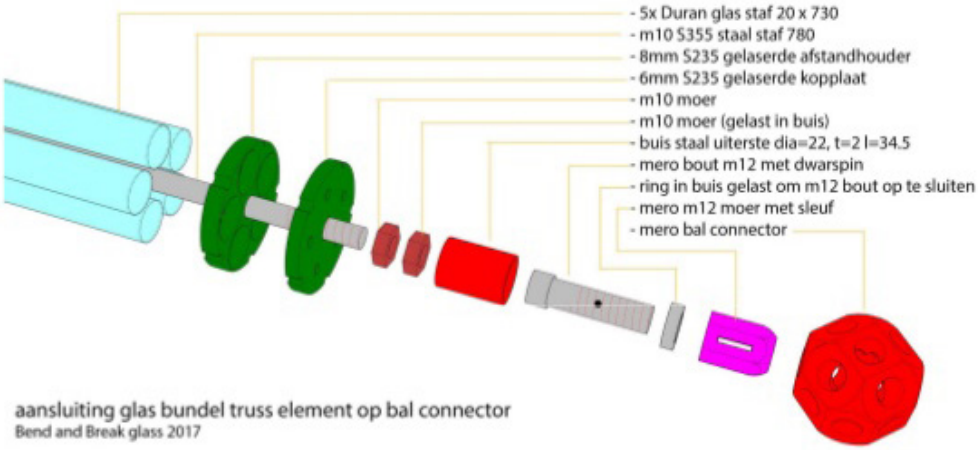

Fig. 61 *Design of a glass rod beam for application in a spaceframe*

	Laminated glass	*Cast glass, solid*	*Cast glass, optimised*	*Glass rod bundle*	*Glass tube*
Transparency	+	++	-	--/-*	-/+*
Fabrication	-	-	--	+	++
Safety	++	+	+	+	+
Weight	-	-	++	+	+

* with/without metal ends

Table 1 *Overview of the various considered glass beam designs*

easily be combined with a cable. To prevent damage to the load-bearing glass tube, a sacrificial, thinner glass tube can be placed around it.

Visually, the bundled rod beams are translucent, but not transparent as the multiple solid beams distort the light falling through them. This does mean that the centrally placed metal cable is never clearly visible. The glass tube design is more transparent as it distorts the view very little, but leaves the metal rod visible in the middle. For both designs, the metal end caps will be very visible in a fully transparent structure. However, these could possibly be integrated within the cast node, reducing the amount of parts required and greatly increasing transparency.

An overview of the available options can be seen in Table 1. From these alternatives, the extruded glass tube element (reinforced with a steel cable) was selected, due to its combination of ease of assembly and modification, and its transparency. To fully make use of this transparency, an alternative should be found for the metal end cap element.

7.3 Connection detailing

Within a conventional glass tube beam design, the internal cable serves a double function. Structurally it takes up any tensile loads that might occur in the beam, leaving the glass only loaded in compression. Secondly, the cable is used to keep the glass tube clamped in place, pulling together two metal end caps. These metal caps usually contain a bolt mechanism to fasten the beam to the remaining structure, in a design comparable to the MERO spaceframe system (Fig. 62).

As suggested before, it will be attempted to eliminate these metal connectors and integrate their functionality within the cast glass node.

Fig. 62 *MERO-system based glass tube beam, with metal capping elements*

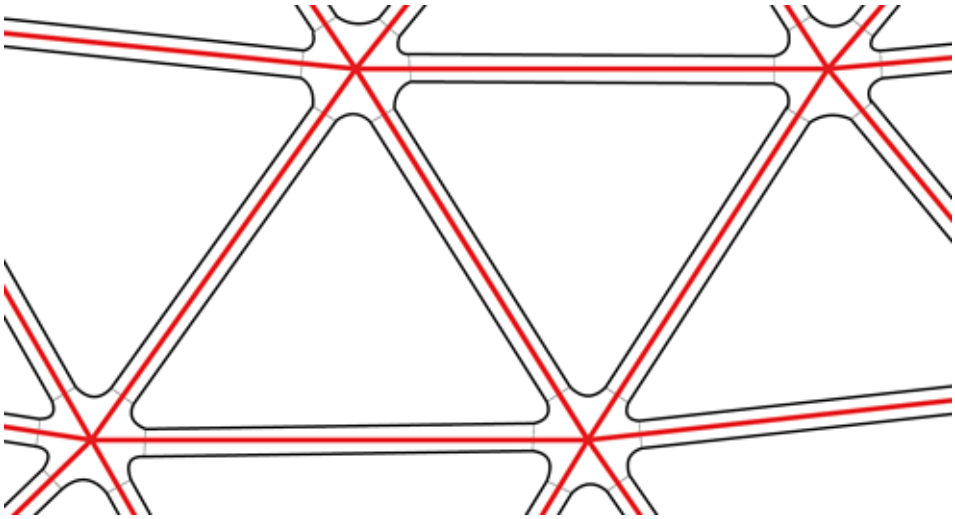

Fig. 63 *Assembly concept. Hybrid structure of glass beams and nodes (black) and steel cables (red)*

Figure (Fig. 63) shows the basic design for the assembly of the glass shell structure. It consists from two sets of elements: a steel cable mesh to withstand tension and hold the structure together, and a series of glass nodes and tubes to withstand compression, and provide stiffness to the structure. By directly clamping the glass tubes between the nodes, no more connecting caps are required.

Where the glass node and tube meet, there is a risk of stress concentrations appearing, due to imperfections in both adjacent glass surfaces. This can potentially lead to localised failure of the material, which will lead to cracks. These stress concentrations can be avoided by placing a softer material between the two layers. This interlayer will deform locally, ensuring that the loads are equally distributed over the entire surface of the connection. A material that is suitable as an interlayer is Polyoxymethylene, or POM (Fig. 64). This is a translucent high-performance engineering plastic, which has seen applications as glass interlayers in comparable situations (Eekhout & Staaks, 2010; Snijder et al., 2018). A data sheet of this material has been included in appendix B.

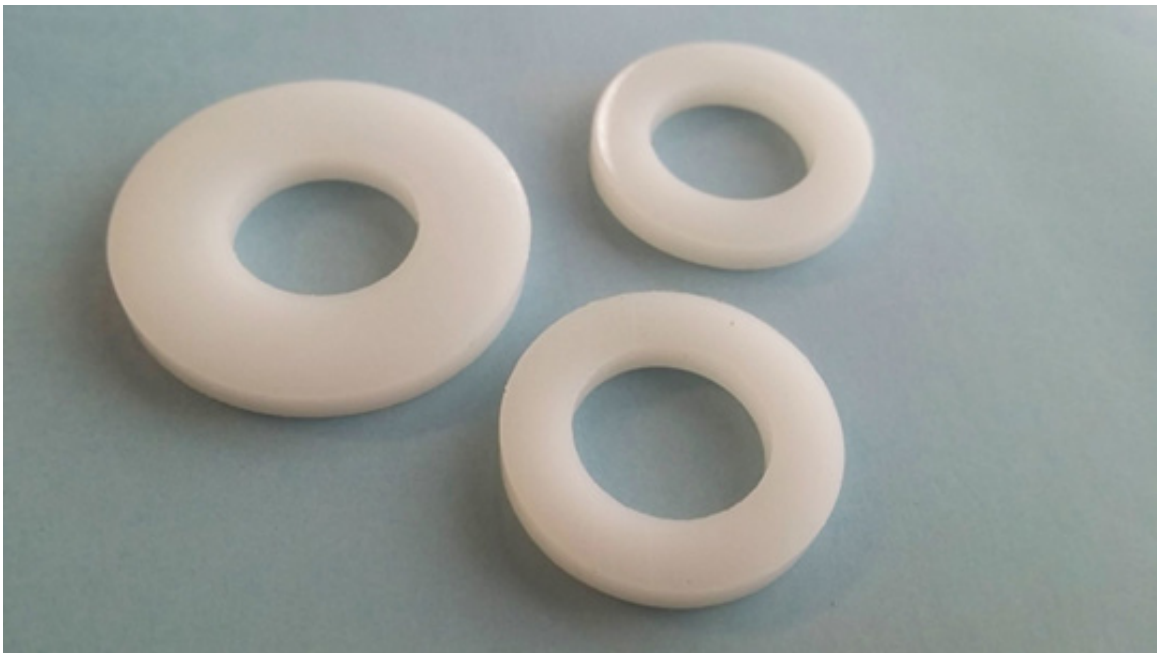

Fig. 64 *Elements of Polyoxymethylene, or POM*

Fig. 65 *Schematic of the new beam assembly, using minimised POM elements as interlayer and assembly component*

Pre-assembling the glass beams by inserting and fastening the steel cable beforehand will considerable speed up on-site assembly. The POM material can be used for this. By closing the glass tube with two POM caps, and fastening the steel cable between them, a complete beam assembly can be made. The POM elements can be light, as they do not need to carry any additional load apart from keeping the cable in place and serve as interlayer between the glass elements (Fig. 65).

The inclusion of an internal cable mesh has a couple of additional benefits. First of all, it provides an additional measure of safety. If a single node or a couple of adjacent glass beams fail, the steel cables will keep the façade elements attached to that node from falling down, while also still providing support in tension.

Secondly, pre-stressing the cable mesh might be used to improve the structural behaviour of the shell. As the pre-tension pulls the shell together, it could serve to reduce unwanted tension and bending moments in the shell. Under eccentric loading, such as a wind load, this would improve the overall stability of the shell. A pre-stressed glass geodesic dome using a similar principle has been realised by Octatube, in their Selimiye mosque project (Eekhout & Staaks, 2010). Within this all-glass dome, the chosen semi-spherical shape would have led to too high bending moments and tensile stresses for the glass to withstand. By applying a pre-stress, the entire dome is loaded in compression (Fig. 66).

7.4 Cable connection assembly

To create the cable mesh, up to six steel cables or bars need to be connected at each node. As this connection serves to attach the glass tube beams to the node, it needs to be simple to assemble to reduce building times on-site. In addition, this connection needs to be able to join steel rods or cables coming from unique angles for each node. As stated before, one of the design goals is to condense the complex unique geometries to the cast glass node, and use general, repeating elements for

Fig. 66 *Pre-tensioned structural glass dome at the Selimiye mosque*

the remaining structure. Therefore, this central connection should be able to connect cables from varying angles without complicated customised elements. Finally, as it will be visible within the glass element, the aesthetics of the connection should be taken into account.

Two designs for the central node have been proposed, the 'ring' design and the 'bar' design (Fig. 66).

Ring design

For this design, a metal ring is placed at the centre of the node. From the inside of this ring, bolts can be inserted that go outward towards to fasten the beams (Fig. 68). This allows for a fast and simple assembly of the shell on site. To insert the steel ring and the bolts, a cylindrical void is needed in the middle of the node. For the bolts to reach far enough, the diameter of the central ring needs to be at least as large as the distance from the ring to the connection point of the beam.

This design has a few downsides. First of all, it requires a large cavity in the middle of the glass node, which might reduce structural performance. However, instructing the TO process to design around it might very well compensate for this.

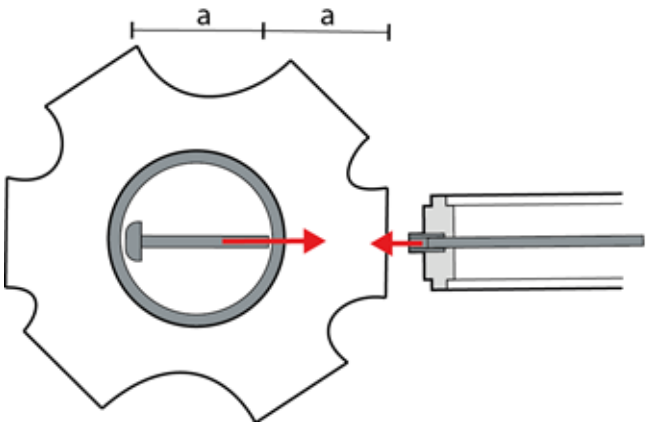

Fig. 68 *Assembly of the ring design*

Additionally, this design limits the changeability of the nodes diameter. Changing between a larger or smaller node, either the ring has to scale with the node, or an oversized ring needs to be chosen. Neither of these is preferable, as it means respectively increasing fabrication complexity or increasing the amount of metal in the node.

Lastly, a way needs to be found to connect the façade cladding to the noce assembly, adding an additional design challenge.

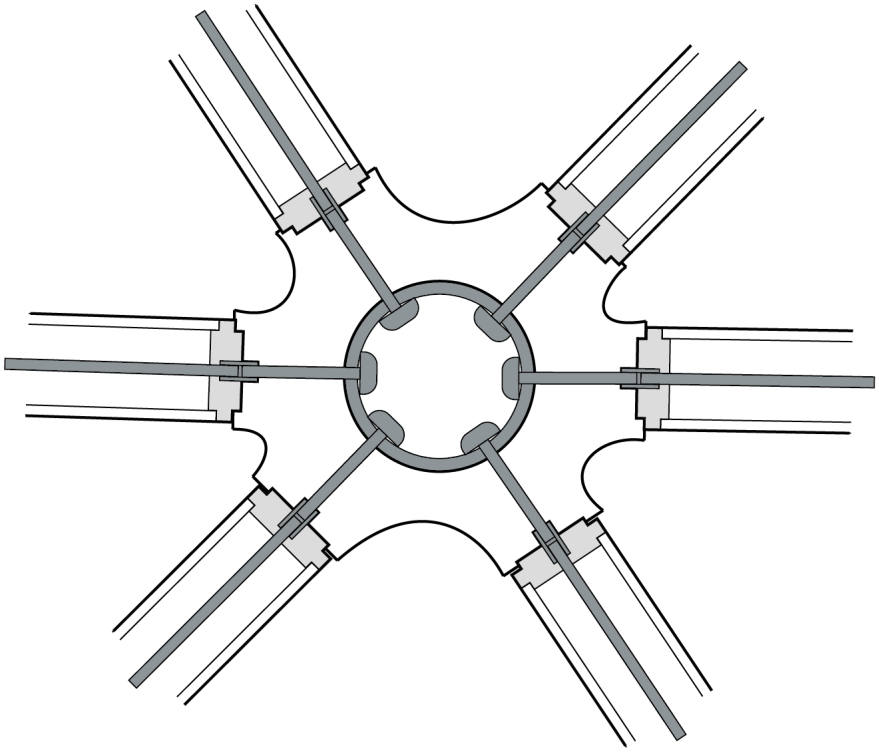

Fig. 67 *Schematic impression of the ring design.*

Bar design

For this design, a metal bar is placed in the centre of the joint, perpendicular to the shells direction. This provides a convenient anchor point for connecting the façade to the node. In the middle of the bar, a connecting plate is placed, with six holes that can serve as an attachment point for the steel cables. These are connected to the ring using a tension fork and a coupling nut (Fig. 69). Most of the metal elements can be added into the node before assembly, reducing assembly time on-site. The central metal plate can easily be fabricated using a waterjet cutter, and can be the same for each node. The remaining elements are all readily available.

This design too has a couple of disadvantages. First of all, the area of the connection between the glass and the metal bar are much smaller than with the ring, bringing with it much higher risk of failure due to local peak stresses. Furthermore, though using only commercially available or simple-to-manufacture elements, many different parts are needed, which makes it more prone to

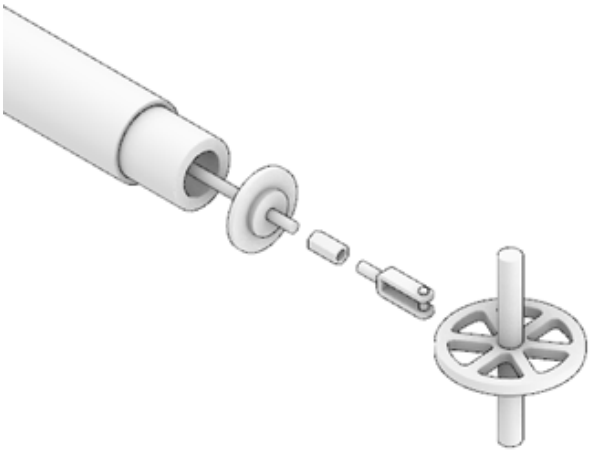

Fig. 69 *Assembly principle of the bar design*

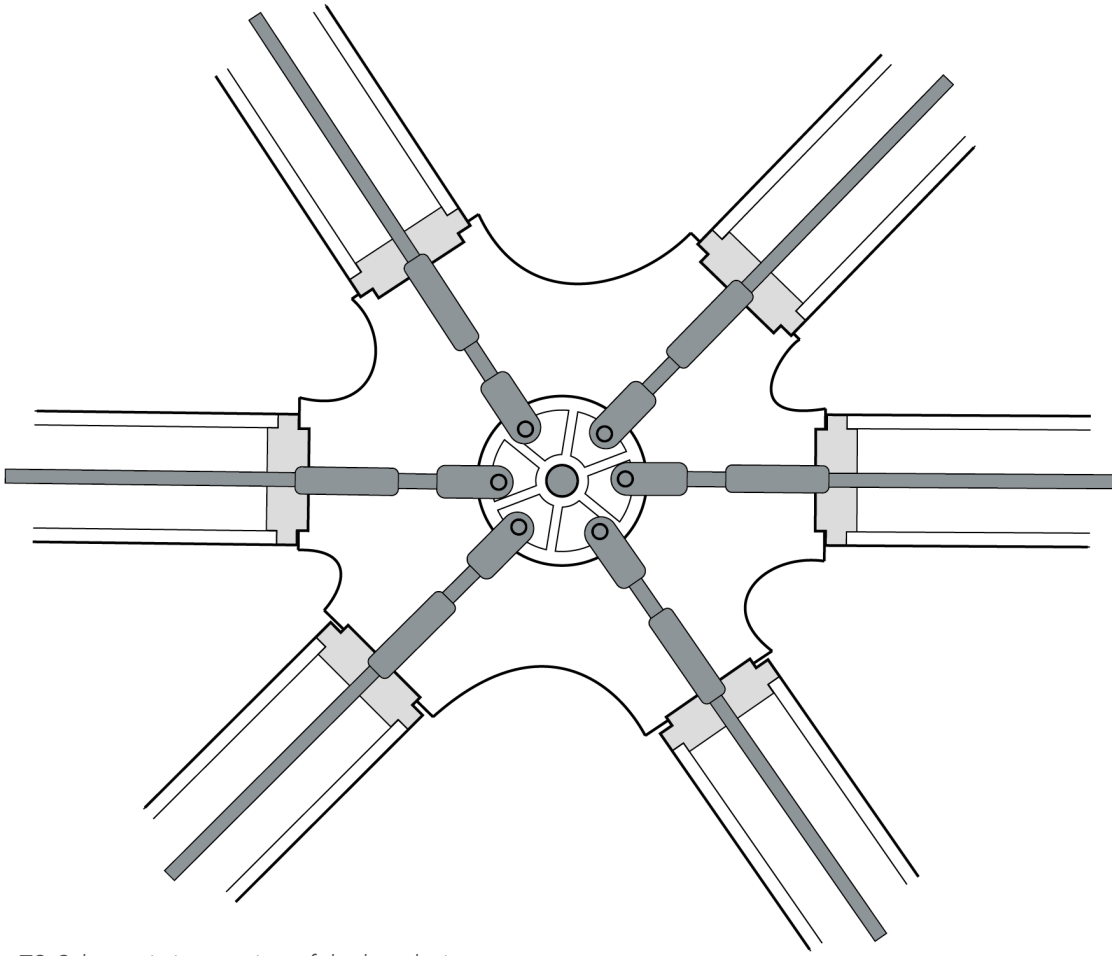

Fig. 70 *Schematic impression of the bar design.*

mistakes and complication during assembly.

7.5 Glass pavilion analysis

The redesigned shell using the glass tube assembly has been structurally analysed using Karamba3D. For the beams, a default SCHOTT glass tube profile of 50 mm in diameter with a 9 mm wall thickness was chosen. The properties of the glass used can be seen in Table 2. At its base, the shell has pinned supports, blocking translation but allowing rotation.

The orientation of the local beam axes has been modified. To differentiate between in-plane and out of plane membrane forces and moments, the local Z direction has been set to always be perpendicular to the shell, to analyse out of plane behaviour. The X axis is set in the direction of the beam, for normal forces and torsion. The local Y axis will therefore represent in-plane behaviour in the results (Fig. 71).

Loads

To check the structural performance of the shell, the following loads have been applied. For a small pavilion such as this, the lowest safety category CC1 as determined by the Dutch NEN-norms can be applied. This means an additional safety factor of 1.1 for permanent loads, and 1.35 for changing loads (Nijsse, 2013).

Family	Glass
Young's Modulus [MPa]	63000
In-plane shear modulus [MPa]	26000
Transverse Shear modulus [MPa]	26000
Density [kg/m³]	2240
Yield strength [MPa]	200

Table 2 *Material properties of the glass used for the structural analysis of the shell*

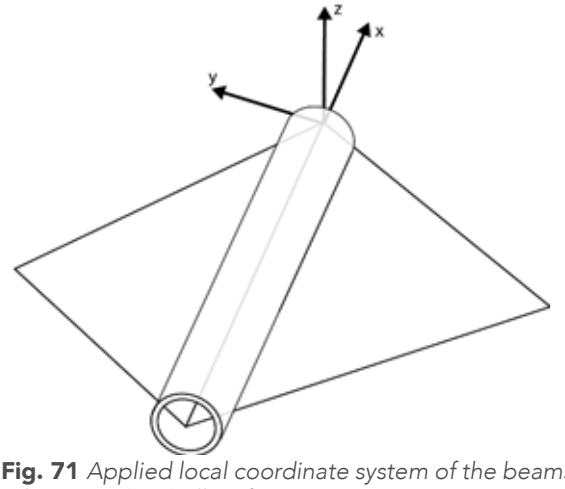

Fig. 71 *Applied local coordinate system of the beams in relation to the shell surface*

The dead load of the structure is applied. This consists of the gravity load of the chosen beams, and an additional load of 0.5 kN/m2 to account for the weight of the glass covering and the various elements used for assembly. The area for which the additional load is calculated is a mesh of the shell, with the resulting loads being transferred to the nearest nodes. This ensures that a node will be loaded more if it supports a larger piece of the shell covering. A 1.1 safety factor is used for these loads.

For the the snow load, a base load of 0.7 kN/m2 is taken, which is the general value used in the Netherlands. This load can be reduced depending on how steep each panel of the shell is, using the following formula.

$$Fsnow = 0.7 \times \mu 1$$

$$0° \leq \alpha \leq 30° \quad \mu 1 = 0.8$$

$$30° < \alpha < 60° \quad \mu 1 = 0.8 \times (60 - a) / 30$$

$$a \geq 60° \quad \mu 1 = 0.0$$

With α being the angle of each panel compared to the ground plane. If the panel is at an angle of 30° of smaller, the load is multiplied by 0.8. If the panel is at 60° or steeper, no snow remains and the load is assumed 0. Angles in between are extrapolated linearly (Nijsse, 2013). Just as with the load of the façade covering, the wind load is added as a mesh load and applied to the nodes. A safety factor of 1.35 is used for this snow load.

A wind load of 0.6 kN/m2 was applied. This is the value given for an unsheltered inland Dutch location for structures under 4 m in height. (Nijsse, 2013) The load is applied to a projected mesh, meaning that a panel that is perpendicular to the wind direction will receive a full wind load, whereas a panel parallel to the wind direction will receive no wind. The wind load is applied on both sides of the shell, to simulate both direct wind pressure and suction on the lee-side. This simulation of the wind is greatly simplified, but is sufficient for the current goals.

Wind angle (°)	No wind	0	60	120	180	240	300
Minimal stress [N/mm2]	-22	-52	-23.3	-33.3	-54.8	-32.4	36.1
Maximum stress [N/mm2]	14.2	38.1	27	15	32.5	25.2	27.4
Maximum displacement [cm]	7.7	18	15	15.6	32	13.8	8.3

Table 3 *Behaviour of the shell under various wind loads*

7.6 Structural results

The analysis was performed using second order theory analysis. Wind loads have been applied with a 30° interval, the resulting axial stresses in the beams, and maximum deflection can be seen in Table 3. It can be seen that wind has a large influence in the behaviour of this shell, adding significant stress and deformation to the structure.

The compressive stresses are within limits of what glass can carry, and the deflections are acceptable. The tensile forces indicated here are too high to be carried by glass. However, these results are an approximation. In practice, the tensile stresses will not be carried by the glass tubes, but by the steel rod inside, likely changing the compression/tension ratio of the results. Furthermore, it is found that the indicated stresses are mainly peak stresses, found along the inner corner of the shell where the mesh was extended. In a detailed materialisation of the shell, this can be taken into account by choosing a larger diameter metal rods, and choosing thicker glass tubes for this area. For the purpose of this project, the current element dimensions are retained.

7.7 Load export

To be used in the ANSYS optimisation, the forces and moments on each node need to be extracted. As Karamba3D shows results per beam, a grasshopper script has been written that identifies all adjacent beams to each node, and extracts the forces and moments in these beams. The loads are taken at a distance along the beam equal to the radius of the node, to obtain the correct loads that are transferred to the node at the connection to the beam (Fig. 72). The found forces are exported to a .CSV file, which can be copied into ANSYS.

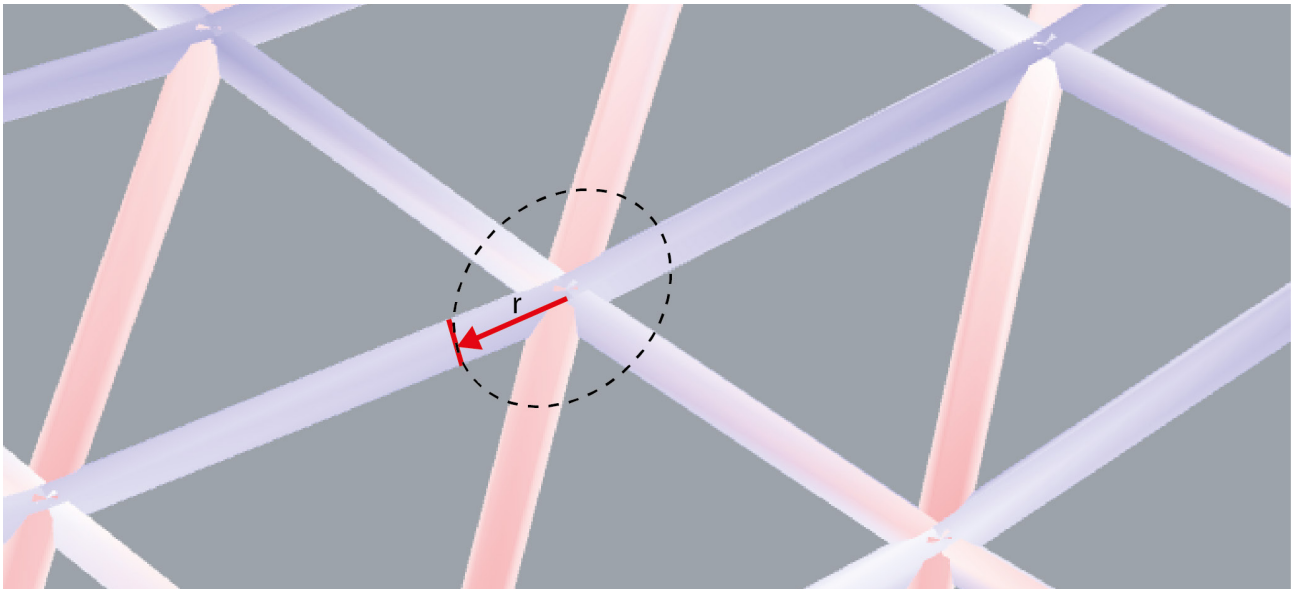

Fig. 72 *The beam loads for the optimisation are selected from Karamba at a distance from the node equal to the radius of the node*

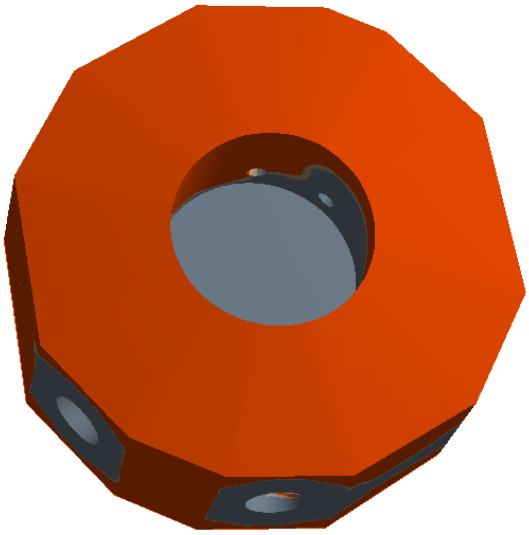
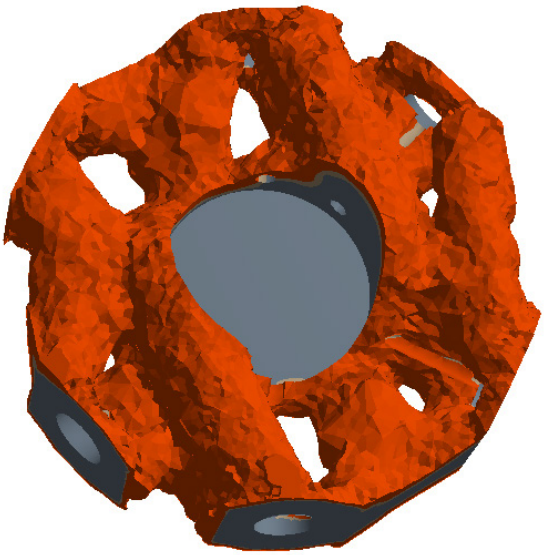

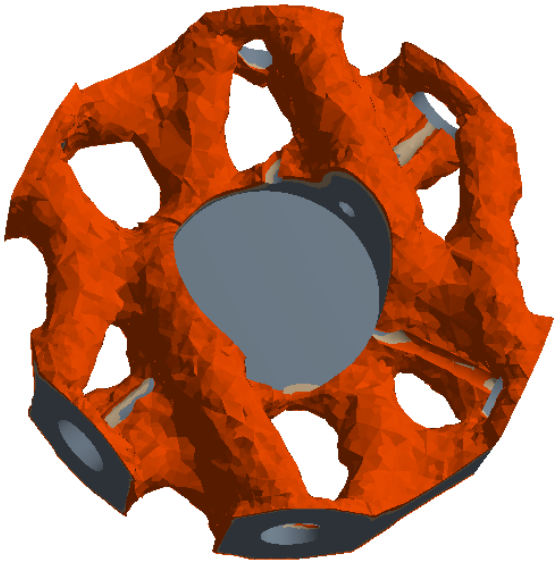
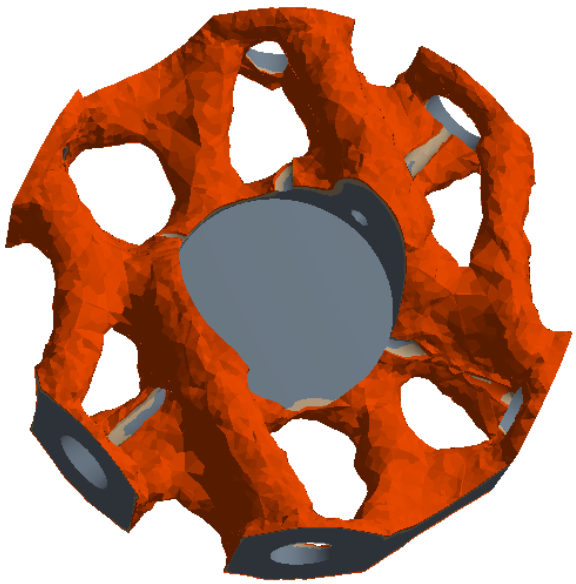
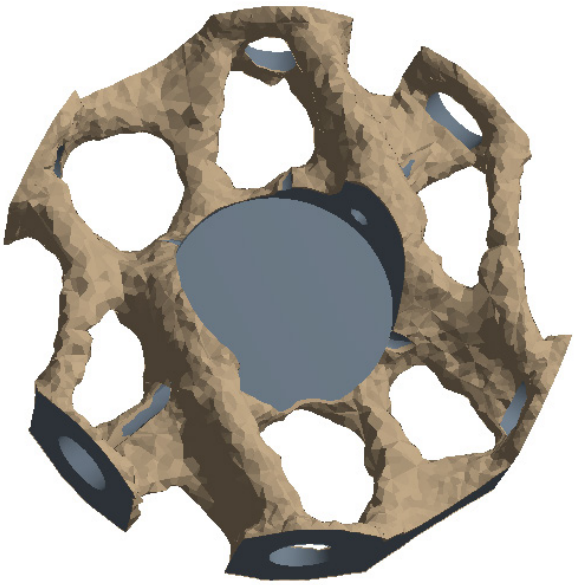

8. Optimisation Methodology

8.1 Design goals

Based on the findings so far, the criteria for the optimised geometry can be formulated. These include both geometrical criteria based on the fabrication process, and structural criteria based on the limitations of the material. These criteria will help define the restrictions and settings of the optimisation process, and allow for clear assessment of the found results.

Designing for cast glass, keeping in mind both the casting and the annealing process, has been discussed in chapter 2.5. Based on that, the following goals can be specified.

Minimising the mass of the element should be the main goal. Apart from reducing material use, keeping the mass of the element low will limit annealing times. Lighter elements are also preferable for on-site construction, making the elements easier to handle.

In addition, each part of the node should have a thickness of at least 15 mm, as thinner elements are estimated to be difficult to cast reliably, and would likely be too fragile for structural applications. In addition, a maximum element thickness of 30 mm has been chosen, as keeping the thickness of the glass limited will help in further reducing cooling times. In addition, limiting the thickness of the element to a 15 to 30 mm range should keep material equally distributed throughout the object.

Sharp corners should be avoided. Within the topology optimisation algorithm this generally happens inherently, as sharp corners result in stress concentration and are therefore avoided. Any sharp corner that remain should be filleted. Based on the bricks used at the Crystal Houses, a minimal fillet radius of 3 mm should be used.

Besides these shape limitations, there are the structural limitations of the material. In tension, a maximum stress of 20 N/mm2 is allowed. In compression, a much higher stress of 200 N/mm2 is deemed acceptable.

At this point, no minimal stiffness requirement is formulated. It is expected that failure due to tensile stress will be the limiting factor in the design.

8.2 Settings and methodology

The optimisations have been performed using a mid-range desktop PC. Its hardware include a i5-6400 2.7 GHz CPU, 8 GB of RAM and a NVIDIA GeForce GTX 970 graphics card.

The following settings for the TO process have been formulated based on the goals stated above (Table 4). As described in chapter 3.3, a compliance-based optimisation is the most suitable when working with a brittle material such as glass. The volume goal indicates the amount of material left in the model after optimisation, for which various values has been tried.

topology optimisation goal	Minimise compliance
Volume goal [%]	15-40
Minimum element size [mm]	15-20
Maximum element size [mm]	30-50

Table 4 *Settings tried for the various optimisations*

For the initial design domain of the node, the smallest possible node for assembly is chosen. Using a grasshopper script, for each node the intersection points between the beams is taken, and the distance from node centre to this point is taken as the radius of the node (Fig. 73). This ensures that each beam can be connected to the node, while using as little material as possible. The height of the node is set at 0.6 times the radius. This was found to generally leave enough space to not limit the TO process, while minimising the volume of the design area. The connections to the surrounding beams are modelled as spring-like elastic supports (Fig. 74).

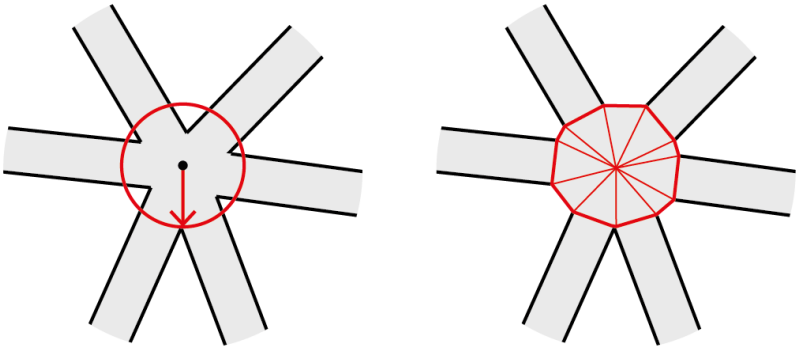

Fig. 73 *Defining the diameter of the node.*

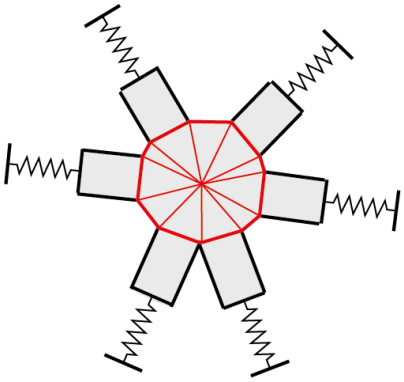

Fig. 74 *Optimisation/FEA setup with connections modelled as elasticsupports.*

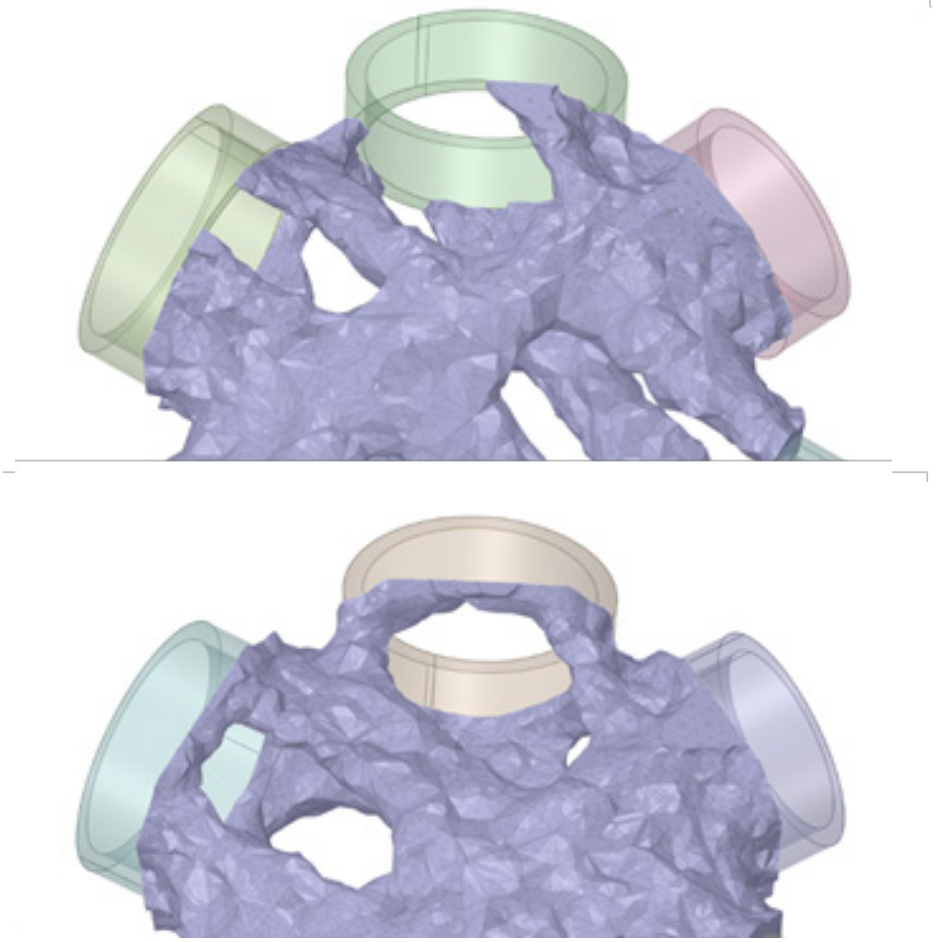

Fig. 75 *Two methods of defining the design area around the beams. Top: all material may be removed. Bottom: a ring of material is retained at the contact area of the beams*

When generating the TO design domain, special care needs to be taken for surfaces where the loads are. Usually the load is applied directly to the design domain, which allows for the removal of material at the contact area of the load. Though more material can be removed this way, it leaves a relatively small contact area for connecting with the remaining structure. Whereas in for example steel this can be remedied by welding this connection, in glass this is not possible. Furthermore, the resulting sharp connections are likely to cause peak stresses in the glass.

It is therefore chosen to exclude the surface area that the load is applied to from the optimisation. This means this surface will be retained in the final model, leading to a smoother transition between beam and node (Fig. 75).

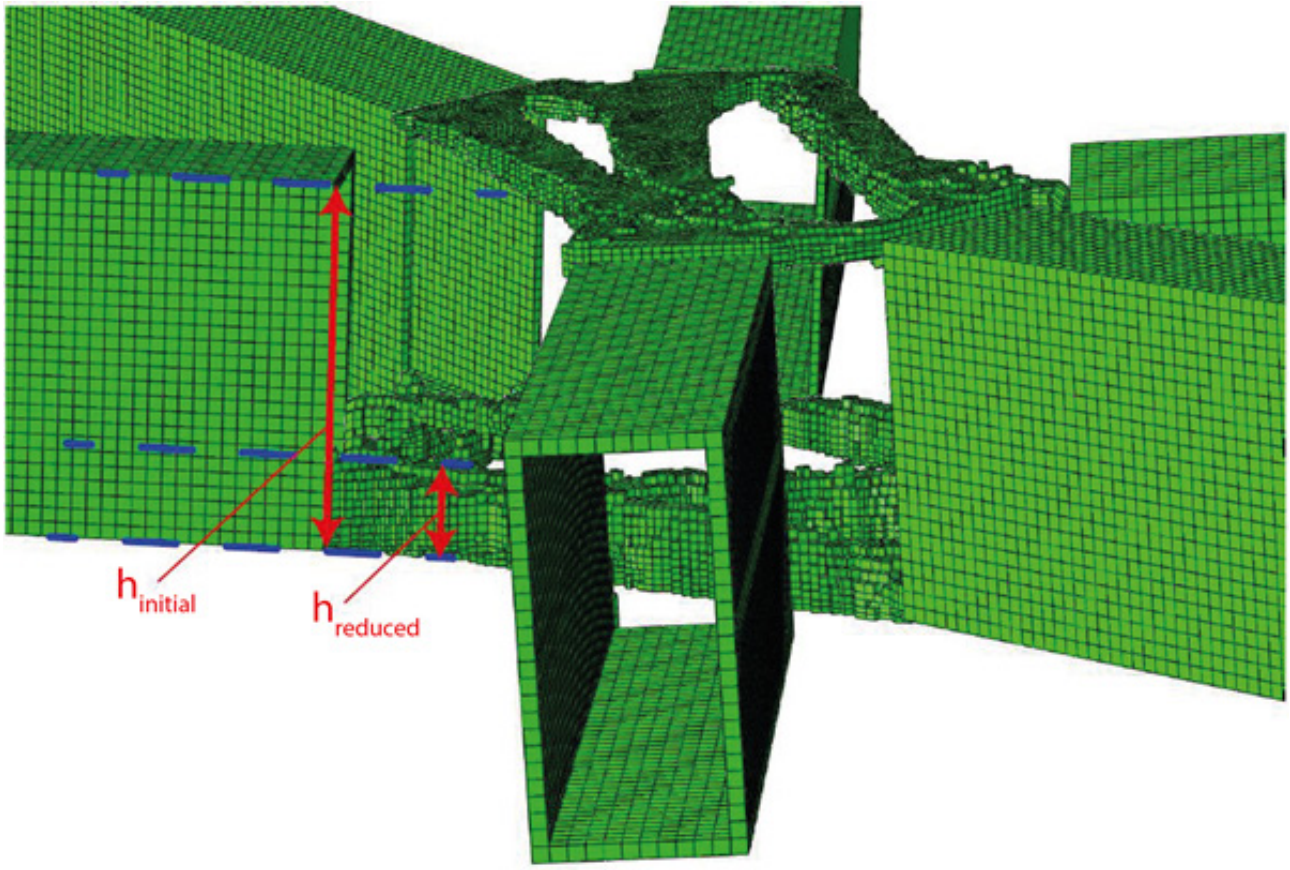

Fig. 76 *Optimised node by van der Linden, 2015. On the right, it can be seen that a fragile connection with reduced height was created under this specific load condition.*

The loads on the shell that are used for the optimisation are based on the different loads that have been described in chapter 6.6. For the optimisation, the self-weight of the shell is used as the main load case. This is the primary load on the node, which needs to be carried under all circumstances.

When optimising for a single load case, there is a risk of creating unstable, over-optimised geometries. In such a case, though capable of withstanding the design load, it lacks the stiffness to properly withstand loads diverging from the main load case. An element designed purely for a dead-load has therefore the risk of failing if an external wind load is placed on the structure. A good example of this is shown in van der Linden, 2015 (Fig. 76.) Here, some connections were found to have greatly reduced and fagile conncection heights compared to the original node height. This was solved by adding additional bending moments to each beam during optimisation, giving the beam a minimal stiffness, sufficient to withstand snow- and wind loads.

In this project, this will be attempted by adding an additional, compressive normal force. Using both the ring and the bar design, reversed tensile loads are added at the central metal element, to simulate any tensile loads on those components that might be expected, while also balancing out the added compressive loads.

In addition, alternatively a pre-stress load obtained from the steel cable mesh will applied, to see whether this results in structurally sound geometries.

8.3 ANSYS

ANSYS Workbench has been chosen for the topology optimisation. Workbench offers various components for different functions, such as Acoustics or Thermal-electric analysis. In this case, the Static structural and the Topology optimisation components will be used.

First, the base geometry is set up and analysed in a structural static component. This includes importing the geometry, applying material properties, defining the connections between the different elements in the geometry and meshing the geometry. After this, the results of the un-optimised element can be fed into a topology optimisation system. Here, the boundary conditions of the optimisation are set: the design domain, the optimisation goal and optional limitations are set. Loads, mesh and material settings are retained from the structural static component. The resulting mesh is then placed into a new static structural element, where it can be cleaned and smoothed into a useful geometry. This cleaned geometry can then be analysed in a new structural static analysis system. The ANSYS workflow is summarised in Fig. 77.

Two materials have been used: structural S235 steel, and float glass. The properties used for these materials can be found in Table 5.

Material	*Glass*	*Steel*
Density	2240	7850
Young's Modulus [MPa]	63000	200000
Poisson's Ratio	0.22	0.3
Bulk Modulus[1] [MPa]	37500	167000
Shear Modulus[1] [MPa]	25820	769200
Tensile Yield strength[2] [MPa]	20	235
Compressive Yield strength[2] [MPa]	200	235

1: Derived from Young's Modulus
2: Not used during TO

Table 5 *Materials used for the ANSYS structural analysis and optimisation*

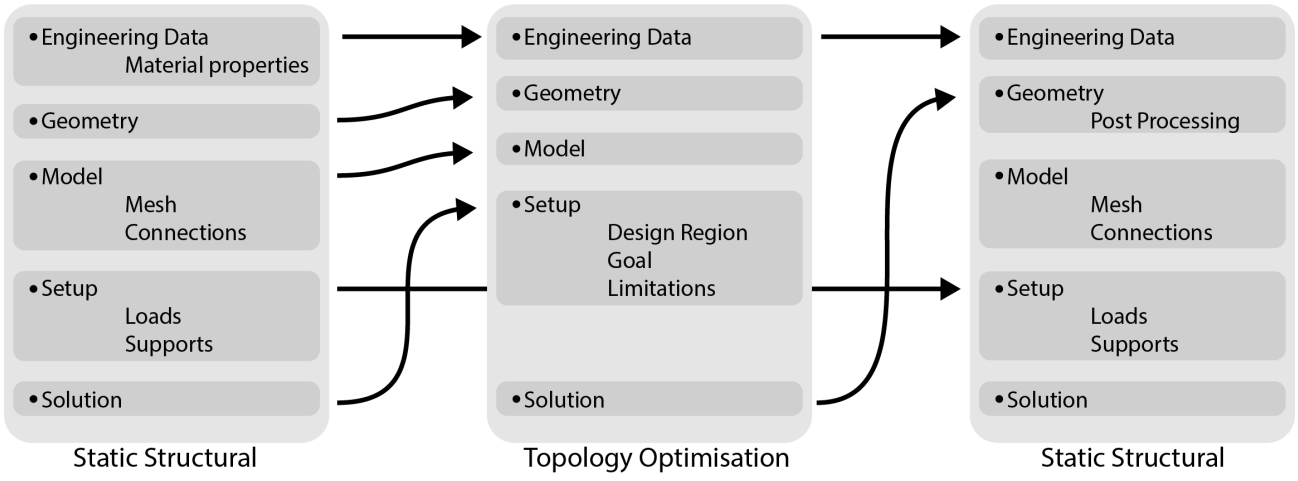

Fig. 77 *Ansys workbench topology optimisation and structural analysis workflow*

8.4 Geometry-post processing

The output mesh from the TO process is very rough, and often contains invalid and unusable mesh elements. A couple of steps need to be taken before further analysis and fabrication is possible. The program SpaceClaim, now included within ANSYS, offers useful tools for post processing geometries.First of all, the shrink-wrapoption offers a useful tool to regularise and smoothen the mesh. As the name implies, it functions by draping a triangle mesh around the entire object. The fineness of this mesh determines the amount of detail in the final model. Using a sufficientlylarge mesh, small bumps and missing mesh elements can be bridged. Where needed, manually drawn elements can be added to the geometry before wrapping, to fill gaps or add material where needed.

Spaceclaim further offers a mesh smoothing tool. This includes approximate and locals moothing. Approximate smoothing inserts additional mesh elements to reduce sharp angles in the model. Local smoothing deforms the existing mesh to remove sharp edges over a certain angle threshold. For this project, local smoothing was primarilly used

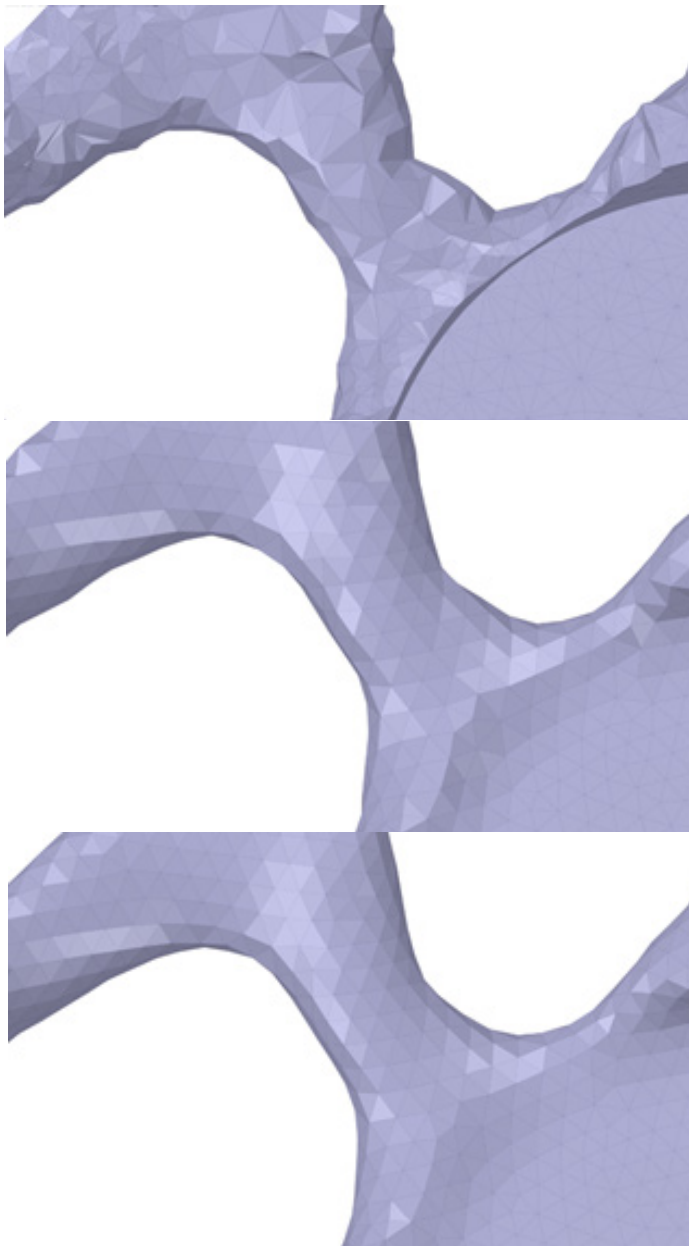

Fig. 78 *Mesh post-processing using Spaceclaim. Top: initial optimised geometry. Middle: Shrink-wrapped geometry. Bottom: shrink-wrapped geometry after smoothing*

9. Optimisation results

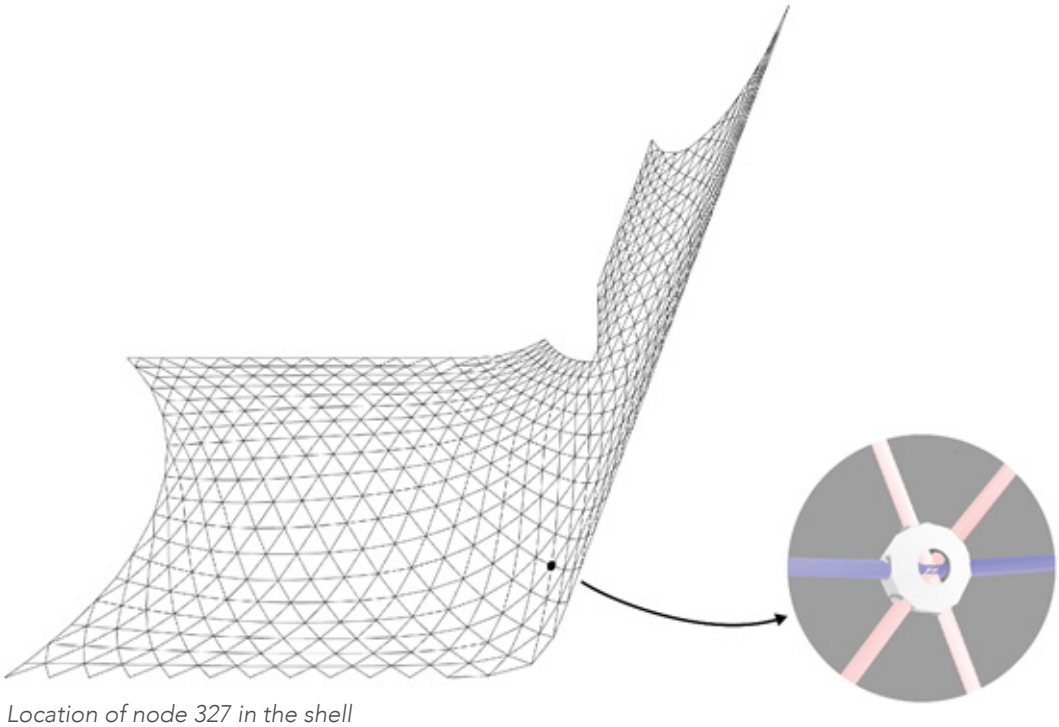

Fig. 79 *Location of node 327 in the shell*

9.1 First iteration

Ring Model

For the first optimisations, node 327 was chosen, indicated in Fig. 79. This node was chosen as it receives a great variety of loads under self-loading: two beams are subjected to high axial compression, two beams receive low compression and two beams are loaded in tension. The loads applied can be found in Table A1-Table A2 in appendix A.

In the design area, a cylindrical void is left open in the centre of the node, in which the metal ring is placed. Between the ring and the beams, voids are left for the steel bolts. For this stage, as the chosen node has a diameter of 140 mm, the diameter of the cylindrical void is set at 60 mm to ensure enough room for the length of the bolt.

Fig. 80 shows the first input geometry that was drawn for this node. It consists of the generic node with a cylindrical void at the centre. At this design stage, the ring is extended up to the top edge of the node. The moment loads of each beam are applied at the connection point between beam and node, as are any compressive axial forces. Any tensile axial force is applied at the central ring. The load applied by the façade pressing down on de node is applied at the top of the ring.

The settings of the TO process are minimising compliance, with a volume goal

Fig. 80 *Initial design volume for node 327 for the 'Ring' design*

of 30%. A mesh of 8 mm was used. The final results of this optimisation can be seen in Fig. 81.

One of the limitations of ANSYS TO can be seen here. When modelling connections between different parts for TO, ANSYS allows only fully welded connections, or no connection at all. For this optimisation, the ring is considered fully fastened to the rest of the node. Furthermore, the ring is materialised as being from glass, as fully embedding a steel ring into the node would add unrealistic strength to the node.

This has resulted in thin, branch-like connection spanning out to the central ring (Fig. 82). Though such geometry makes sense in theory from a structural point of view, in practice glass cannot practically be connected like this.

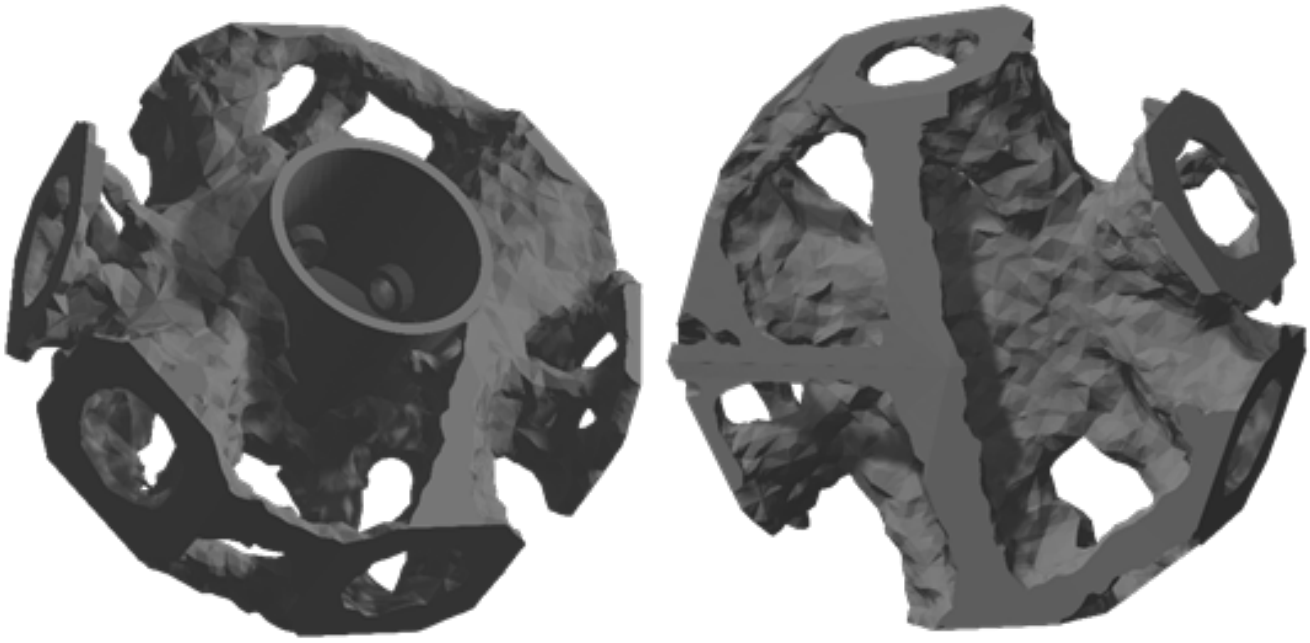

Fig. 81 *Topology optimisation results for the first 'ring' design*

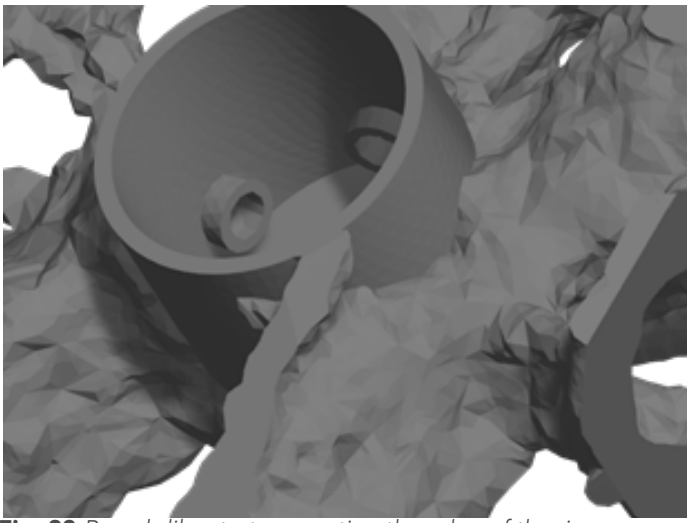

Fig. 82 *Branch-like strut supporting the edge of the ring*

In the following step, the height of the ring is greatly reduced. This has been done mainly for aesthetical reasons, to reduce the amount of unneeded metal in the node. It also simplifies the assembly of the shell, as the bolts to connect the beams can now be inserted much easier. Two optimisation processes were performed, one with the ring materialised as glass, and one as steel (Fig. 83-Fig. 84).

The effect of the connection type, and the material of the ring, can be clearly observed. In the direction of the applied tensile loads, the fully connected steel ring can transfer most of the load, resulting in the total removal of material in this direction. For the weaker glass ring, this effect does not appear.

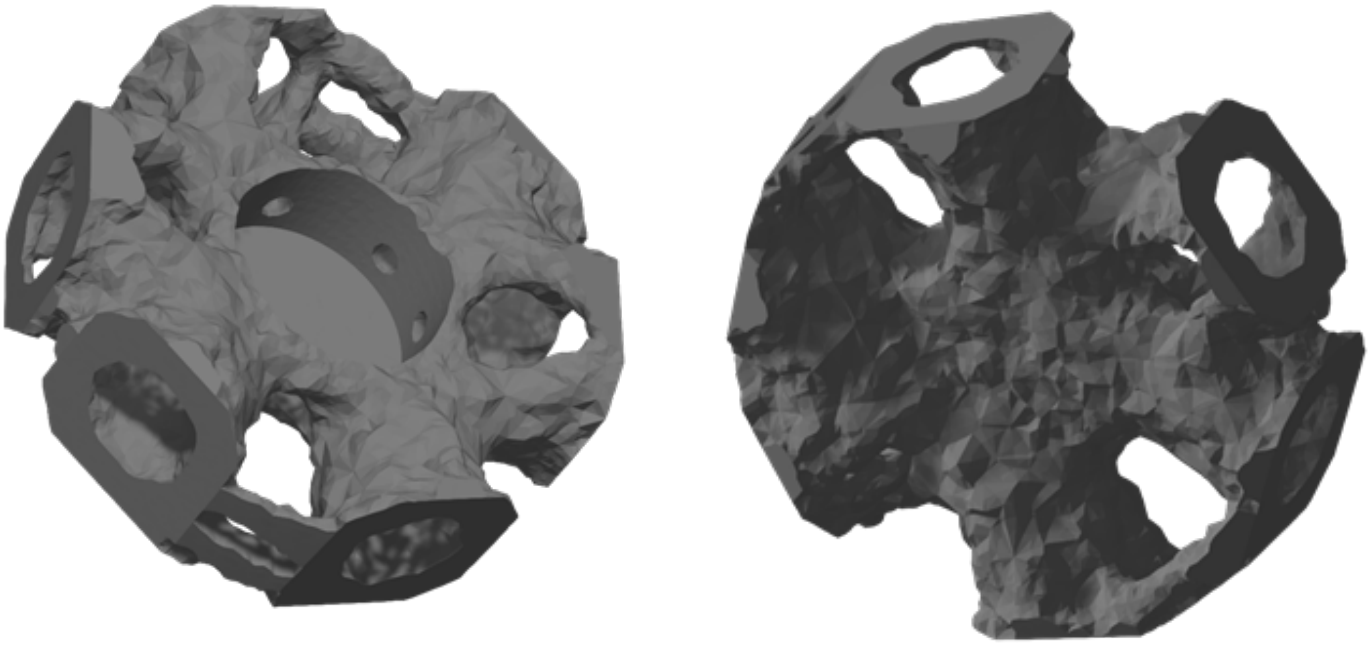

Fig. 83 *Inner ring modelled as glass during optimisation, fully bonded tot the glass node*

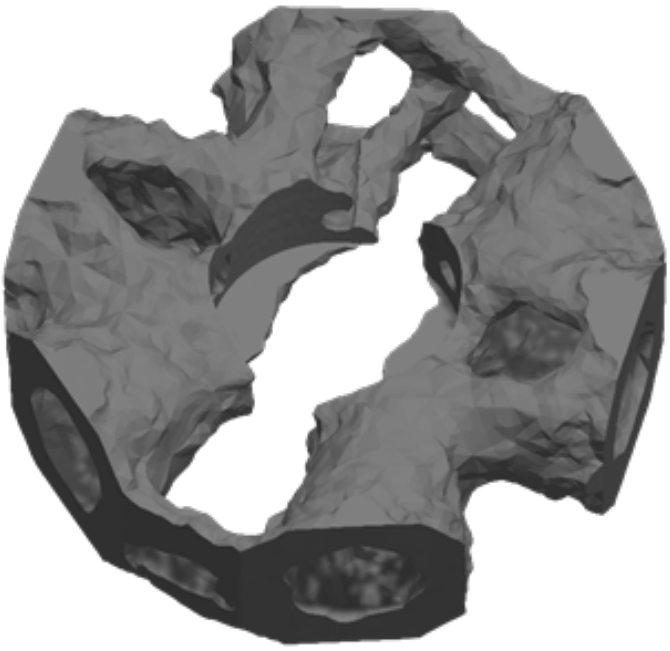

Fig. 84 *Inner ring modelled as steel, fully bonded tot the glass node*

For the next two iterations, the central ring has again been modelled in glass. For the connection, only the bottom surface of the ring was bonded to the glass node. The first optimisation uses the same settings as before, whereas the second has an added fabrication constraint, with an element thickness of between 20 and 50 mm. A fabrication limitation of smaller than 20 mm is found to result in fragmented geometry using the current mesh size (Fig. 85).

As the glass receives much less support at its centre, material is added at the top of the node. This results in a ring-like geometry around the top of the cylindrical void. The manufacturing limitation noticeably increases the thickness of the elements. A 20% to 40% material limit has been used, with the final geometry exceeds by retaining 42.3% of its material. The second node has been shrink-wrapped and smoothed in SpaceClaim (Fig. 86)

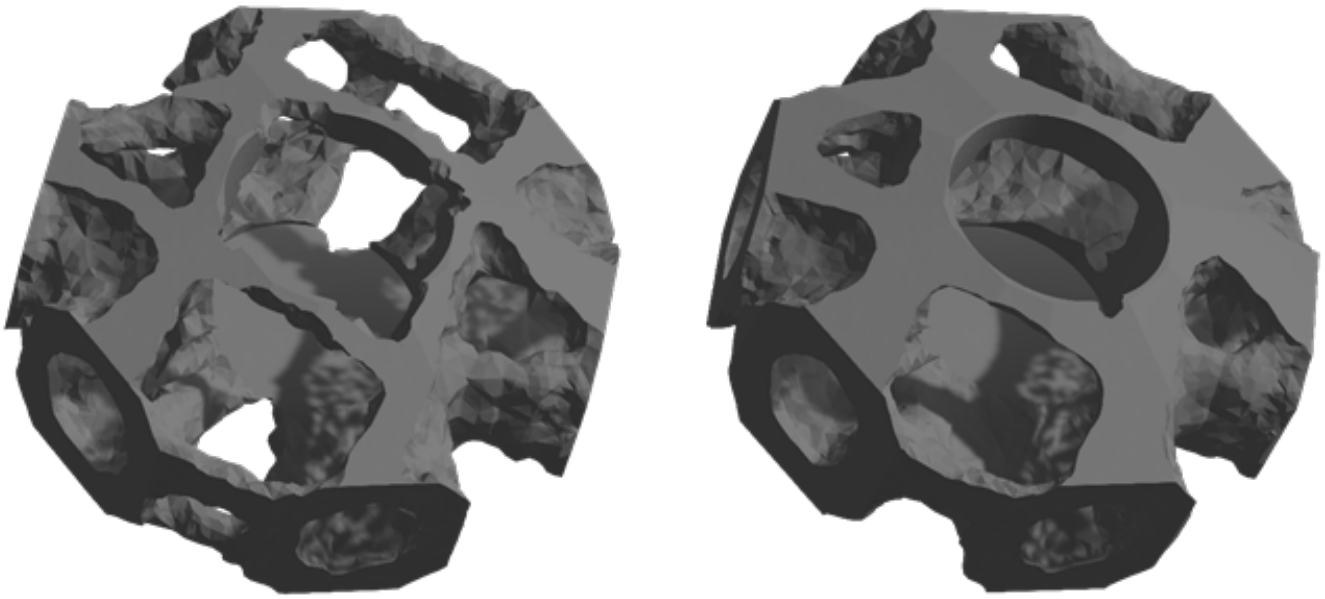

Fig. 85 *Results of central ring bonded to the glass at only its base. Right, a 20 – 50 mm element thickness limitation was added*

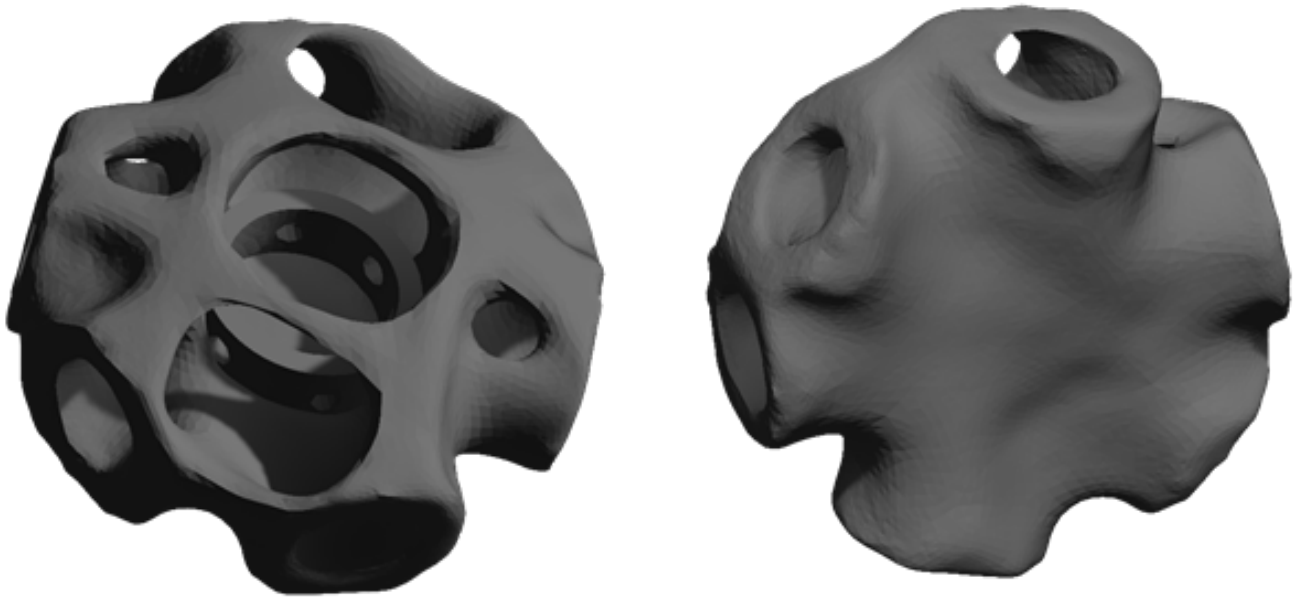

Fig. 86 *Node after shrink-wrapping and smoothing*

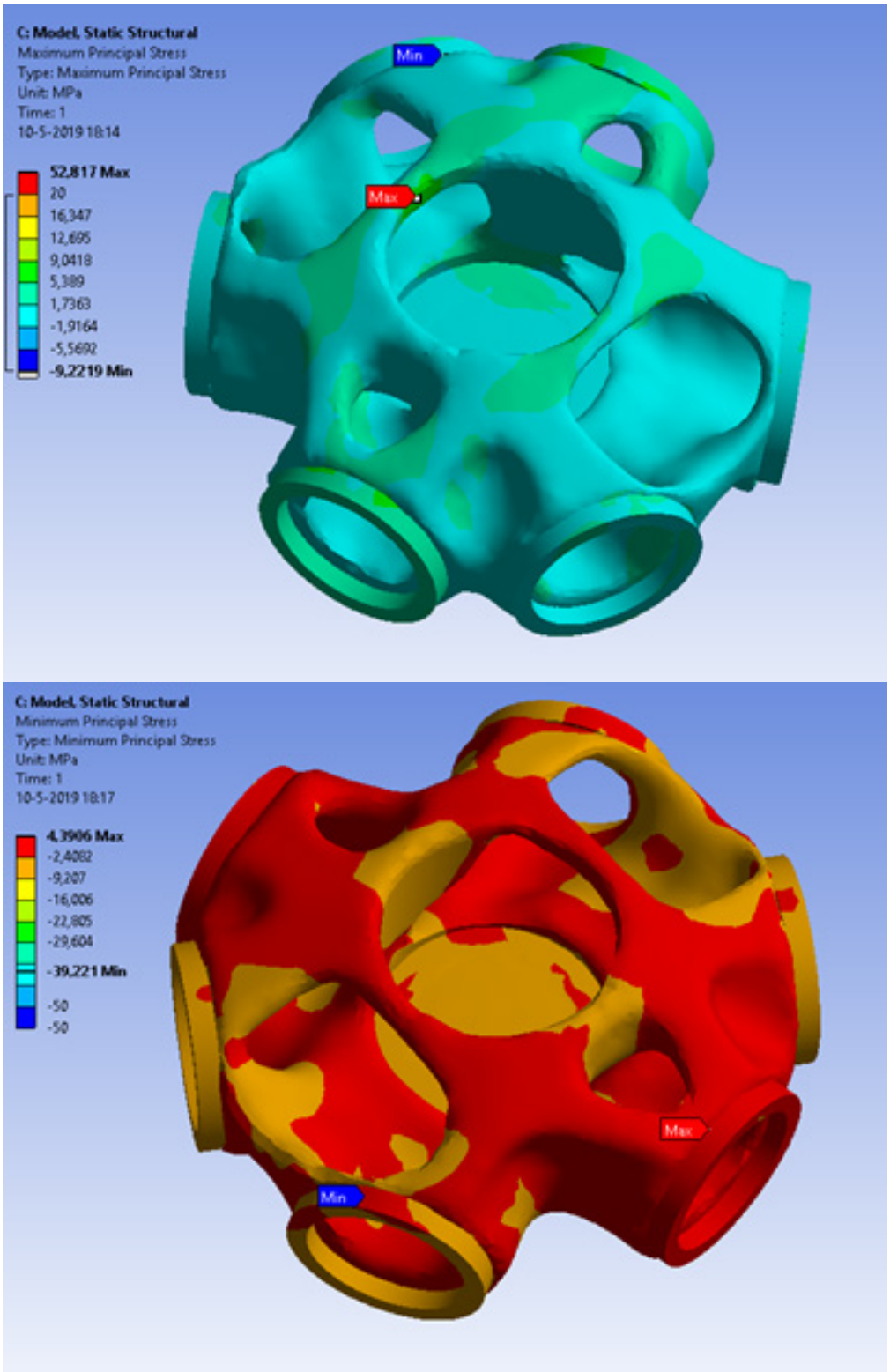

Fig. 87 *Structural static analysis of the smoothened node under optimisation loads. The high stress values in the legend occur in the embedded steel ring which is not shown. Top: principal tensile stresses, Bottom: Principal compressive stresses*

This smoothed geometry was transferred to ANSYS static structural for further analysis. Under the self-weight of the shell, the loads used for optimisation, it is found that neither the compressive nor tensile stresses in the glass exceed 10 N/mm2, which is acceptable (Fig. 87).

Bar model

The second series of optimisations was performed on the 'bar' model, as described before. In the design volume, a couple changes are made (Fig. 88). First of all, a 12 mm diameter bar is placed between the top and bottom point of the node. Along the middle third of the bar, a cylindrical void is placed, where the steel ring element around the bar will be placed.

Due to the size of the assembly connecting this ring to the beams, the diameter of the node has been increased from 140 mm to 220 mm.

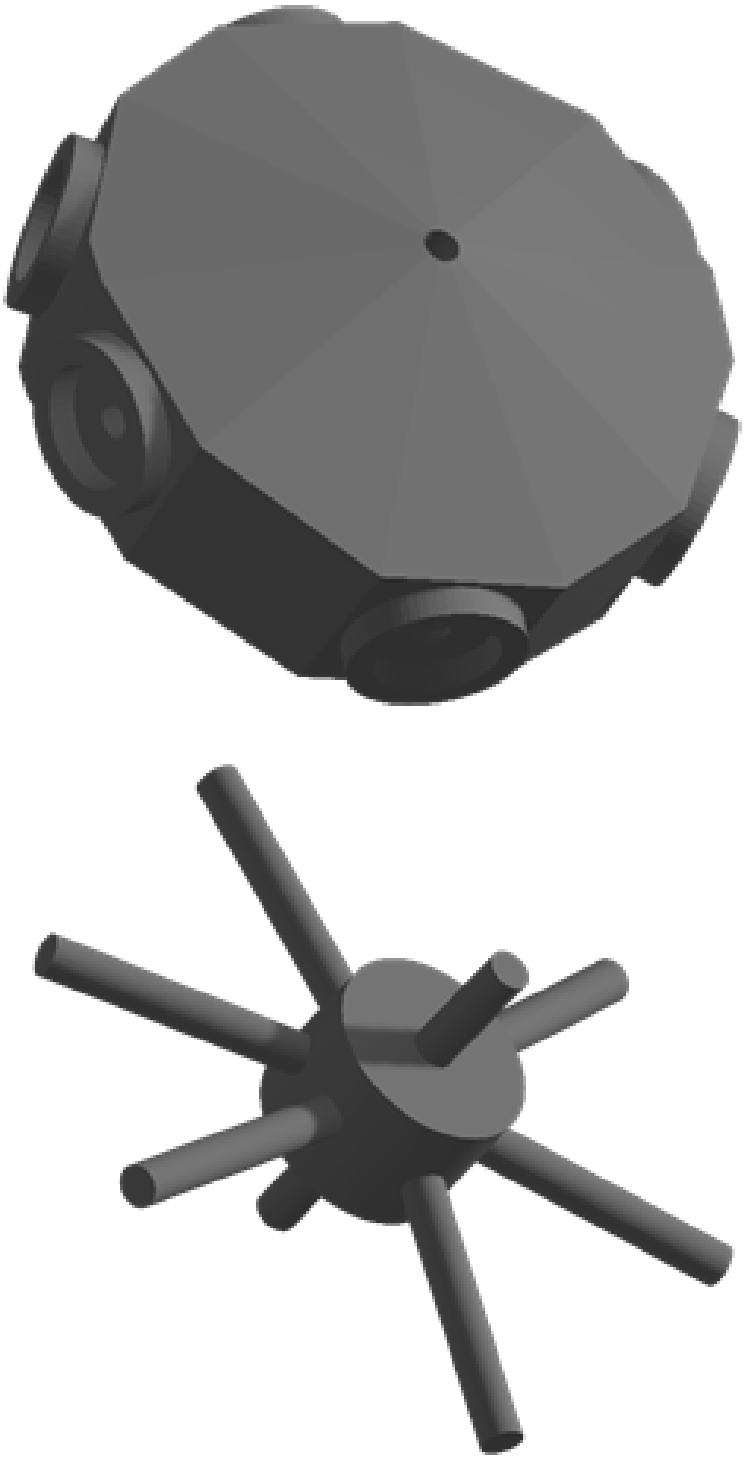

Fig. 88 *Top: Optimisation volume for the 'Bar' design. Bottom: the non-design void within the optimisation volume*

The set goal for these optimisations is maximising compliance, the material volume goal is 25%. Two rounds of optimising were run, respectively using a 20-30mm and a 30-40mm fabrication constraint (Fig. 89-Fig. 90). The same loads as before were used.

A geometry that consists of two, almost fully separated layers is the result. Only at the edges, and at a single point at the centre are the layers connected. The influence of the fabrication constraint is clearly visible. The geometry with the 20-30 mm constraint has much thinner elements; the 30-40 mm constrained geometry has fewer, but noticeably thicker elements.

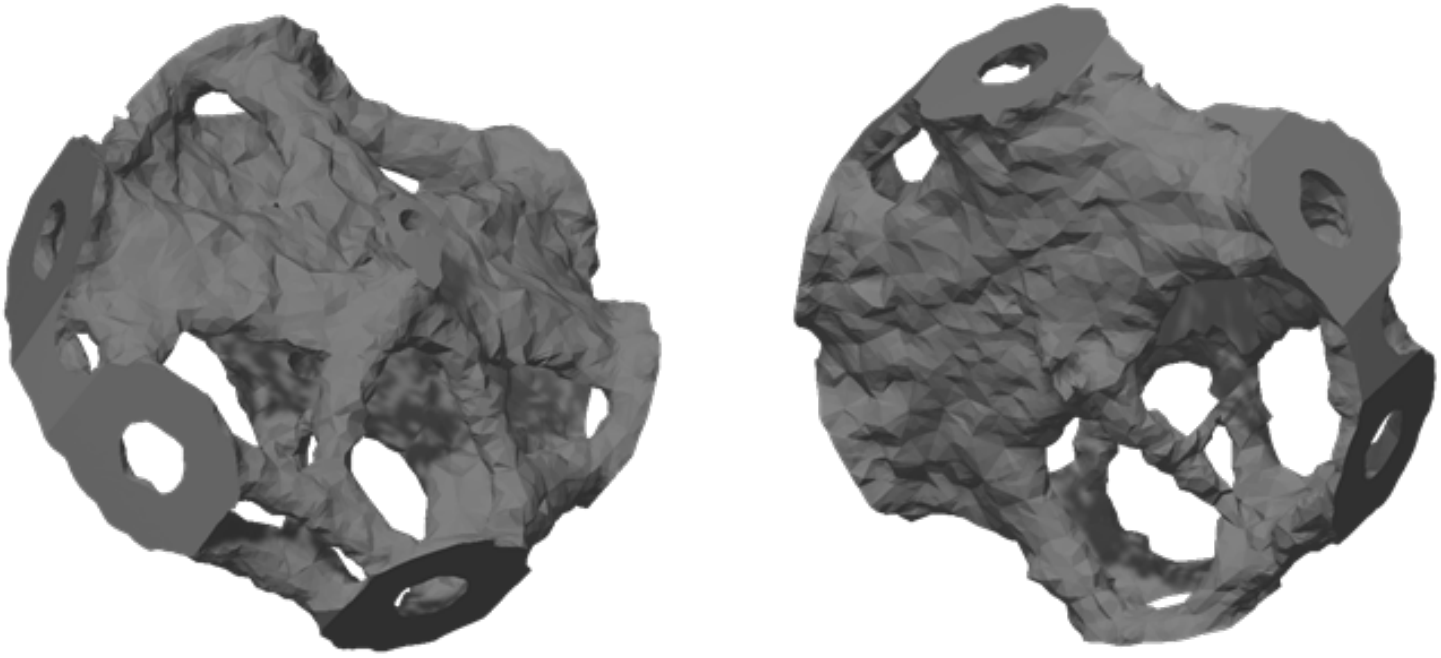

Fig. 89 *Optimisation result of the 'bar' model, with a 20 – 30 mm element thickness limit*

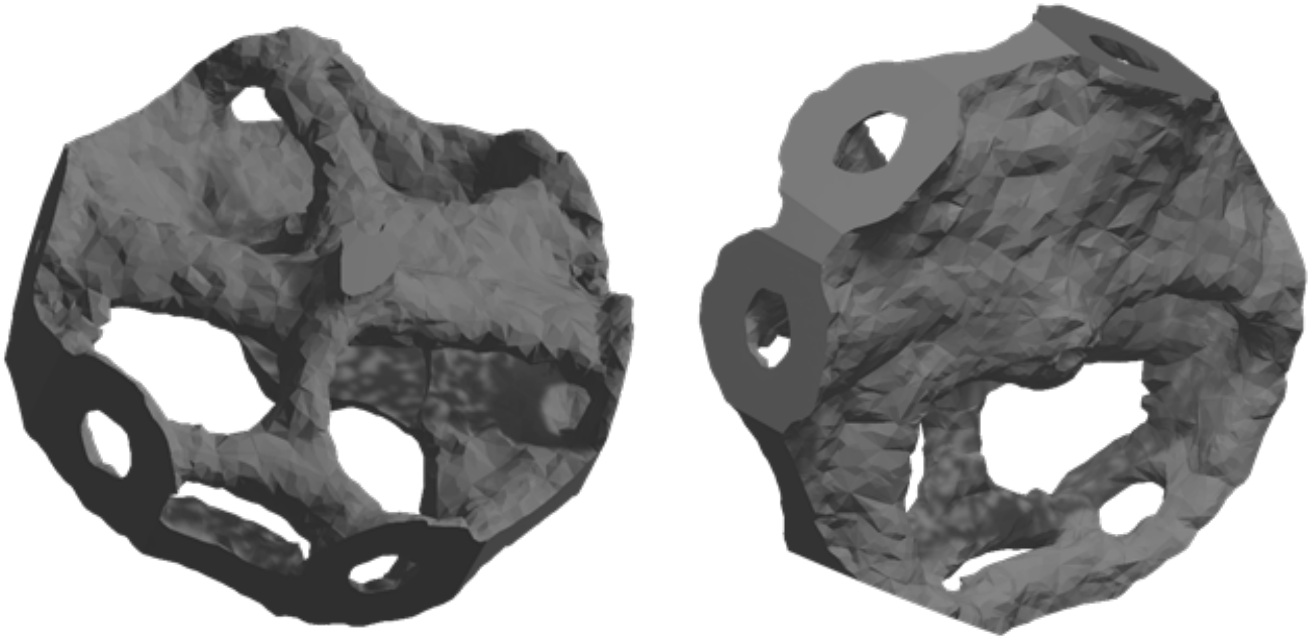

Fig. 90 *Optimisation result of the 'bar' model, with a 30 – 40 mm element thickness limit*

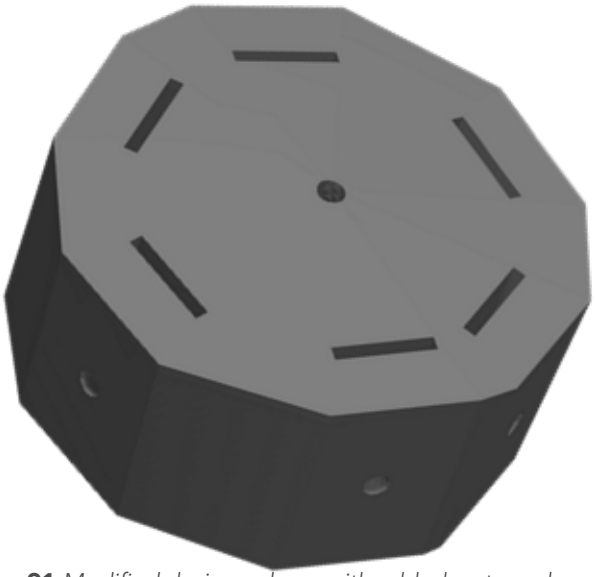

Fig. 91 *Modified design volume with added rectangular voids for assembly, and the resulting optimised geometry*

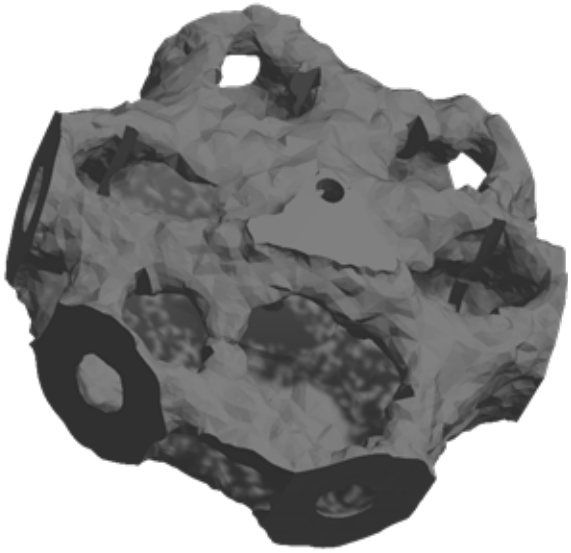

Fig. 92 *Optimisation of the geometry from Fig. 91.*

Fig. 93 *Geometry after shrink-wrapping and smoothing*

To be able to assemble this model, it is required to reach the coupling bolts between the central bar and the beams with a wrench. Within this current geometry, this is not possible for all six connections. The geometry at the top however does seem to generate large openings. A possible solution for assembly is shifting these openings to coincide with the coupling bolts. A new design domain, with rectangular voids that would allow for a wrench to reach the bolts was generated for this. (Fig. 91) A topology optimisation with a 20-30 mm fabrication limitation was used, with a 30% material limitation (Fig. 92-Fig. 93).

It can be seen how the optimisation transfers the loads around these new obstacles and moving the location of the voids. Structural analysis of both optimisations, before and after adding the new voids, shows that the stresses have not noticeably changed by this shift. It shows how well TO performs, even within limited space.

More problematic is the structural behaviour of the connection between the glass and the steel bar (Fig. 94). Even using a fully bonded connection, which is an optimistic assumption, for both models tensile peak stresses of around 125 N/mm2 are found. For glass, this will certainly lead to localised cracks and failure. A better solution is needed if this design is chosen.

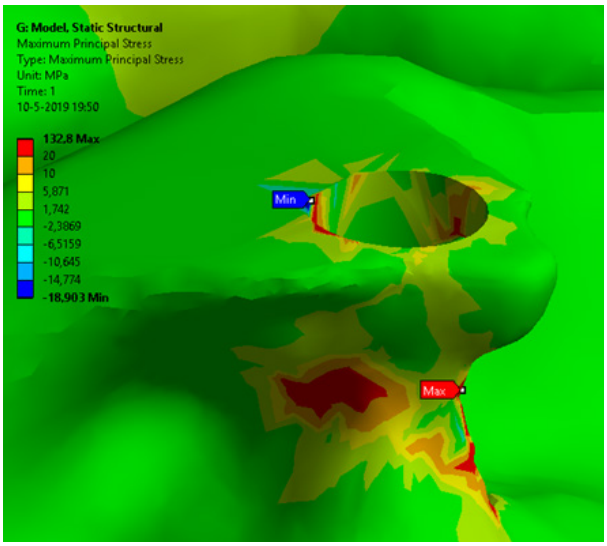

Fig. 94 *Tensile stress concentrations around the metal bar*

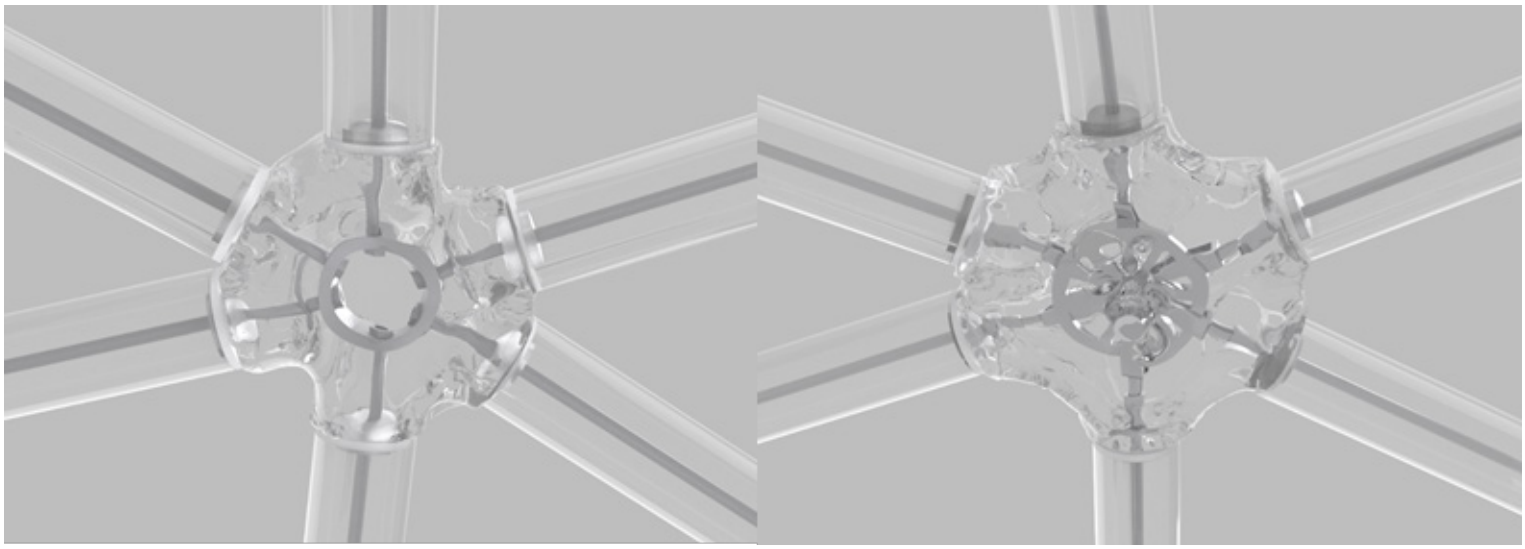

Fig. 95 *Visualisation of the optimised design after assembly. Left: the ring design. Right: the bar design*

9.2 Discussion

Fig. 95 shows an impression of both node assemblies after optimisation. A couple of preliminary conclusions can be drawn from the results so far.

It can be seen that topology optimisation is a powerful tool that is suitable for its task. Material usage is reduced by up to 80% without excessive stresses appearing. Further decreasing the amount of material in the model leads to incomplete, interrupted geometries, as mesh elements are removed that are required to connect different parts of the structure together. Increasing the resolution of the calculation by decreasing the mesh element size will likely improve this, though this will also greatly increase calculation time.

Assembly of the shell will be challenging at this scale. For this pavilion, relatively small nodes could be realised. However, assembling these elements either with either of the connection designs mentioned here before is expected to be difficult. In the ring design, the middle ring is simply too small for a bolt to be inserted and fastened with a wrench (Fig. 96). For the bar model, the size of the node already needed to be increased to fit the connecting elements. Despite this, there is still very little room to make the connections, and no room for inserting the central plate. Thought structurally viable and possible to cast, these nodes are too small from an assembly point of view.

Fig. 96 *Small scale of optimised element makes assembly complicated*

Due to the many different elements used in the bar model, visually it seems to contain a lot of steel. This not only reduces the transparency of the node, but is also fully visible after assembly. The ring design, in this aspect, is deemed much more elegant, though a solution for the middle façade connection is still required.

On aesthetics of glass in general: Cast glass is mostly known for its applications in art, as its transparency and optical qualities make it a very sculptural material. Whereas in a steel grid shell it makes sense to minimise the dimensions of the nodes to make them less visible, glass is not limited by this. Instead, an argument can be made that the node should be larger and visible instead. It can be seen as a functional sculpture, a structural piece of art. The topology optimisation ensures that material use remains low.

9.3 Second iteration

Based on the results of the first results, a second series of optimisations was performed. The ring design has been chosen for further development, based on the previous results. In addition to this, it was chosen to increase the diameter of the node from 140 mm to 240 mm, and to use this as a fixed diameter for all nodes. This ensures that a single size of ring can be used in the entire shell, which simplifies construction, while also giving the structure a more uniform look.

The Grasshopper script generating the loads for optimisation was improved, slightly changing its output. The 1 kN added load on all beams is replaced by a pretension load that is generated by pre-tensioning the steel cable mesh. In Karamba, this is modelled as a 0.5 kN/m^2 distributed mesh load over the entire shell. All loads can be found in Table A3 - Table A4 in Appendix A.

The TO was performed using an 8 mm mesh, a 30 – 50 mm manufacturing constraint and a 20% material limitation. (Fig. 97-Fig. 99) A couple additional elements have been added to the model after optimisation. To ensure a properly distributed load transfer between the steel ring and the glass, a 15mm glass ring and bottom plate have been fused into the geometry. In addition, glass rings have been added to the node/beam connections, as these were too thin for fabrication. (Fig. 98)

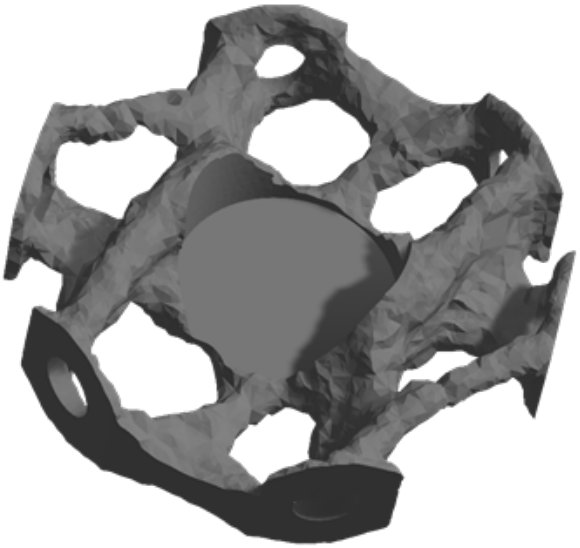

Fig. 97 *Node 327 optimised with a larger diameter*

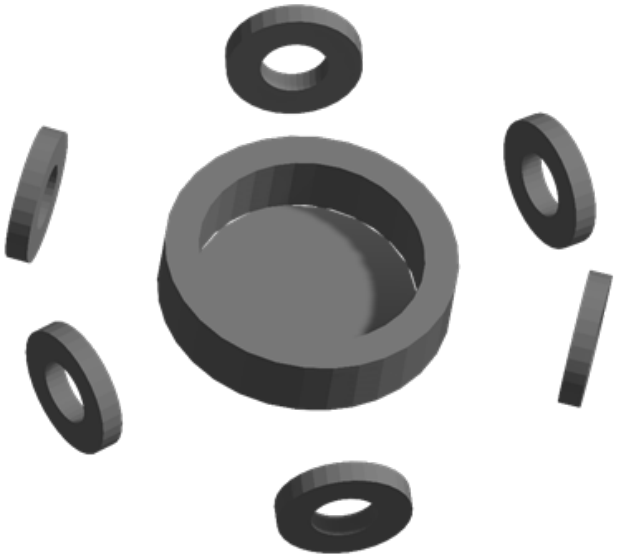

Fig. 98 *Additional elements added before shrink-wrapping to improve structural behaviour and fabrication*

Fig. 99 *Shrink-wrapped and smoothed result*

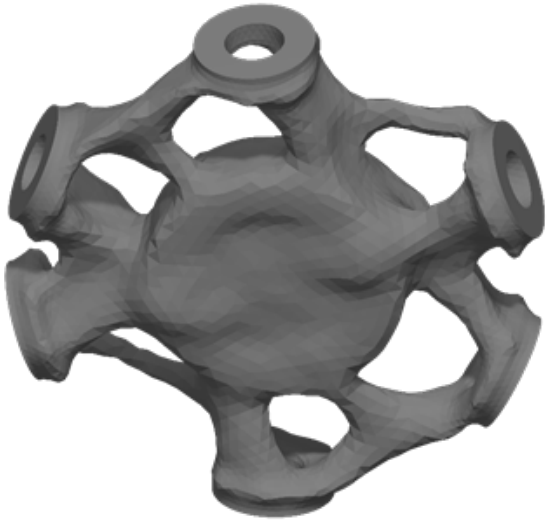

Structural analysis of this element under optimisation loads shows that tensile stresses are low throughout the node, with a couple of areas of higher stress in the added ring. Throughout the node, no stresses exceed the acceptable 20 N/mm^2 (Fig. 100).

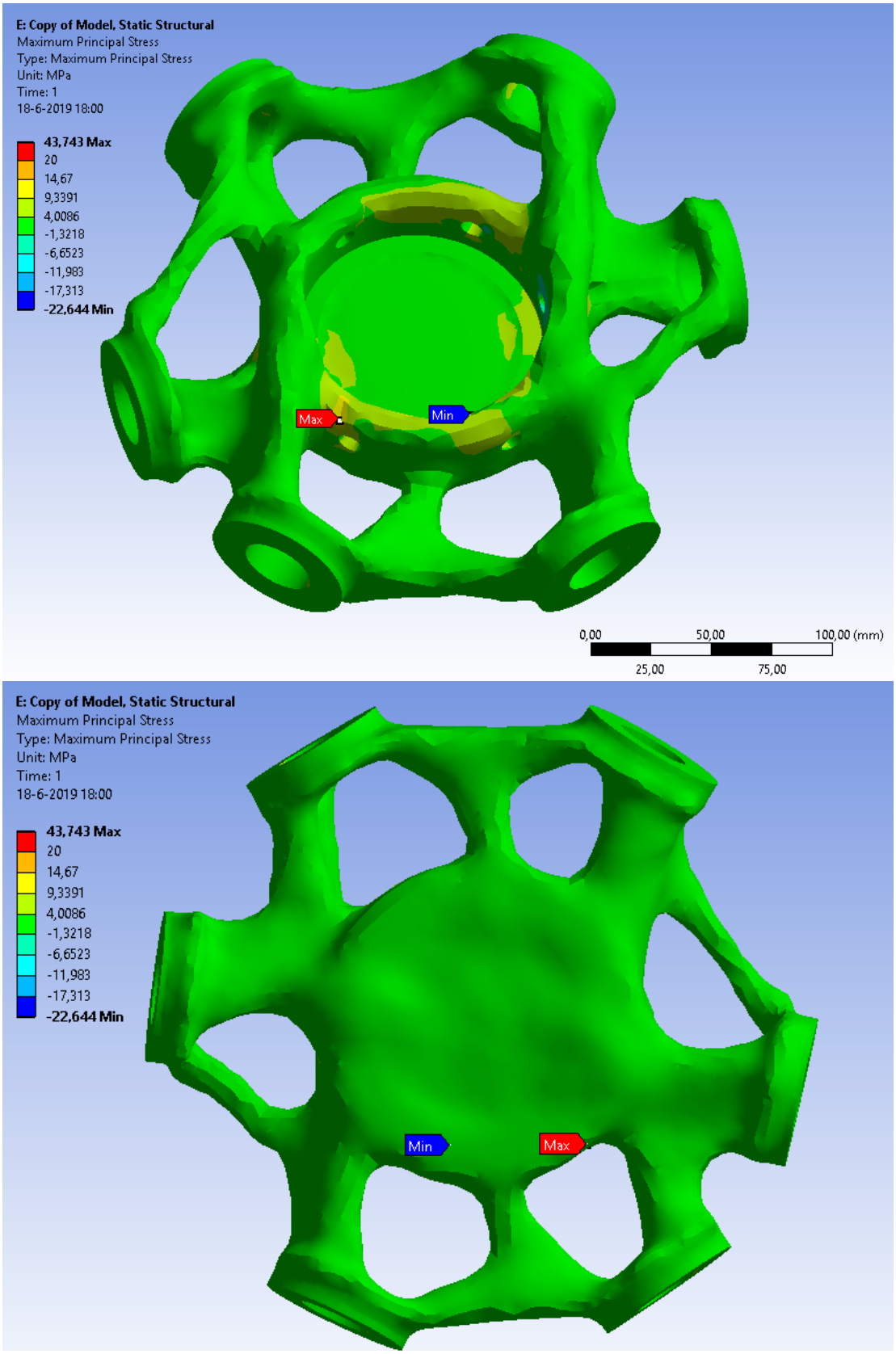

Fig. 100 *Principle tensile stresses in the node under self-weight loading*

To further test the structural behaviour of this node, a wind load is applied. The direction is assumed to be perpendicular to the node, as this is the wind load that exerts the highest loads on the node. The applied loads can be seen in Table A5 in Appendix A.

This leads to noticeably higher stresses throughout the node (Fig. 101). The maximally found tensile stress in the glass is 24 N/mm2, at the outer edge of the added glass ring. This exceeds the allowed stress for glass. The tensile principle stress is found to be close to failure at a couple of more points around the node. Due to the much higher compressive yield strength, no failure due to compression can be seen.

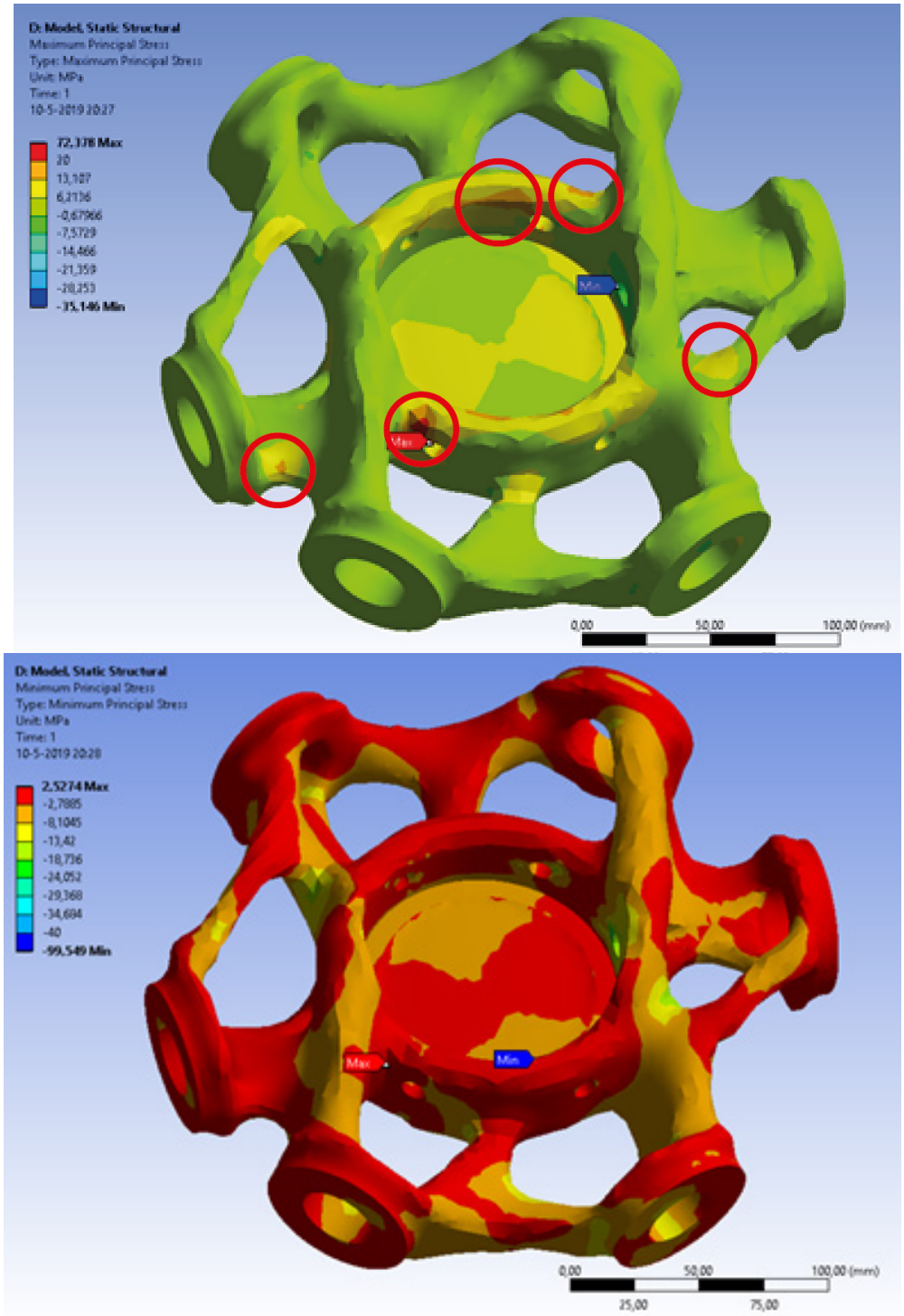

Fig. 101 *Structural analysis under wind load. Left: principle tensile stress, locations of stress concentrations are indicated. Right: principle compressive stress.*

To check if these results are representative for the shell, a different node was optimised using the same methodology. Node 174 was chosen, as it is a typical node at the base of the shell, loaded under heavy compression. (Fig. 102).The loads applied to this node can be found in Table A6 - Table A7 in Appendix A. The resulting geometry is shown in Fig. 103.

Structural analysis using both the form-finding self-load and a wind load has been performed. The wind load perpendicular to this was node, as it causes the highest loads on the node. These loads can be found in Table A11.

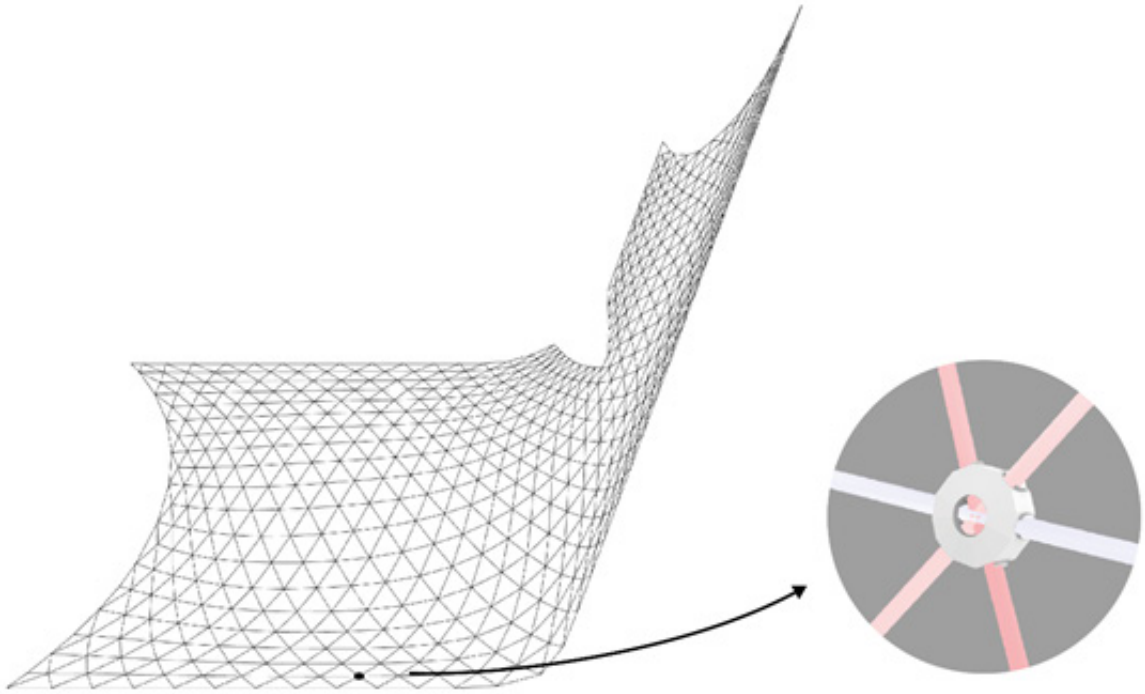

Fig. 102 *Location of node 174 in the shell*

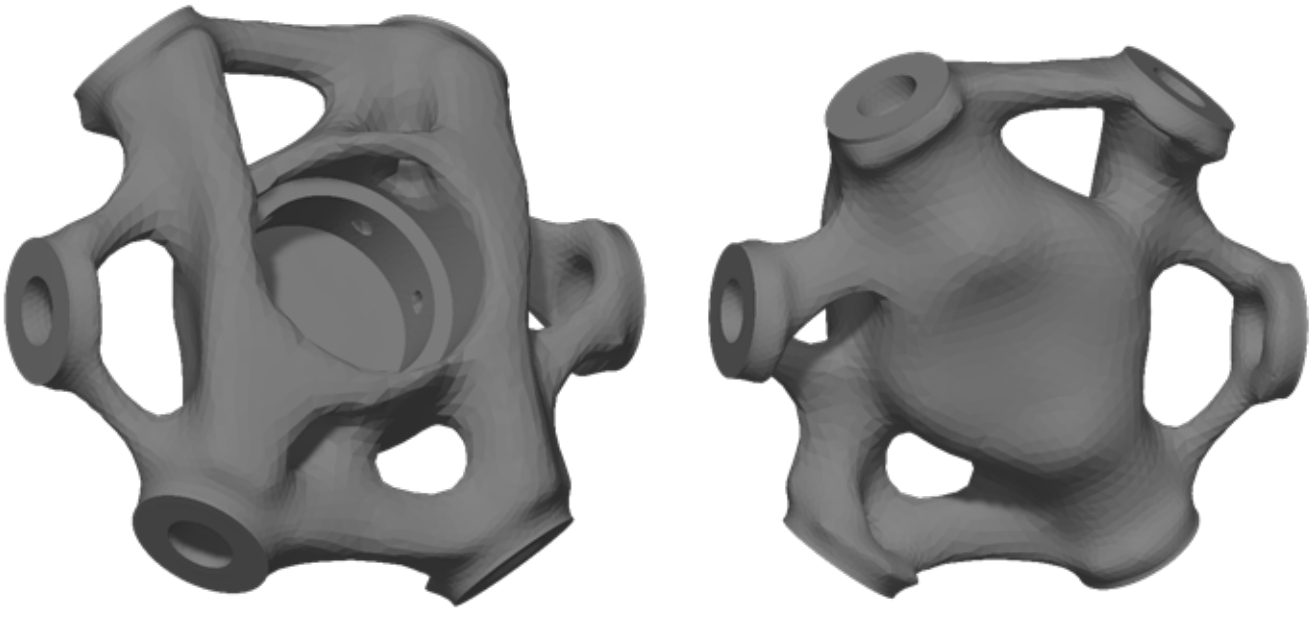

Fig. 103 *Resulting geometry for node 174*

The results are comparable to node 327 (Fig. 104). Under self-weight loading stresses are low, and the node seems over-dimensioned. Once an external wind load is applied, the node fails. At the underside of the node, tensile stresses of up to 45 N/mm2 can be found. Clearly, this design methodology is insufficient to deal with changing loads on the shell.

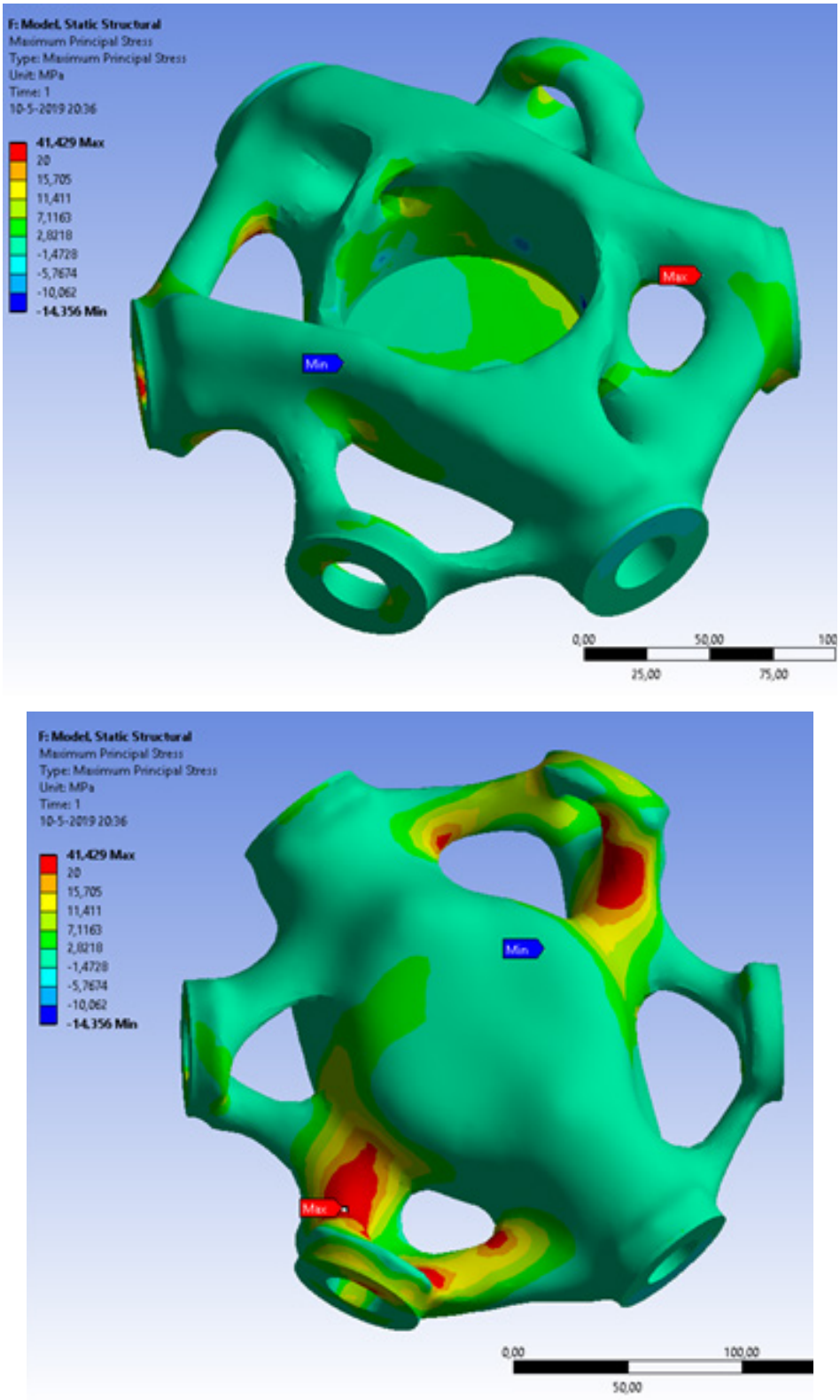

Fig. 104 *Static structural analysis of node 174 under wind loading, principle tensile stresses*

9.4 Discussion

A couple of conclusions can be drawn from the optimisations so far. It has been shown that Topology Optimisation is a powerful design tool, capable of finding material efficient solutions even within highly limited design space. However, this high level of optimisation is also a weakness. Buildings are constantly subjected to changing loads, such as wind loads, and therefore require a certain level of flexibility in their loadbearing structure. Topology optimisation gives optimal solutions for a fixed load case, but becomes unreliable when the loading conditions are uncertain.

Looking at other comparable projects, some possible solutions can be found. In the work of van der Linden, 2015, a grid shell node was designed using topology optimisation for the Złoty Tarasy shopping mall roof (Fig. 105). This is a 100 by 130 m roof, with a total weight of around 1300 tons. The roof structure placed between a series of high-rise buildings, mostly sheltering it from direct wind. Due to this, the variable and changing wind loads are of little influence on the shell, in comparison to its self-weight. The self-weight will therefore always remain the governing loading condition. Under these circumstances, topology optimisation is a viable tool, as there is a clear single load case on the shell that can be optimised for.

In comparison, the SUTD grid shell is a free-standing structure, light-weight in design. This makes it highly susceptible to wind, with forces and moments increasing manifold, or changing direction completely. Under these conditions, topology optimisation is ineffective, as it is simply not clear what to optimise for.

Combining multiple optimised geometries can be a way to deal with this uncertainty. If the changing loadcases can be simplified to a few distinct loads, it is possible to optimise for each of these loads, and merge the resulting geometries. These geometries will not be fully optimal, as intersecting elements is likely to add additional stiffness to the structure, leading to over dimensioning. However, they should ensure resilience against multiple loads.

In his design of a TO gridshell node, Prayudhi (2016) takes a similar approach. He creates a 'standard node', that is strong enough to provide the shell with a base stiffness. On top of this, he adds an optimised geometry to deal with the main loads on the shell. Combined, this results in a node that can efficiently carry the main self-load, while providing sufficient redundancy to withstand changing load cases.

Fig. 105 *Gridshell roof of the Złoty Tarasy shopping mall, case study for van der Linden, 2015*

9.5 Third iteration

Taking into account the conclusions of the previous optimisations, two different variations of the topology optimisation have been tried. First, a design is made by combining two distinct load cases, to investigate what kind of geometry this results in. For the second optimisation, a larger and heavier shell structure is used. This should result in the self-weight of the shell being the governing load-case even when wind loads are applied.

Combined loads

The two distinct load cases used for this optimisation are the self-weight of the shell, and the wind load perpendicular to the node. This is the wind load that causes the highest loads and stresses in the node.

The applied loads can be found in Table A10 - Table A13 in appendix A. The other used settings are an 8 mm mesh size, a compliance-based optimisation goal, a 20 – 50 mm manufacturing constraint and a 15% volume limitation. The resulting geometries are shown in Fig. 106 - Fig. 107. In post-processing, these geometries have been merged, shrink-wrapped and smoothed. Some elements that were deemed too thin for manufacturing have been manually thickened (Fig. 108).

Fig. 106 *Optimisation of node 174 for wind load*

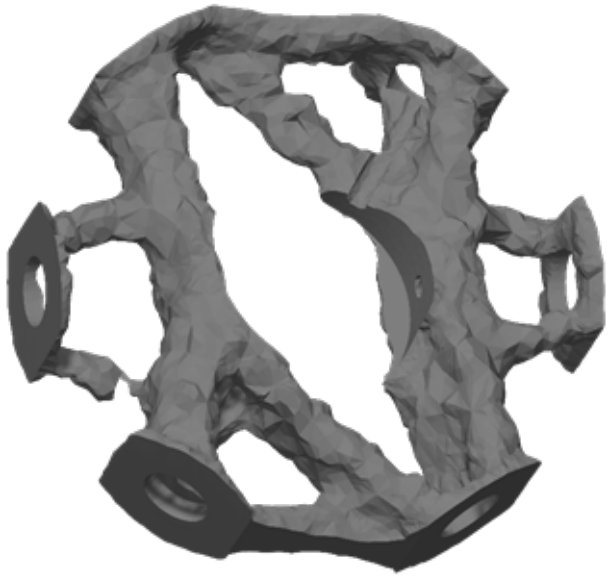

Fig. 107 *Optimisation of node 174 for self weight*

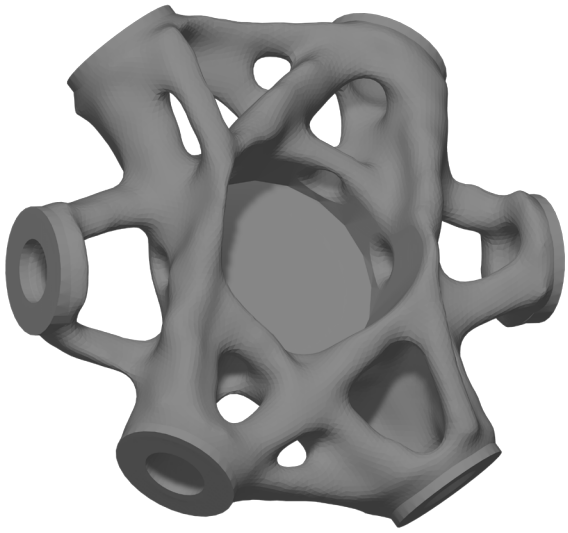

Fig. 108 *Resulting combined optimisation of node 174 for wind and self weight*

This element has been structurally tested with both the optimisation loads, and a wind load from a reversed direction, loading the shell in suction. The results can be seen in Fig. 109-Fig. 110.

As is expected, the element can withstand the design loads with ease. The reversed wind load leads to unacceptable tensile stresses in the structure, showing once again the vulnerability of topologically optimised structures to deal with loads it was not designed for.

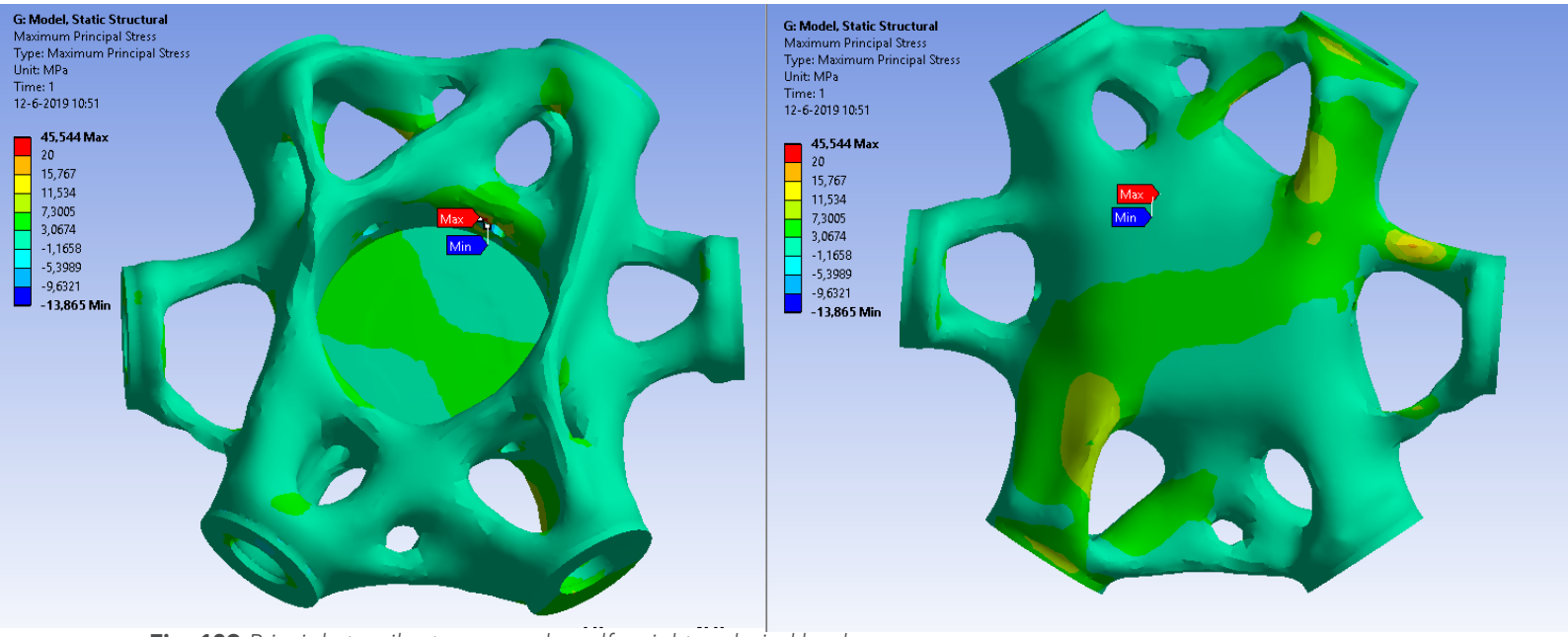

Fig. 109 *Principle tensile stresses under self-weight and wind load*

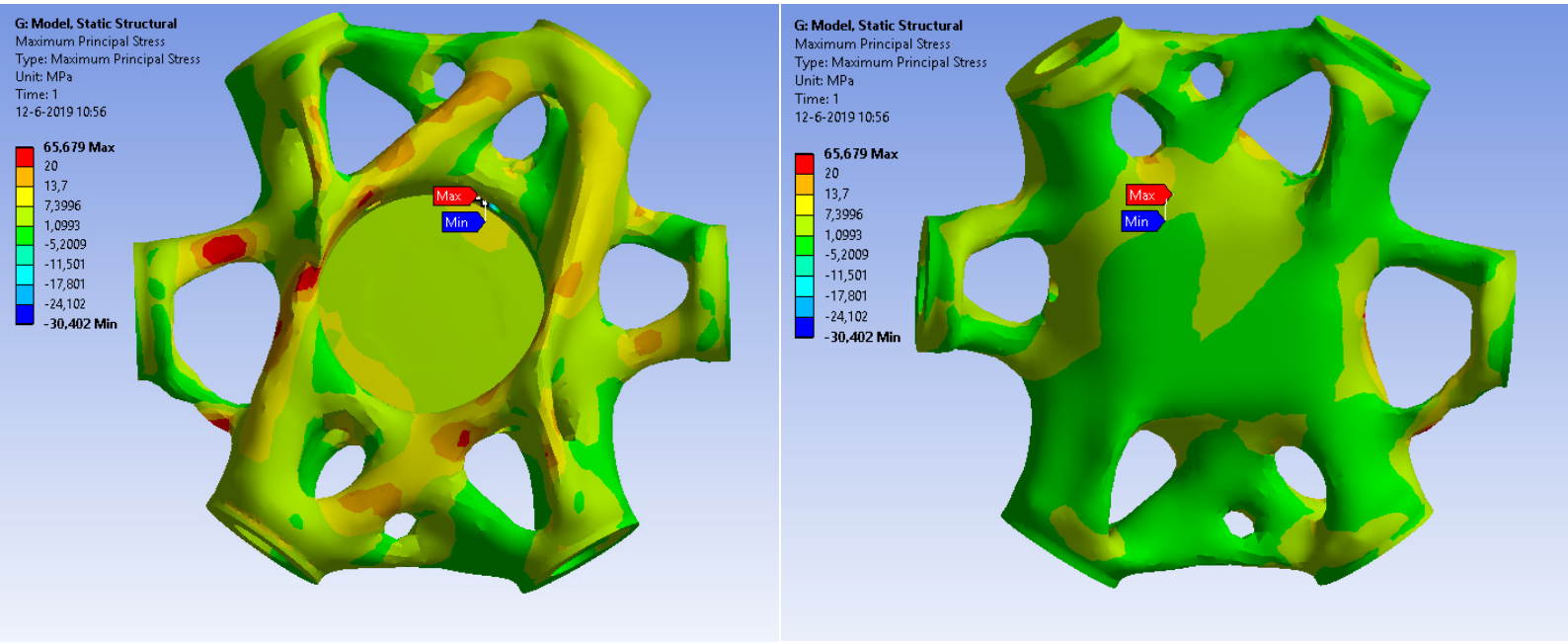

Fig. 110 *Principle tensile stresses under wind loading in reverse direction*

The same methodology was used on node 327, using the self-load, and a wind perpendicular to the node (Table A11 - Table A12 in appendix A). To improve the quality of the geometry, this optimisation was also performed with a reduced mesh size of 5mm, down from 8mm. This resulted in a smoother geometry, and increased calculation time for this model from 6 minutes to 2 hours and 12 minutes (Fig. 111-Fig. 113).

Both of these designs are of little use in practice, as they are only able to withstand a wind load from a single wind direction. It does however show that TO can be used if a few distinct load cases are present, by combining these geometries. This can help in providing more redundancy and flexibility in topologically optimised structures.

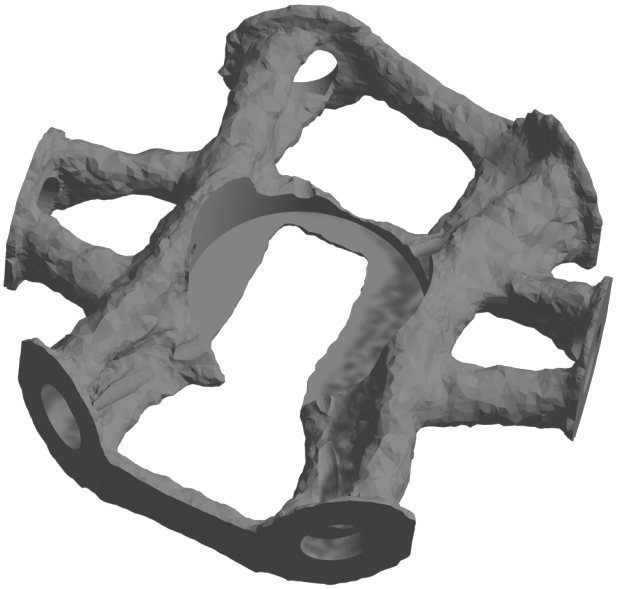

Fig. 111 *Optimisation of node 174 for self weight*

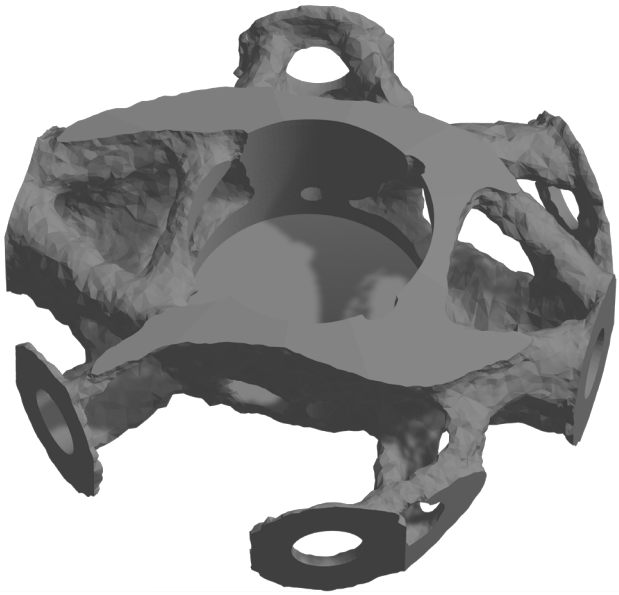

Fig. 112 *Optimisation of node 174 for wind load*

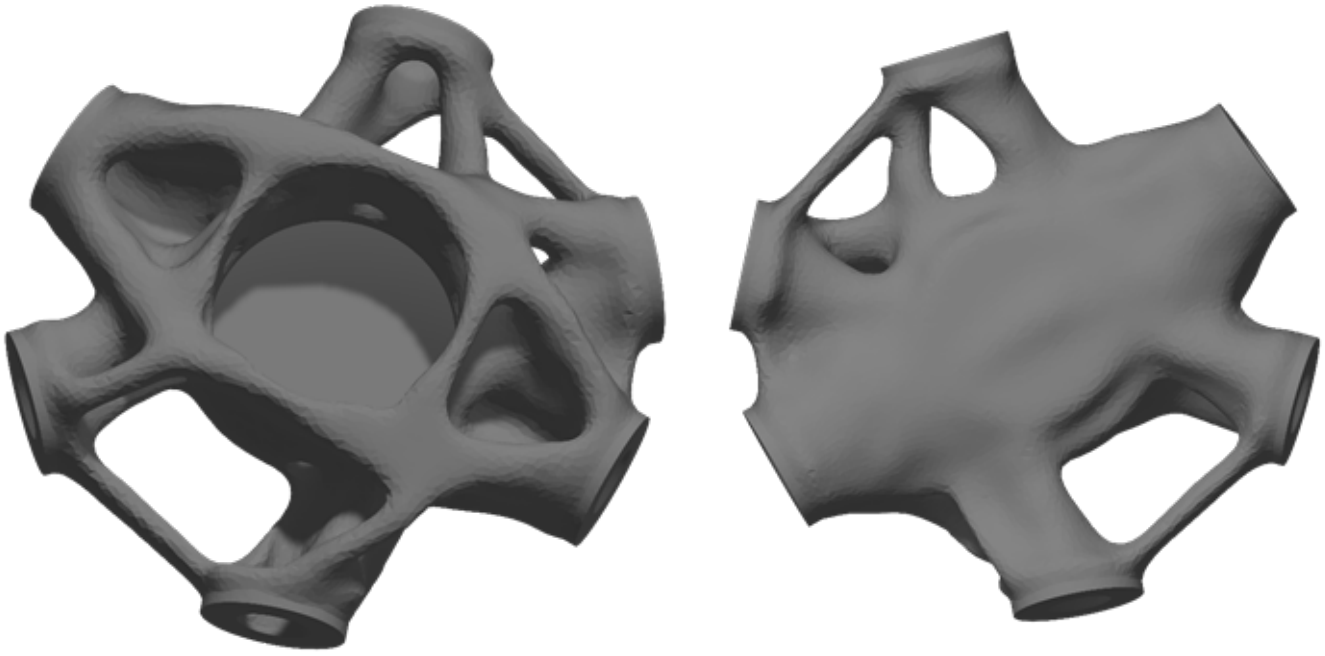

Fig. 113 *Resulting combined optimisation of node 327 for wind and self weight*

Heavy shell optimisation

To test a heavier and larger shell, the entire shell geometry has been scaled up by 50%. In addition, the mesh load representing the weight of the shell cladding has been increased from 0.5 kN/m2 to 1.2 kN/m2. This is a value that can still be considered realistic, assuming a multi-layer, double glazed glass covering. To account for the greater loads, the beam dimension has been increased to an 80mm diameter glass tube, with a 12 mm wall thickness.

Once again node 174 used. The resulting loads from Karamba are displayed in appendix A, Table A13 - Table A14. Due to the heavier weight of the shell, the compressive axial force in the four diagonal beams has increased noticeably. To ensure that the remaining two horizontal beams are fully connected to the node, an additional load of 3.5 kN was applied at these connections. For this optimisation, a manufacturing constraint of 20 – 40 mm was used, with a 37% material goal. The resulting geometry after smoothing is shown in Fig. 114.

This node was tested in ANSYS FEA under a wind load perpendicular to the node, which causing the highest loads on this node. Compared to the previous tests, a slightly lower wind load of 0.49 kN/m2 was used, which is representative for a more inland Dutch location (Nijsse, 2013). The exact loads used are in Table A15 in appendix A. It is found that this node performs well, even under a wind load that was not included in the optimisation. No tensile stresses of over 20 N/mm2 can be found in the glass (Fig. 115).

9.6 Annealing time reduction

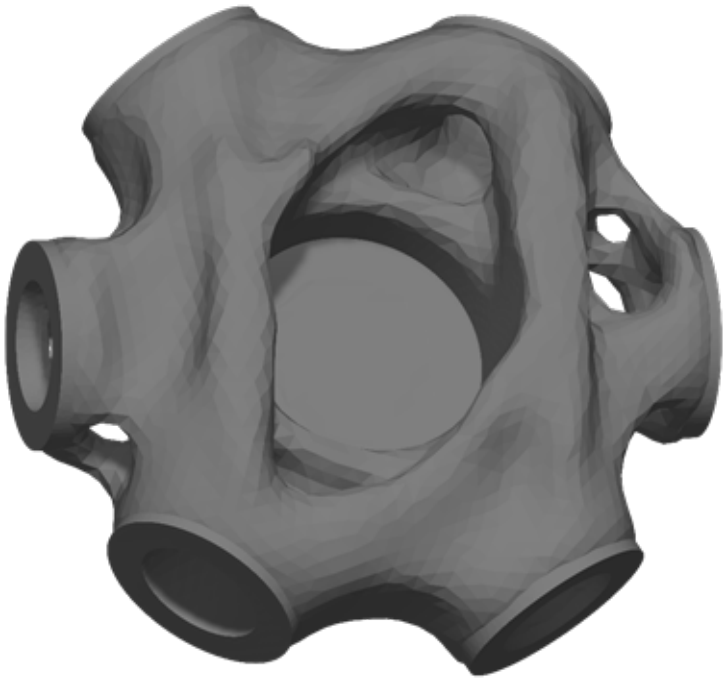

Fig. 114 *Node 174 optimised for a high self weight*

As described in chapter 2.4, a couple factors determine how long a glass object needs to be annealed. These are object weight, element thickness, material distribution and the presence of sharp corners in the design. How has the optimisation process affected this?

For weight, considerable weight reductions have been achieved compared to the initial design domain. In the two-load optimisation, node 174 has been reduced from 8.72 kg to 2.69 kg, a reduction of 69%. For the larger and heavier shell, the node was optimised from 10.83 kg to 5.13 kg, a mass reduction of 47.4%. It should be noted that these numbers are somewhat optimistic, as the initial geometry

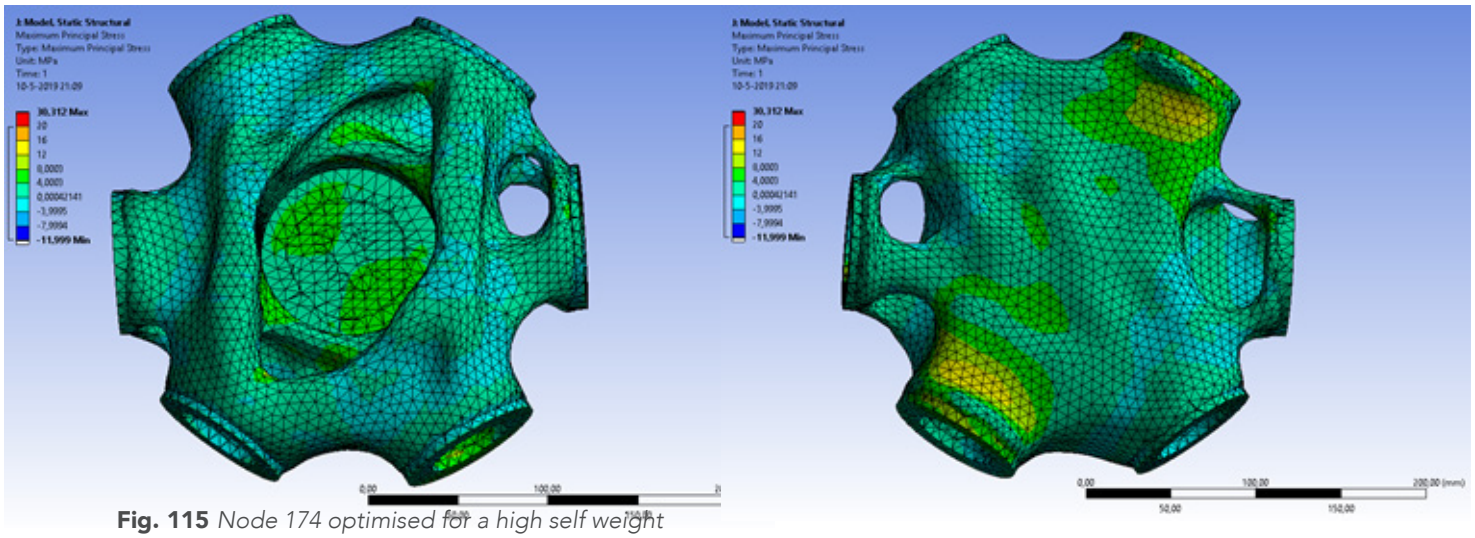

Fig. 115 *Node 174 optimised for a high self weight*

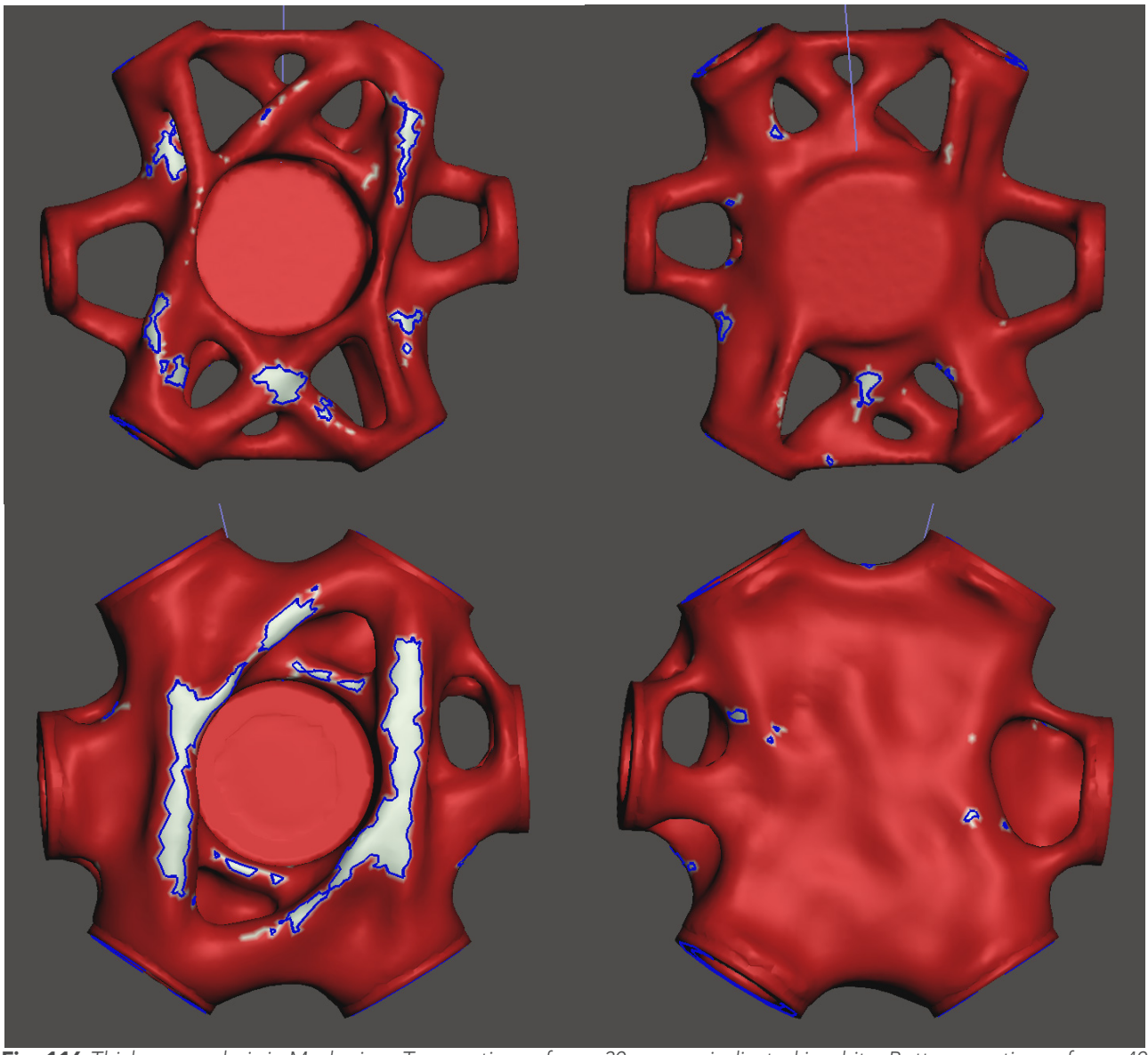

Fig. 116 *Thickness analysis in Meshmixer. Top: sections of over 30 mm are indicated in white. Bottom: sections of over 40 mm are indicated in white*

used was over-dimensioned. Compared to a more carefully designed conventional node, the weight reduction would certainly be less. Despite this, the weight reductions are significant, and will greatly help in decreasing fabrication time.

To judge element thickness and material distribution, a section thickness analysis has been performed using Autodesk Meshmixer (www.meshmixer.com). For the two-load optimisation, the majority of elements is found to have a thickness of between 8 and 30 mm. For the heavier shell node, the thickness of most elements lies between 15 and 40 mm. In the combined node, most thicker elements occur where the two merged geometries intersect. This is difficult to predict beforehand, and might lead to unwanted thicker sections. However, as each added element of itself is rather thin, it is expected that the combined geometry will generally remain thin.

It can be concluded that the manufacturing constraints used during the TO process can ensure an equal material distribution is achieved in the node. More narrowly defined fabrication constraints in combination with a finer mesh should help to further equalise the section thicknesses.

Finally, few sharp angles are to be found in the final geometry, which is highly organically shaped. This should pose no additional complications during cooling.

Taking these points into account, it can

be confidently said that the annealing time of these elements will be noticeably lower compared to the un-optimised geometry. Precisely calculating annealing times is complicated and dependant on many different variables, as described in chapter 2.3. An estimation of the annealing times required of these elements can be made by comparing it to realised examples from casting practice. The Crystal Houses project in Amsterdam is used for this comparison. In this project, multiple dimensions of cast soda-lime glass bricks have been produced, for which the annealing times have been documented (Oikonomopoulou et al., 2016).

The large blocks made for the Crystal Houses project measure 210 x 210 x 65 mm and weigh 7.2 kg. This is comparable to the un-optimised node geometry, with a diameter of 240 mm, a height of 95 mm and a mass of between 9 and 11 kg. (Fig. 117-Fig. 118). The Crystal Houses blocks required 38 hours of annealing. Considering the higher weight, it is reasonable to assume that the completely un-optimised node should take roughly 48 hours to anneal.

The smallest dimension of bricks produced for the Crystal Houses are 210 x 105 x 65 mm with a weight of 3.6 kg, and required 8 hours to fully anneal. Compared to this, the optimised two-load node is 25% lighter and has a maximum wall thickness of 30 mm, which is less than half of the smallest thickness of the brick (Fig. 119-Fig. 120) . Furthermore, generally much less sharp angles can be found in the geometry of this part, compared to the brick. Especially due to the low thickness, it is reasonable to assume that the annealing time

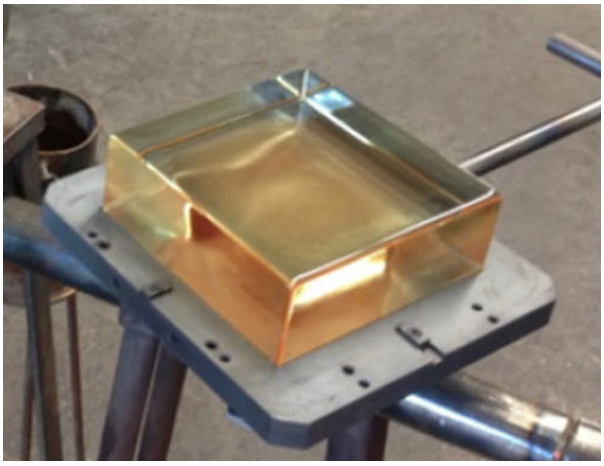

Fig. 117 *210 x 210 x 65 mm brick from the Crystal Houses project*

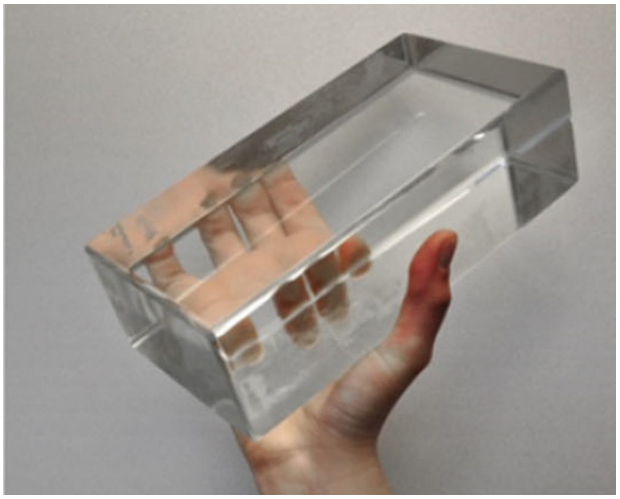

Fig. 119 *210 x 105 x 65 mm brick from the Crystal Houses project*

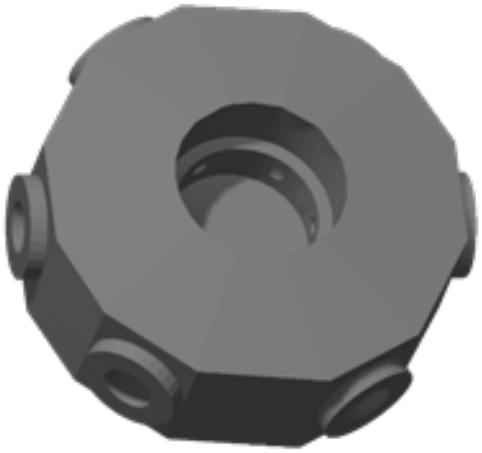

Fig. 118 *Unoptimised node element*

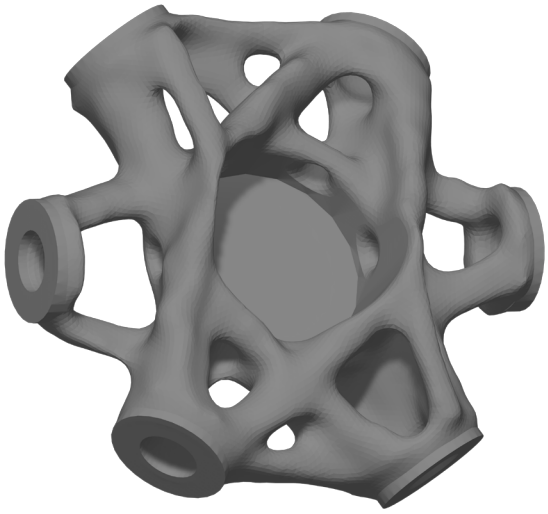

Fig. 120 *The lightest combined-load optimised node*

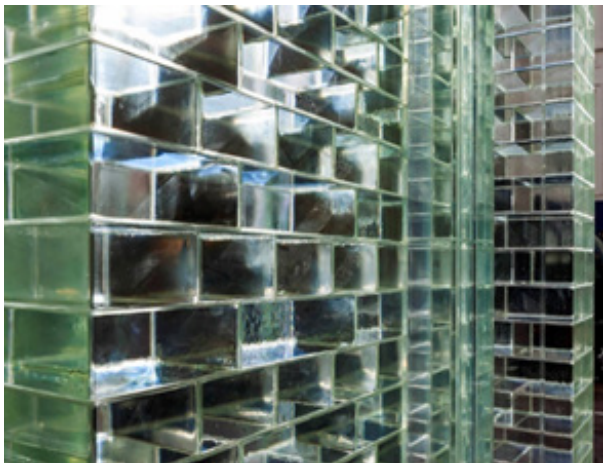

Fig. 121 *Detail of the Crystal Houses project, with a 210 x 167.5 x 65 bricks visible at the corner*

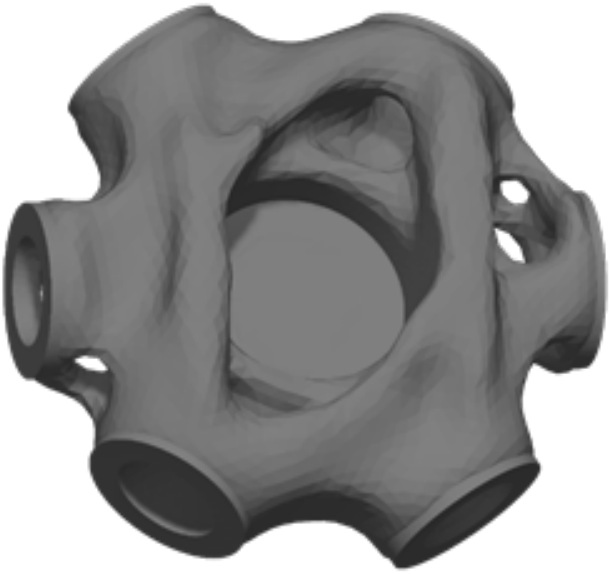

Fig. 122 *Optimised node for a heavy shell*

of this element might be as low as 4 hours.

The heavy-shell node can be compared to the 5.4 kg brick used at the Crystal Houses (Fig. 121-Fig. 122). These bricks have a size of 210 x 167.5 x 65 mm, and required approximately 20 hours to anneal. The heavy-shell node has a somewhat lower mass and a lower overall wall thickness, which will make it anneal faster. It is therefore reasonable to assume that this element will anneal in around 16 hours.

The Crystal Houses bricks were cast in soda-lime glass. Using the faster annealing Borosilicate glass, these annealing time could be even further reduced. Borosilicate glass is more expensive, but the reduced cooling time often makes it a feasible alternative to soda-lime glass for solid cast glass projects. Considering these low-weight optimised nodes the annealing times are already relatively short, which means the gain of using borosilicate glass are lower. The final choice of material would be a financial one, depending on whether the reduced annealing costs offset the higher material price of borosilicate glass.

9.7 Conclusions

TO for the built environment

The initially chosen shell design has been found to be difficult to adapt to topology optimisation design. Topology optimisation is designed to give an optimised material distribution under one specific load case, reaching highly optimised geometries to carry that load case. This high level of optimisation, however, brings with it a lack of flexibility to deal with loads that diverge from the design load.

Due to its small size and light weight, the case study structure is very susceptible to wind, causing highly varying loads on the loadbearing structure. This makes it impossible to formulate a clear single load case to optimise for. Due to this, a node optimised for the self-weight of the structure will fail when loaded with an external wind load.

It was shown that a larger, heavier shell can be optimised in TO. In these cases, loads on each node is dictated by the self-weight of the structure, and variable loads such as wind loads have relatively less influence. This gives a much clearer load to optimise for, and means the actual loads will diverge much less from the design load.

A different way to optimise an element under different loads is to run the optimisations separately, and merging the results. This is mainly useful if multiple different, clear loads on the element can be distinguished.

Weight reduction and annealing

Glass geometries formed by topology optimisation are estimated to have much low annealing times due to their lightweight and organic geometries. The element size limitation chosen in ANSYS was successful at limiting element thickness to a small range. This should further improve annealing time, by forming thin objects with equally distributed weights. An estimated annealing time of only around four hours was found for the lightest optimised node, compared to up to 48 hours for the full, un-optimised element. For the heavy-shell node, a reduction from over 48 hours to around 16 hours was found. This great improvement means that annealing time is much less of a limiting factor in the fabrication process of the element, which will help in making cast glass a much more attractive solution as a structural material in the built environment.

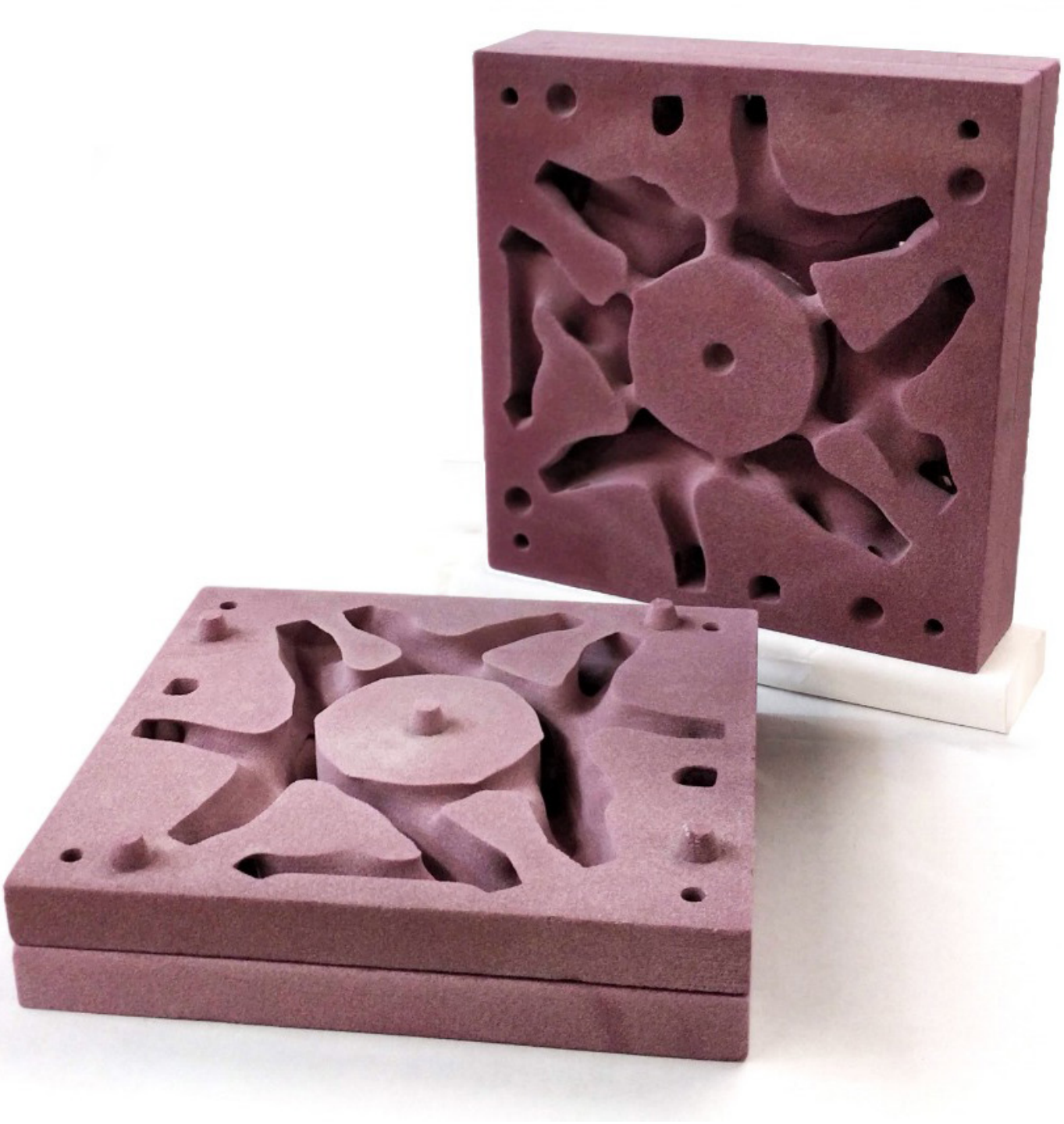

10. Casting tests

In the various designs made so far, the limitations of the fabrication process were taken into account, using design criteria and limitations in the optimisation software. These were however based on assumptions, as the exact behaviour of glass during casting is difficult to predict. To more reliably investigate how the node can be cast, a physical cast of the node should be performed. This also offers a chance to test two fabrication methods of the mould using additive manufacturing.

10.1 Methodology

Geometry modification

Some additions need to be made to the node to make it suitable for casting. These elements ensure the mould properly filled with glass during casting, and need to be removed after casting (Fig. 123).

It was decided to place the node flatly, with the cylindrical void facing downwards. A large, central additional channel has been added to provide an opening where the molten glass can be poured in (shown in red). Next, six channels of 6mm diameter have been added from across the node to the top of the mould to allow air to escape during casting, and avoid air bubbles being trapped in the mould (shown in yellow) (Fig. 124). Finally, multiple 6mm interconnecting channels have been added throughout the node to ensure the molten glass can easily distribute itself throughout the mould (shown in green).

Moulds

Two mould making techniques will be tested. The first method is an additively manufactured sand mould, made using binder jet printing. In this process, a fine sand is deposited layer by layer. Where a solid geometry is required, a binder is added to solidify the sand. After the binder has hardened, any remaining loose sand without binder is removed.

Additive manufacturing using this method has the advantage that it does not require any additional support material, as any sand without binder remains in the model until said binder has hardened, providing support to the entire model. This allows for relatively complex shapes to be printed, and also means no printed supports are needed that need to be removed from the model after printing. Furthermore, large elements can be printed fast and at high precision. Finally, the sand used is heat resistant, making it possible to directly use the printed object as a mould. Because of this, printed sand moulds have already been extensively used in metal foundries. Removing the mould can be greatly simplified by utilising a water-soluble binder during printing.

The main downsides of this technique are the specialised, expensive machines required for printing the mould, and the need of special coatings on the mould to ensure a good

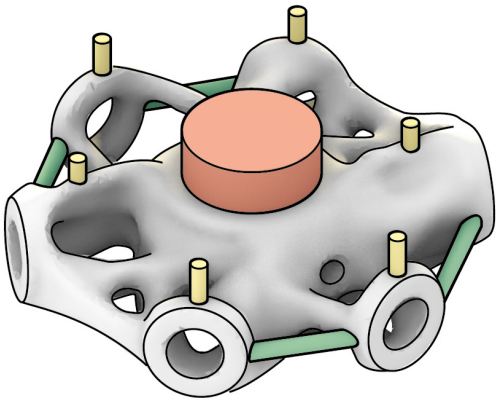

Fig. 123 *Additons for casting node 174*

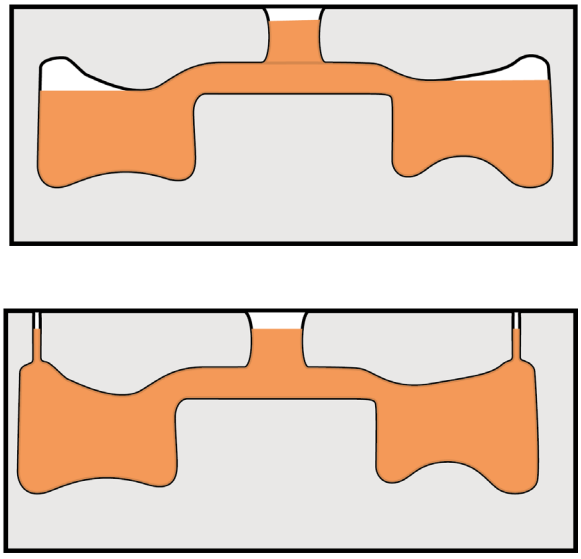

Fig. 124 *Preparations for casting. Top: air trapped within the mould. Bottom: adding air channels to let the air escape.*

surface quality of the cast material. Applying this coating can be challenging if small elements or large overhangs are involved.

The second alternative is investment casting using lost-wax. For this technique, the object that needs to be cast is sculpted in wax, after which mould material is placed around it. Once the mould has solidified, the wax is removed by heating, leaving an empty mould that can be used for casting. An additively manufactured node geometry using a special wax-based filament will be used.

This methodology has the advantage that it does not require specialised equipment, as the wax filament can be printed using widely available 3d-printer setups. Furthermore, the wax can be sculpted before placing it into the mould, which makes it easy to tweak the geometry or to fix flaws in the printing. However, the wax 3d printing is relatively slow, and the mould casting and wax removal makes this a comparatively slow and labour-intensive process.

The mould in the lost-wax process will be made from silica plaster, which has been described in chapter 2.6.

Glass

Two types of glass will be used. For the lost-wax cast, recycled art glass panes are used. Due to various material additions, a lower melting temperature of 827C° is used. This glass has an annealing temperature of 482 C°.

The sand mould casts will be made using lead glass. This variation of lead glass has a melting temperature of 810 degrees, and an annealin temperature of 430 degrees.

Kiln casting will be applied, as this is the only method available at this lab, and is the simplest casting method for small batches of glass.

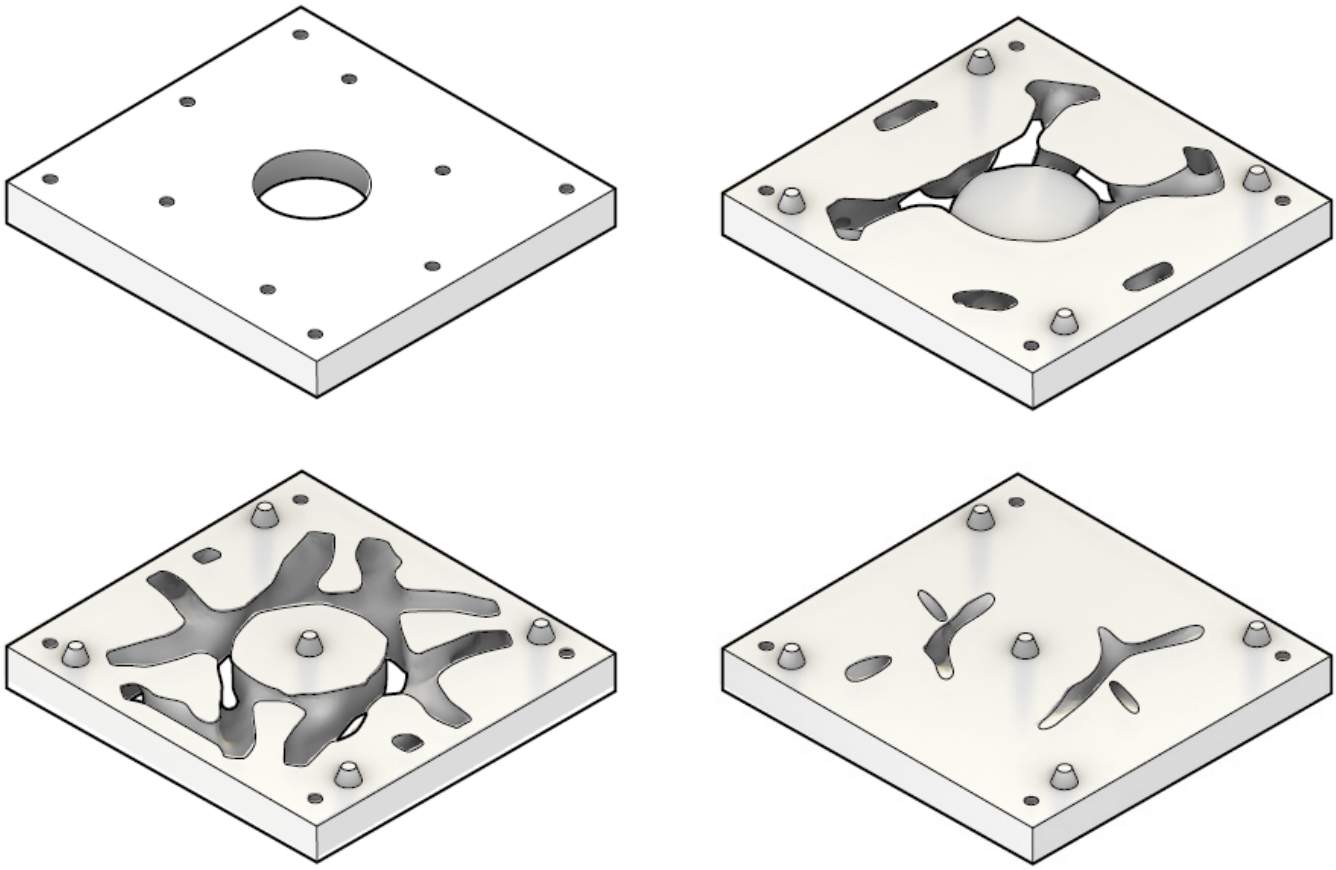

Fig. 125 *The design of the sand mould in four parts. Iterlocking pin and hole elements have been added to align the layers of the mould*

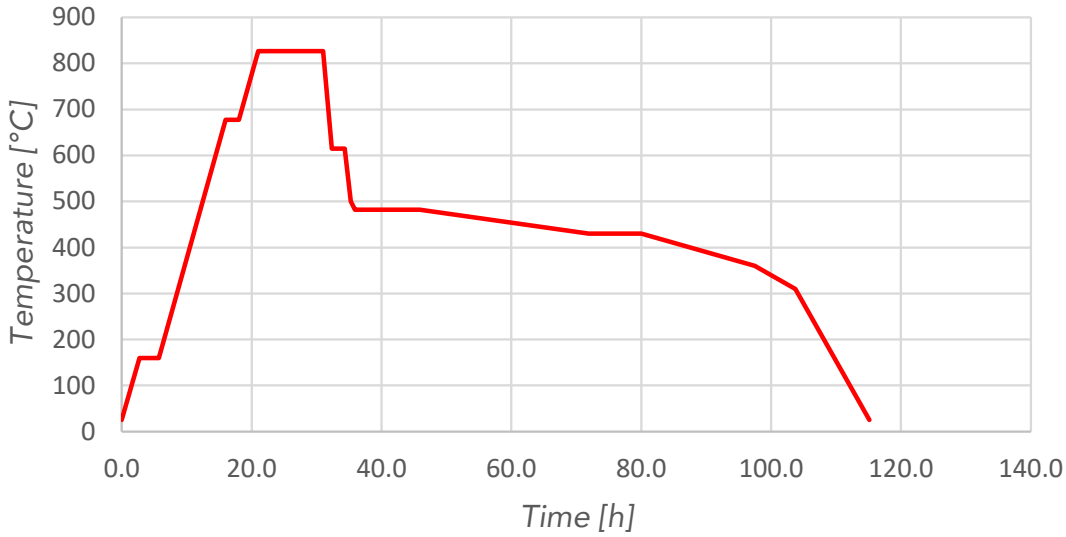

Fig. 126 *Firing schedule for the lost-wax casting*

Firing schedule

The firing schedule used for the lost-wax casting can be seen in Fig. 126. At the beginning of the firing, the oven is left at 160C° for two hours to ensure all remaining moisture has a chance to evaporate from the silica-plaster moulds. After this, as the mould is placed in the oven together with multiple different elements from other projects, a generic, slow annealing schedule is followed. First, the oven is heated to 827C°, where it remains to let the glass melt and fullt settle into the mould. The glass is then rapidly cooled to its annealing temperature of 482C° to avoid crystalisation. After this, the glass is slowly cooled to around 310C° over the course of a few days to ensure any internal stresses have dissapated. The glass can then be cooled to room temperature.

For the sand mould casting, a comparable schedule is used, with a slighly lower melting temperature of 810C°.

10.2 Mould making

Sand mould

A sand mould has been made based on the light combined-load node. ExOne, a company specialised in the development and sale of binder-jet printers was so kind to provide the mould (https://www.exone.com/). A mould was printed using CHP-binder. In small-scale testing, this binder appeared to be sufficiently hear-resistant to withstand the casting and annealing process. In addition, this binder can be dissolved in water. This means the node can be demoulded without risking to damage the glass. (Paper Ivneet, 2019) After dissolving the binder, the sand can be reused for a new mould, reducing waste and material use.

To guarantee a smooth finish of the glass, the sand mould needs to be coated to avoid sand at the surface of the mould fusing to the molten glass. A thin coat of silica-plaster was used, applied to the inside of the mould using a brush. (Bhatia, 2019). To be able to reach the entire inside of the mould, it was decided to split the mould into four slabs, as shown in Fig. 125. This also greatly simplifies the removing of leftover sand from the mould. A Grasshopper script was used to automatically generate the mould and split it.

To join this split mould together, an interlocking pin-and-hole system was used. In addition, four steel rods were used to bolt the mould together. Direct contact between the sand mould and the metal was avoided, as this might damage the mould due to different thermal behaviour of the mould. A rod of a diameter smaller than the holes was used, and at the top and bottom, fire resistant cloth was placed between the washer and the mould. An additional coating of plaster was added along the outer seams of the mould, to prevent any glass that might flow between the mould layers to flow into the oven.

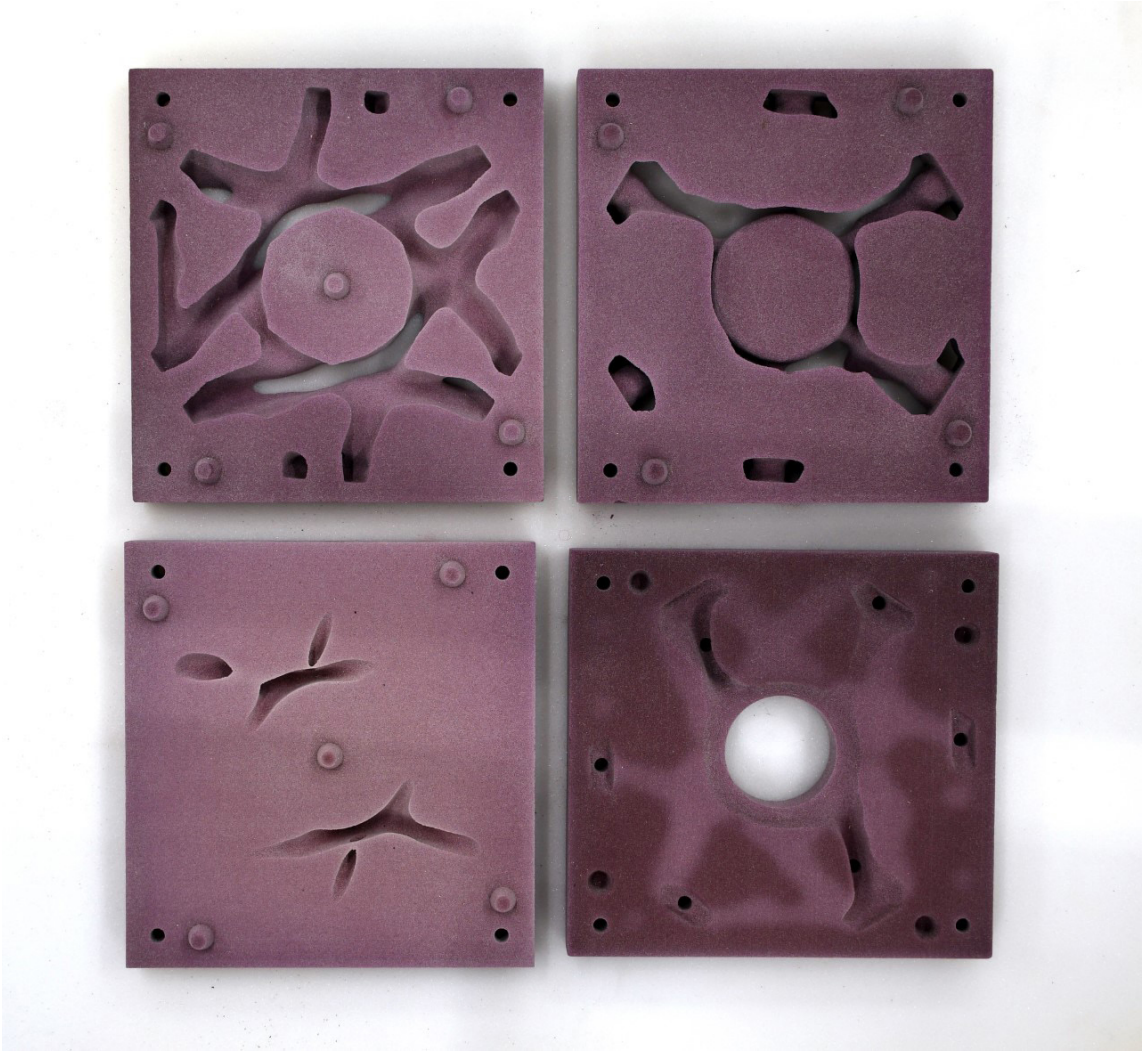

Fig. 127 *The printed sand mould elements provided by ExOne.*

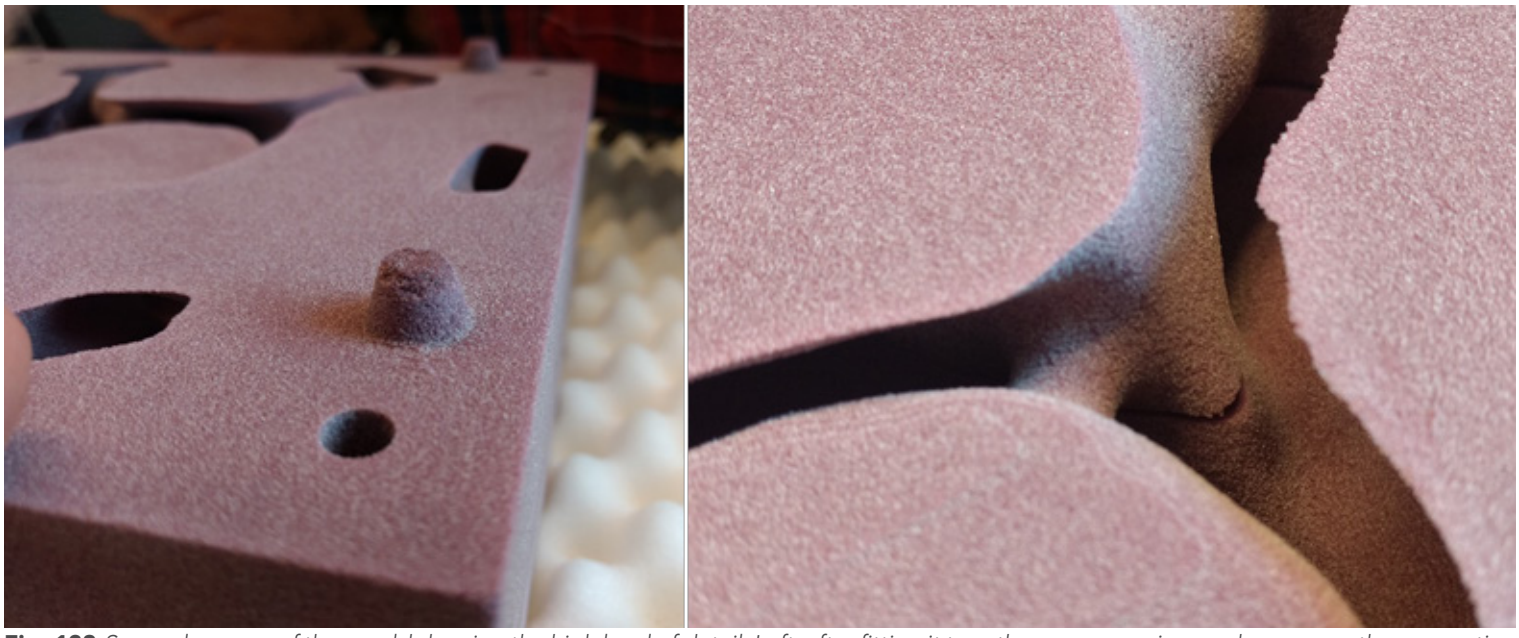

Fig. 128 *Some close-ups of the mould showing the high level of detail. Left: after fitting it together, some erosion can be seen on the connecting pin-and hole connection. Right: Despite the accuraty of the print, some seams can be seen where the layers of the mould connect.*

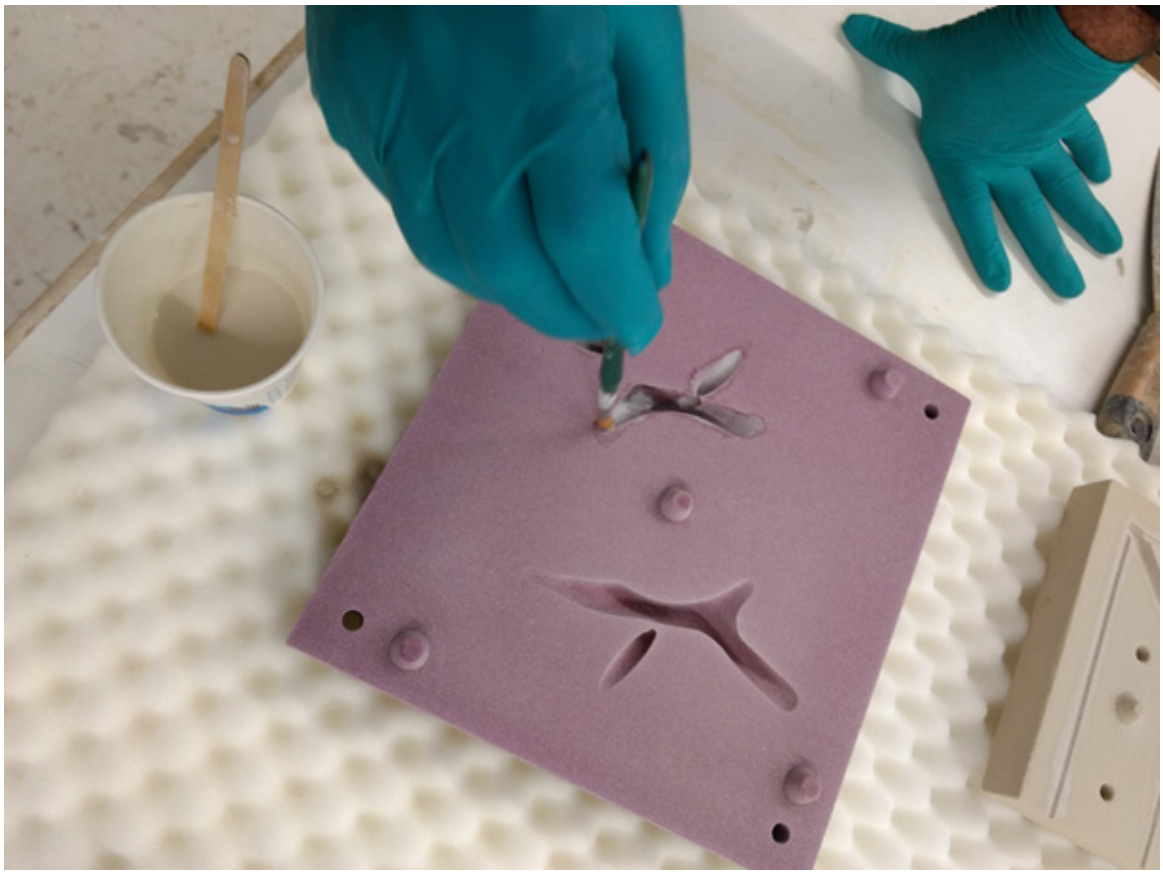

Fig. 129 *Coating the inside of the mould with silica-plaster*

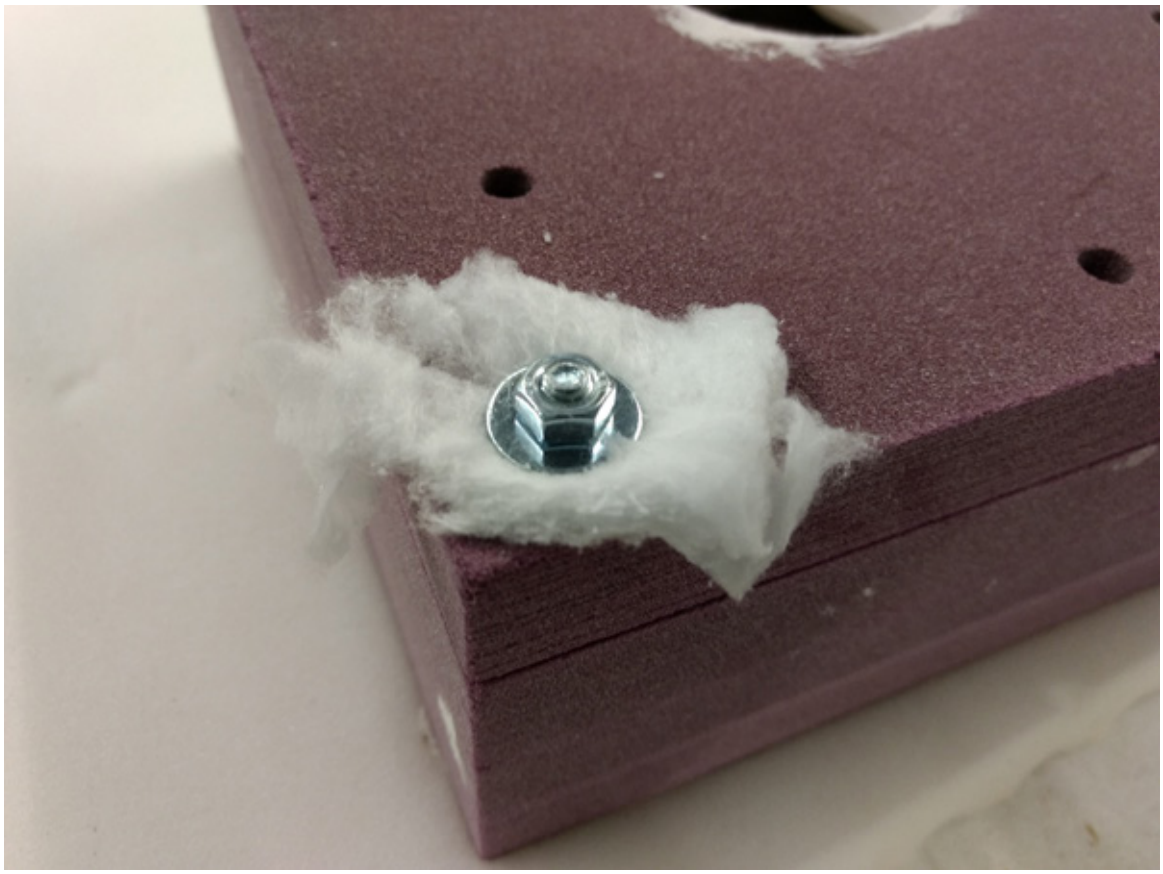

Fig. 130 *Fire resistant cloth to avoid direct contact between the steel washers and the mould*

Fig. 131 *Setup for the kiln casting. The flower pot with the needed amount of glass is placed on the sand mould*

Lost wax mould

For the investment casting, the node was printed at 1:2 scale using a special wax-based filament from Machineable Wax was used. (www.machineablewax.com) This material has very different properties compared to regular plastic printing filaments, which resulted in a challenging printing process. The printing process and final settings used have documented in appendix C.

The printed geometry contained some rough surfaces and cracks, which were filled in using regular candle wax. The different casting and air channels needed for casting have also been manually added in wax. Once this was completed, the wax was secured with clay, and a simple wooden mould was constructed around it. More clay was used to close any potential gaps in this mould. Once this was done, the silica plaster could be cast, and left to harden for an hour.

After removing the mould and any clay left in the mould, the wax needed to be burned out. Regular wax can be removed by steaming, which heats the wax sufficiently for it to liquefy and flow out of the mould. The printable wax proved to have a noticeably higher melting point, and could not be steamed out.

Because of this, it was tried to place the mould in an oven and heat it sufficiently for the wax to flow out. Steadily increasing temperatures from 140 degrees C and up were used. Around 280 degrees C, the wax started to melt and flow out, but also became black and partly remained stuck to the mould. It was decided to attempt to fully evaporate the wax using a higher temperature. At 515 degrees, the wax was fully evaporating. The mould was left at this temperature for six hours to ensure it was fully clean; though it is expected that a shorter time would have been sufficient.

Casting

Before casting, the glass was cleaned to minimise contamination of the molten glass. The required amount of glass was then weighted and placed in ceramic flower pots. An additional 15% of material added to account for material remaining within the flower pot. The pots were placed over the mould, and put in the oven.

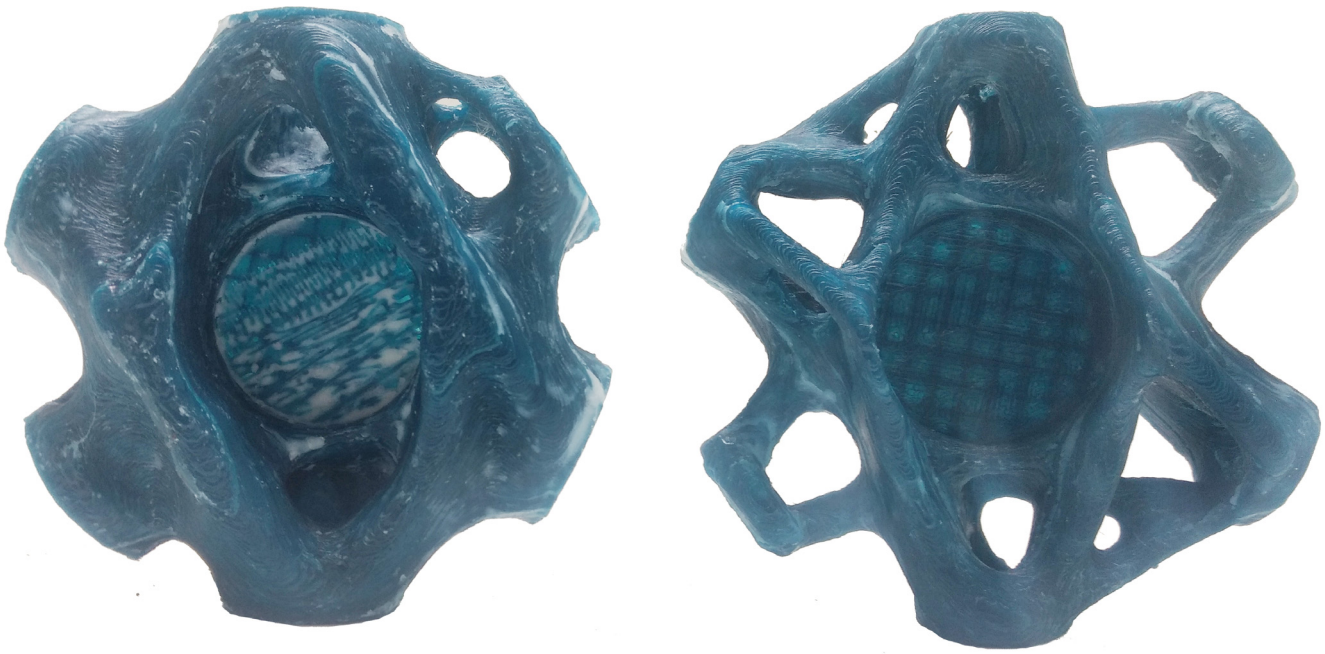

Fig. 132 *The two printed wax nodes, with candle wax finishing*

Fig. 133 *Mould setup, with added elements for casting in wax and clay*

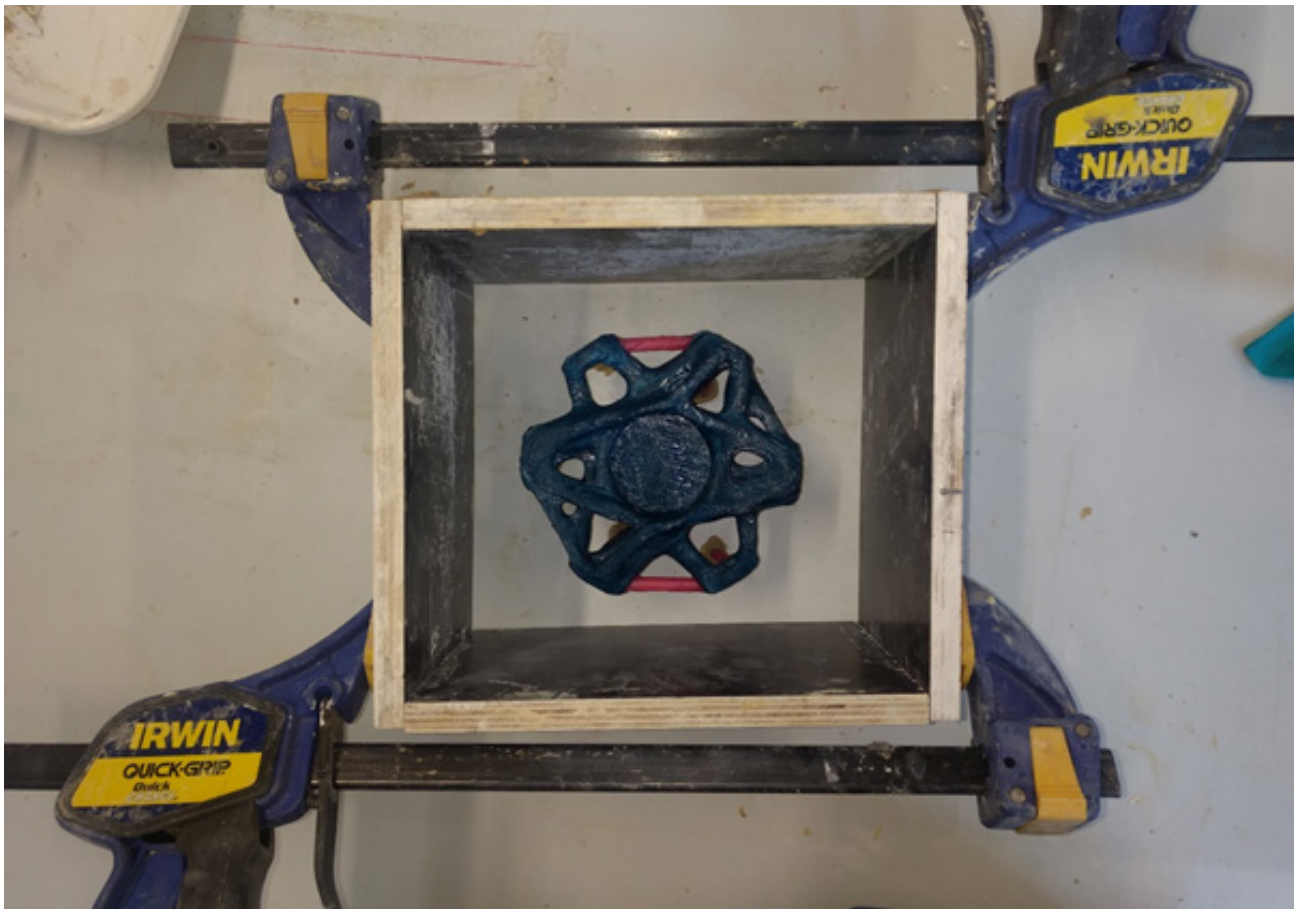

Fig. 134 *Temporary mould for the casting of the silica mould*

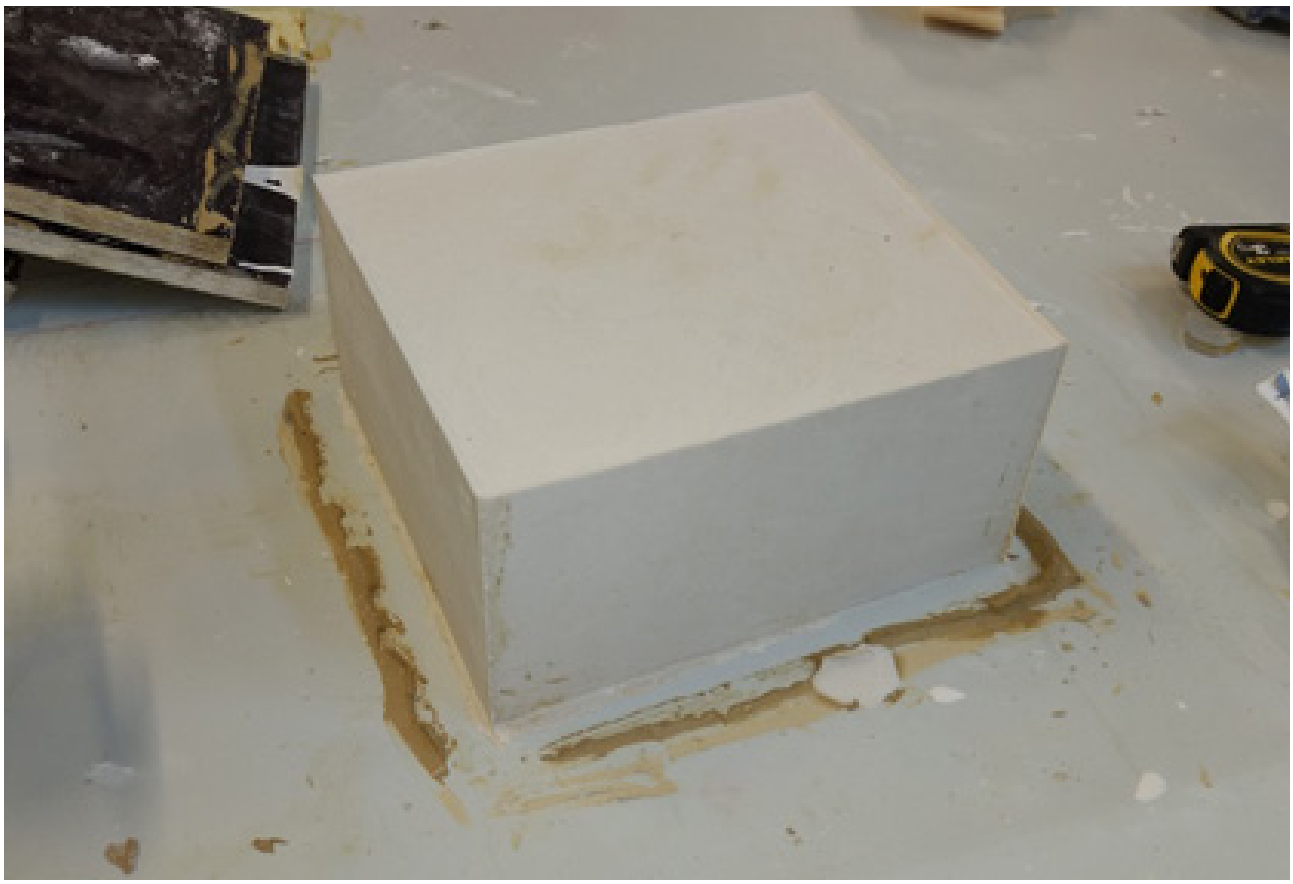

Fig. 135 *The disposable mould after one hour of solidifying*

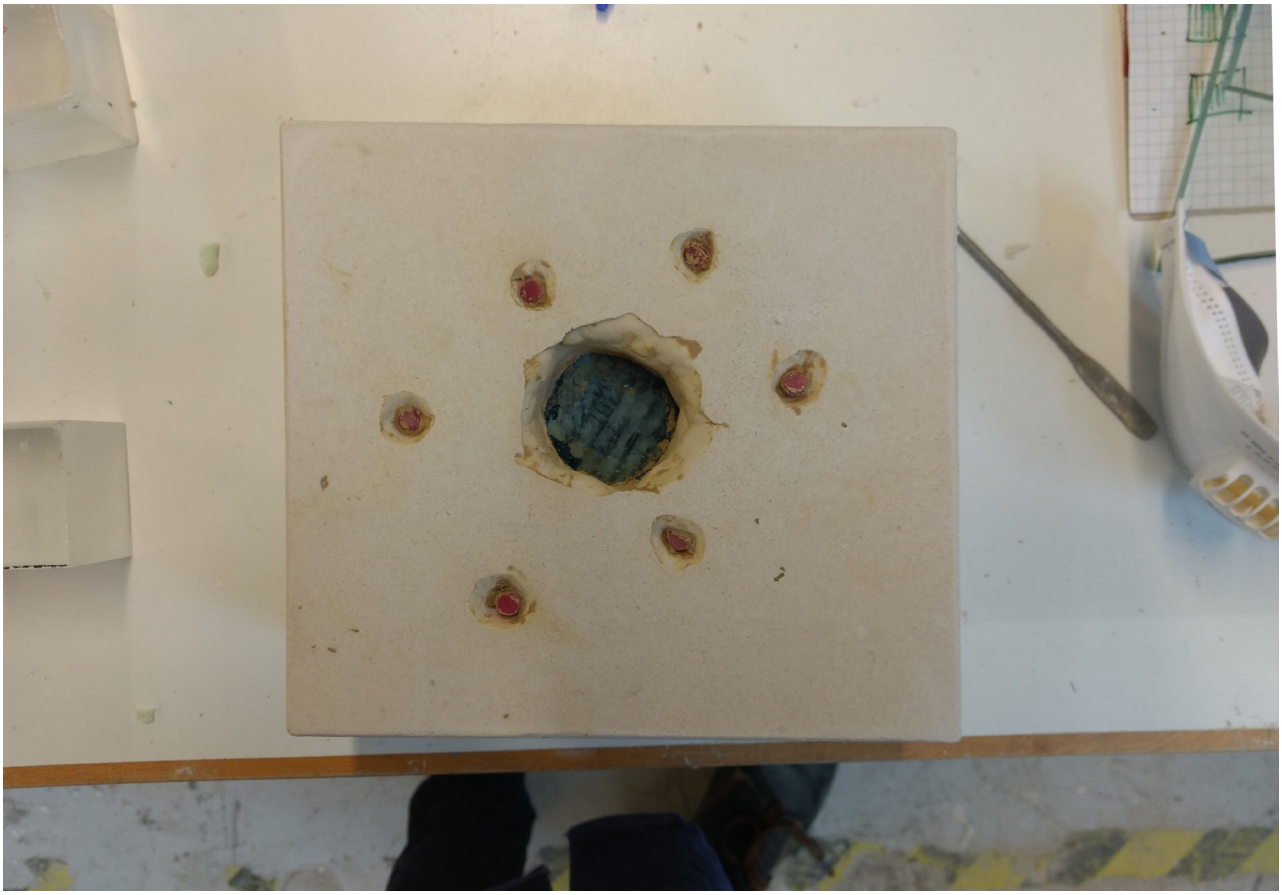

Fig. 137 *The silica-plaster mould with the wax element inside*

Fig. 136 *The clean silica-plaster mould after the wax was burned out*

10.3 Results

Lost wax demoulding and finishing

For the lost-wax model, the oven was around 60 °C as the firing was finished. The mould was taken out of the furnace and left to cool at room temperature. Once it had sufficiently cooled, the plaster mould was placed in water and left to soak. After around a quarter of an hour, the mould had become sufficiently soft to be removed by hand. Removing the silica from in between the glass geometry took some time due to the complex shape of the element.

Using the silica mould, the surface of the glass remained transparent. The mould and the glass casting were of such high detail that the lines of the 3D printed wax element were clearly visible, which resulted in a rather rough surface. Some further post-processing was needed to remove the added casting channels from the node. The thinner elements could be removed using a Dremel cutting tool, whereas a large cutting machine was required to remove the large casting element. After cutting, the remains of these casting elements were sanded down for a smooth finish.

Some small white inclusions were found in the glass of the cast node. These appear to be pieces of silica plaster. Most likely, these were part of the mould, and have become detached during casting. Additionally, there are some small, drop-like glass pieces on the surface at a couple of points. These are caused by small air bubbles that have remained stuck to the printed wax geometry during the plaster mould casting.

Fig. 138 *Demoulding the lost wax cast. The silica mould becomes soft after submergin it in water*

Fig. 139 *Demoulding the lost wax cast, removing the silica-plaster around the complex node geometry*

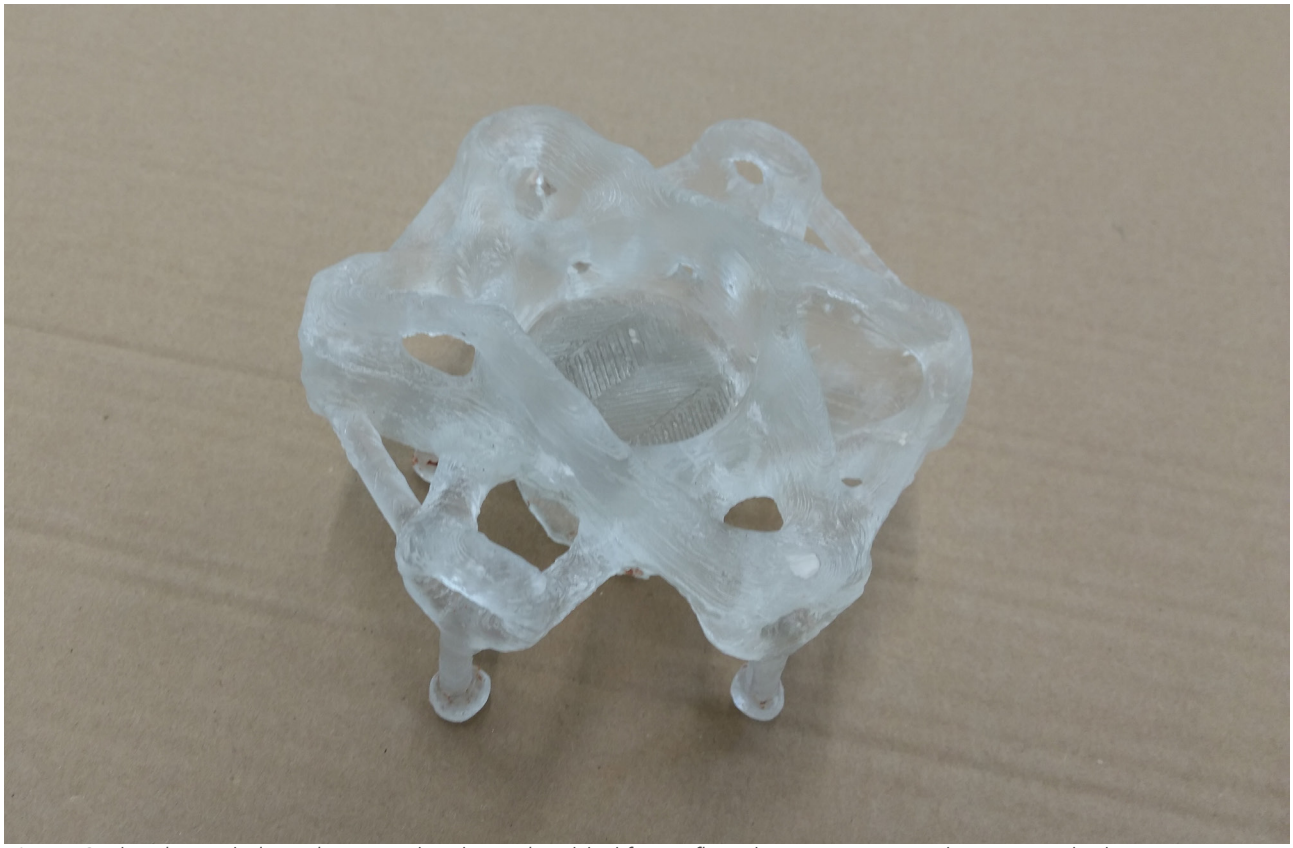

Fig. 140 *The cleaned glass element. The channels added for air-flow during casting can be seen at the bottom*

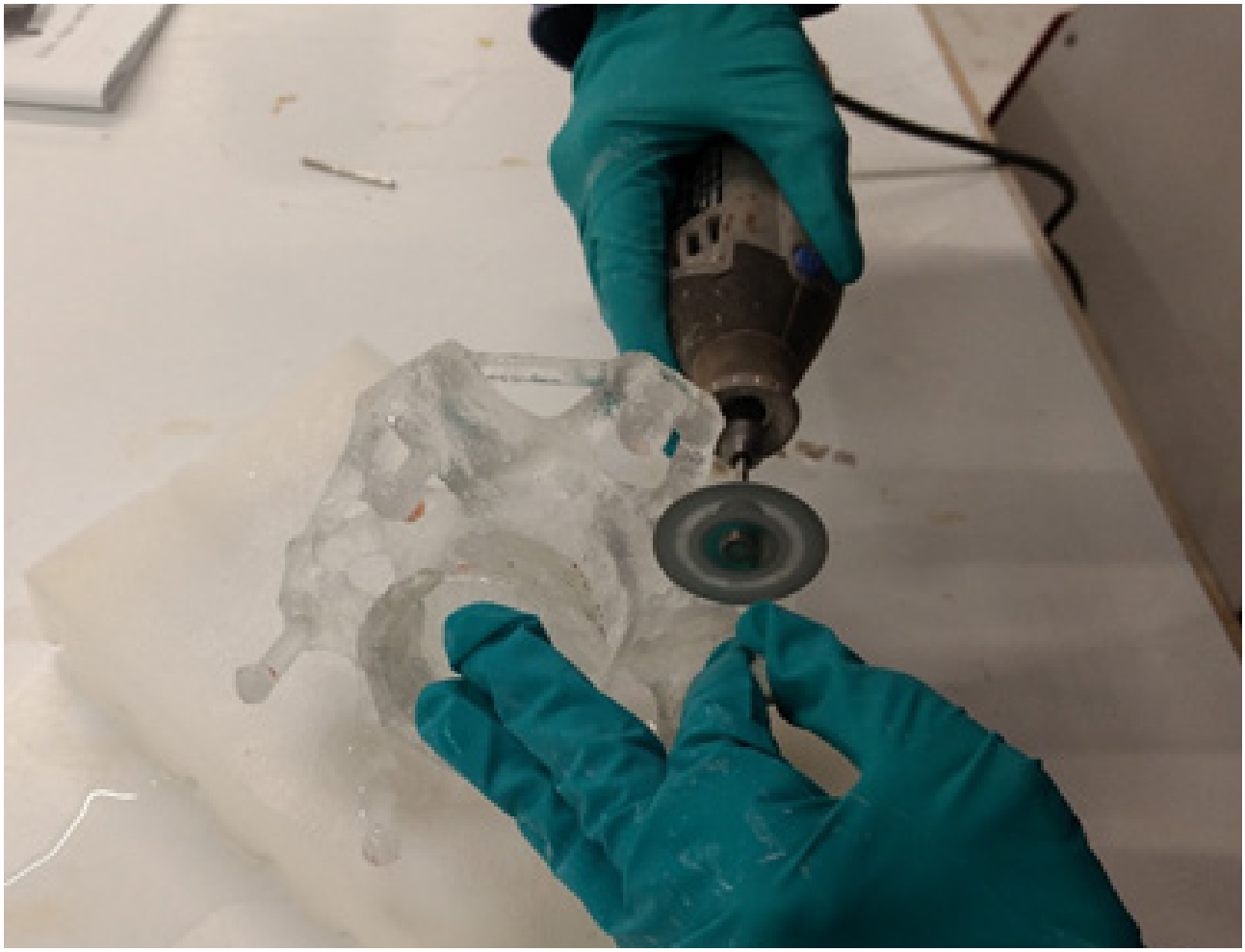

Fig. 141 *Removing the elements added for casting*

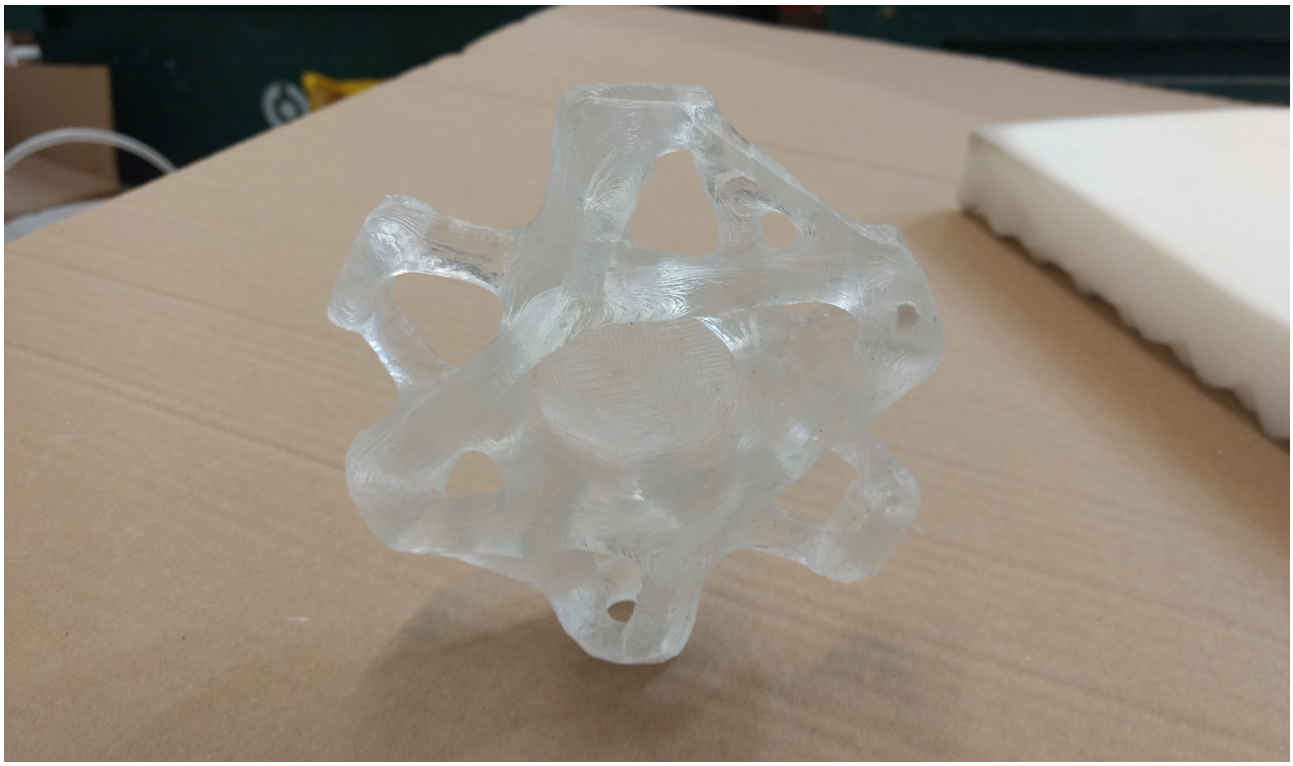

Fig. 142 *The cleaned glass element*

Fig. 143 *The sand mould casting after the oven had cooled. In the foreground, the mould of the optimised node.*

Sand mould casting

The casting of a node using the printed sand mould failed to produce a usable geometry. Upon opening the cooled furnace, it was found that the sand mould had partly collapsed on itself (Fig. 143-Fig. 144). It appears that the binder used to print the sand was less heat-resilient than assumed and has evaporated, leaving the sand returned to its original colour and highly fragile, falling apart under touch. This appears to have happened before the glass had time to distribute itself throughout the mould, as little glass was found inside the mould.

While taking apart the mould, it could be seen that the silica coating had successfully formed a solid layer on the inside of the mould (Fig. 145). As shown with the lost-wax casting, glass cast in silica has a very clean surface quality. From this it can be concluded that, had the sand mould not collapsed, a clean glass geometry requiring little processing might have been achieved.

Fig. 144 *Collapse of the mould, seemingly caused by the weight of the glass-filled flowerpot*

Fig. 145 *The thin interior layers formed by the silica-plaster coating.have stayed intact where the mould was not crushed by the flowerpot.*

Based on these results, some further experiments can be proposed to explore the use of sand moulds for glass. First of all, different binders are available. At least one of these is potentially stronger and more heat resistant, but was not chosen here as removing a mould of this material was expected to be more difficult (Bhatia, 2019).

Additionally, the mould seems to have collapsed at least partly due to the weight of the flower-pot and glass placed on top of it. These can be supported by a separate structure, reducing the load on the mould, possibly preventing collapse.

Finally, hot-pouring could be used as an alternative to kiln casting. As the glass is molten in a separate oven and then cast into the mould, the mould itself can be subjected to high temperatures for a much shorter time. Once the glass has filled the entire mould and has cooled to its softening point, it is self-supporting. If the mould fails after this point due to the heat of the annealing oven, this should no longer disturb the glass object, and possible even simplify demoulding.

Conclusion

The investment casting using a sand mould was successful. It was shown that even a complexly shaped design with small elements can be cast with great accuracy using 3D printed wax. During design, a minimal element thickness of 15mm was used to ensure that the element could be easily cast; the result of an element at 1:2 scale shows that much smaller elements can be achieved. The high level of detail does mean that the quality of the initial wax print should be high to ensure a smooth glass element. Apart from this, the glass surface is clear. This removes the need for sanding of the entire surface, which would be challenging for a geometry of this complexity.

A lot of manual work is required in this process. The preparation and casting of the mould, the complete demoulding, cutting and polishing of the final result all require manual work. In addition, the printing of the wax geometry and the burning out of each mould require significant time. Significant improvements in the fabrication process are required to make large scale production feasible.

The casting of glass using a printed sand mould failed, as the binder used for printing could not resist the heat of the kiln-casting. Despite this, further research on these moulds is proposed. A different binder can be used, which is potentially more heat-resistant. Additionally, a different setup can be used which exerts less load on the sand mould, possibly preventing failure. Finally, hot pouring might be more suitable for the sand moulds, as this exposes the mould to less heat.

The coating of the mould with silica-plaster successfully created a thin plaster shell that should improve the surface quality of the glass, though this could not be ascertained due to the failure of the mould.

11. Final design

11.1 Pavilion overview

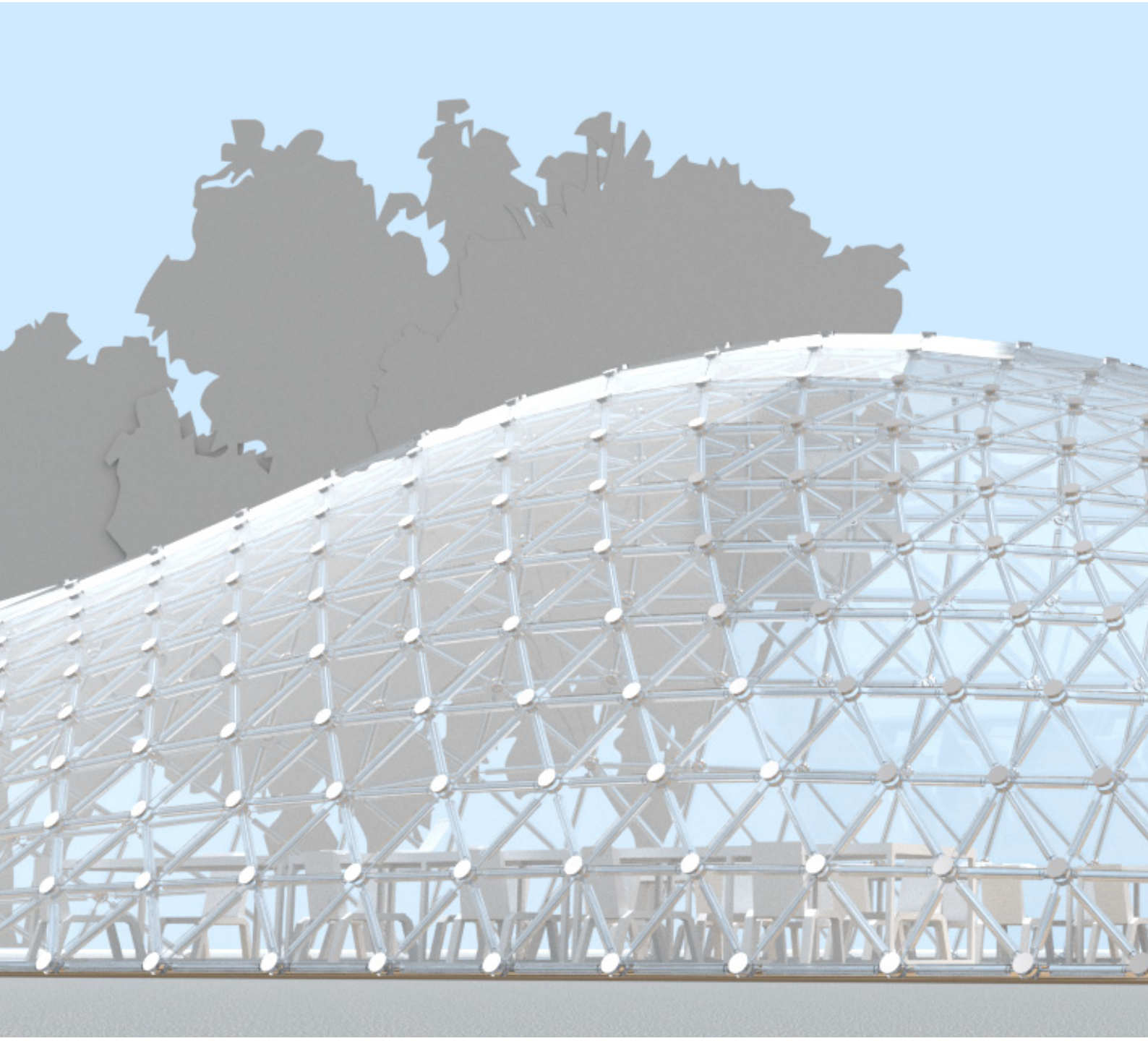

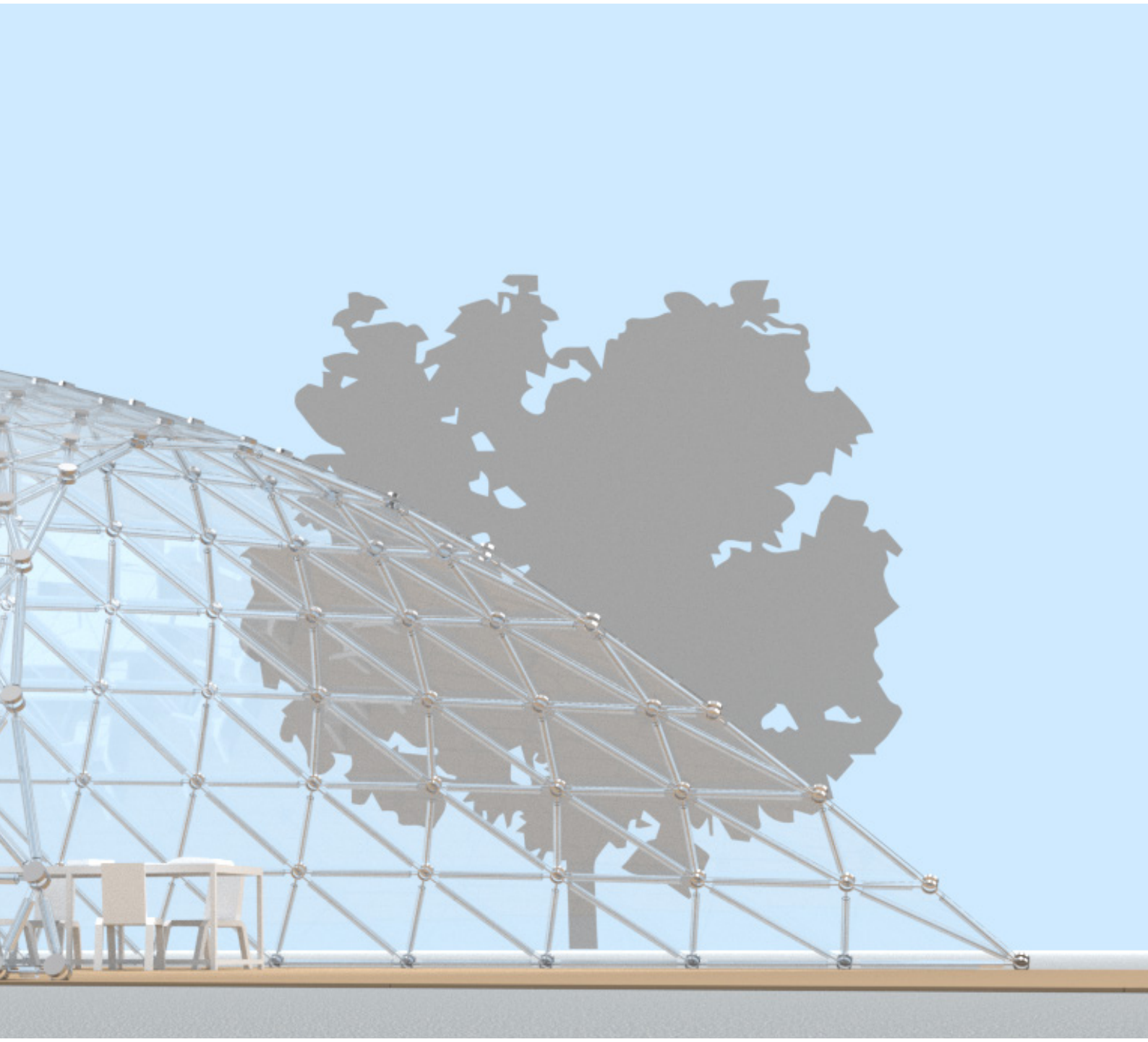

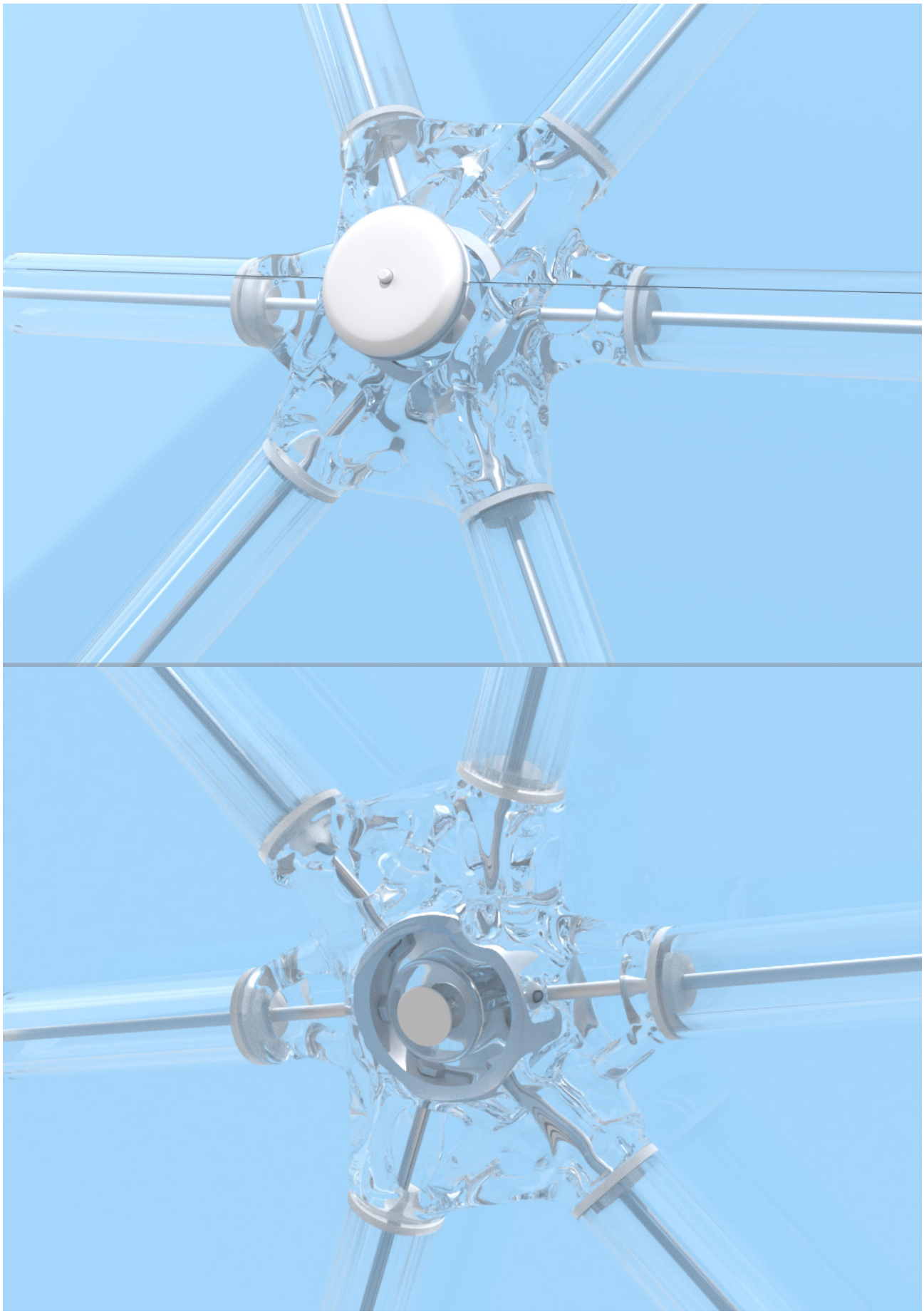

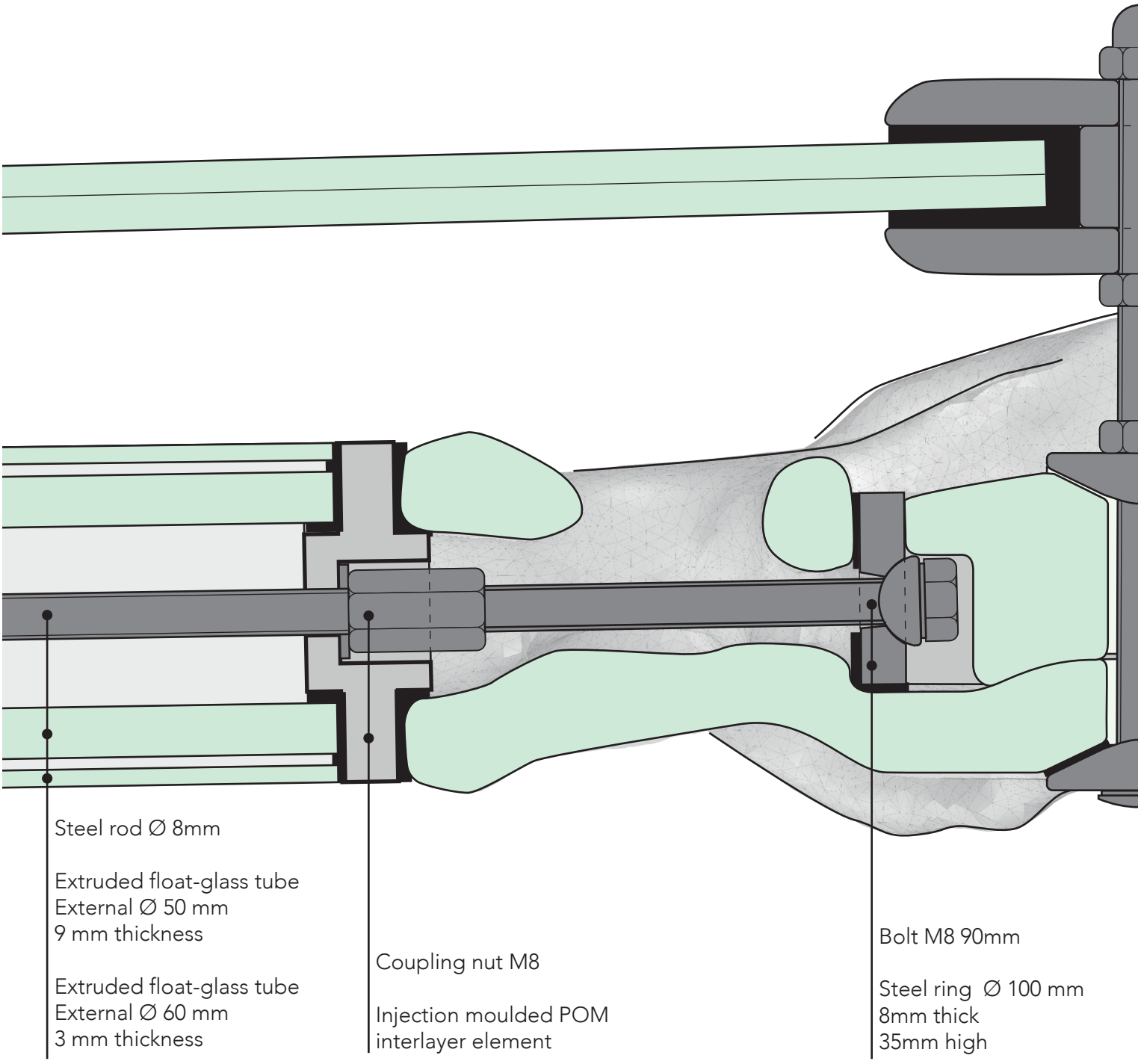

Fig. 146 *Node section, scale 1:1*

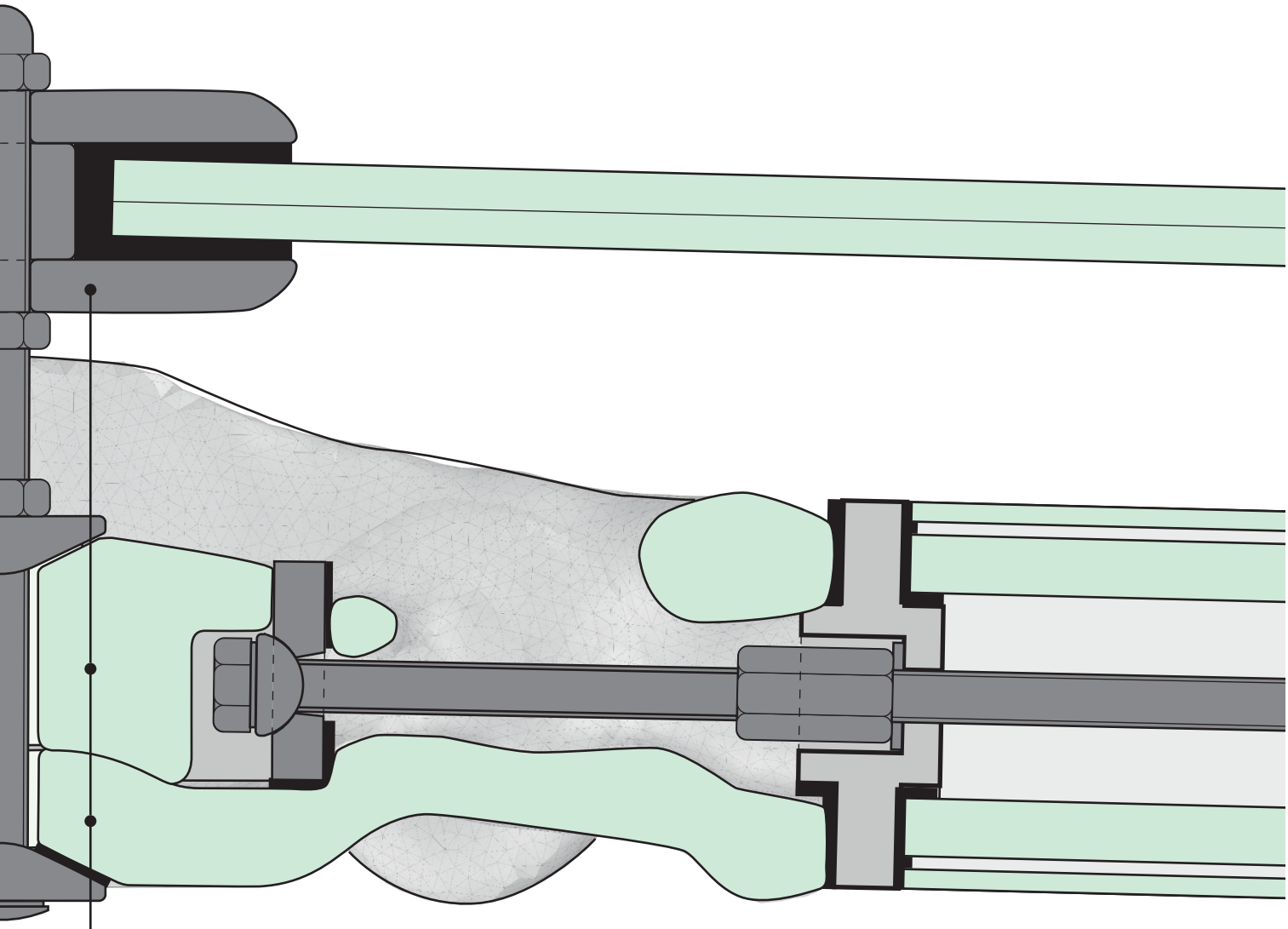

Facade connector

Injection moulded
PMMA centre element

Cast glass node

11.2 Node assembly detailing

The assembly process of the node consists of multiple steps.

The base of the node is formed by the optimised cast glass element (Fig. 147). Within the circular void of this node, the steel ring used for assmbly is placed. An interlayer is placed around the steel ring to avoid direct contact between the metal and the glass (Fig. 148).

The beams elements are pre-fabricated. This involves cutting the metal rod and the glass elements to the correct length. Two glass tubes are used: a main loadbearing tube and a thinner one placed around it to serve as a sacrificial layer. These can be joined together using two POM end caps, and fastened using two coupling bolts (Fig. 149).

On site, each beam is attached to the node using a single bolt, inserted through the steel ring (Fig. 150). This forms the load-bearing structure of the shell. For the cladding of the shell, a transparent plastic centre piece is added in the centre, and clamped in place Fig. 151). This gives a stable central bar that the facade can be attached to, while also closing the node, keeping out dirt and sand, and protecting the bolts that keep the strucure connected (Fig. 152).

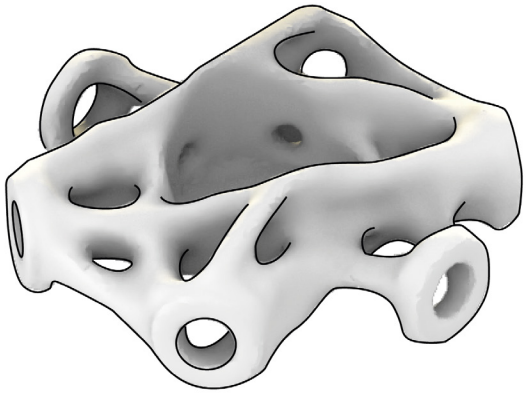

Fig. 147 *An optimised glass node*

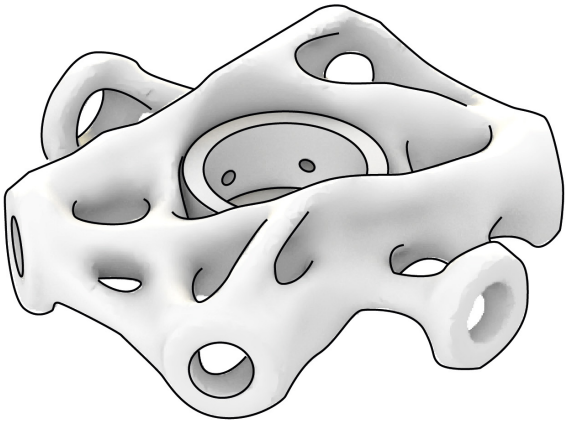

Fig. 148 *Adding the steel ring*

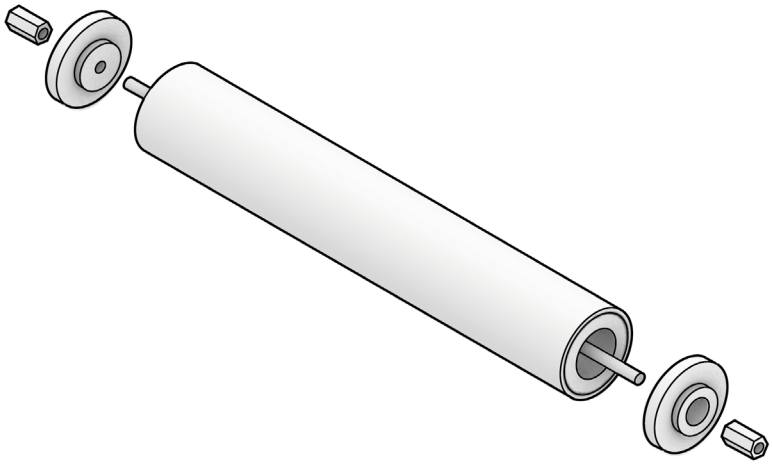

Fig. 149 *Pre-assembling the beam*

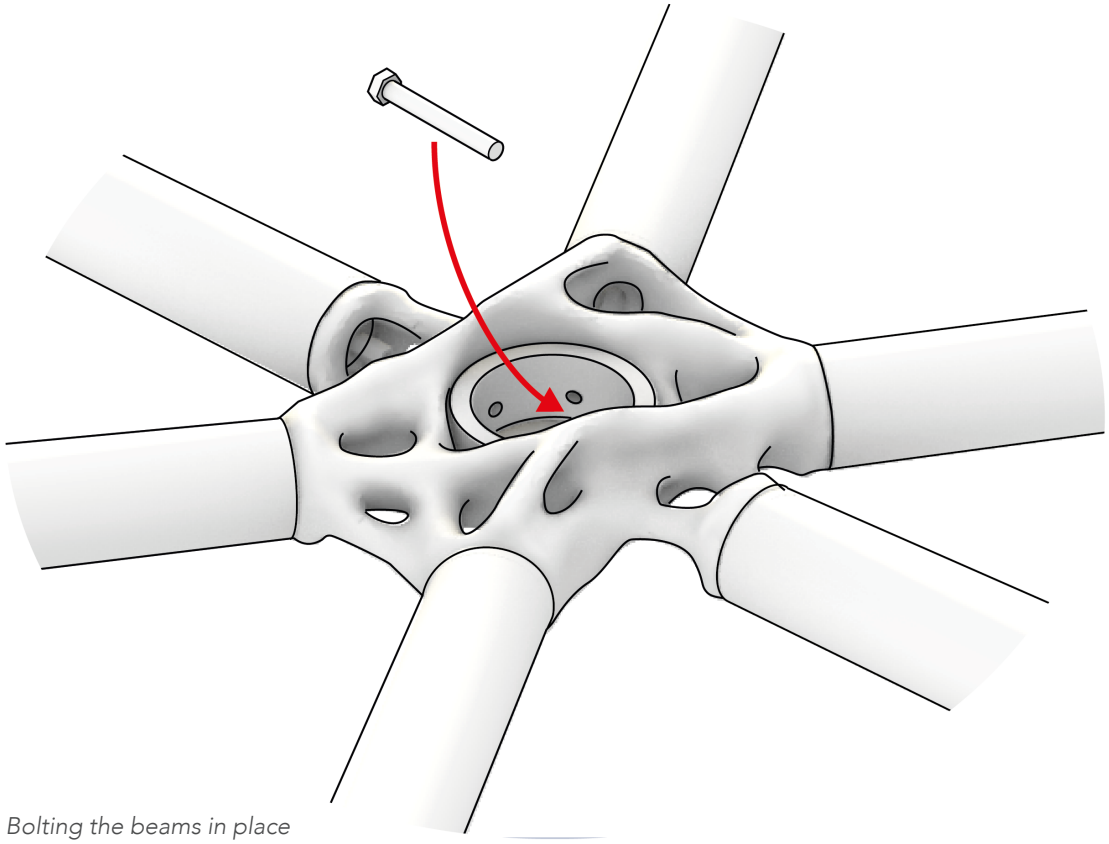

Fig. 150 *Bolting the beams in place*

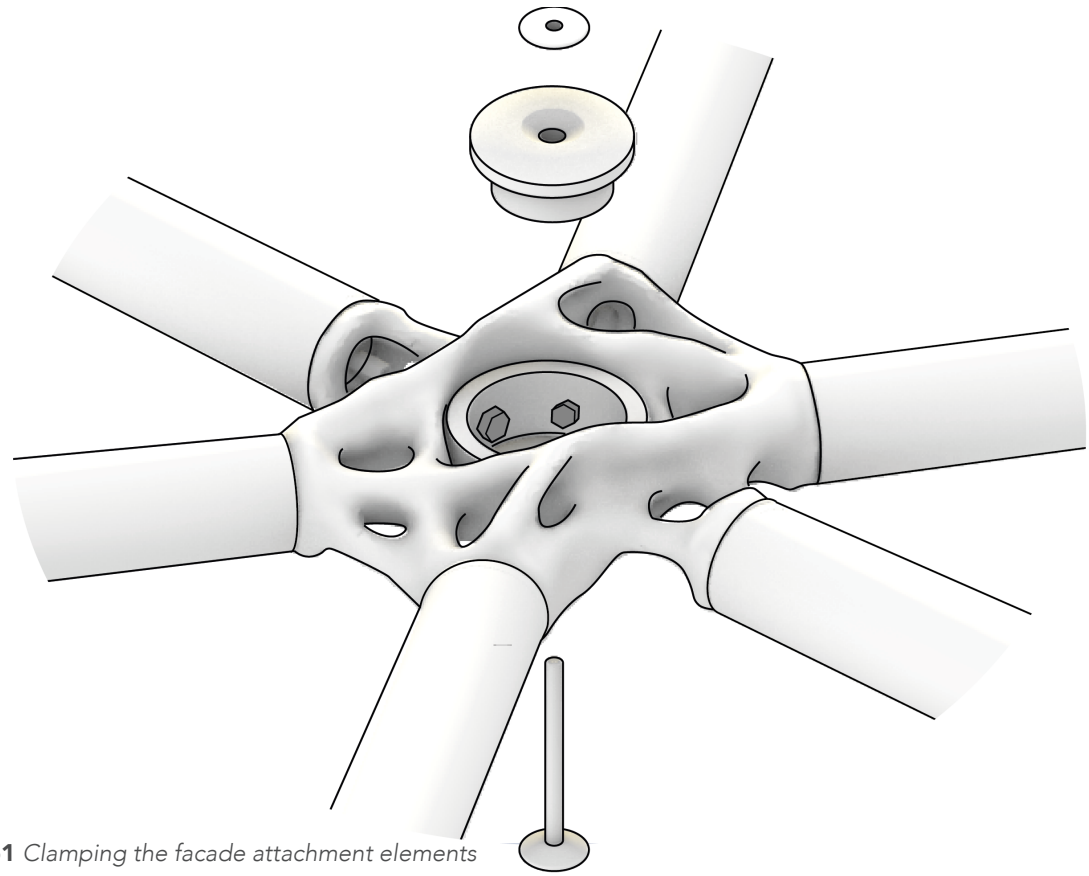

Fig. 151 *Clamping the facade attachment elements*

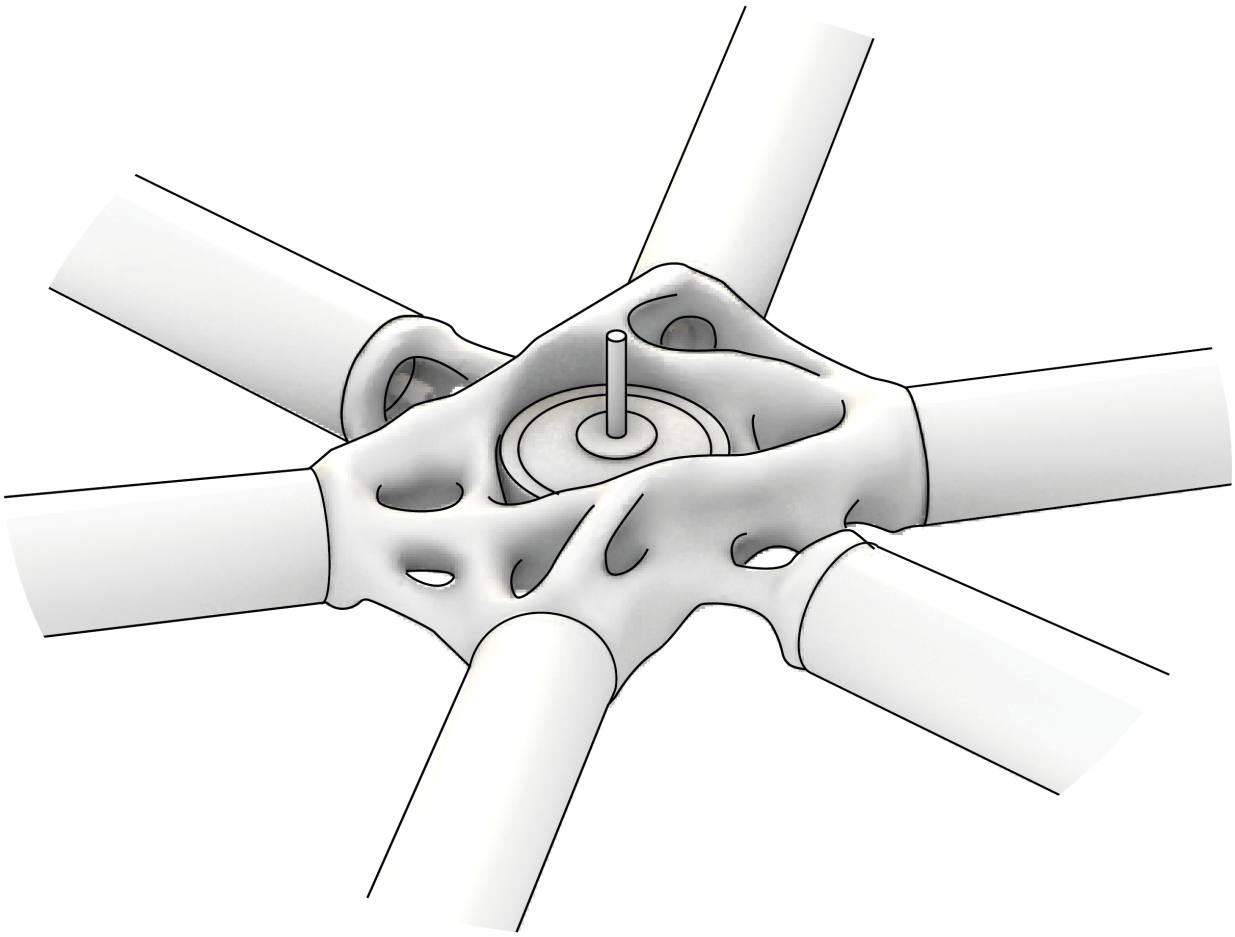

Fig. 152 *The completed node, ready for the placement of the cladding*

11.3 Fabrication and mass production

So far, it has been shown how cast glass can be used to design and make a grid shell element, with the aid of topology optimisation and additive manufacturing. When used in practice, however, these elements will need to be produced at large quantities. Even a relatively small grid shell structure such as the redesigned SUTD grid shell used for this project contains over five hundred nodes. The shape of the structure and the design methodology mean that each of these nodes will be fully unique. This raises a question about mass production: to what degree would it be possible to automate the various steps of the design process, in a way to make optimised cast glass elements viable and affordable at a large scale?

The following pages give an overview of the entire fabrication process, from digital model to physical structure. Along the way, it is discussed what parts of the process could be automated, and where human intervention will remain required.

Topology optimisation process

To begin with, a complete model of the shell structure is required. A structural analysis of this structure has to be performed to formulate inputs for the optimisation process. This involves determining the expected loads (or combinations of loads) on the node, and the design volume to optimise (Fig. 153). Using scripting and programming, this can be automated relatively simply, as has been shown by the Grasshopper script that was created for this project.

Depending on software chosen for the actual fabrication, it is likely that this data needs to be transmitted between different programs. Though this was done largely manually for this project, this too is something that can be automated. Software such as the GeometryGym plug-in for Grasshopper (https://geometrygym.wordpress.com/) allows for the transmission of data between different programs with minimal manual interference. A well-integrated BIM setup is therefore of essence to viably produce a shell like this.

For TO, many settings, such as materialisation and fabrication limitations remain unchanged between nodes. However, the exact material infill percentage used has so far been chosen manually. The material infill was chosen with a trial-ad error process to ensure a continuous and viable geometry is formed. Removing too much material can lead to very thin or even disconnected elements, as the thickness of geometry becomes smaller than the mesh elements used. Using a finer mesh of a higher resolution will should alleviate this issue. ANSYS recommends a mesh size that is one-third of the smallest element; for a minimal element size of 15mm this gives a 5mm mesh. In addition, if it is possible within the optimisation software, the element size limitation should be given a larger priority in the optimisation process. Though this might lead to somewhat reduced material efficiency, as material is added where it is not necessarily required from a structural point of view, it will ensure that the resulting geometry can reliably be fabricated.

The calculation times of the topology optimisation software cannot be neglected. The calculation times are largely determined by the amount of mesh elements present in the computational model. A finer mesh will result in smoother and more reliable thin elements, but will exponentially increase calculation times, whereas a rough mesh will solve faster, but might cause complications in post-processing and production. Using a mid-range PC, a node with relatively rough mesh of 8mm was optimised down to 20% material in 6 minutes, whereas the same calculation using a 5mm mesh increased the calculation time to 2 hours and 12 minutes. For the 500 nodes of the pavilion, this fine mesh would result in a calculation time of over 1000 hours. This value further increases if combined multi-load topology optimisations are used, as multiple optimisation iterations are then required for each node.

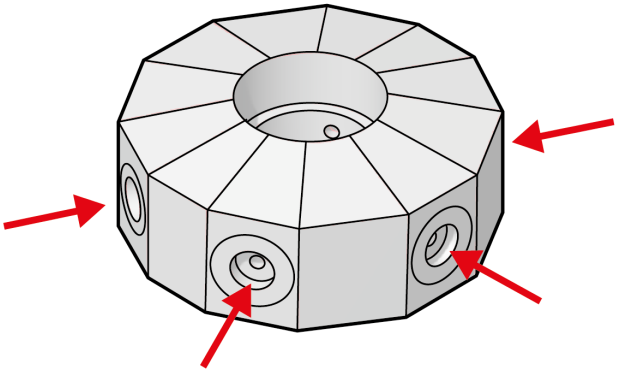

Fig. 153 *TO input: design area and loading conditions*

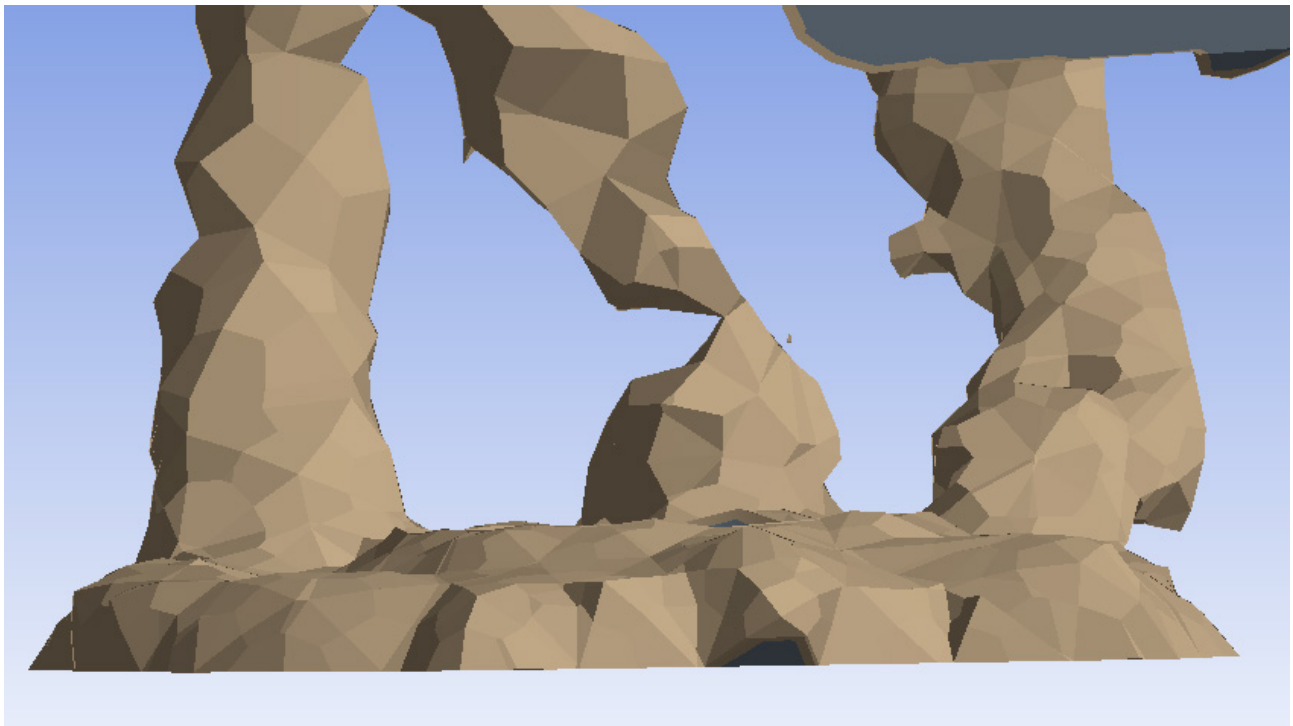

Fig. 154 *Unreliable, interrupted geometries caused by a too coarse mesh*

With a fully automated optimisation workflow, calculations could run day and night without interruptions. In addition, the work could be split between multiple computers, or even use an online cluster of computers in Cloud computing, which can potentially greatly reduce calculation times. However, this once again underlines the importance of automating the optimisation process.

Preparation for fabrication

The optimised geometry needs to be post-processed to prepare it for fabrication. Inserting additional geometries around the centre ring and supports, shrink-wrapping the geometry using a 4mm mesh and then smoothing the result was found to reliably result in geometries that are suitable for glass casting. As described before, a fine mesh and strictly defined fabrication constraints during optimisation should minimise the amount of manual work during post-processing. However, before fabrication it is recommended that each node should be inspected manually to ensure that they are viable for fabrication (Fig. 155).

To make the elements suitable for casting, tubes for airflow and circulation need to be added (Fig. 156). It is rather difficult to predict where these need to be placed, as this is greatly dependent on the geometry of the optimised node. Currently, when casting elements such as these, the placement of these casting aids is done manually, based on the experience and intuition of the caster. In computerised design, this should be made as simple as possible for the designer. A simple point and click system indicating the start and end point of each channel would be a possible way to do this. Ideally, the generation of the casting geometry could also be fully automated, taking into account the flow and cooling behaviour of the molten material as it flows through the mould. This is already partly possible (Sama et al., 2019), though fully integrating this within the optimisation workflow is expected to greatly increase the required calculation times.

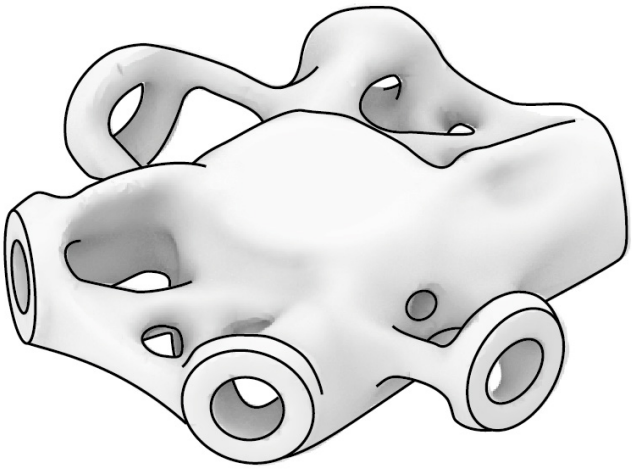

Fig. 155 *Optimised and cleaned up geometry*

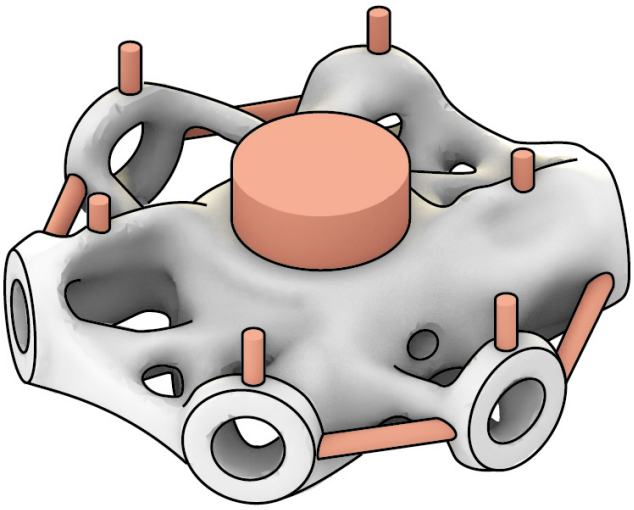

Fig. 156 *Preparation for casting*

Mould making

Once the geometry is fully prepared for casting, a mould design needs to be made. Sand printing has little restrictions on what geometries can be printed, which means the node geometries can be directly converted to a mould. For this project, Grasshopper script was used to automatically generate the mould.

The mould is made in slices to make sure the entire geometry is accessible. This has two reasons. After the binder jet printing is completed, loose sand without binder remains within the model. Keeping the mould accessible will make it easier to completely remove it from the mould. Secondly, a coating needs to be applied to the sand mould to improve the surface quality of the glass. Multiple coatings are available for this (Bhatia, 2019), for all of them, direct access is needed to properly apply it. An interlocking pin and hole system is automatically added to make sure the moulds are properly aligned during casting (Fig. 157-Fig. 158)

The sand moulds can be printed relatively fast if compared to other additive manufacturing techniques. The printing time is roughly 30 minutes for every 20-25mm in height . Using a print bed of 1800 x 1000mm (https://www.exone.com/Systems/Production-Printers/-S-Max), up to 18 moulds of 300 x 300 x 100mm can be printed simultaneously. This gives an average printing time of under 10 minutes per mould.

Alternatively, investment casting is used. For this, the geometry is 3D printed directly using a material that can melt and evaporate at a low temperature. Material and printing process chosen, there are limitations to what can be fabricated. Too steep overhanging angles for example, will require considerable support material to be printed, which means longer printing times, more material wasted and more post-processing required after printing. If this method is chosen for mass fabrication, additional optimisation is needed to take into account the limitations of the process. For the example of steep overhangs, the geometry can be changed to a steeper, pointed arch shape that can be printed without support. This will, however, take considerable remodelling (Fig. 159).

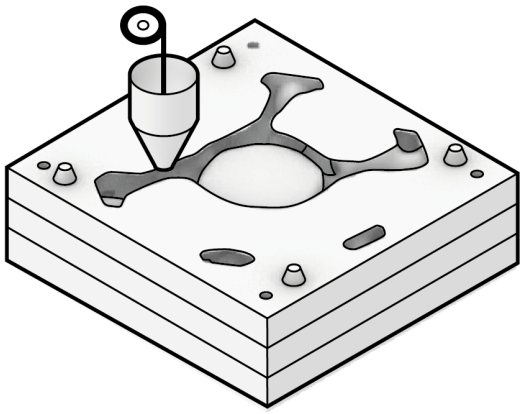

Fig. 157 *Additive manufacturing of the sand mould*

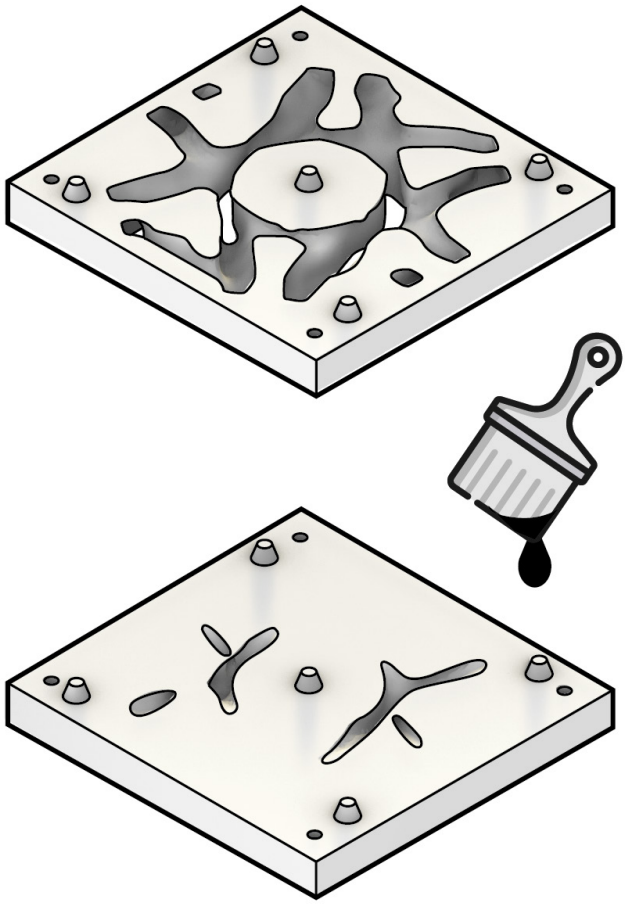

Fig. 158 *Sliced mould allowing the application of coatings*

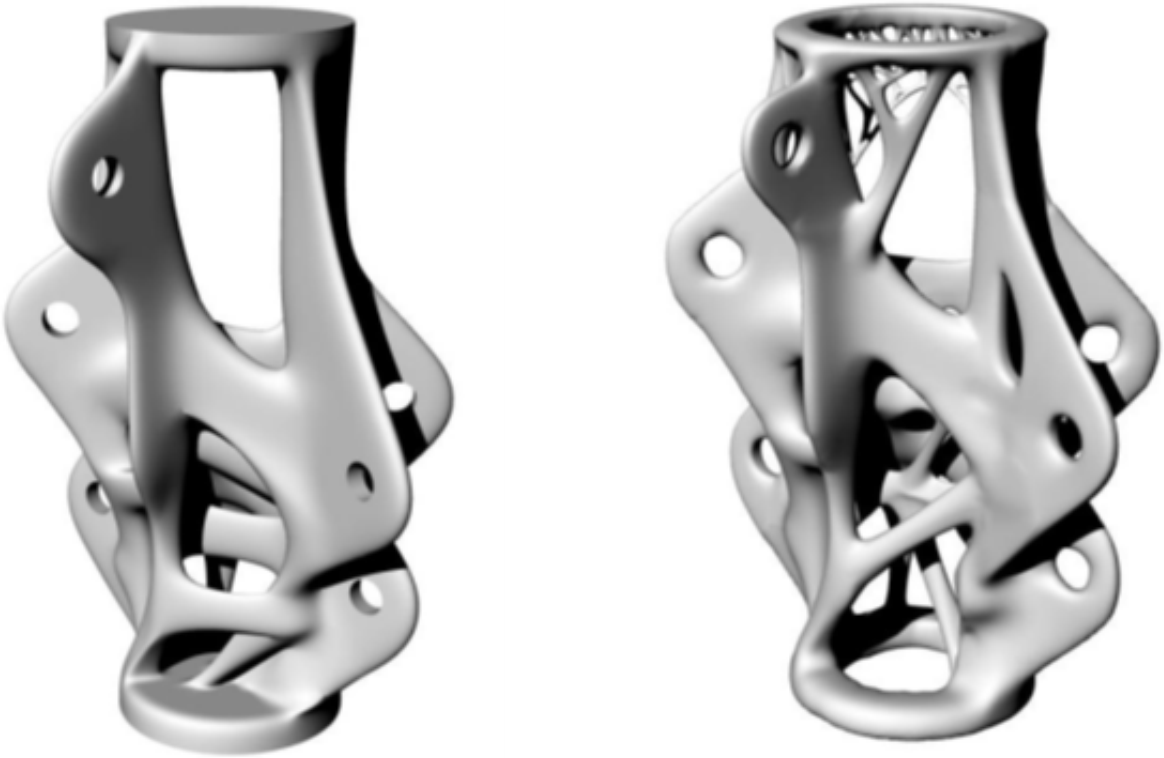

Fig. 159 *Design for additive manufacturing in the ARUP node. Left: the original optimised geometry. Right: the geometry, optimised for additive manufacturing without supports*

In addition, conventional additive manufacturing is a slow process compared to other fabrication methods. The 1:2 scale wax-printed prototype shown in chapter 9 took around 13 hours to print. This was partly because printing had to be slowed down due to the material, however even if printing speeds can be sped up, a full scale node will take considerable time to print.

After printing, the mould is cast around the object. For disposable glass casting moulds, Silica-plaster is generally used (Fig. 160). After the plaster has been left to harden, the printed geometry needs to be removed. This is generally done by burnout, where the mould is heated until the printed geometry evaporates. The temperature and duration for the burn-out is mainly determined by the material used for the printing; for example the wax filament used in this project had fully evaporated after around three hours at 515 °C. After burn-out, the mould is ready for casting.

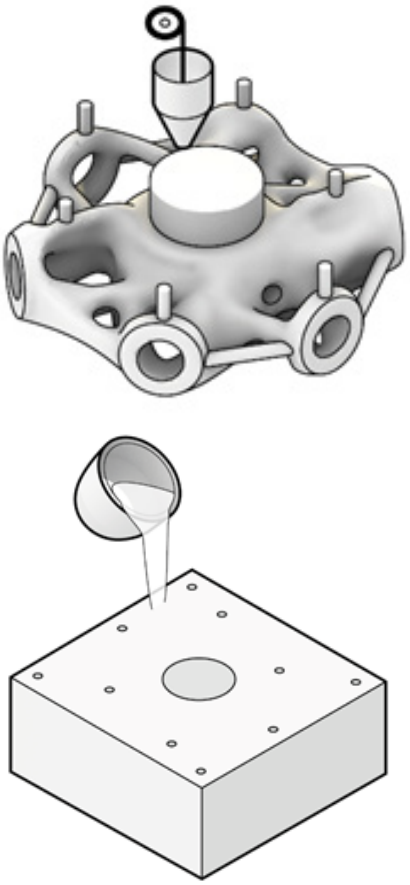

Fig. 160 *Additive manufacturing and casting of the investment mould*

Casting and post-processing

For the casting, either soda-lime or borosilicate glass can be used. Borosilicate glass is often used in solid glass casting because of its shorter annealing times compared to soda-lime glass. Due to the optimisation of the node however, annealing times are already relatively low, which reduces the gains that can be made by using borosilicate glass. In comparison, soda-lime glass is cheaper and can be cast at a lower temperature than borosilicate glass. Structurally, the performance of both types of glass is comparable. The final choice of material is dependant on cost, considering whether the further reduced annealing times of Borosilicate can be offset by its higher cost involved.

In chapter 2.3, the two methods of glass casting by either kiln-casting or hot-pouring were introduced. For large-scale fabrication, hot-pouring is employed. Though a larger setup with multiple ovens is required, it allows for many elements to be cast in quick succession. This is a process that can be fully automated, making it suitable for full mass-production of glass elements.

A challenge for hot pouring is precisely determining the amount of glass that needs to be poured on each mould, as this will differ between elements. A casting setup is required that can precisely determine how much material is being poured into each mould.

The alternative is kiln-casting. For this technique, more setup time per piece is needed, as both the moulds and the glass need to be placed in the oven beforehand, which will require a lot of manual labour. This does have the advantage is that the amount of glass that is put in each mould can be easily checked, though at large scale this might become prone to human error. Kiln-casting can be done for a single, smaller project, it is generally not viable for mass production.

Due to the optimised, low-mass elements, annealing times will be relatively short. The cooling times can be further reduced by placing elements of comparable mass together, as they will have similar annealing times. This means no element has to remain in the annealing oven longer than strictly necessary.

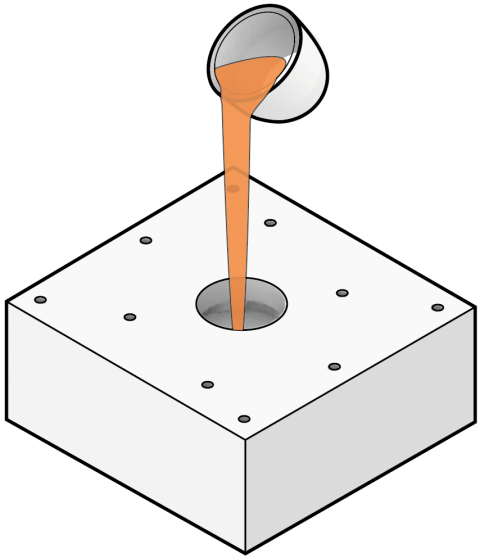

Fig. 161 *Hot-pouring*

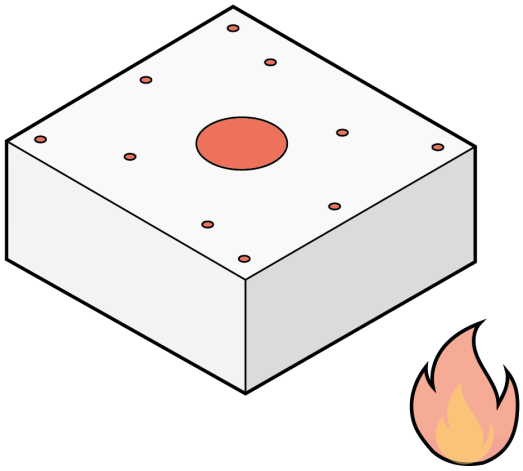

Fig. 162 *Annealing*

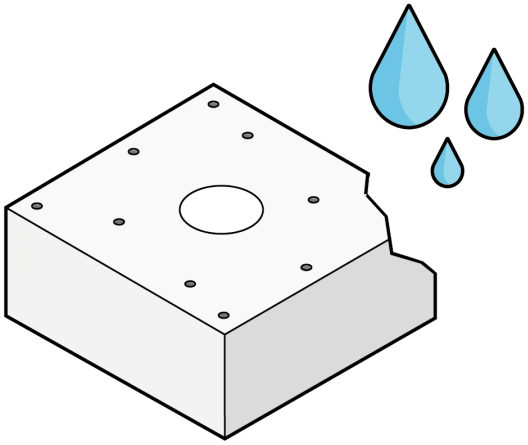

Fi

Both the printed sand moulds and the cast plaster moulds can be dissolved in water (Fig. 163). This means demoulding the nodes after cooling is relatively simple, and can be done without risk of damaging the glass. For the sand moulds, the sand can be cleaned and re-used.

After demoulding, the glass elements need to be cleaned up. This includes removing the tubes and channels added for the casting process, and polishing surface flaws that might have occurred during casting. Currently, this is mostly done by hand in a rather slow and labour intensive process. Ideally, a form of automated CNC milling could be used for mass production. The data for this milling is available, as the exact geometry of each node is known. In this case, the cylindrical void in the centre of each node could be used as a point where each node can be held while being milled.

For on-site assembly, it is important to keep in mind that all beam and node elements have a single specific place in the structure. A clear labelling system should be used, to ensure each element is placed correctly and any delays in assembly are avoided (Fig. 164). This can be taken into account during fabrication. Within the parametric model of the shell, each node and beam is labelled with a unique number. As the model of the node is prepared for printing, is would be possible to automatically add these labels into the node, as it can easily be printed together with the rest of the node without noticeably increasing production time. This provides the construction workers a clear guide for assembly that cannot get lost or mislabelled; while being still being practically invisible from a distance.

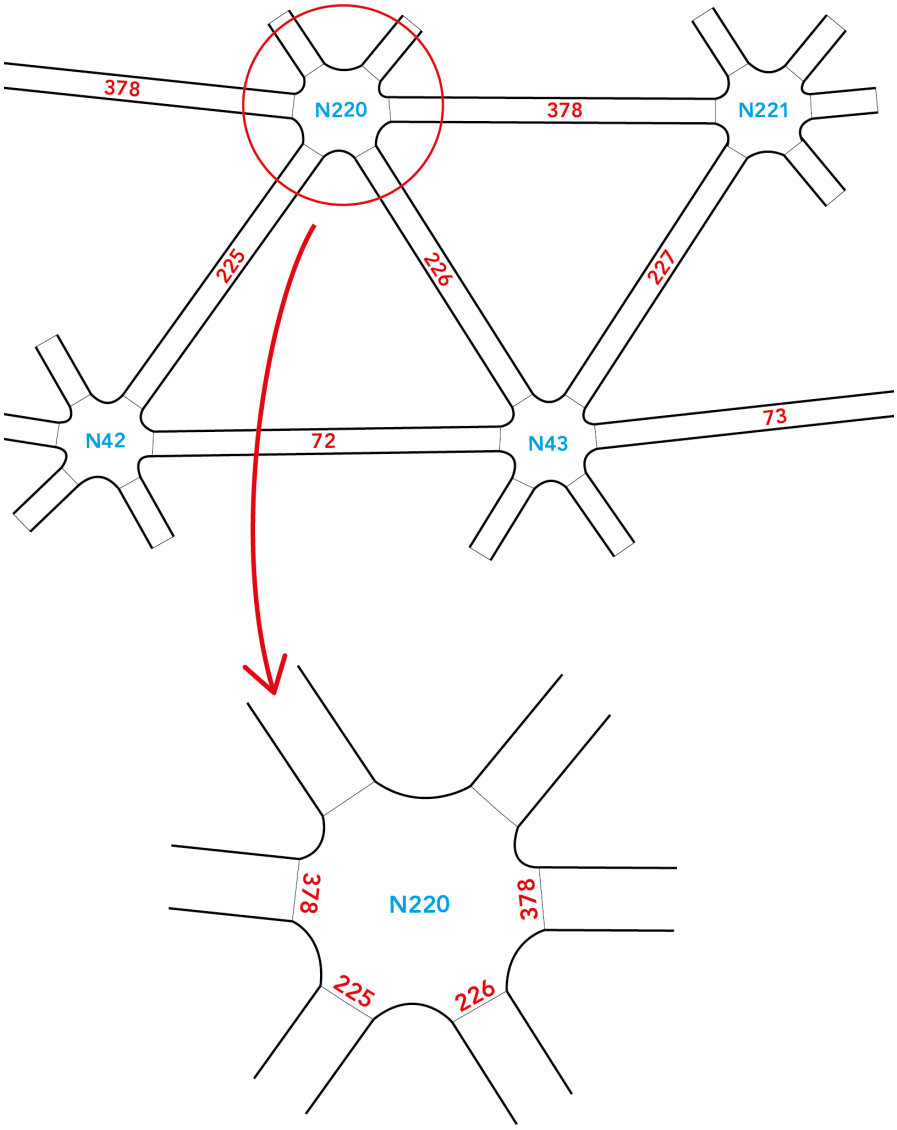

Fig. 164 *Numbering of the nodes and beams to simplify the assembly process*

Assembly preparation

Meanwhile, the remaining elements required for the assembly can be prepared.

The central steel ring has the same dimensions for each node, and can therefore simply be cut from a single size tube. The locations of the holes used to bolt the beams to the node are different for each node; these can be drilled by hand.

The glass tube beams can be pre-fabricated. For a free-form pavilion, nearly all beams will have a unique length. As described in chapter 6.2, this design of beam was chosen as it is relatively easy to modify its length by cutting the extruded glass beam and metal rod to the correct length. The POM end caps and the plastic node centre piece are all identical, and can be easily mass produced with injection moulding (Fig. 165).

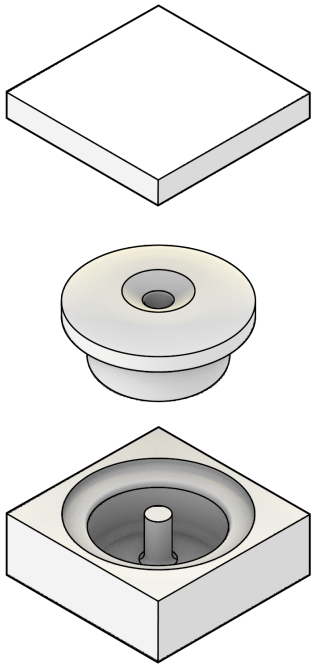

Fig. 165 *Central element is suitable for injection moulding*

Assembly

The assembly of the shell pavilion would start with the placement of foundations. On top of this, the bottom nodes are fastened. Due to the vulnerable location at the base of the shell, and the need for a strong connection to the foundations, these first nodes would likely be fabricated in steel. After the first layer of beams is bolted to these nodes, the first glass nodes can be placed. Due to the specific optimisation of the nodes, it is not guaranteed that they can withstand the loads of the unfinished shell under construction. Therefore, it is required to support the structure while it is being built.

Once a node is fully connected, the central glass element can be added in. This allows the façade cladding to be added, while also ensuring the bolted connections to the beams cannot easily be removed.

Conclusion

For affordably fabrication of a glass grid shell structure at this scale, the entire process from optimisation to assembly needs to be streamlined. Especially in the digital part of the process, from shell model to optimised node, most steps can be automated. Some parts of the process will always require a certain amount of time, such as the topology optimisation process, or the additive manufacturing. These can be made faster by running them multiple times, parallel to each other. Picking a faster production method, for example sand printing instead of wax printing, can also help.

Some steps require manual work. In some cases, this is due to a task that is relatively hard to automate, such as preparing the moulds for casting, or cutting off unwanted parts of the cast element. Other steps, such as checking the optimised geometry, and adding channels for casting, require some experience and insight to perform well.

With this in mind, does it make sense to design a shell structure using all unique, optimised nodes? Due to the complex shapes used, disposable moulds made with the help of additive manufacturing are the most suitable option. For the printing process it matters little if each component made is unique; it can be said that in additive manufacturing, complexity is given for free. This makes it much more attractive to create complex-shape shells where each node has a unique shape, and is uniquely optimised, as this adds relatively little to the fabrication process.

The sheer amount of optimised elements required for a relatively small pavillion such as the SUTD shell, makes it rather unlikely it would be realised in practice. However, it should be kept in mind that the grid shell was not designed with complex nodes in mind. For a glass grid shell, reducing the amount of nodes needed should be given priority

12. Conclusions

12.1 Research question

At the beginning of this thesis, the following central research question was formulated: What is the potential of using Topology Optimisation as a design tool for a structural cast glass grid shell node that is optimised for fabrication, structural behaviour and assembly? This question was split up in several sub-questions, each covering a different aspect of the research. Based on the research done, an answer can be formulated to these questions:

What design criteria should be used when using topology optimisation for cast glass design?

The design criteria for topology optimisation of glass can be subdivided in fabrication and structural criteria. For fabrication, the main thing that needs to be taken into account is designing for annealing. There are a couple of steps that can be taken to reduce annealing time. First and foremost, the mass of the element should be minimised. Less material is easier to cool down safely, in addition to being less resource-intensive and easier to transport and fabricate. Furthermore, using thin elements improves cooling time, as this makes it easier for the glass to lose its heat. This can be further improved by ensuring the element thickness and mass distribution is uniform throughout the element, as this allows for more homogeneous cooling, reduces the risk of internal stresses occurring within the material. Finally, sharp edges and corners should be avoided, as these are likely to cause localised stresses, both during cooling and under structural loading.

These criteria can be met within topology optimisation. It was shown that TO can be used to greatly reduce the mass of a structural element, with minimal loss of strength and stiffness. A minimal and maximal element size constraint can be used to ensure thin sections in the material, and homogenising material distribution throughout the element. Finally, the form-follows-force approach of TO avoids the occurrence of sharp edges in the material, generating smoothed, rounded shaped instead.

It was found that the casting process of the glass poses few limitations to the shape that can be achieved. Though cast glass is relatively viscous, when given sufficient time to settle within the mould, highly detailed geometries can be cast. The largest limitation here is the fabrication of the moulds, which will be discussed further on.

How should the connection between the glass node and the remainder of the structure be designed?

When designing the connections between the glass node and the surrounding glass beams, the structural limitations of the material need to be taken into account. As a brittle material, glass is vulnerable to tensile stresses. A clamped connection using a steel cable was developed to account for this. The included steel elements ensure that the glass is loaded under compression, as any tensile loads occurring due to axial loads or bending moments are carried in the steel members of the assembly. In addition, the lack of glued connections makes it possible to easily assemble, and disassemble the structure.

Glass is unable to deform plastically under heavy stress, and will instead fail, causing continuous cracks throughout the material. This behaviour makes it very vulnerable to localised stresses that can occur where glass comes into contact with metal, or other glass elements, due to flaws and inaccuracies in the material surface. A softer interlayer material should be introduced at these surfaces, to evenly distribute the load on the glass. For the cast node design, an interlayer was designed using POM, a high performance plastic.

Specific production techniques using additive manufacturing are required to create the complex-shaped elements found by the topology optimisation. This is a challenge, but also an opportunity. In contrast to conventional fabrication processes, additive manufacturing can be used to add more complexity to the node without greatly increasing fabrication time and cost. This makes it possible to reduce the amount of unique elements within the assembly, by including their functionality within the node. In the design made for the grid shell pavilion, the bulky metal end caps usually needed for this type of glass beam connections could be left out of the model,

as their function was included within the glass node. This reduced the amount of separate parts required for the design, while also increasing the transparency of the structure.

What are the most suitable methods to fabricate the nodes with the aid of additive manufacturing?

For the fabrication of the node, a disposable mould has been used. Not only is the topology of the design is too complex for a re-usable mould, but the load-based optimisation means that each node within the structure is unique, which makes single-use moulds the more suitable choice.

Two methodologies of additive manufacturing has been tried for the fabrication of this mould. Lost-wax investment casting, using a printed wax model of the node, was successfully used to cast a scale model. It was shown that this methodology is suitable for complex and detailed models, while using widely available tools. Though very useful for prototyping, this method is generally too slow and labour intensive to be viable when a large quantity of elements needs to be produced.

The second methodology employed was using additively manufactured sand moulds.

What is the influence of TO design on the annealing time of the glass elements?

The annealing time required to safely cool the glass nodes was estimated by comparing them to glass bricks produced in the Crystal Houses project. It was estimated that the initial, un-optimised glass node would take over two days to cool, due to its thickness and weight. The lightest optimised node weights 2.7 kg, which is 70% lighter than the starting geometry. In addition, it has a maximal section thickness of only 30 mm throughout the element. Due to this, it was estimated that this element would require only around 4 hours to cool down fully. The heavier node that was designed for a larger shell is heavier, weighing 5.4 kg, and has a slightly thicker geometry of maximum 40 mm throughout. Based on this, an annealing time of roughly 16 hours is predicted. Though considerably longer than the lightest node, this still implies that cooling time was cut by two thirds compared to the initial geometry. It can therefore be concluded that topology optimisation is an effective tool to reduce annealing times of cast glass elements.

To answer the main question, it can be concluded that topology optimisation does indeed have potential to be used for structural elements from cast glass. The variety of shapes that can be created using cast glass has great synergy with the organic shapes that are found with topology optimisation; together they can be used to create durable, light and aesthetically unique architectural elements. Additive manufacturing offers the freedom of shape required to fabricate these components, while also offering the opportunity to make the nodes more multi-functional within the structure of a shell.

It should be noted that there are some clear limitations to using topology optimisation within the built environment, which are discussed below.

12.2 Lessons learned

Some of the more broadly applicable lessons learned about using topology optimisation will be discussed in this chapter. Some of the things that worked and did not work are described.

First of all, it should be understood that Topology Optimisation is a specific tool, with specific applications. Within a given area, it will formulate a highly efficient way of distributing material to carry a specific load. TO is very good at this, giving viable results using only a fraction of the original material. This high level of optimisation is also its weakness: it is no longer viable when the boundary conditions change. In many applications in the built environment this can problematic, as structures are subjected to a variety of shifting loads. People and goods moving through the building, wind, snow or seismic activity can all greatly affect the loading on a structural element, and will cause structural failure of an over-optimised component if the loads diverge too far from the design load.

Increasing the redundancy of an optimised element can make it more flexible to withstand changing loads. Simply removing less material during optimisation is one method to achieve this, albeit an inefficient one, as the

optimisation process will use this material to further improve the resistance to the design load. This will lead to over-dimensioning for a specific load case, while adding little to overall strength.

Using dummy loads during form finding can be used to guide the optimisation process. Adding a bending moment or force in addition to the basic design load will force the TO to add material to account for this load. This can be used to reinforce elements that would otherwise be too fragile. It is however difficult to predict what loads should be added and where, as this is completely dependent on the geometry, existing loads and expected loading conditions.

A different issue can arise when multiple loads are applied that are wildly different in magnitude. Most of the material will be placed around the heavier loads, potentially leaving the lightly loaded parts fragile, or even fully disconnected. Again, an artificial base load can be added at the fragile parts to equalise the material distribution through the model, though finding the correct load to use is mostly a matter of trial-and-error.

If a couple of clear, different loads on the element can be defined, it is possible to optimise separately for these loads, and combine the resulting geometries. Though this makes it possible to optimise for multiple loads, structural behaviour during in-between loads cannot be guaranteed and should be tested.

It should therefore be carefully considered beforehand whether TO is a suitable tool for the design challenge at hand. TO is a very efficient tool if a single or only a couple of specific loads are expected, but lacks the rigidity to deal with a broad variety of load cases. It is possible to steer the TO in a way to make it more flexible. These solutions however have a risk of being inefficient or unreliable, while requiring a lot of manual work, to overcome an inherent weakness of the tool.

12.3 Discussion

Relevance

Though fully glass structures have become increasingly accepted within the built environment, it is still regarded as a two-dimensional material, based on float glass construction. Cast glass allows the creation of complex, solid objects, transforming glass to a fully three-dimensional material. Most research into structural cast glass, however, has been limited to relatively simple, repetitive geometries of stacked components; copying the design language of brick or stone blocks.

This research proposes a different design language for cast glass. Glass design using Topology Optimisation can be used to make structurally viable elements with only little material. These geometries can be annealed much faster than conventional solid glass elements, due to their low mass, organic shapes and thin material sections. The short annealing times eliminate one of the major challenges of cast glass fabrication, and can significantly help in making cast glass a competitive alternative to conventional glass structures.

Additive manufacturing has been used to simplify the mould-making process required for fabricating cast glass components. Conventional mould making is a complex, labour intensive process, which limits the casting of customised complex geometries. It has been shown that additive manufacturing of moulds can be used to streamline this process. Together with the reduced annealing times achieved with topology optimisation, this shows that cast glass has great potential to be used as a structurally sound and economically feasible construction material in the built environment.

This project combines an aesthetic design goal with a thorough technical approach, taking into account fabrication and assembly. The fusion of a challenging structural design with new materials, utilising innovative production techniques, make this project fitting for the Building Technology master.

That being said, it is doubtful whether a project like this would ever become reality. The nature of a grid shell brings with it that a great quantity of elements need to be produced. Considering the amount of work required for large scale production, in its current shape this specific design will likely remain a niche solution. However, cast glass nodes can also be used in smaller applications, such as small

scale trusses and space-frames, which are likely more realistic due to the smaller number of elements required. Finally, it serves to show that cast glass can absolutely be used as a viable structural material. Thin looking structural laminated glass, despite being proven to be safe, is still often looked at with suspicion by both users and lawmakers. These much more solid, cast glass components could be an important step in telling that glass structures can be trusted.

Limitations and Follow-up research

The results of the optimisation have been analysed only numerically, using FEA modelling. Though an attempt was made to make the setup as accurate as possible, some simplifications and assumptions had to be made. In addition, glass is a notoriously unpredictable material, and effects can occur that might not have been included in the simulations. Extensive physical testing should be performed to validate the analysis, but could not be performed due to a lack of time.

The final design made makes poor use of the compressive strength of glass. The compressive strength of glass is around ten times as high as its tensile strength, but in the node compressive and tensile stresses are comparable, with the tensile stresses being the defining failure criteria of the design. This is a result of the chosen optimisation methodology: the research was limited to using commercially available topology optimisation software's. As described in chapter 3, these are developed to be used with ductile materials, such as steel of plastics, with no distinction made between tension and compression

A possible follow-up topic could focus on using some of the more specialised, stress based optimisation algorithms, such as described by for example Jackson & Carstensen, 2019. By distinguishing between the tensile and compressive capacity of the material, the glass can be used much more efficiently.

In a similar direction, a multi-material optimisation such as for described by Gaynor et al., 2013, might be used (Fig. 166). This methodology has been developed for the optimisation of reinforcement in concrete structures, to minimise the amount of steel used and to ensure no tensile forces appear in the concrete. This makes it potentially useful for the design of a hybrid glass and steel structure, using the strengths of both materials to deal with respectively compression and tension. This can be used for lightweight and reliable glass structures at a large scale.

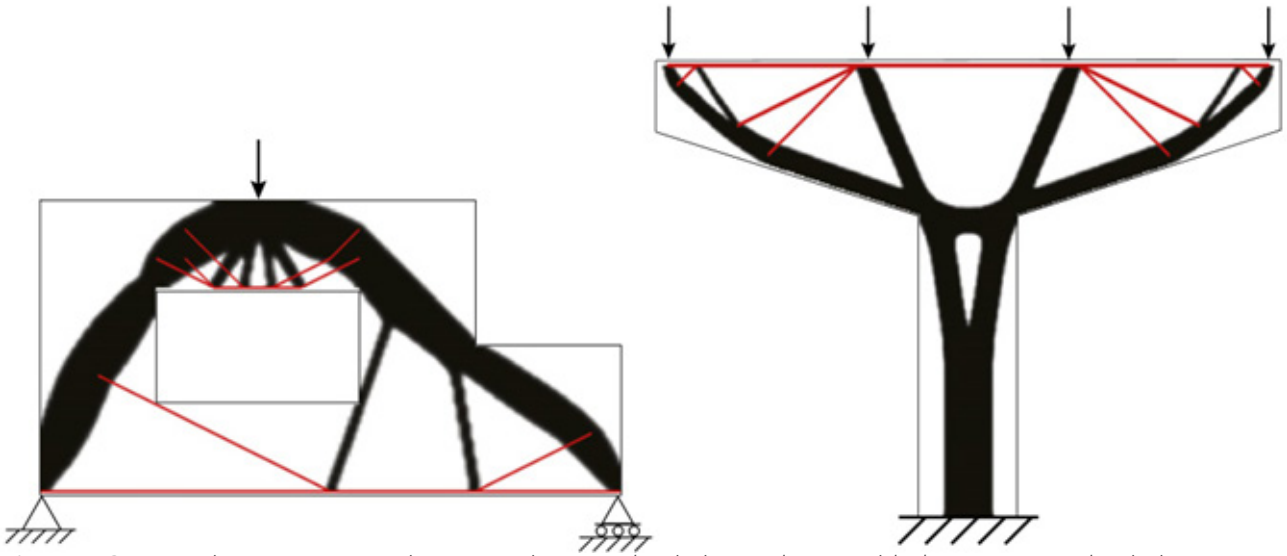

Fig. 166 *Optimised strut-continuum designs. Red: tension loaded strut elements, black: compression loaded concrete*

13. References

13.1 Literature

1. Introduction

Bendsoe, M.P., Sigmund, O. (2003) Topology Optimisation; Theory, Methods and Applications. Springer-Verlag, Berlin/Heidelberg, Germany.

Göppert, K., Paech, C., Arbós, F., Teixidor (2008) Glass Monument in Remembrance of the Terrorist Attacks in Madrid of March 11, 2004. Retrieved from: http://www.bellapart.com/uploads/files/entradas/glass-monument-in-remembrance-of-the-terrorist-atta.pdf in December 2018.

Niehe, P. (19 September 2017) Sand printing makes complex casted structural parts affordable. Retrieved from: https://www.arup.com/news-and-events/sand-printing-makes-complex-casted-structural-parts-affordable in November 2018.

Oikonomopoulou, F., Bristogianni T., Veer, F.A., Nijsse, R. (2017) The construction of the Crystal Houses façade: challenges and innovations. Glass Structural & Engineering, DOI 10.1007/s40940-017-0039-4

Oikonomopoulou, F., Bristogianni, T., Barou, L., Veer, F.A., Nijsse, R. (2018) The potential of cast glass in structural applications; Lessons learned from large-scale castings and state-of-the art load-bearing cast glass in architecture. Journal of Building Engineering 20, 213-234.

Saadlaoui, Y., Milan, J.L., Rossi, J.M., Chabrand, P. (2017) Topology optimisation and additive manufacturing: Comparison of conception methods using industrial codes. Journal of Manufacturing Systems 43, 178-186.

2. Glass

Arbab, M., Finley, J.J. (2010) Glass in Architecture. International Journal of Applied Glass Science, 1, 118-129.

Bristogianni, T., Nijsse, R., Oikonomopoulou, F., Veer, F. A. (2016) Design and production of a structural cast glass element for a transparent dome. Insights and Innovations in Structural Engineering, Mechanics and Computation: Proceedings of the 6th International Conference on Structural Engineering, Mechanics and Computation, SEMC 2016, 1662-1667.

Cai, K., Shi, J. (2010) A Bionic Approach for Topology Optimisation for Tension-only or Compression-only Design. Journal of Bionic Engineering, 7, 397-404.

Corning museum of Glass (December 8, 2011) Types of Glass. Retrieved from: https://www.cmog.org/article/types-glass in December 2018.

Cummings, K. (2001) Techniques of kiln-formed glass. A&C Black Publishers Limited/University of Pennsylvania Press, London/Philadelphia, UK/USA.

Göppert, K., Paech, C., Arbós, F., Teixidor (2008) Glass Monument in Remembrance of the Terrorist Attacks in Madrid of March 11, 2004. Retrieved from: http://www.bellapart.com/uploads/files/entradas/glass-monument-in-remembrance-of-the-terrorist-atta.pdf in December 2018.

Guan, H., Steven, G.P., Xie, Y.M. (1999) Evolutionary Structural Optimisation Incorporating Tension and Compression Materials. Advances in Structural Engineering, 2, 273-288.

Haldimann, M. (2006) Fracture strength of structural glass elements; analytical and numerical modelling, testing and design. Doctoral Dissertation, Department of Civil Engineering, École Polytechnique Fédérale de Lausanne, France. Retrieved from: https://infoscience.epfl.ch/record/89658/files/EPFL_TH3671.pdf

Klein, J., (2015) Additive Manufacturing of Optically Transparent Glass. Master Thesis, School of Architecture and Planning, Massachusetts Institute of Technology, USA.

Luo, J., Pan, H., Kinzel, E.C. (2014) Additive Manufacturing of Glass. Journal of Manufacturing Science and

Engineering 136, DOI 10.1115/1.4028531.

MVRDV (2018) Crystal Houses. Retrieved from: https://www.mvrdv.nl/projects/crystal-houses in January 2019.

Niehe, P. (19 September 2017) Sand printing makes complex casted structural parts affordable. Retrieved from: https://www.arup.com/news-and-events/sand-printing-makes-complex-casted-structural-parts-affordable in November 2018.

Oikonomopoulou, F., Bristogianni T., Veer, F.A., Nijsse, R. (2017) The construction of the Crystal Houses façade: challenges and innovations. Glass Structural & Engineering, DOI 10.1007/s40940-017-0039-4

Oikonomopoulou, F., Bristogianni, T., Barou, L., Veer, F.A. (2018) The potential of cast glass in structural applications. Lessons learned from large-scale castings and state-of-the-art load-bearing cast-glass in architecture. Journal of Building Engineering 20, 213-234

O'Regan, C. (Ed.) (2014). Structural use of glass in buildings (Second edition), The institution of Structural Engineers, London, United Kingdom.

Veer, F.A. (2007) The strength of glass, a non-transparent value. Heron, vol. 52, no ½.

Watson, D.M. (1999) Practical Annealing. Retrieved from: http://www.gafferglass.com/technical/practical-annealing-by-dan-watson/, in December 2018.

Whitney, D., Kipnis J. (1993) Philip Johnson, The Glass House. Pantheon Books, New York, xi–xxxiii.

Witzendorff, P., Pohl, L., Stuttmann, O., Heinrich, P., Heinrich, A., Zander, J., Bragard, H., Kaierle, S. (2018) Additive manufacturing of glass: CO2-Laser glass deposition printing. 10th CIPR Conference on Photonic Technologies, Procedia CIRP 74, 272-275.

Zirker, J.B., (2005) An Acre of Glass: A History and Forecast of the Telescope. John Hopkins University Press, Baltimore, USA.

3. Topology Optimisation

Bendsoe, M.P., Sigmund, O. (2003) Topology Optimisation; Theory, Methods and Applications. Springer-Verlag, Berlin/Heidelberg, Germany.

Gaynor, A., Guest, J., Moen C. (2013) Reinforced Concrete Force Visualisation and Design Using Bilinear Truss-Continuum Topology Optimisation. Journal of Structural Engineering 139, 607-618.

Huang, X., Xie, Y.M. (2010) Evolutionary topology optimization of continuum structures with an additional displacement constraint. Structural and Multidisciplinary Optimisation, 40, 409-416.

Jewett, J., Carstensen, J. (2019) Topology-optimised design, construction and experimental evaluation of concrete beams. Automation in Construction 102, 59-67.

Jipa, A., Meibodi, M.A., Bernhart, M., Dillenburger, B. (2016) 3D-Printed Stay-in-Place Formwork for Topology Optimised Concrete Slab. TxA Emerging Design + Technology Conference, San Antonio, Texas, USA.

Lundgren, J., Palmqvist, C. (2012) Structural Form Optimisation; Methods of numerical optimisation and applications on civil engineering structures. Master Thesis, Department of Civil and Environmental Engineering, Chalmers University of Technology, Göteborg, Sweden. Retrieved from: http://publications.lib.chalmers.se/records/fulltext/162939.pdf (December 2018).

Rozvany, G. (2009) A critical review of established methods of structural topology optimisation. Structural Multidisciplinary Optimisation, 37, 217-237.

Suzuki, K., Kikuchi, N. (1991) A homogenisation method het shape and topology optimisation. Computer

Methods in Applied Mechanics and Engineering, 93, 291-318.

Wang, M.Y., Wang, X., Guo, D. (2003) A level set method for structural topology optimisation. Computer methods in applied mechanics and engineering, 192, 227-246.

Weaver, T. (September 2016) Inside Track; 3D printing the Light Rider. Develop 3D, 20-24.

4. Shell

Bulenda, Th., Knippers, J. (2001) Stability of grid shells. Computers and Structures, 79, 1161-1174.

Blauwendraad, J., Hoefakker, J.H. (2014) Structural Shell Analysis; Understanding and Application. Springer Science+Business Media, Dordrecht, The Netherlands.

El-Sheikh, A. (1996) Development of a New Space Truss System. Journal of Constructional Steel Research, 3, 205-227.

Fritzsche, J.C. (2013) Gridshell Efficiency optimisation; optimising efficiency form- & grid-configuration through iterative approximation and minimising strain energy. Master thesis, Department of Architecture Building and Planning, TU Eindhoven, Netherlands. Retrieved from: https://pure.tue.nl/ws/portalfiles/portal/46942029/761229-1.pdf in December, 2018.

Garlock, M.M., Billington D.P. (2014) Félix Candela and Heinz Isler; A comparison of two structural artists. In Adriaenssens, S., Block, P., Veenendaal, D., Williams, W. (Eds.) Shell structures for Architecture; Form Finding and Optimisation, 247-257. Routlegde, London/New York, UK/USA.

Harvard Business Review (2018) The Next Wave of Intelligent Design Automation. Briefing paper

Linden, L. (2015) Innovative joints for gridshells; joints designed by topology optimisation and to be produced by additive manufacturing. Master Thesis, Faculty of Civil Engineering, TU Delft. Retrieved from: https://repository.tudelft.nl/islandora/object/uuid:8bf193c3-eece-4fc1-a259-06ae5d275f45 in November 2018.

Ney, L., Adiaenssens, S. (2014) Shaping forces. In Adriaenssens, S., Block, P., Veenendaal, D., Williams, W. (Eds.) Shell structures for Architecture; Form Finding and Optimisation, 15-19. Routlegde, London/New York, UK/USA.

Prayudhi, B. (2016) 3F3D: Form Follows Force with 3D printing; Topology Optimisation for Free-form Building Envelope design with Additive Manufacturing. Master Thesis, Faculty of Architecture and the Built Environment, TU Delft. Retrieved from: https://repository.tudelft.nl/islandora/object/uuid%3Ab068f81c-1561-4733-a07d-05e60368184b in November 2018.

Seifi, H., Javan, A.R., Xu, S., Zhao, Y. (2018) Design optimisation and additive manufacturing of nodes in gridshell structures. Engineering Structures, 160, 161-170.

Williams, C. (2014) What is a Shell? In Adriaenssens, S., Block, P., Veenendaal, D., Williams, W. (Eds.) Shell structures for Architecture; Form Finding and Optimisation, 21-31. Routlegde, London/New York, UK/USA.

6. Pavilion Design

Eekhout, M., Staaks, D. (2010) All-Glass Dome for Mosque in Haarlem, Challenging glass 2 – Conference on Architectural and Strucutral Applications of Glass, May 2010.

Galjaard, S., Hofman, S., Perry, N., Ren, S. (2015) Optimizing Structural Building Elements in Metal by uaing Additive Manufacturing. Proceedings of the International Association for Shell and Spacial Structures Symposium, August 2015, Amsterdam, The Netherlands.

Nijsse, R. (2013) Dictaat Draagconstructies I, TU Delft, Faculty Bouwkunde.

Snijder, A., Nijsse, R., Louter, C. (2018) The glass truss bridge, HERON, 63, 139-157.

7. Optimisation Methodology
Linden, L. (2015) Innovative joints for gridshells; joints designed by topology optimisation and to be produced by additive manufacturing. Master Thesis, Faculty of Civil Engineering, TU Delft. Retrieved from: https://repository.tudelft.nl/islandora/object/uuid:8bf193c3-eece-4fc1-a259-06ae5d275f45 in November 2018.

8. Optimisation Results
Linden, L. (2015) Innovative joints for gridshells; joints designed by topology optimisation and to be produced by additive manufacturing. Master Thesis, Faculty of Civil Engineering, TU Delft. Retrieved from: https://repository.tudelft.nl/islandora/object/uuid:8bf193c3-eece-4fc1-a259-06ae5d275f45 in November 2018.

Oikonomopoulou, F., Bristogianni, T., Barou, L., Veer, F.A. (2018) The potential of cast glass in structural applications. Lessons learned from large-scale castings and state-of-the-art load-bearing cast-glass in architecture. Journal of Building Engineering 20, 213-234

Prayudhi, B. (2016) 3F3D: Form Follows Force with 3D printing; Topology Optimisation for Free-form Building Envelope design with Additive Manufacturing. Master Thesis, Faculty of Architecture and the Built Environment, TU Delft. Retrieved from: https://repository.tudelft.nl/islandora/object/uuid%3Ab068f81c-1561-4733-a07d-05e60368184b in November 2018.

9. Casting tests
Bhatia, I. (2019) Shaping Transparent Sand in Sand; Fabricating geometrically optimized glass column using 3d printed sand moulds. Master Thesis, Faculty of Architecture and the Built Environment, TU Delft.

10. Final Design
Bhatia, I. (2019) Bhatia, I. (2019) Shaping Transparent Sand in Sand; Fabricating geometrically optimized glass column using 3d printed sand moulds. Master Thesis, Faculty of Architecture and the Built Environment, TU Delft.

Sama, S., Wang, J., Manogharan, G. (2018) Non-conventional mold design for metal casting using 3D sand-printing. Journal of Manufacturing processes 34, 765-775.

11. Conclusion
Gaynor, A., Guest, J., Moen C. (2013) Reinforced Concrete Force Visualisation and Design Using Bilinear Truss-Continuum Topology Optimisation. Journal of Structural Engineering 139, 607-618.

13.2 Internet Sources

Software
Ameba: topology optimisation plug-in for Grasshopper. Retrieved from: https://ameba.xieym.com/ in December, 2018.

Sawapan Millipede: structural design and topology optimisation plug-in for Grasshopper. http://www.sawapan.eu/, retrieved in December, 2018.

ANSYS topology optimisation. https://www.ANSYS.com/products/structures/optimization, retrieved in December, 2018.

Autodesk Fusion 360: modelling and structural design software. https://www.autodesk.com/products/fusion-360/overview, retrieved in May, 2019.

Autodesk Generative Design: automated design software. https://www.autodesk.com/solutions/generative-design, retrieved in June, 2019

Autodesk MeshMixer: analysis and editing of mesh objects. https://www.meshmixer.com, retrieved in May , 2019.

GeometryGym: plug-in allowing for easy transfer of data from grasshopper to different software packages. https://geometrygym.wordpress.com/, retrieved in June, 2019.

Materials
Machineable Wax: filmanent used in the lost-wax printing. https://www.machinablewax.com/product.php?product=52, retrieved in April, 2019.

MOLDLAY wax filament: https://www.matterhackers.com/store/3d-printer-filament/moldlay-filament-1.75mm, retrieved in April, 2019.

PolyCast filament: https://eu.polymaker.com/product/polycast/, retrieved in April, 2019.

POM/Delrin interlayer plastic: https://www.ridderflex.nl/wp-content/uploads/POM-Delrin%C2%AE-naturel.pdf, retrieved in April, 2019.

Schött: glass manufacturer with a wide range of extruded glass products. https://www.schott.com/tubing/english/product_selector/, retrieved on January 2019.

Additive manufacturing
ExOne: producer of tools and materials for additive manufacturing of sand. https://www.exone.com/, retireved in May, 2019.

13.3 Illustrations

Any figures not included in this list have been drawn by the author

Fig. 1
Estudio de Arquitectura FAM, https://en.wikiarquitectura.com/building/monument-11-m/

MVRDV: https://www.mvrdv.nl/projects/240/crystal-houses, April 3, 2016

Fig. 2
Galjaard, S., Hofman, S., Perry, N., Ren, S. (2015) Optimizing Structural Building Elements in Metal by uaing Additive Manufacturing. Proceedings of the International Association for Shell and Spacial Structures Symposium, August 2015, Amsterdam, The Netherlands.

Fig. 3
Foster and Partners, https://www.fosterandpartners.com/media/2632341/hero_0793_fp276124.jpg?width=1920&quality=85

Fig. 4
Oikononomopoulou, F., Glass structures Sustainability & Innovation Lectures, TU Delft, September 20, 2017.

Fig. 5
Haldimann, M. (2006) Fracture strength of structural glass elements; analytical and numerical modelling, testing and design. Doctoral Dissertation, Department of Civil Engineering, École Polytechnique Fédérale de Lausanne, France. Retrieved from: https://infoscience.epfl.ch/record/89658/files/EPFL_TH3671.pdf

Fig. 6
Rubem, O., Montedo, O., Hotza, D., Oliveira, A., Meszaros, R., Travitzky, N., Greil, P. (2012) Crystallisation Kinetics of a -Spodumene-Based Glass Ceramic, Advances in Materials Science and Engineering 4.

Fig. 8
Devon Murphy, http://devon-murphy.blogspot.com/2012/04/how-i-make-some-of-things-i-make.html April 27 2012

Washington Glass School, http://washingtonglassschool.com/category/cast-float-glass . July 15, 2014

Fig. 9
SCHOTT/ESO, https://www.eso.org/public/images/eso1715a/ May 22, 2017

Fig. 10
Oikonomopoulou, F., Bristogianni, T., Barou, L., Veer, F.A. (2018) The potential of cast glass in structural applications. Lessons learned from large-scale castings and state-of-the-art load-bearing cast-glass in architecture. Journal of Building Engineering 20, 213-234

Fig. 12
Giant Magellan Telescope https://www.gmto.org/gallery/mirror-lab/, 2019

Fig. 13
Bristogianni, T., Nijsse, R., Oikonomopoulou, F., Veer, F. A. (2016) Design and production of a structural cast glass element for a transparent dome. Insights and Innovations in Structural Engineering, Mechanics and Computation: Proceedings of the 6th International Conference on Structural Engineering, Mechanics and Computation, SEMC 2016, 1662-1667.

Fig. 14
Oikonomopoulou, F., Bristogianni, T., Barou, L., Veer, F.A. (2018) The potential of cast glass in structural applications. Lessons learned from large-scale castings and state-of-the-art load-bearing cast-glass in architecture. Journal of Building Engineering 20, 213-234

Fig. 15
MVRDV: https://www.mvrdv.nl/projects/240/crystal-houses, April 3, 2016

Fig. 16
Oikonomopoulou, F., Bristogianni, T., Barou, L., Veer, F.A. (2018) The potential of cast glass in structural applications. Lessons learned from large-scale castings and state-of-the-art load-bearing cast-glass in architecture. Journal of Building Engineering 20, 213-234

Fig. 17
Estudio de Arquitectura FAM, https://en.wikiarquitectura.com/building/monument-11-m/

Fig. 18
Klein, J., (2015) Additive Manufacturing of Optically Transparent Glass. Master Thesis, School of Architecture and Planning, Massachusetts Institute of Technology, USA.

Fig. 19
Bendsoe, M.P., Sigmund, O. (2003) Topology Optimisation; Theory, Methods and Applications. Springer-Verlag, Berlin/Heidelberg, Germany.

Fig. 20
Belblidia, F., Bulman, S. (2002) A hybrid topology optimization algorithm for static and vibrating shell structures, International Journal for Numerical Methods in Engineering 54, 835 - 852

Fig. 21
Liu, X., Li, Z., Wang, L., Wang, J. (2011) Solving topology optimization problems by the Guide-Weight method, Frontiers of Mechanical Engineering 6, 136-150.

Fig. 22
Zhao, F. (2014) A nodal variable ESO (BESO) method for structural topology optimization, Finite Elements in Analysis and Design 86, 34-40.

Fig. 23
Cai, S., Zhang, W. (2015) Stress constrained topology optimization with free-form design domains, Computer Methods in Applied Mechanics and Engineering 289

Fig. 24
Jewett, J., Carstensen, J. (2019) Topology-optimised design, construction and experimental evaluation of concrete beams. Automation in Construction 102, 59-67.

Fig. 25 - Fig. 26
Weaver, T. (September 2016) Inside Track; 3D printing the Light Rider. Develop 3D, 20-24.

Fig. 27 - Fig. 28
Jipa, A., Meibodi, M.A., Bernhart, M., Dillenburger, B. (2016) 3D-Printed Stay-in-Place Formwork for Topology Optimised Concrete Slab. TxA Emerging Design + Technology Conference, San Antonio, Texas, USA.

Fig. 29 - Fig. 30
Oikonomopoulou, F. Pictures taken on the Milan Design Week, April 13, 2019.

Fig. 31
Williams, C. (2014) What is a Shell? In Adriaenssens, S., Block, P., Veenendaal, D., Williams, W. (Eds.) Shell structures for Architecture; Form Finding and Optimisation, 21-31. Routlegde, London/New York, UK/USA.

Fig. 32
http://projects.mcah.columbia.edu/amiens-arthum/image/hookes-law-1, 2017

Fig. 33
Fernandes, J., Kirkegaard, P.H., Branco, J.M. (2016) Tectonic design of elastic timber gridshells, World Conference on Timber Engineering, Vienna, Austria.

Fig. 34
Adriaenssens, S., Barnes, S., Harris, S., Williams, C. (2014) Dynamic relaxation. In Adriaenssens, S., Block, P., Veenendaal, D., Williams, W. (Eds.) Shell structures for Architecture; Form Finding and Optimisation, 15-19. Routlegde, London/New York, UK/USA.

Fig. 35
A. López, I. Puente, and M. a. Serna, (2007) Numerical model and experimental tests on single-layer latticed domes with semi-rigid joints, Comput. Struct 85, 360–374.

Fig. 36 - Fig. 37
P. J. Knippers and T. Helbig, (2009) Recent Developments in the Design of Glazed Grid Shells," Intern. J. Sp. Struct. 24

Fig. 38
Seele, https://seele.com/references/chadstone-shopping-centre/

Fig. 39 - Fig. 40
Prayudhi, B. (2016) 3F3D: Form Follows Force with 3D printing; Topology Optimisation for Free-form Building Envelope design with Additive Manufacturing. Master Thesis, Faculty of Architecture and the Built Environment, TU Delft. Retrieved from: https://repository.tudelft.nl/islandora/object/uuid%3Ab068f81c-1561-4733-a07d-05e60368184b in November 2018.

Fig. 41 - Fig. 42
Linden, L. (2015) Innovative joints for gridshells; joints designed by topology optimisation and to be produced by additive manufacturing. Master Thesis, Faculty of Civil Engineering, TU Delft. Retrieved from: https://repository.tudelft.nl/islandora/object/uuid:8bf193c3-eece-4fc1-a259-06ae5d275f45 in November 2018.

Fig. 43
Seifi, H., Javan, A.R., Xu, S., Zhao, Y. (2018) Design optimisation and additive manufacturing of nodes in gridshell structures. Engineering Structures, 160, 161-170.

Fig. 44
P. Aldrupp., 2014. Recieved in personal correspondence with A. Sevtsuk.
Fig. 54 - Fig. 55
Galjaard, S., Hofman, S., Perry, N., Ren, S. (2015) Optimizing Structural Building Elements in Metal by uaing Additive Manufacturing. Proceedings of the International Association for Shell and Spacial Structures

Symposium, August 2015, Amsterdam, The Netherlands.

Fig. 56
GlassCon GmbH, https://www.glasscon.com/projects/structural-glass-roof-glass-fins

Fig. 57
Oikonomopoulou, F. Picture taken on the Milan Design Week, April 13, 2019.

Fig. 58
Jose Galan, from https://www.slideshare.net/booosting/20181120-booosting-glasontwikkelingen-glass-swing-ate-snijder-tud

Fig. 59
Carpeter Lowings, https://carpenterlowings.com/portfolio_page/glass-tube-field/, June 2014

Fig. 61
Ate Snijder, from https://www.slideshare.net/booosting/20181120-booosting-glasontwikkelingen-glass-swing-ate-snijder-tud

Fig. 62
Ate Snijder, from private correspondence

Fig. 64
https://www.gastechniek24.nl/a-49253351/cilinder-aansluitingen/10-stuks-dichtringen-voor-nen-cilinderaansluitingen-delrin-pom/

Fig. 66
Octatube, from https://www.octatube.nl/nl_NL/project-item.html/projectitem/157

Fig. 105
Linden, L. (2015) Innovative joints for gridshells; joints designed by topology optimisation and to be produced by additive manufacturing. Master Thesis, Faculty of Civil Engineering, TU Delft. Retrieved from: https://repository.tudelft.nl/islandora/object/uuid:8bf193c3-eece-4fc1-a259-06ae5d275f45 in November 2018.

Fig. 157
Galjaard, S., Hofman, S., Perry, N., Ren, S. (2015) Optimizing Structural Building Elements in Metal by uaing Additive Manufacturing. Proceedings of the International Association for Shell and Spacial Structures Symposium, August 2015, Amsterdam, The Netherlands.

Fig. 166
Gaynor, A., Guest, J., Moen C. (2013) Reinforced Concrete Force Visualisation and Design Using Bilinear Truss-Continuum Topology Optimisation. Journal of Structural Engineering 139, 607-618.

Appendix A. Optimisation loads

Node 327 Self-weight

Beam #	Normal force [N]	V_z [N]	V_y [N]	Torsion [Nmm]	M_y [Nmm]	M_z [Nmm]
1	-1.808,7	-3,0	-17,2	-1208,8	-12532,1	-4690,3
2	-2.155,9	10,4	3,3	-2816,4	-5461,8	3468,9
3	3.257,5	17,3	-0,6	-518,0	-3640,9	1230,2
4	-1.515,8	-2,4	-21,0	6152,1	-8593,1	-6211,4
5	-2.501,9	33,9	4,4	-7496,0	-27684,7	3417,0
6	3.696,6	0,7	3,0	1645,2	-2659,1	2661,6

Table A1 *Self weight loads for the first iteration of optimisations, following local coordinates of the beams*

Node 327 Added loads

Beam #	Normal force 1 [N]	Normal force 2 [N]
1	-1000	1000
2	-1000	1000
3	-1000	1000
4	-1000	1000
5	-1000	1000
6	-1000	1000

Table A2 *Added axial loads for the first iteration of optimisations*

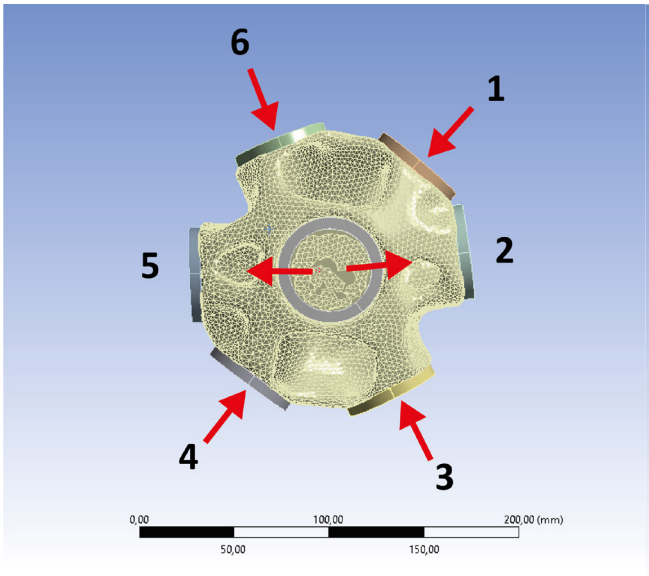

Fig. A1 *Location of forces from Table A1. Moments are all applied at the outer edge of the node*

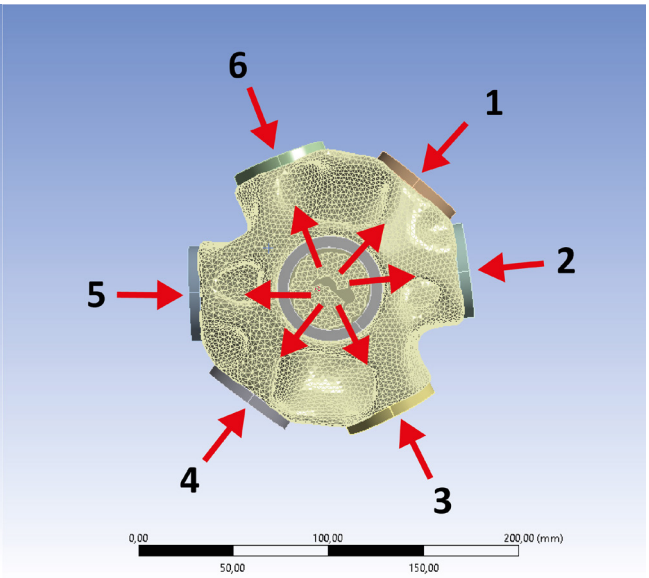

Fig. A2 *Location of normal forces as displayed in Table A2*

Node 327 Self-weight

Beam #	Normal force [N]	V_z [N]	V_y [N]	Torsion [Nmm]	M_y [Nmm]	M_z [Nmm]
1	-1.970,3	-2,1	-23,7	-1.004	-16.208,0	-5.778
2	-2.288,4	16,4	2,2	-3.589	-7.351	4.341
3	3.373,4	21,5	-3,6	-879	-4.356	1.557
4	-1.715,7	12,5	-27,4	7.599	-13.947	-7.613
5	-2.566,5	-26,3	21,0	-8.809	-8.218	4.048
6	3.763,3	10,2	19,5	1.586	-5.321	3.634

Table A3 *Self weight loads for the second iteration of optimisations, following local coordinates of the beams*

Node 327 Pre-stress

Beam #	Normal force [N]	V_z [N]	V_y [N]	Torsion [Nmm]	M_y [Nmm]	M_z [Nmm]
1	-1.210,5	48,7	10,8	-8.573	-614	309
2	-819,7	-13,5	-3,0	4.078	1.788	-1.569
3	-1.818,7	-2,6	-3,8	9.909	-3.149	-1.682
4	-980,3	-9,1	4,2	-10.809	-2.919	467
5	-891,1	-1,6	1,4	323	15.325	804
6	-1.559,9	-7,5	-1,8	9.764	-1.374	385

Table A4 *Loads caused by pre-tensioning the shell, for the second iteration of optimisations. Using local coordinates of the beams*

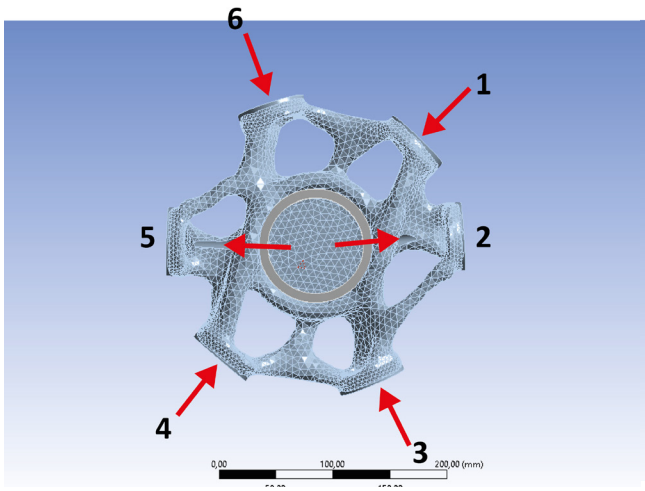

Fig. A3 *Location of forces from Table A3. Moments are all applied at the outer edge of the node*

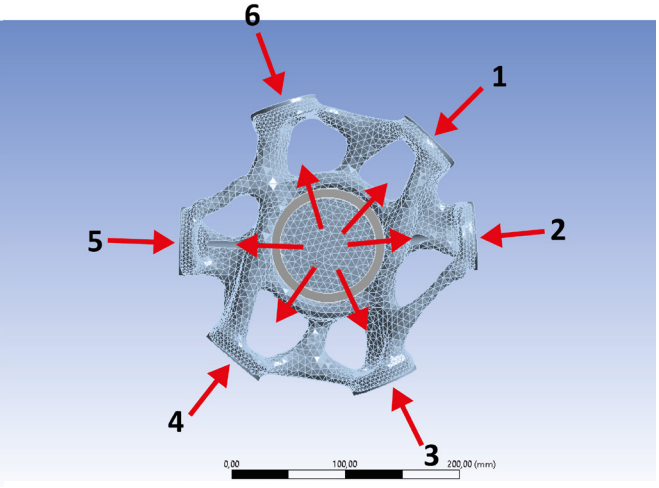

Fig. A4 *Location of normal forces as displayed in Table A4.*

Node 327 Wind

Beam #	Normal force [N]	V_z [N]	V_y [N]	Torsion [Nmm]	M_y [Nmm]	M_z [Nmm]
1	-241.162	33.476	-23.539	4.961	-1.823	-6.404
2	-434.081	6.558	11.678	-838	-14.262	4.722
3	4.665.501	4.443	1.814	-6.597	-5.323	614
4	-142.437	20.602	-12.161	3.213	579	-3.402
5	851.875	21.596	7.726	2.537	-11.559	2.377
6	3.568.519	14.694	4.614	-5.426	-4.785	1.088

Table A5 *Additional wind loads for testing the second iteration of optimisations. Using local coordinates of the beams*

Node 174	Self-weight					
Beam #	*Normal force [N]*	*V_z [N]*	*V_y [N]*	*Torsion [Nmm]*	*M_y [Nmm]*	*M_z [Nmm]*
1	-2.181,4	0,9	-1,4	266,0	-3.492,0	2.282,0
2	566,1	0,4	-1,5	-268,0	1.762,0	-1.777,0
3	-2.969,8	-0,1	-1,4	4.101,0	1.247,0	-3.749,0
4	-1.948,4	-0,5	1,5	-2.818,0	-1.807,0	3.765,0
5	649,3	0,6	1,2	-2.143,0	249,0	727,0
6	-3.469,3	0,5	1,5	1.148,0	3.101,0	-1.413,0

Table A6 *Self weight loads for the second iteration of optimisations, following local coordinates of the beams*

Node 174	Pre-stress					
Beam #	*Normal force [N]*	*V_z [N]*	*V_y [N]*	*Torsion [Nmm]*	*M_y [Nmm]*	*M_z [Nmm]*
1	-7.010,3	-83,1	2,7	17.187,0	91.932,0	1.793,0
2	-995,5	-10,5	10,4	11.669,0	10.721,0	4.556,0
3	-562,7	-18,3	-11,1	-3.675,0	71.107,0	-4.777,0
4	-6.707,7	-39,4	0,6	28.994,0	93.166,0	17,0
5	-139,0	-4,5	13,0	15.221,0	8.297,0	5.557,0
6	-426,7	-102,3	-14,2	-23.559,0	73.827,0	-5.225,0

Table A7 *Loads caused by pre-tensioning the shell, for the second iteration of optimisations. Using local coordinates of the beams*

Node 174	Wind					
Beam #	*Normal force [N]*	*V_z [N]*	*V_y [N]*	*Torsion [Nmm]*	*M_y [Nmm]*	*M_z [Nmm]*
1	-10.926,4	-128,3	-5,1	24.519,0	125.394,0	-788,0
2	-2.478,6	-14,9	22,7	12.711,0	16.457,0	10.198,0
3	3.663,6	-35,0	-12,7	-50.041,0	102.822,0	-5.819,0
4	-10.443,6	-40,1	-11,0	41.989,0	127.492,0	-4.944,0
5	-3.256,6	-9,0	27,8	19.086,0	13.399,0	11.772,0
6	4.147,0	-126,9	-21,3	-31.495,0	107.212,0	-7.881,0

Table A8 *Additional wind loads for testing the second iteration of optimisations. Using local coordinates of the beams*

Node 174	Self-weight					
Beam #	*Normal force [N]*	*V_z [N]*	*V_y [N]*	*Torsion [Nmm]*	*M_y [Nmm]*	*M_z [Nmm]*
1	-1.913	2	-2	553	-1.718	1.392
2	507	3	-12	-217	1.503	-1.568
3	-3.073	-9	-10	2.822	2.228	-2.304
4	-1.691	-7	11	-1.777	-28	2.567
5	598	5	10	-1.648	209	485
6	-3.563	2	2	627	3.815	-716

Table A9 *Self loads for the two-load optimisation*

Node 174	Wind					
Beam #	*Normal force [N]*	*V_z [N]*	*V_y [N]*	*Torsion [Nmm]*	*M_y [Nmm]*	*M_z [Nmm]*
1	-11.694	-102	-3	21.888	108.144	-353
2	-280	-15	15	9.746	15.709	6.826
3	3.36	-28	-9	-41.433	92.479	-3.847
4	-1.109	-35	-7	35.304	11.072	-3.179
5	-3.708	-10	19	15.151	12.315	8.154
6	3.938	-142	-16	-27.267	96.978	-5.536

Table A10 *Wind loads for the two-load optimisation*

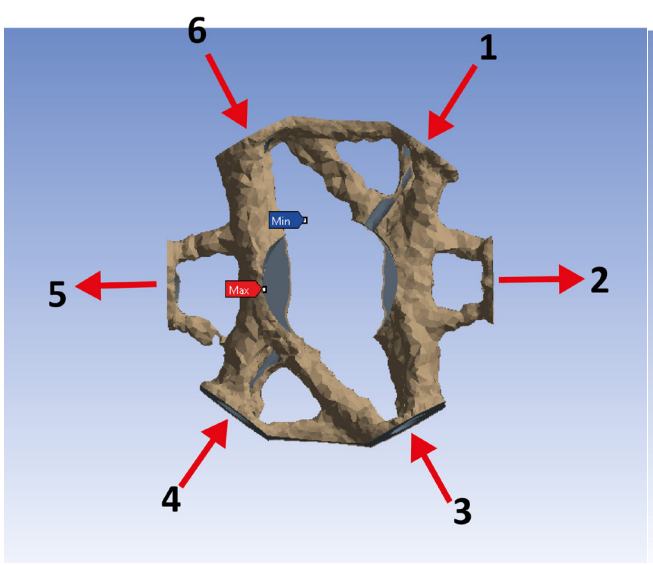

Fig. A5 *Location of loads for the self-weight only optimisation from Table A9*

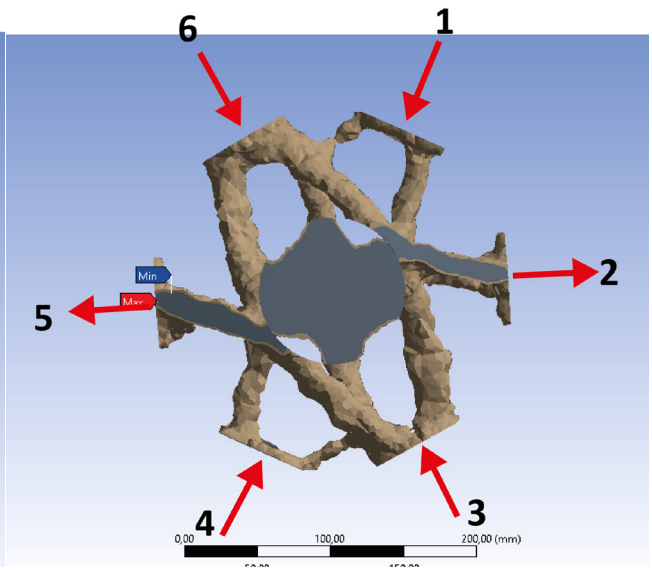

Fig. A6 *Location of loads for the wind-only optimisation from Table A10.*

Node 327	Self-weight					
Beam #	*Normal force [N]*	*V_z [N]*	*V_y [N]*	*Torsion [Nmm]*	*M_y [Nmm]*	*M_z [Nmm]*
1	-1.395,6	-3,0	-9,5	-653,0	-2.861,0	-2.368,0
2	-137,4	7,7	-4,3	-816,0	-1.073,0	1.756,0
3	1.026,4	1,1	-6,6	-277,0	-887,0	506,0
4	-1.059,9	0,6	-11,2	1.743,0	-1.792,0	-3.244,0
5	-1.460,5	-2,5	14,1	-1.622,0	-1.566,0	1.959,0
6	1.229,8	4,1	13,4	662,0	-1.238,0	1.604,0

Table A11 *Self loads for the two-load optimisation*

Node 327	Wind-load					
Beam #	*Normal force [N]*	*V_z [N]*	*V_y [N]*	*Torsion [Nmm]*	*M_y [Nmm]*	*M_z [Nmm]*
1	-233,6	-33,6	-23,5	4.858,0	-1.844,0	-6.352,0
2	-437,5	6,4	11,6	-825,0	-1.404,0	4.679,0
3	4.630,8	5,1	1,6	-6.481,0	-5.305,0	613,0
4	-1.402,9	20,6	-1,2	3.144,0	51,0	-3.403,0
5	833,2	22,4	7,7	2.506,0	-11.374,0	2.366,0
6	3.548,2	14,8	4,6	-5.321,0	-4.799,0	1.104,0

Table A12 *Wind loads for the two-load optimisation*

Node 174 Self-weight

Beam #	Normal force [N]	V_z [N]	V_y [N]	Torsion [Nmm]	M_y [Nmm]	M_z [Nmm]
1	-15.712,2	-34,3	38,6	26.936,0	1.221,0	1.559,0
2	345,4	13,0	53,5	20.279,0	8.385,0	16.867,0
3	-10.954,7	-66,7	-10,4	-28.579,0	92.624,0	-15.226,0
4	-17.555,6	-59,4	-4,8	18.961,0	113.126,0	10.979,0
5	715,3	-3,3	-29,5	16.535,0	2.201,0	437,0
6	-8.914,1	-12,2	-51,3	-41.166,0	76.226,0	-25.984,0

Table A13 *Self loads for the heavy shell optimisation*

Node 174 Added loads

Beam #	Normal force 1 [N]	Normal force 2 [N]
1	0	0
2	-3000	3000
3	0	0
4	0	0
5	-3000	3000
6	0	0

Table A14 *Additional loads for the heavy shell optimisation*

Node 174 Wind

Beam #	Normal force [N]	V_z [N]	V_y [N]	Torsion [Nmm]	M_y [Nmm]	M_z [Nmm]
1	-20.408,8	-73,9	-16,3	109.126,0	34.283,0	-12.007,0
2	-6.512,1	-19,1	42,6	48.334,0	37.748,0	30.174,0
3	7.767,2	-187,4	-31,3	-83.712,0	304.104,0	-20.375,0
4	-21.420,0	-213,0	-7,4	65.993,0	346.573,0	-199,0
5	-4.939,8	-27,9	34,3	32.432,0	46.749,0	25.513,0
6	6.791,0	-87,8	-18,0	-128.911,0	27.773,0	-14.553,0

Table A15 *Added wind loads to analyse the heavy shell optimisation*

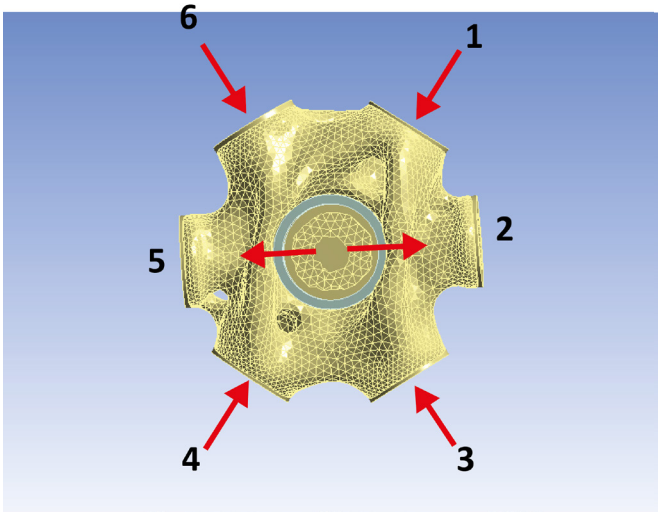

Fig. A7 *Location of forces from Table A13. Moments are all applied at the outer edge of the node*

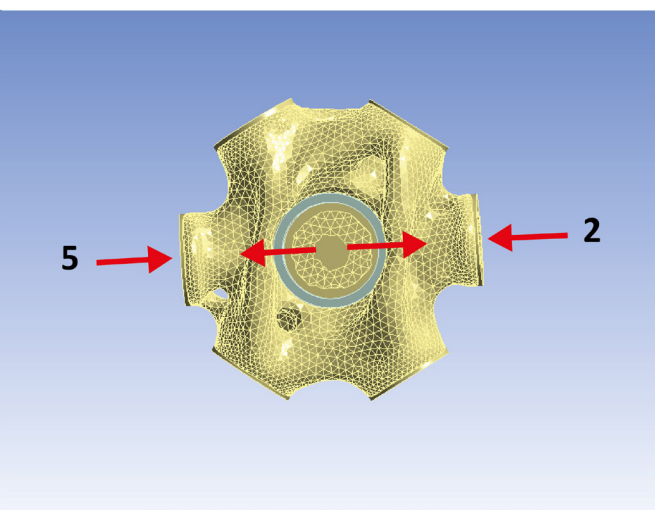

Fig. A8 *Location of forces from Table A15. Moments are all applied at the outer edge of the node*

Appendix B. Delrin POM

Ridderflex®

WEAR RESISTANT PLASTIC / SLIJTVASTE KUNSTSTOFFEN

DELRIN®

MAIN FEATURES

- Good slide and wear properties
- Resistant to cleaning agents
- High hardness
- High stiffness
- High strength
- Very good electrical insulation

COLOUR	Natural

PROPERTIES

	Typical value	Units	Test method
DENSITY	1.41	g/cm³	
WATER ABSORPTION	0.05/0.1	%	DIN EN ISO 62
FLAMMABILITY (UL94)	HB		DIN IEC 60695-11-10

MECHANICAL PROPERTIES

	Typical value	Units	Test method
MODULUS OF ELASTICITY (TENSILE TEST)	2800	Mpa	DIN EN ISO 527-2
TENSILE STRENGTH	67	Mpa	DIN EN ISO 527-2
TENSILE STRENGTH AT YIELD	67	Mpa	DIN EN ISO 527-2
ELONGATION AT YIELD	9	%	DIN EN ISO 527-2
ELONGATION AT BREAK	32	%	DIN EN ISO 527-2
FLEXURAL STRENGTH	91	MPa	DIN EN ISO 178
MODULUS OF ELASTICITY (FLEXURAL TEST)	2600	Mpa	DIN EN ISO 178
COMPRESSION STRENGTH	20/35	MPa	EN ISO 604
COMPRESSION MODULUS	2300	Mpa	EN ISO 604
IMPACT STRENGTH	Not broken	kJ/m²	DIN EN ISO 179-1eU
NOTCHED IMPACT STRENGTH	8	kJ/m²	DIN EN ISO 179-1eA

THERMAL PROPERTIES

	Typical value	Units	Test method
GLASS TRANSITION TEMPERATURE	-60	°C	DIN 53765
MELTING TEMPERATURE	166	°C	DIN 53765
SERVICE TEMPERATURE (LONG TERM)	100	°C	
SERVICE TEMPERATURE (SHORT TERM)	140	°C	

ELECTRICAL PROPERTIES

Appendix C. Wax printing

Lost-wax casting is an ancient and proven way of creating intricately shaped metal objects. As 3d-printing metal is relatively complicated and expensive, the lost-wax technique is more often employed to cast metal objects from 3d-printed geometries. This can be done using regular PLA plastic, which will evaporate if sufficiently heated. However, during this 'burnout', there is a risk of residue being left in the mould, potentially disrupting the casting. Different printing filaments have been designed to minimise residue left after burnout, for example MOLDLAY or PolyCast filaments. These filaments still need to be placed in an oven for extended amounts of time to be fully removed from the mould.

A different alternative is the wax filament offered by MachinableWax. This wax-like filament claims to leave minimal residue, and can be removed from the mould at much lower temperatures. Being able to obtain a role of the material easily, this was the material that was used for the node casting.

The wax filament is a rather different material than ordinary printing plastics. Compared to regular plastics, it is a very flexible material. Furthermore, it has a low recommended printing temperature of between 140-150° C, compared to regular plastic filaments that are printed at over 200° C. The producer offers a list of suggested printing settings, however, considerable trial-and-error is needed to find the optimal settings for each machine.

A small sample element was printed with different settings to find the most fitting printer and settings (Fig. A9). The samples consist of a rectangular tube, with different radii of filleting, to test how these affect the printing.

The major issue found with the wax filament was that is shrinks a lot when cooling. Due to this it is challenging to keep the material stuck to the printing bed, as the material tends to curl up during cooling, causing very deformed prints, or even complete failure when the model moved from its place. A second issue is adhesion between the layers. This material does not always stick together properly. Combined with the heavy shrinking behaviour, this quickly leads to cracks in the printed elements (Fig. A10).

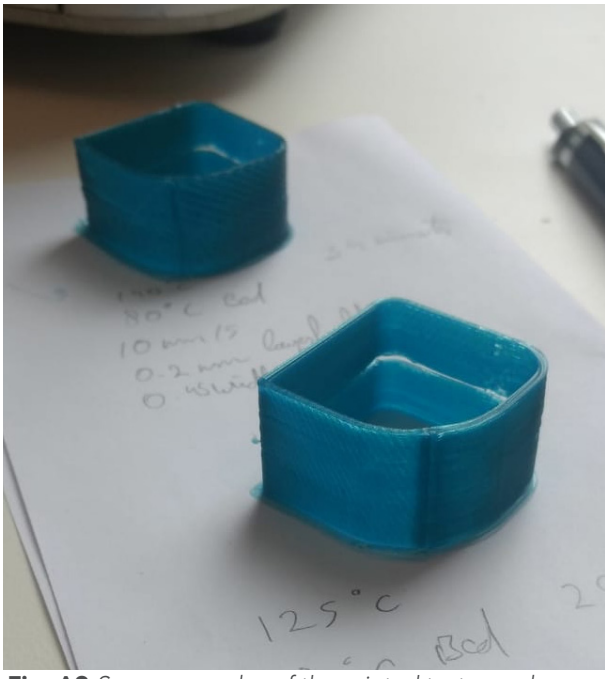

Fig. A9 *Some examples of the printed test samples*

A printer with a direct extruder is preferred. Many printers use a so called Bowden extruder, which places the motor pushing the filament away from the extruder. For regular printing this has certain advantages, as it allows the printing head to be lighter, and therefore more accurate. However it was found that due to the flexibility of the wax filament it will often curl up and jam the printer when fed like this. A direct extruder should be used to avoid this.

A heated bed is highly recommended for this material. First of all, it improves adhesion to the print bed, which is essential for this material. In addition, it heats entire model, which reduces shrinkage during printing and improves adhesion between layers.

Multiple methods have been tried to improve adhesion to the bed. It was found that regular printing paper offers a good base for printing, as the hot wax sticks to this strongly. However, when printing at high temperatures, the geometry detached from the paper due to the high shrinkage of the material (Fig. A12) For the final prints, double-sided sticker was the only material tried that ensured almost full adhesion to the printing bed. A two layer raft was printed under the entire object to further improve adhesion to the bed.

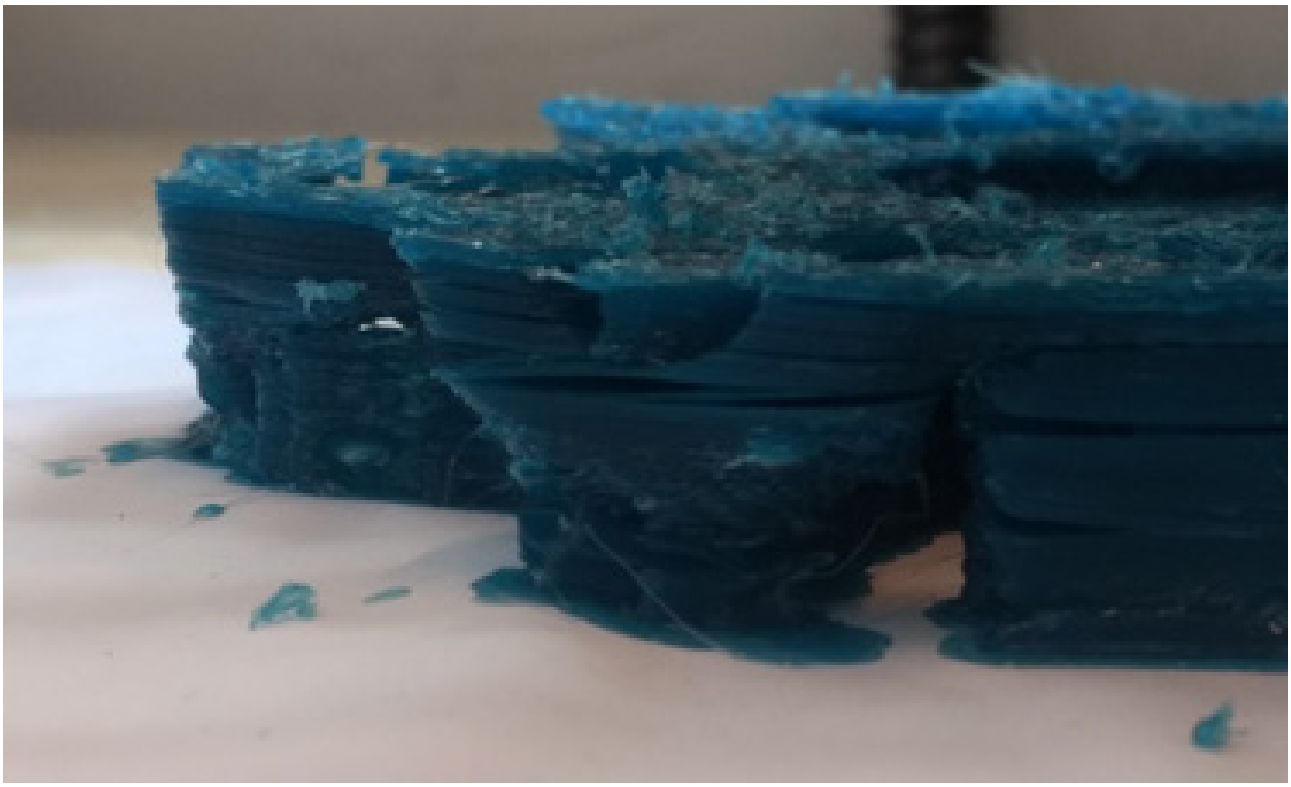

Fig. A10 *Significant layer separation in the first print*

Achieving proper adhesion between the different printing layers also proved challenging. To improve this, different layer heights, printing speeds and printing temperatures have been tried. The most successful result was found with 0.20 mm high layers with a 0.35 mm nozzle, at a temperature of 165° C. This is higher than the recommended printing temperature, though it is possible the printer used was indicating a too high temperature. 100% material extrusion and a low printing speed of 25 mm/s was used. No cooling was used, as this seemed to worsen the adhesion between layers.

Though the higher temperature improved layer adhesion, it also increases warping of the model. Minimising the amount of material in the model helps offset this. In the final model, a shell thickness of only one layer was used, with only 10 percent infill. Support material was generated to support any material at an angle steeper than 35°. This is more support than would be necessary, but in this case it meant that the supports were a continuous structure, as small, loose pieces of support were found to easily snap or detach during printing (Fig. A11).

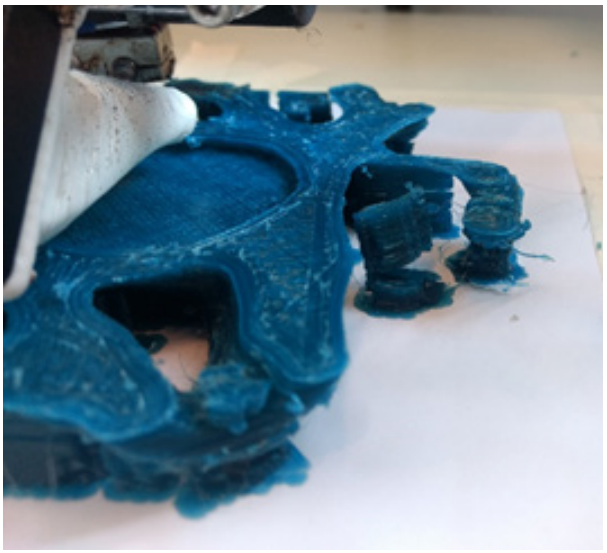

Fig. A11 *Breaking supports due to layer separation*

Despite these precautions, the adhesion between the layers still failed at multiple spots along the outer edge of the model, as this is where the largest stresses due to shrinkage occur. Candle wax was used after printing, to fill any cracks and smooth out irregularities.

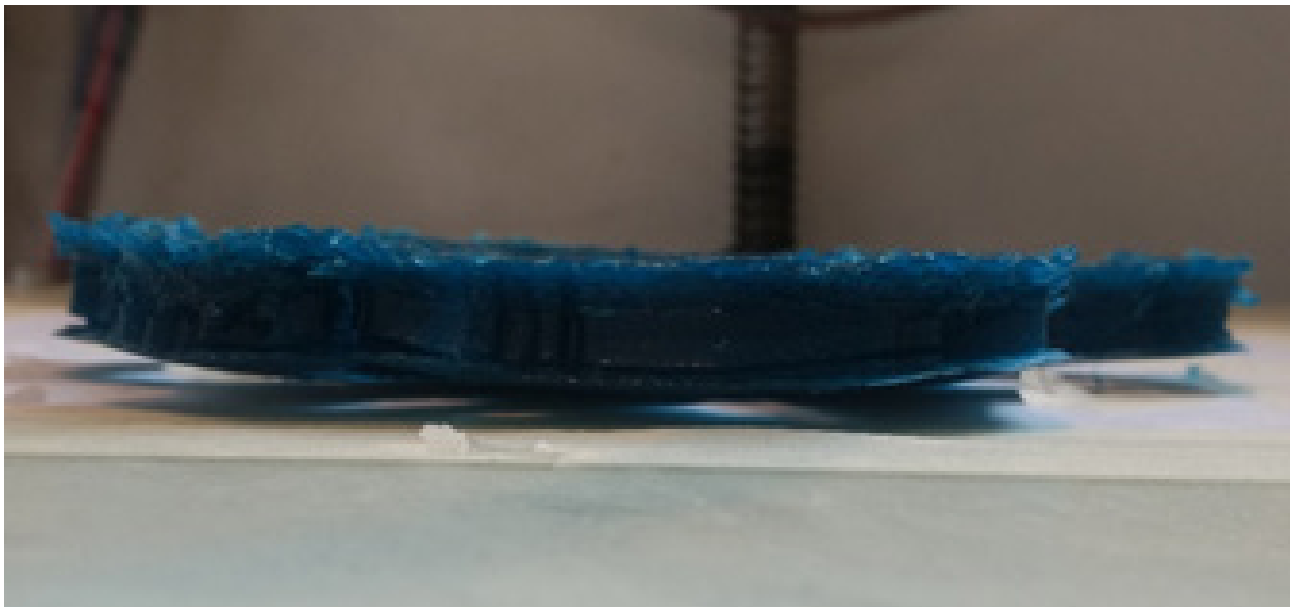

Fig. A12 *Loss of bed adhesion on the second printing test, showing the heavy warping of the material*

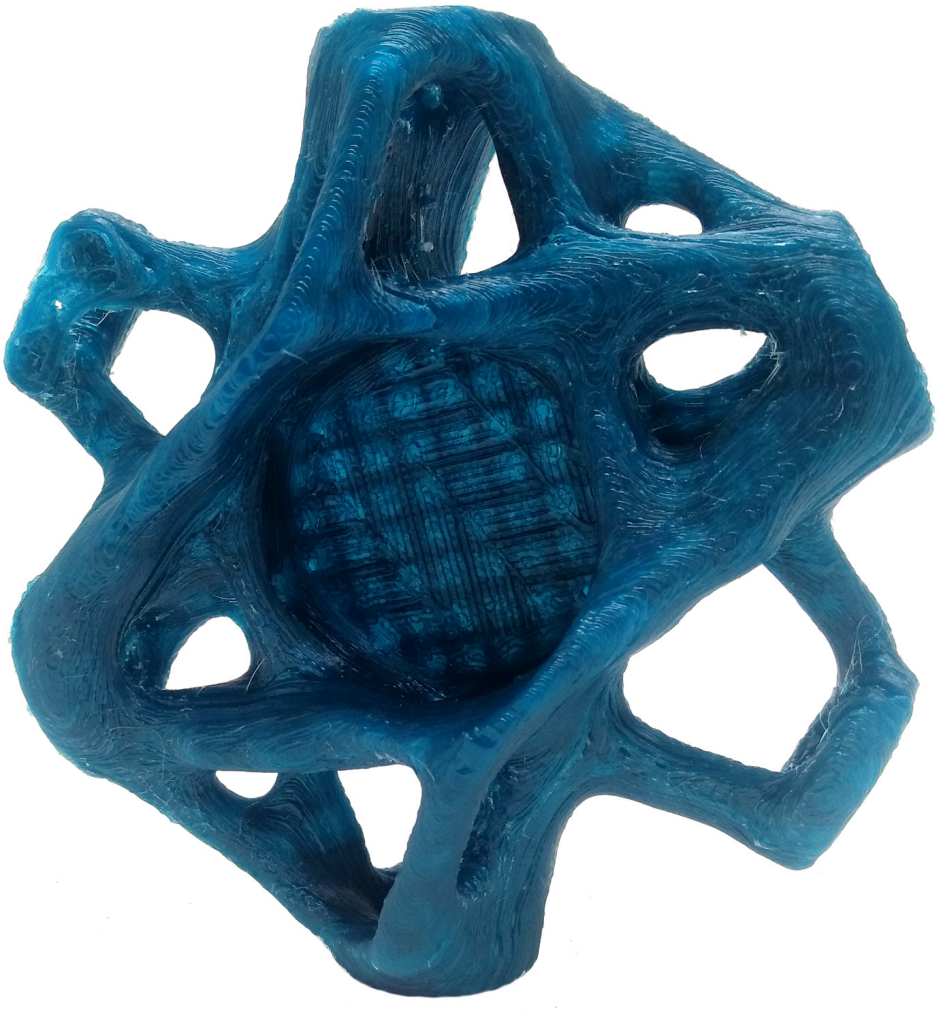

Fig. A13 *Result of the third print*

Fig. A14 *Printing in layers, to reduce shrinkage and minimise the amount of support material required*

An alternative print was performed, where the geometry was split into three layers, each printed separately. As each layer contained less material, the overall shrinkage of the model was reduced, almost completely eliminating cracks in the material. Furthermore, each part layer can be oriented separately. Printing the bottom part of the node upside down, the amount of overhang, and therefore support material needed, can be reduced to a minimum (Fig. A14).

Due to the shrinkage, however, the separate layers ended up warping during printing, locally detaching itself from the printing bed. Because of this, when fixing the separate parts together, considerable seams were found between the layers (Fig. A15). These were filled with wax as well as possible (Fig. A16).

Object made using regular wax can easily be made smooth by carefully heating the surface using for example a hairdryer, and letting the material flow a little. The filament used has a considerably higher melting temperature, which made it impossible to smoothen its surface in this way. Because of this lack of surface treatment, the layers of the printing process were still clearly visible within the cast glass geometry. Improving the surface quality of the printed geometry is therefore essential if a transparent geometry is to be achieved. A possible solution could be dipping the model into molten candle wax, which should cover the surface with a smooth finish.

Fig. A15 *Assembled layers. Some warping has occured, causing large seams between the layers*

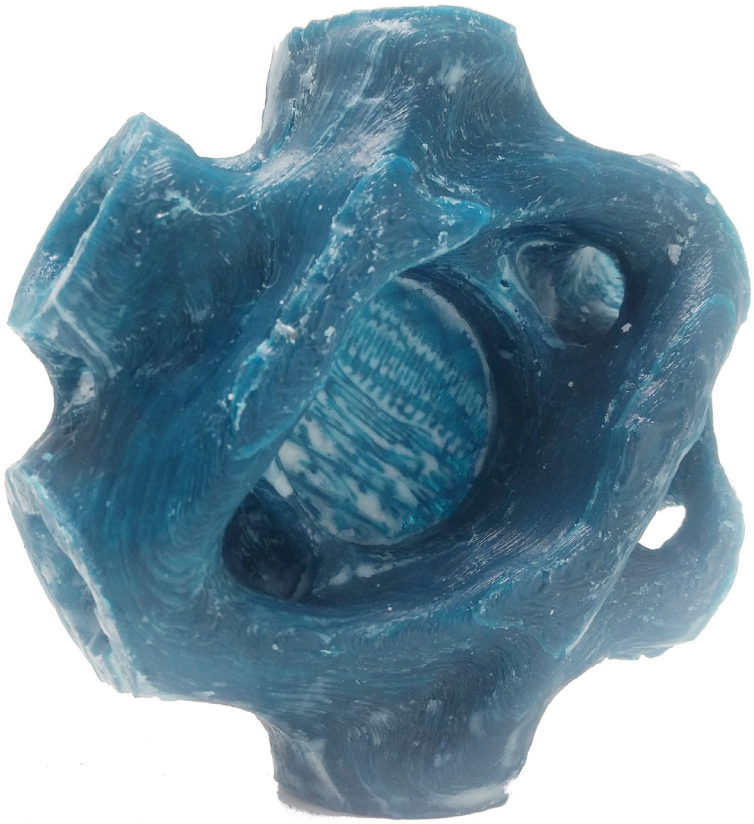

Fig. A16 *Final result of the printing in layers. Candle wax has been used to fill any seams and holes.*